



Drake, Thomas M. (2023) *Mechanisms of immunotherapy resistance in hepatocellular carcinoma*. PhD thesis.

<https://theses.gla.ac.uk/84000/>

Copyright and moral rights for this work are retained by the author

A copy can be downloaded for personal non-commercial research or study, without prior permission or charge

This work cannot be reproduced or quoted extensively from without first obtaining permission from the author

The content must not be changed in any way or sold commercially in any format or medium without the formal permission of the author

When referring to this work, full bibliographic details including the author, title, awarding institution and date of the thesis must be given

Enlighten: Theses

<https://theses.gla.ac.uk/>
research-enlighten@glasgow.ac.uk

Mechanisms of Immunotherapy Resistance in Hepatocellular Carcinoma

Thomas M Drake

MBChB BMedSci

School of Cancer Sciences
College of Medical, Veterinary and Life Sciences
University of Glasgow



University
of Glasgow

Submitted in fulfilment of the requirements for the degree of
Doctor of Philosophy in Cancer Science of the University of Glasgow, May 2023

Declaration

This thesis is my own work. The experiments and analysis described were performed by myself or in collaboration with others who are attributed in the text. Figures are my own work. This work has not been submitted for any other degree nor qualification.

Thomas M Drake

2023

Abstract

Hepatocellular Carcinoma is the 7th most common cause of cancer and 2nd highest cause of cancer mortality worldwide. For patients who present with early stage disease, cure can be achieved by surgical resection or liver transplantation. The majority of patients, however, present with late stage disease where palliative therapies are the only treatment option.

Immunotherapy is an emerging and promising treatment option for patients with advanced HCC. It allows a cytotoxic response to be directed against tumours and in some cases, can provide complete and durable disease control. However, not all patients will respond to immune checkpoint inhibition. Evidence suggests this is likely due to tumour intrinsic molecular processes that induce primary or secondary resistance to immunotherapy. Therefore, there is an urgent need to identify new strategies to increase the efficacy of immunotherapy for all patients.

Here, I show the development of genetically engineered mouse models which recapitulate key aspects of the human HCC tumour microenvironment. Using a range of techniques including immunohistochemistry and sequencing, I demonstrate response to immunotherapy in these models is associated with the presence of immune cells and go on to identify potential mechanisms responsible for immunotherapy resistance.

This work will underpin the basis for testing new treatments in relevant model systems, with the overall objective of improving patient care through translation of new therapies which improve responses to immunotherapy.

Acknowledgements

Science is about people and teams, without the support of one another nothing worthwhile is achieved.

First and foremost, thank you to all at the Cancer Research UK Beatson Institute for Cancer Research for supporting me over the past 5 years. Although too numerous to list individually, I am very grateful to the help and expertise provided to me by the teams in the animal unit, histology, molecular technology, high-performance computing, stores and laboratory management services.

Thank you to members of R09 including Ee Hong Tan, Toshiyasu Suzuki, Christos Kiourtis, Anastasia Georgakopoulou and Stephanie May for your friendship and support over the past 5 years. I would like to say a huge thanks to my supervisors Professor Thomas Bird and Professor Owen Sansom. Your support and trust was invaluable, allowing me to explore exciting new ideas and grow.

I would also like to thank Cancer Research UK, The Beatson Cancer Charity, Wellcome Trust, the Royal College of Surgeons of Edinburgh, Tenovus, Iterion therapeutics and Aligos therapeutics for funding my research. The complimentary mouse model service from Ingenious Targeting Laboratories was also very appreciated.

Finally – thank you to my Family and Friends (and your pets) for supporting me throughout.

Publications

Selected articles arising during this fellowship (including COVID-19 secondment)

Drake, Thomas M; Bird, Thomas G. Simplifying screening for primary liver cancer-do the LCR1 and LCR2 tests hold the key? *Alimentary Pharmacol Therapeutics* **49**, 612-613 (2019)

Knight, Stephen R; Shaw, Catherine A; Pius, Riinu; **Drake, Thomas M**; Norman, Lisa; Ademuyiwa, Adesoji O; Adisa, Adewale O; Aguilera, Maria Lorena *et al.*. Global variation in postoperative mortality and complications after cancer surgery: a multicentre, prospective cohort study in 82 countries. *The Lancet* **397**, 387-397 (2021)

Bloom, Chloe I; **Drake, Thomas M**; Docherty, Annemarie B; Lipworth, Brian J; Johnston, Sebastian L; Nguyen-Van-Tam, Jonathan S; Carson, Gail; Dunning, Jake; Harrison, Ewen M; Baillie, J Kenneth. Risk of adverse outcomes in patients with underlying respiratory conditions admitted to hospital with COVID-19: a national, multicentre prospective cohort study using the ISARIC WHO Clinical Characterisation Protocol UK. *The Lancet Respiratory Medicine* **9**, 699-711 (2021)

Haq, Mohammad Inamul; **Drake, Thomas M**; Goh, Tee Lin; Ahmed, Asma; Forrest, Ewan; Barclay, Stephen; Gillespie, Ruth; Priest, Mathew *et al.*. Effect of hepatocellular carcinoma surveillance programmes on overall survival in a mixed cirrhotic UK population: a prospective, longitudinal cohort study. *Journal of Clinical Medicine* **10**, 2770 (2021)

Drake, Thomas M; Riad, Aya M; Fairfield, Cameron J; Egan, Conor; Knight, Stephen R; Pius, Riinu; Hardwick, Hayley E; Norman, Lisa; Shaw, Catherine A *et al.*. Characterisation of in-hospital complications associated with COVID-19 using the ISARIC WHO Clinical

Characterisation Protocol UK: a prospective, multicentre cohort study. *The Lancet* **398**, 223-237 (2021)

Fairfield, Cameron J; **Drake, Thomas M**; Pius, Riinu; Bretherick, Andrew D; Campbell, Archie; Clark, David W; Fallowfield, Jonathan A *et al.*. Genome-wide association study of NAFLD using electronic health records. *Hepatology Communications* **6**, 297-308 (2022)

Fairfield, Cameron J; **Drake, Thomas M**; Pius, Riinu; Bretherick, Andrew D; Campbell, Archie; Clark, David W; Fallowfield, Jonathan A *et al.*. Genome-wide analysis identifies gallstone-susceptibility loci including genes regulating gastrointestinal motility. *Hepatology* **75**, 1081-1094 (2022)

Leslie, Jack; Mackey, John BG; Jamieson, Thomas; Ramon-Gil, Erik; **Drake, Thomas M**; Fercoq, Frédéric; Clark, William; Gilroy, Kathryn *et al.*. CXCR2 inhibition enables NASH-HCC immunotherapy. *Gut* **71**, 2093-2106 (2022)

Knight, Stephen R; Shaw, Catherine A; Pius, Riinu; **Drake, Thomas M**; Norman, Lisa; Ademuyiwa, Adesoji O; Adisa *et al.*. Effects of hospital facilities on patient outcomes after cancer surgery: an international, prospective, observational study. *The Lancet Global Health* **10**, e1003-e1011 (2022)

Villar, Victor H; Allegra, Maria Francesca; Deshmukh, Ruhi; Ackermann, Tobias; Nakasone, Mark A; Vande Voorde, Johan; **Drake, Thomas M** *et al.*. Hepatic glutamine synthetase controls N 5-methylglutamine in homeostasis and cancer. *Nature Chemical Biology* **19**, 292-300 (2023)

Abbreviations

AAV	Adeno associated virus
ALIOS	American lifestyle induced obesity syndrome
ATAC	Assay for transposase-accessible chromatin
BCLC	Barcelona clinic liver cancer
CAR	Chimeric antigen receptor
CCL	CC chemokine ligand
CCR	CC chemokine receptor
CD	Cluster of Differentiation
cGAMP	Cyclic guanosine monophosphate–adenosine monophosphate
cGAS	Cyclic GMP-AMP synthase
CXC3	C-X3-C motif
CXCL	CXC chemokine ligand
CXCR	CXC chemokine receptor
DAMP	Damage-associated molecular pattern
DEN	Diethylnitrosamine
DNA	Deoxyribonucleic acid
ER	Estrogen receptor
GC	Genomic copies
H&E	Haematoxylin and eosin
HBV	Hepatitis B virus
HCC	Hepatocellular carcinoma
HCV	Hepatitis C virus
HIV	Human immunodeficiency virus
IFN	Interferon
LIHC	Liver hepatocellular carcinoma
LSEC	Liver sinusoidal endothelial cell
NAFLD	Non-alcoholic fatty liver disease
NASH	Non-alcoholic steato hepatitis
PAMP	Pathogen-associated molecular pattern
PCR	Polymerase chain reaction
PTEN	Phosphatase and tensin homolog
RAS	Rat sarcoma virus protein
RB	Retinoblastoma
RNA	Ribonucleic acid
ROS	Reactive oxygen species
RTK	Receptor tyrosine kinases
SDI	Service delivery indicators
STING	Stimulator of interferon genes
TBG	Thyroxine-binding globulin
TCGA	The Cancer Genome Atlas
TERT	Telomerase reverse transcriptase
TP53/Trp53	Transformation related protein 53
WES	Whole exome sequencing

Contents

Declaration	i
Abstract	iii
Acknowledgements	v
Publications	vii
Abbreviations	ix
1 Introduction	1
1.1 Liver biology	2
1.2 Primary liver cancer	3
1.3 Hepatocellular carcinoma	4
1.4 Aetiology and risk factors for hepatocellular carcinoma	4
1.4.1 Viral infection	5
1.4.2 Environmental carcinogens	8
1.4.2.1 Alcohol	8
1.4.2.2 Smoking	9
1.4.2.3 Aflatoxin	9
1.4.2.4 Other mutagens	10
1.4.3 Non-alcoholic fatty liver disease	10
1.4.4 Other causes of liver disease	12
1.4.5 Additional risk factors	13
1.4.5.1 Age	13
1.4.5.2 Sex	13
1.4.5.3 Cirrhosis	14

1.4.5.4	Protective factors	17
1.5	Clinical management	17
1.5.1	Diagnosis and surveillance	17
1.5.2	Classification, staging and treatment	18
1.5.3	Systemic therapy	22
1.5.3.1	Immune checkpoint therapy for HCC	23
1.6	Biology of hepatocellular carcinoma	26
1.6.1	Molecular subclassification of HCC	27
1.6.2	Tumour microenvironment	28
1.6.3	Immune surveillance and anti-tumour immunity	29
1.6.4	Evasion of anti-tumour immunity and resistance to immunotherapy	31
1.6.5	Factors influencing immunotherapy response	34
1.7	Mouse models of hepatocellular carcinoma	34
1.7.1	Genetically engineered HCC models for studying immunotherapy response and resistance	37
2	Hypothesis and aims	40
2.1	Hypothesis and aims	41
2.1.1	Hypotheses	41
2.1.2	Aims	42
3	Materials and methods	43
3.1	Mouse models	44
3.1.1	Adeno-associated virus preparation	44
3.1.2	Mouse husbandry	44
3.1.3	Orthotopic transplantation	46
3.1.4	Alleles	48
3.1.4.1	Conditional β -Catenin exon 3 deletion	48
3.1.4.2	Conditional Trp53 deletion	48
3.1.4.3	Conditional c-MYC expression	49

3.1.4.4	TetO- Δ N89 β -Catenin expression	49
3.1.4.5	Tetracycline controlled systems	49
3.1.4.6	Generation of the NeoTAP mouse model of conditional antigen expression	50
3.1.5	Diethylnitrosamine american lifestyle-induced obesity syndrome model of NASH-HCC	51
3.1.6	Drug administration	51
3.2	Histology	53
3.2.1	Tissue processing	53
3.2.2	Immunohistochemistry	53
3.2.3	RNA in-situ hybridisation	54
3.2.4	Tissue analysis	56
3.2.5	Computer vision for slide labelling	56
3.3	Protein and molecular assays	57
3.3.1	Cytokine assays	57
3.3.2	Nucleic acid extraction from tissue	57
3.3.3	Whole exome library preparation and sequencing	58
3.3.4	Whole exome sequencing analysis	58
3.3.5	mRNA stranded library preparation and sequencing	58
3.3.6	RNA sequencing analysis	59
3.3.7	Assay for transposase-accessible chromatin library preparation and sequencing	60
3.3.8	ATAC sequencing analysis	60
3.3.9	Single cell RNA library preparation and sequencing	61
3.3.10	Single cell RNA sequencing analysis	62
3.4	Cell culture	63
3.4.1	2-D Cell culture	63
3.4.2	3-D Cell culture	64
3.5	Statistical analyses	65

4	Development of immunotherapy resistant and immunotherapy responsive genetically engineered mouse models of hepatocellular carcinoma	67
4.1	Introduction	68
4.2	Hypothesis	69
4.3	Model development	69
4.3.1	Overview of Cre mediated recombination	69
4.3.1.1	Function of β -Catenin and the canonical WNT signalling pathway	72
4.3.1.2	Function of c-MYC	73
4.3.2	Selection of genetic drivers for inflamed HCC model	74
4.3.3	Optimising the Trp53 ^{fl/fl} Rosa26 ^{c-MYC/c-MYC} mouse model	80
4.3.4	Response to immune checkpoint inhibition of Trp53 ^{fl/fl} Rosa26 ^{c-MYC/c-MYC} mouse model	89
4.3.5	Generating a genetically defined orthotopic transplantation model	94
4.4	Summary	98
4.5	Future directions	100
5	Multomic analysis of hepatocellular carcinoma models to identify pathways associated with immune exclusion	103
5.1	Introduction	104
5.2	Hypothesis	105
5.3	Whole exome sequencing	106
5.3.1	Comparison of whole exome sequencing in Ctnnb1 ^{exon3/Wt} Rosa26 ^{c-MYC/c-MYC} and Trp53 ^{fl/fl} Rosa26 ^{c-MYC/c-MYC} tumours	109
5.3.2	Comparison of copy number variation in Ctnnb1 ^{exon3/Wt} Rosa26 ^{c-MYC/c-MYC} and Trp53 ^{fl/fl} Rosa26 ^{c-MYC/c-MYC} tumours	115
5.4	Transcriptomic comparison of Ctnnb1 ^{exon3/Wt} Rosa26 ^{c-MYC/c-MYC} and Trp53 ^{fl/fl} Rosa26 ^{c-MYC/c-MYC} mouse models	121
5.4.1	Comparison of transcriptome sequencing in Ctnnb1 ^{exon3/Wt} Rosa26 ^{c-MYC/c-MYC} and Trp53 ^{fl/fl} Rosa26 ^{c-MYC/c-MYC} tumours	121

5.4.2	Expression of immune checkpoint genes	127
5.4.3	Spatial validation of RNA sequencing results	131
5.5	Comparison of chromatin accessibility and transcription factor footprints	133
5.5.1	Results of ATAC sequencing and differences in chromatin accessibility by genotype and tissue	134
5.6	Protein-level quantification of cytokine expression in HCC mouse models	146
5.6.1	Comparison of cytokine expression in $Ctnnb1^{exon3/Wt}$ $Rosa26^{c-MYC/c-MYC}$ and $Trp53^{fl/fl}$ $Rosa26^{c-MYC/c-MYC}$ HCC models	146
5.7	Summary	151
5.8	Future directions	153
6	Targeting the cGAS-STING pathway to induce cytokine expression in models of immune excluded hepatocellular carcinoma	156
6.1	Introduction	157
6.2	Hypothesis	160
6.3	Targeting the cGAS-STING pathway	160
6.3.1	Stimulation of $Ctnnb1^{exon3/Wt}$ $Rosa26^{c-MYC/c-MYC}$ and $Trp53^{fl/fl}$ $Rosa26^{c-MYC/c-MYC}$ tumour cells in-vitro with 2'3'cGAMP	163
6.3.2	Comparison of transcriptome sequencing of $Ctnnb1^{exon3/Wt}$ $Rosa26^{c-MYC/c-MYC}$ and $Trp53^{fl/fl}$ $Rosa26^{c-MYC/c-MYC}$ tumour cells following 2'3'cGAMP	165
6.4	Summary	174
6.5	Future directions	175
7	New genetically engineered mouse models to study epithelial-immune interactions in the tumour microenvironment	177
7.1	Introduction	178
7.2	Development of a temporally controlled model of β -Catenin driven HCC	179
7.2.1	Results from whole-body and conditional expression of TetO- Δ N89 β - catenin	181

7.2.2	Summary	186
7.2.3	Future directions	186
7.3	Development of the NeoTAP model	188
7.3.1	Requirements for the ideal mouse model of neoantigen expression	188
7.3.2	Design of a mouse model for study of neoantigen expression	189
7.3.2.1	Production of the NeoTAP model	191
7.3.3	Comparison with the inversion controlled joined neoantigen mouse model	192
7.3.4	Validation of tissue-specific expression	195
7.3.5	Summary	195
7.3.6	Future directions	197
8	Conclusions	200
8.1	Key findings	201
8.1.1	Cancer cell intrinsic mechanisms underpinning immune exclusion	203
8.1.2	Epithelial cytokine expression can be induced by targeting the cGAS-STING pathway	207
8.2	Further research questions and limitations	209
8.2.1	Do other cell types contribute to immunotherapy resistance in HCC?	209
8.2.2	How does c-MYC cooperate with different drivers to limit or promote anti-tumour immunity?	212
8.2.3	Can β -Catenin be targeted as an adjuvant to immunotherapy?	212
8.3	Immunotherapy for HCC in context	214
	Bibliography	216
	Appendix	242
A	Resistance to immune checkpoint inhibitors in non-alcoholic steatohepatitis induced hepatocellular carcinoma	243
A.1	Introduction	244
A.2	Hypothesis	245

A.3	Neutrophils in human NASH/NAFLD-HCC	246
A.4	Investigating the effect of CXCR2 inhibition on the tumour microenvironment .	248
A.4.1	Results of single-cell RNA sequencing analysis	249
A.4.2	Effect of CXCR2 inhibition in myeloid compartments of the tumour microenvironment	253
A.4.3	Cytokine signalling in neutrophil populations	257
A.4.4	Effect of CXCR2 inhibition in T-cell compartments of the tumour microenvironment	259
A.4.5	Effect of CXCR2 inhibition on cell state and RNA velocity in T-cell compartments	267
A.4.6	Effect of combination CXCR2 inhibition on cell state and RNA velocity in tumour associated neutrophils	271
A.5	Summary	274
A.6	Future directions	276

List of Tables

1.1	Hepatocellular carcinoma TNM staging	20
1.2	Comparison of different <i>in-vivo</i> models	38
3.1	Clinical signs and grading for determining endpoints in mouse models	45
3.2	Drug dosing and administration	53
3.3	Antibody list	56
4.1	Selection of alleles for development of an immunotherapy responsive mouse model of HCC	78
5.1	Top 20 most frequent CNVs in $Ctnnb1^{\text{exon3/Wt}}$ $Rosa26^{\text{c-MYC/c-MYC}}$ and $Trp53^{\text{fl/fl}}$ $Rosa26^{\text{c-MYC/c-MYC}}$ HCC models	119
5.2	Transcription factors in cytokine TSS regions found exclusively in either $Trp53^{\text{fl/fl}}$ $Rosa26^{\text{c-MYC/c-MYC}}$ or $Ctnnb1^{\text{exon3/Wt}}$ $Rosa26^{\text{c-MYC/c-MYC}}$ tumours	139
5.3	Summary of mechanisms contributing to immune exclusion and therapy resistance	152

List of Figures

1.1	Disability adjusted life years lost from primary liver cancer worldwide	6
1.2	Disability adjusted life years lost worldwide by sex and development index	7
1.3	Progression of liver disease	15
1.4	Barcelona Clinic Liver Cancer staging system	22
1.5	The cancer immunity cycle	32
1.6	Overview of inhibitory immune checkpoints	35
4.1	Immune infiltration in HCC patients in the Cancer Genome Atlas by molecular subclass	71
4.2	Immune infiltration in $Ctnnb1^{\text{exon3/Wt}}$ $Rosa26^{\text{c-MYC/c-MYC}}$ tumours	75
4.3	Frequency of somatic mutations in TCGA-LIHC patient cohort by aetiology of liver disease	77
4.4	Overview of conditional strategy used to generate genetically engineered mouse models	81
4.5	Optimisation of AAV8-TBG-Cre in $Trp53^{\text{fl/fl}}$ $Rosa26^{\text{c-MYC/c-MYC}}$ model	83
4.6	Histological appearance of tumours in $Trp53^{\text{fl/fl}}$ $Rosa26^{\text{c-MYC/c-MYC}}$ mice by dose of AAV8-TBG-Cre	84
4.7	Phenotypic markers in $Trp53^{\text{fl/fl}}$ $Rosa26^{\text{c-MYC/c-MYC}}$ tumours	85
4.8	Immune infiltration in $Trp53^{\text{fl/fl}}$ $Rosa26^{\text{c-MYC/c-MYC}}$ tumours	88
4.9	Systemic blood counts of $Trp53^{\text{fl/fl}}$ $Rosa26^{\text{c-MYC/c-MYC}}$ HCC models compared to empty vector controls	90
4.10	Systemic blood counts of $Ctnnb1^{\text{exon3/Wt}}$ $Rosa26^{\text{c-MYC/c-MYC}}$ versus $Trp53^{\text{fl/fl}}$ $Rosa26^{\text{c-MYC/c-MYC}}$ HCC models	91
4.11	Treatment of $Trp53^{\text{fl/fl}}$ $Rosa26^{\text{c-MYC/c-MYC}}$ mice with anti-PD1	92

4.12 Overall survival with anti-PD1 in $Ctnnb1^{exon3/Wt}$ $Rosa26^{c-MYC/c-MYC}$ and $Trp53^{fl/fl}$ $Rosa26^{c-MYC/c-MYC}$ HCC models	93
4.13 Generating an immunotherapy responsive orthotopic transplantation model from $Trp53^{fl/fl}$ $Rosa26^{c-MYC/c-MYC}$ tumours	95
4.14 Immune infiltration in $Trp53^{fl/fl}$ $Rosa26^{c-MYC/c-MYC}$ orthotopic transplant model	97
5.1 Overview of experimental design used for multiomic comparison of $Ctnnb1^{exon3/Wt}$ $Rosa26^{c-MYC/c-MYC}$ and $Trp53^{fl/fl}$ $Rosa26^{c-MYC/c-MYC}$ HCC models	108
5.2 Exome mutations by type and location across genome in tumours from $Trp53^{fl/fl}$ $Rosa26^{c-MYC/c-MYC}$ and $Ctnnb1^{exon3/Wt}$ $Rosa26^{c-MYC/c-MYC}$	112
5.3 Overview of variants by type and annotation in tumours from $Trp53^{fl/fl}$ $Rosa26^{c-MYC/c-MYC}$ and $Ctnnb1^{exon3/Wt}$ $Rosa26^{c-MYC/c-MYC}$	114
5.4 Uniform Manifold Approximation Projection (UMAP) plot of mutations from whole exome sequencing of $Ctnnb1^{exon3/Wt}$ $Rosa26^{c-MYC/c-MYC}$ and $Trp53^{fl/fl}$ $Rosa26^{c-MYC/c-MYC}$ tumours.	115
5.5 Copy Number Variations in $Ctnnb1^{exon3/Wt}$ $Rosa26^{c-MYC/c-MYC}$ and $Trp53^{fl/fl}$ $Rosa26^{c-MYC/c-MYC}$ tumours	117
5.6 Uniform Manifold Approximation Projection plot of copy number variations from $Ctnnb1^{exon3/Wt}$ $Rosa26^{c-MYC/c-MYC}$ and $Trp53^{fl/fl}$ $Rosa26^{c-MYC/c-MYC}$ tumours	120
5.7 Overview of transcriptomic differences in $Ctnnb1^{exon3/Wt}$ $Rosa26^{c-MYC/c-MYC}$ tumour model compared with $Trp53^{fl/fl}$ $Rosa26^{c-MYC/c-MYC}$ model	123
5.8 Gene Set Enrichment Analysis for Gene Ontology Biological Process Terms in $Trp53^{fl/fl}$ $Rosa26^{c-MYC/c-MYC}$ tumours compared to $Ctnnb1^{exon3/Wt}$ $Rosa26^{c-MYC/c-MYC}$ tumours	125
5.9 Gene Set Enrichment Analysis of specific anti-viral or PAMP/DAMP associated pathways significantly enriched in $Trp53^{fl/fl}$ $Rosa26^{c-MYC/c-MYC}$ tumours compared to $Ctnnb1^{exon3/Wt}$ $Rosa26^{c-MYC/c-MYC}$ tumours	126
5.10 Expression of cytokine genes across tumour and control liver tissue	128
5.11 Venn diagrams of differential gene expression in $Trp53^{fl/fl}$ $Rosa26^{c-MYC/c-MYC}$ versus $Ctnnb1^{exon3/Wt}$ $Rosa26^{c-MYC/c-MYC}$ HCC models	129

5.12	Expression of inhibitory and stimulatory immune checkpoint genes across tumour and control liver tissue	130
5.13	Spatial validation of immune checkpoints in $\text{Trp53}^{\text{fl/fl}}$ $\text{Rosa26}^{\text{c-MYC/c-MYC}}$ and $\text{Ctnnb1}^{\text{exon3/Wt}}$ $\text{Rosa26}^{\text{c-MYC/c-MYC}}$ tissue	132
5.14	Overview of ATAC sequencing results	135
5.15	Overview of ATAC sequencing results by tissue type according to proximity to transcription start sites	136
5.16	Annotated regions of open chromatin across different tissue types	137
5.17	Differentially accessible genomic features identified by ATAC sequencing of $\text{Trp53}^{\text{fl/fl}}$ $\text{Rosa26}^{\text{c-MYC/c-MYC}}$ tumours compared with $\text{Ctnnb1}^{\text{exon3/Wt}}$ $\text{Rosa26}^{\text{c-MYC/c-MYC}}$ tumours	138
5.18	Transcription factor footprints comparing immune infiltrated $\text{Ctnnb1}^{\text{exon3/Wt}}$ $\text{Rosa26}^{\text{c-MYC/c-MYC}}$ tumours to $\text{Trp53}^{\text{fl/fl}}$ $\text{Rosa26}^{\text{c-MYC/c-MYC}}$ tumours	140
5.19	Selected plots of normalised counts of RNA for cytokine associated genes and transcription factors which are found within 500 bp of the TSS	143
5.20	Selected plots of normalised counts of RNA for cytokine associated genes and transcription factors which are found within 500 bp of the TSS (continued) . . .	144
5.21	Examples of transcription factor binding in regulatory regions of STING signalling pathway	145
5.22	Multiplex cytokine array results by cytokine and tissue type	148
5.23	Multiplex cytokine array results by cytokine and tissue type (continued)	149
5.24	Multiplex cytokine array results by cytokine and tissue type (continued)	150
5.25	Summary of cytokine array results by cytokine and tissue type comparisons . . .	150
6.1	Overview of the cGAS-STING pathway	159
6.2	STING staining and STING target gene expression in $\text{Ctnnb1}^{\text{exon3/Wt}}$ $\text{Rosa26}^{\text{c-MYC/c-MYC}}$ and $\text{Trp53}^{\text{fl/fl}}$ $\text{Rosa26}^{\text{c-MYC/c-MYC}}$ models of HCC	162
6.3	Expression of cGAS-STING genes and Gene Set Enrichment of Gene Ontology terms in the Cancer Genome Atlas	164
6.4	Overview of the 2'3'cGAMP stimulation experiment	165

6.5	Overview of transcriptional differences in 2'3'cGAMP response	167
6.6	Differentially expressed genes by 2'3'cGAMP treatment and tumour organoid genotype	168
6.7	Normalised cytokine gene counts by 2'3'cGAMP treatment and tumour organoid genotype	170
6.8	Normalised immune checkpoint gene counts by 2'3'cGAMP and tumour organoid genotype	171
6.9	Gene Set Enrichment Analysis of Gene Ontology terms following 2'3'cGAMP treatment	173
7.1	Overview of tetracycline controlled TetO- Δ N89 β -catenin	182
7.2	Confirmation of nuclear β -Catenin expression in 'tet-on' Col1a1 ^{TetO-ΔN89 β-catenin} Rosa26 ^{M2-rtTA} model	183
7.3	Confirmation of nuclear β -Catenin expression in 'tet-off' Col1a1 ^{TetO-ΔN89 β-catenin} Igs2 ^{CAG-lsl-tTA2-T2A-H2B-TagBFP/Wt} model	184
7.4	Histological appearance, expression of canonical WNT/ β -Catenin marker GS and immune infiltration in doxycycline controlled Col1a1 ^{TetO-ΔN89 β-catenin/Wt} Rosa26 ^{c-MYC/c-MYC} Igs2 ^{CAG-lsl-tTA2-T2A-H2B-TagBFP/Wt} mouse model of HCC	185
7.5	Overview of the NeoTAP model	193
7.6	Expression of mCherry in experimental NeoTAP mice	196
8.1	Potential mechanisms underpinning immunotherapeutic resistance in β -Catenin mutant HCC arising from this thesis.	204
8.2	Potential therapeutic targets for reversing immunotherapeutic resistance in β -Catenin mutant HCC	207
A.1	Pathological assessment of neutrophil infiltrate and automated quantification of CD66B in a HCC resection patient cohort	247
A.2	Overview of single-cell RNA sequencing experiment in a DEN-ALIOS NASH-HCC model with CXCR2smi therapy	250

A.3	Summary of clusters by treatment group in DEN-ALIOS NASH-HCC model with CXCR2smi therapy	251
A.4	Overview of a selection of cluster defining canonical epithelial and immune cell markers	254
A.5	Re-clustered myeloid populations	256
A.6	Gene set enrichment analysis of Gene Ontology terms for myeloid cell clusters .	258
A.7	Pseudotime trajectory analysis of differentially expressed genes within neutrophils	260
A.8	Re-clustered T-cell populations	263
A.9	Gene set enrichment analysis of Gene Ontology terms for T-cell clusters	265
A.10	Cytotoxicity and cytokine gene expression in T-cell populations	268
A.11	RNA velocity stream across T-cell clusters	269
A.12	Gene expression heatmaps of T-cell RNA velocity by latent time	271
A.13	RNA velocity stream across neutrophil clusters	273
A.14	Gene expression heatmaps of neutrophil RNA velocity by latent time	274

Chapter 1

Introduction

1.1 Liver biology

The liver is a major organ which forms a key part of the digestive system in vertebrate species. It performs essential roles such as removing toxic substances, synthesis of key proteins, drug and carbohydrate metabolism, and production of hormones[1]. In humans, the liver is found in the upper right quadrant of the abdomen, affixed to the diaphragm by the left and right triangular ligaments, and to the anterior abdominal wall by the falciform ligament.

The liver has a dual circulatory supply, with oxygenated blood coming in from the hepatic artery (~30%) and nutrient rich blood supplied through the portal vein (~70%). Venous drainage is through the hepatic veins which drain directly into the vena cava. This arrangement gives rise to the microscopic structure of the liver, where blood travels along sinusoids from the hepatic artery and portal vein and into the hepatic veins.

Along the course of the sinusoids is highly fenestrated endothelium which allows the passage of waste molecules into the liver parenchyma for processing by hepatocytes[2]. Hepatocytes are the primary epithelial cell found within the liver responsible for many of its key functions. These cells process the waste and produce bile which runs in a counter current direction from the blood flow, along the biliary tree and eventually drains into the intestine. They are also responsible for many of synthetic functions within the liver.

Lymphatic drainage of the liver is through one of three routes, depending on the tract being drained. Lymphatic capillaries in the portal tract drain into the hilar and coeliac nodes, whereas vessels along the central vein and the subcapsular regions of the convex surface of the liver drain superiorly into the mediastinal nodes[1].

In addition to hepatocytes, the liver contains many highly specialised cells with a diverse range of functions. Cholangiocytes line the biliary tree, liver sinusoidal endothelial cells (LSECs) provide a fenestrated lining to the sinusoids, hepatic stellate cells coordinate production of extracellular matrix in times of liver injury and Kupffer cells are tissue resident macrophages which line the sinusoidal endothelium.

Immunologically, the liver also plays an important role in regulating inflammation[3, 4]. It is a major site of antigen and toxin exposure from dietary and microbial sources. The liver has to be able to tolerate relevant dietary components whilst being able to respond and eliminate any potential pathogens[5]. In health the liver is typically tolerogenic, to prevent autoimmunity and inappropriate activation of immune responses to otherwise necessary dietary exposures.

1.2 Primary liver cancer

Primary liver cancer can be defined as a malignancy arising from within the liver parenchyma or biliary tree, proximal to the hilum[6].

The highest rates of primary liver cancer are found in Eastern Asia (17.8 cases per 100,000 age standardised population), Northern Africa (15.2 cases per 100,000 age standardised population) and South-East Asia (13.7 cases per 100,000 age standardised population)[7]. Globally, the case fatality rate from primary liver cancer is over 90%[7].

Primary liver cancers are comprised of the five following types, in descending order of frequency:

- Hepatocellular Carcinoma (including fibrolamellar hepatocellular carcinoma) – cancer arising in epithelial compartments of the liver.
- Intrahepatic cholangiocarcinoma – cancer of the biliary epithelium
- Combined hepatocellular-cholangiocarcinoma – rare tumour with mixed histological characteristics of both hepatocellular carcinoma and cholangiocarcinoma
- Sarcoma (Angiosarcoma) – cancer arising from endothelial or connective tissues within the liver
- Hepatoblastoma – childhood cancer arising in epithelial compartments of the liver

1.3 Hepatocellular carcinoma

Hepatocellular carcinoma (HCC) is the most common form of primary liver cancer, accounting for 75% to 90% of cases. Intrahepatic cholangiocarcinoma (iCCA) comprises 10% to 15%, with the remaining ~5% comprised of sarcoma and mixed HCC/iCCA[6]. The cell-of-origin of HCC remains subject to debate and there is a degree of plasticity within hepatocytes and cholangiocytes that can give rise to hepatocellular carcinoma or cholangiocarcinoma from either cell population[8]. For the remainder of this thesis, I will focus on HCC.

In recent years, there have been large epidemiological shifts in the incidence of HCC, with increasing numbers of people in high-income countries affected by the disease, whereas incidence in developing countries is decreasing, in large part thanks to Hepatitis B immunisation programmes[9–11]. Despite decreasing incidence in middle- and low-income countries, deaths from HCC disproportionately affect people in middle-income countries (figure 1.1 and figure 1.2) and are expected to rise by 56.4% over the next 20 years[7].

1.4 Aetiology and risk factors for hepatocellular carcinoma

Most people with HCC develop it on the background of pre-existing chronic liver disease[8]. Cirrhosis is the major risk factor, with an annualised risk of between 0.5 and 5%[12–14]. The underlying aetiology driving chronic liver disease and cirrhosis varies globally, across both geography and income status[15].

In low-middle income settings and Asia-pacific regions, communicable diseases such as hepatitis B and C predominate, whereas in Europe and more developed settings, alcohol and non-alcoholic fatty liver disease are the major drivers. Worldwide, Mongolia has the highest rates of HCC and disability adjusted life years lost due to HCC (figure 1.1)[9, 16].

The main causes for chronic liver disease are:

1.4.1 Viral infection

Viral hepatitis, arising from infection with hepatitis B, hepatitis C and hepatitis D viruses, directly causes over 50% of HCC cases worldwide[11].

Hepatitis B virus (HBV) is a *Hepadnaviridae* DNA virus, spread through exposure to infected blood or bodily fluids[17]. Following exposure and initial infection, hepatitis B virus may be cleared, if not this results in chronic hepatitis B infection. Clearance improves with age and female sex, with neonates and males at the highest risk of chronic infection[18]. Treatment is with antivirals, with the aim of reducing the rate of viral replication and viral load[10]. Cure of chronic infection is not possible. The primary means of addressing the global burden of Hepatitis B is through prevention and immunisation. The first hepatitis B vaccine was approved in 1981 and there has been widespread roll-out of vaccination initiatives globally, with the World Health Organisation aiming to eradicate hepatitis B by 2030[7].

HBV causes liver inflammation as cytotoxic immune responses aim to eliminate infected cells, leading to chronic damage and subsequent progression to cirrhosis. HCC arises in 25% of people living with chronic hepatitis B and tumorigenesis is mediated by insertional mutagenesis[10, 12]. Elements of the HBV genome are found to be integrated in specific HCC driver loci, namely TERT promoter regions (up to 40% of people with HBV-HCC). Coinfection with hepatitis D virus (HDV) is strongly associated with HCC development, the mechanism underpinning the apparent synergy between HBV and HDV is currently unclear.

In contrast, Hepatitis C virus (HCV) is a *Flaviviridae* RNA virus, spread mainly through blood borne, iatrogenic or nosocomial routes[19]. The virus will infect around 80% of people

Figure 1.1: Disability adjusted life years lost per 100,000 population from the Global Burden of Disease study[9]. World maps are for all cause primary liver cancer, primary liver cancer due to Hepatitis B virus (HBV), primary liver cancer due to Hepatitis C virus (HCV), primary liver cancer due to non-alcoholic steatohepatitis (NASH) and primary liver cancer due to any other cause.

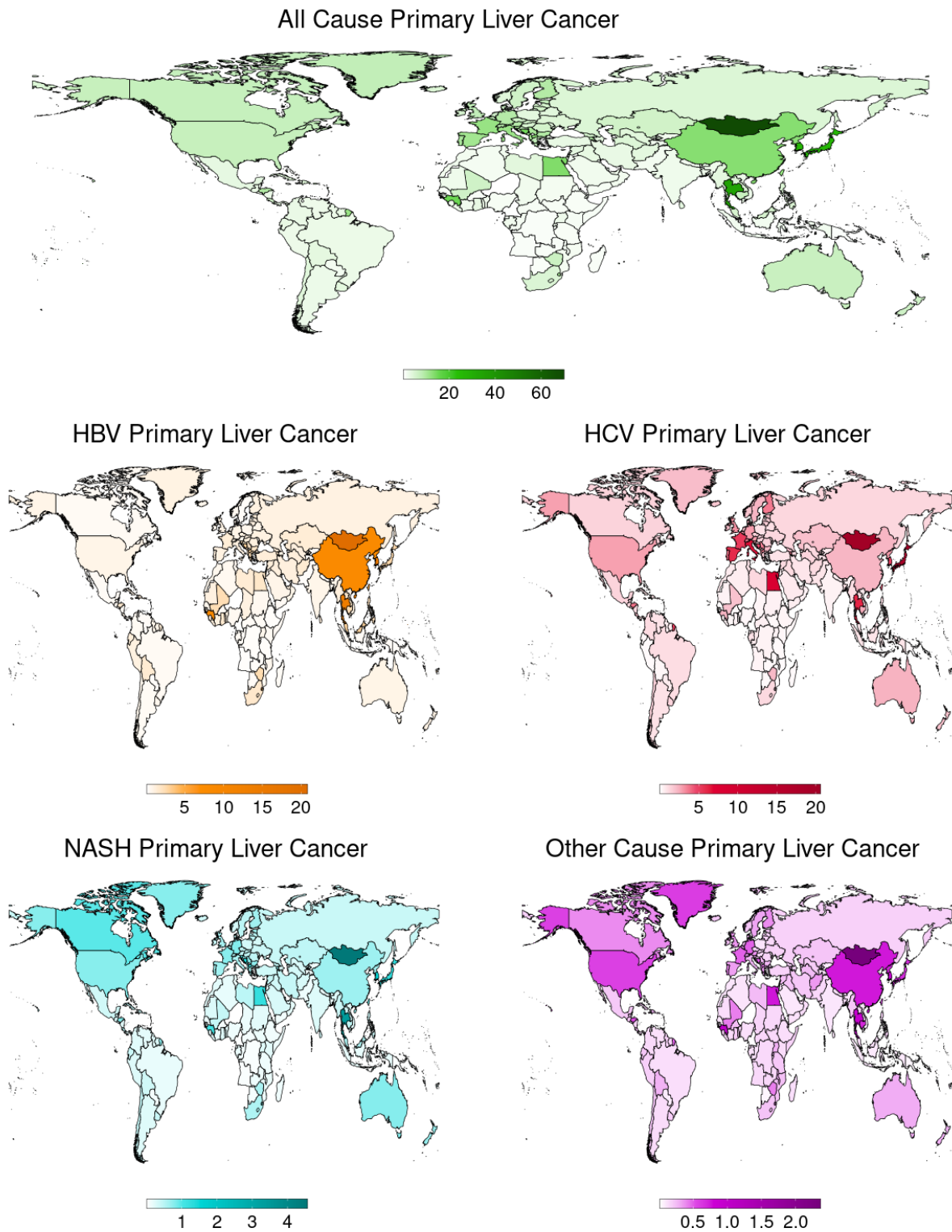
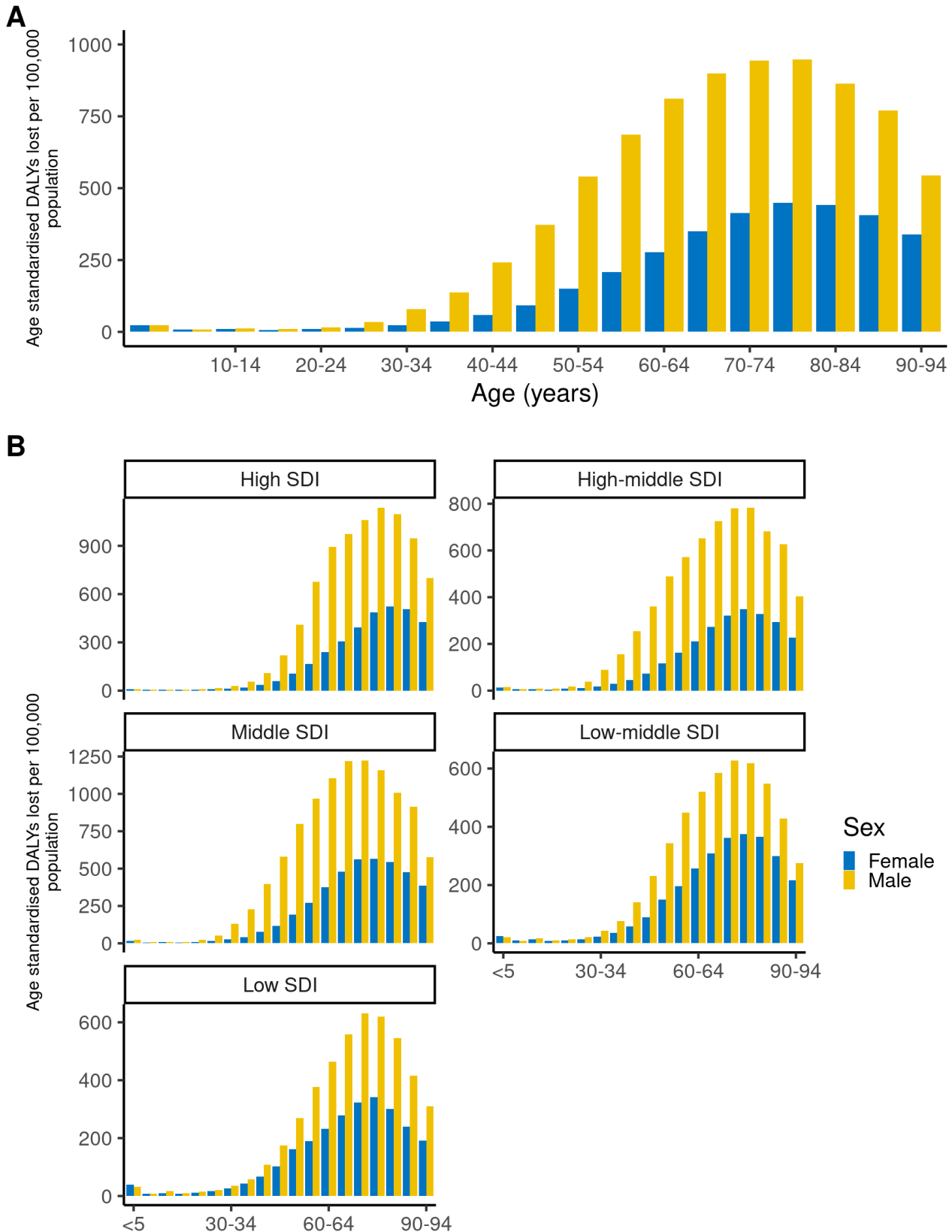


Figure 1.2: Disability adjusted life years lost per 100,000 population from the Global Burden of Disease study[9]. Panel A – DALYs lost to primary liver cancer by age group and sex, demonstrating a much higher male preponderance to HCC. Panel B – DALYs lost to primary liver cancer by age, sex and SDI setting, showing substantially higher burden of disease in middle SDI groups, with more females affected in lower SDI settings.



exposed but will spontaneously clear in majority of cases and not cause severe disease. Recent development of new direct-acting antivirals (DAA) now can provide cure of hepatitis C to almost all patients with minimal side effects and has been one the outstanding successes of modern medicine on a global level.

HCV causes liver inflammation and progression to cirrhosis as cytotoxic immune responses aim to eliminate infected cells, leading to fibrosis and scarring. The rate of HCC in HCV infected people is between 10 and 20%, with the risk significantly lower in those who achieve SVR. HCV promotes carcinogenesis mainly by the progression of chronic inflammation and cirrhosis, rather than mutagenic effects as HBV does. However, there is some evidence which implicates the interaction of HCV proteins with host tumour suppressor proteins (TP53, RB1, DDX3, DDX5), leading to increased cell proliferation and dysregulation of the cell-cycle[20–22].

1.4.2 Environmental carcinogens

Several environmental exposures have been associated with the development of HCC, both in epidemiological studies and in mutational signatures found in HCC tumours. These exposures include alcohol, acetaldehyde, cigarette smoke, aflatoxin, dimethyl sulphate and aristolochic acid amongst others[8, 23, 24].

1.4.2.1 Alcohol

Excess alcohol (ethanol) consumption is major risk factor for chronic liver disease and a major contributing factor to HCC across the world. The burden of alcohol-related HCC is primarily focused on high development countries and European regions[15, 23]. Consumption of excessive quantities of alcohol leads to hepatocyte damage through a diverse range of mechanisms, including production of reactive oxygen species (ROS) and toxic effects of downstream alcohol metabolism products. There are three main metabolic pathways the liver utilises to remove alcohol, the main alcohol dehydrogenase pathway, a secondary microsomal ethanol oxidizing system pathway (MEOS) through Cytochrome P450 2E1, and a tertiary catalase pathway[23, 25]. These pathways all directly or indirectly lead to ROS and NADH production, leading to depletion of intracellular ROS scavengers, damage to the mitochondria

and lipid peroxidation. The presence of damage caused by ROS in turn leads to hepatocyte death, which triggers the release of damage-associated molecular patterns (DAMPs) which trigger immune responses and subsequent hepatic inflammation. This process over time leads to persistent inflammation, fibrosis, scarring and eventual progression to cirrhosis.

In addition to causing liver disease through oxidative stress, the main product of all 3 alcohol metabolism pathways in the liver is acetaldehyde, a potent carcinogen. Acetaldehyde induces interstrand DNA crosslinks, and is subsequently repaired by one of two mechanisms, the Faconi Anaemia pathway or DNA polymerase REV1 replication fork convergence repair. Both are error prone and give rise to the unique CC>AA, CC>AG and CC>AT mutations found in acetaldehyde mutational signatures[21, 26]. Finally, susceptibility to alcoholic liver disease is also affected by NAFLD/NASH risk, and the two can share similar characteristics, including genetic determinants of risk such as PNPLA3, TM6SF2 and MBOAT7 mutation[27].

1.4.2.2 Smoking

Cigarette smoking is associated with around a 1.5-times increased risk for developing HCC[24, 28]. This risk is highest in those smoking more than 15 cigarettes per day. Within cigarette smoke, there are number of potentially mutagenic compounds which may promote HCC formation. The most notable being nitrosamine compounds, tar, vinyl chloride and 4-Aminobiphenyl. Cigarette smoking has multiplicative interactions with other causes of HCC, notably HBV and HCV, leading to substantially increased risk in people with additional risk factors[24]. DNA damage by various agents in cigarette smoke results in multiple C>A substitutions, with the presence of guanine adducts. Mutations in keeping with a cigarette smoking signature are found particularly frequently in the TP53 and TERT promoter regions, which are well-described HCC drivers[20, 21].

1.4.2.3 Aflatoxin

Aflatoxin B1 is a mycotoxin produced by *Aspergillus flavus* and *Aspergillus parasiticus*, which are common contaminants of numerous food sources including grains, peanuts, cottonseed meal and animal feed[29]. Both *A. Flavus* and *A. Parasiticus* thrive in warm, humid climates.

As a result, Aflatoxin contamination is highest in Asia-pacific, South American, and African regions of the world[29, 30]. Aflatoxin B1 is a potent carcinogen and forms covalent adducts on pyrimidine bases which leads to site specific G>T substitution[31]. These lesions are poorly repaired and often bypassed by DNA polymerases, leading to subsequent incorporation into the genome. One hot-spot site is codon 249 in the TP53 gene, where exposure to aflatoxin is found to frequently induct AGG>AGT substitutions, leading to gain-of-function of TP53. Unlike other cancers, the TP53^{R249S} mutation is the only TP53 hotspot mutation found in HCC[20]. Characterisation of R249S gain-of-function in mouse models and *in-vitro* suggests its action is complex and may exert tumorigenic effects through a wide range of pathways, including through c-Myc amplification and downstream signalling[32].

1.4.2.4 Other mutagens

Dimethyl sulphate (DMS) has recently been identified as a potentially causative agent following an exome sequencing study of HCC in Mongolia[16]. In this study, enrichment of T>G substitutions was identified, which was consistent with a DMS mutational signature. The DMS signature was found to be twice as common in HCC from Mongolian people, compared to other regions of the world. DMS is thought to be present in the environment from coal combustion by household stoves, which are widespread across Mongolia and are used for heating and cooking.

Geographic differences in the incidence of HCC can be further explained by aristolochic acid exposure. Aristolochic acids are mutagenic chemicals found in *Aristolochiaceae* plant species. Widely used in Chinese herbal medicine, for poorly understood reasons, exposure to these compounds leads to A>T mutations in similar genes which have been found to be most mutated in non-aristolochic acid exposed HCC. Aristolochic acid signatures are most prevalent in Taiwan (78% of cases), China (47% of cases) and southeast Asia (56%)[16, 22].

1.4.3 Non-alcoholic fatty liver disease

An increasingly prevalent cause of chronic liver disease, the proportion of HCC attributable to non-alcoholic fatty liver disease (NAFLD) has significantly increased, particularly in high

developed countries over the past 20 years[15, 33, 34].

Within the NAFLD umbrella, there are two disease subtypes; non-alcoholic fatty liver (NAFLD) and non-alcoholic steatohepatitis (NASH) which includes inflammation in addition to steatosis found in NAFLD[33]. Although there is a lower risk of progression to cirrhosis with NAFLD/NASH, up to 25% of NASH driven HCC cases occur in the absence of cirrhosis, therefore making it difficult to define a population at risk of NASH HCC[20]. NASH occurs frequently in combination with diabetes, obesity and metabolic syndrome. There is no specific treatment for NAFLD/NASH, other than lifestyle modification through weight loss, increased exercise and reducing dietary fat and calorie intake. Given males are more likely than females to develop diabetes, obesity and metabolic syndrome, this may also help explain the male preponderance to HCC[33].

There is a genetic contribution to NAFLD/NASH risk as well. Genome wide association studies have identified variants implicated in lipid metabolism and scavenging of reactive oxygen species which lead to a higher risk of developing NAFLD/NASH[27, 35]. Most notably the PNPLA3 I148 variant, which has been linked with higher risk of subsequent HCC development. The pathogenesis of NASH induced HCC is likely to be complex and at present is ill-defined. Dysregulation of lipid, protein and redox stress within the microenvironment are hypothesised to increase liver inflammation, leading to hepatocyte damage, fibrosis and scarring[33, 36]. Simultaneously, cytotoxic products from activation of the unfolded protein response (UPR), lipid peroxidation and mitochondrial sources of reactive oxygen species (ROS) drive hepatocyte damage.

The steatotic microenvironment also affects other cells within the liver milieu, with evidence that fatty acids and ROS lead to activation of NF- κ B in Kupffer cells, promoting expression of pro-inflammatory cytokines including TNF- α , CXCL1 and IL-8[37]. Other cells including neutrophils and T-cells (namely CD4+ cells) are found infiltrating areas of NASH, which also release chemotactic cytokines and ROS production in response to inflammation produced by lipotoxic hepatocyte death.

Interestingly, there seems to be no association between NAFLD/NASH and specific HCC driver mutations. In people with advanced HCC and preclinical models, the presence of NAFLD/NASH is associated with T-cell anergy and resistance to immune checkpoint inhibition, making this a key group of people with therapeutic resistance[38].

1.4.4 Other causes of liver disease

In addition to the more common aetiologies of liver disease discussed above, rarer causes include Autoimmune Hepatitis (AIH), cryptogenic liver disease (cirrhosis of an unknown cause), alpha-1-antitrypsin deficiency, haemochromatosis (disorder of iron transport, commonly caused by mutation in the HFE gene) and Wilson's disease (disorder of copper transport caused by mutation of ATP7B)[39–41]. People living with these disorders are at higher risk of developing cirrhosis and subsequent progression to HCC than comparable healthy populations.

Of these rarer causes, people with haemochromatosis are at the highest risk of developing HCC. Hereditary haemochromatosis is largely linked to northern European and Celtic ancestry, leading to a small geographic area where this is an important cause of HCC[39]. Humans lack the ability to excrete excess iron. Accumulation of iron is thought to arise due to mutations in iron transport channels and abnormal interactions with other key players in iron metabolism including the transferrin receptor and hepcidin. These abnormalities lead to an increase in the intestinal absorption of iron and increased intracellular iron generating ROS driving inflammation and DNA damage, can trigger ferroptosis (iron dependent mechanism of cell death) and deposition of haemosiderin in vital organs leading to further damage to a number of organs including the heart and those involved in the endocrine system[39]. Although the disease can be managed through routine venesection, the annualised risk of HCC is estimated to be around 1.2% in people with the disease and rises as cirrhosis develops[42]. This is in contrast with Wilson's disease, where HCC is rare if the disease is well controlled using the copper chelating agent D-penicillamine[40].

1.4.5 Additional risk factors

These causes of liver disease do not invariably result in HCC. Risk is increased when multiple aetiologies are underlying chronic liver disease, and risk of HCC may be further increased by other risk factors:

1.4.5.1 Age

Advancing age is the risk factor most strongly associated with HCC development (figure 1.2A), with most cases of HCC occurring in those aged 60 and over[8, 9]. Both chronic liver disease and HCC require time to develop and are likely sequential processes. Therefore, increased rates of HCC with age reflects both the increasing chances of cancer with age, but also the accumulation of HCC risk due to chronic liver disease. Early-age onset of HCC is more common in lower socio-demographic Index (SDI) settings (figure 1.2B), with greater DALYs lost, which may reflect the higher incidence of untreated viral hepatitis and lower access to healthcare.

1.4.5.2 Sex

There is a strong male preponderance to HCC, with around two to three times the incidence in males versus females[9]. Interestingly, this varies across different SDI settings, with females in lower SDI settings having a relatively higher risk of developing HCC compared with females in higher SDI settings. The mechanisms underpinning these sex-divergent risks are poorly understood and are likely to be multifactorial.

One suggestion to explain this observation is that males are more likely to engage in higher-risk behaviours[43]. Males are more likely than women to consume large amounts of alcohol and take recreational drugs, including injectable drugs. Females who live with substance misuse problems tend to use substances for a shorter period of time, with a lower intensity and are less likely to inject drugs.

In addition to risk-taking behaviours, females who are exposed liver disease causing agents and pathogens are less likely to develop chronic liver disease. In the case of hepatitis B and

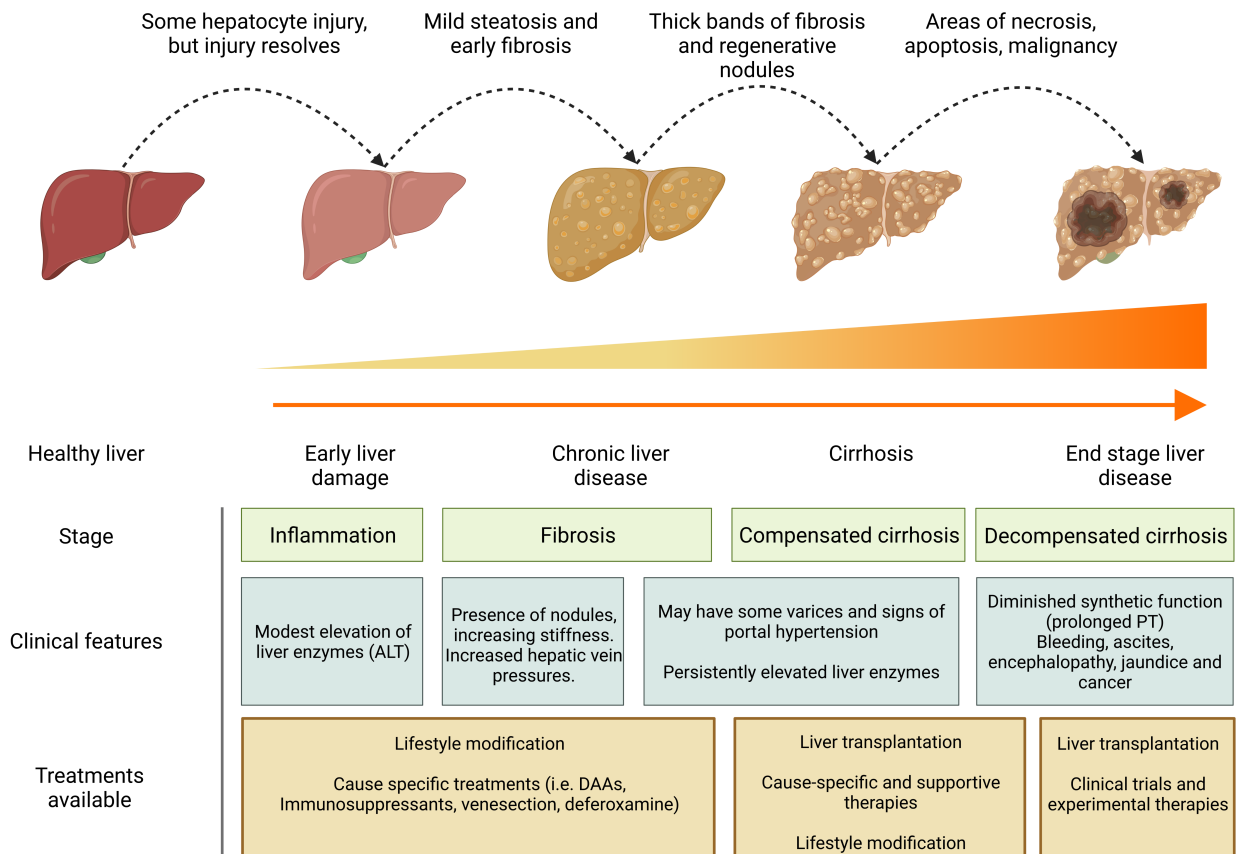
hepatitis C, females are more likely to clear viruses on exposure and therefore do not go on to develop cirrhosis. There are both liver-specific and immunological sexual dimorphisms which could explain this[18].

In the female liver, there are lower levels of IL-6 produced by Kupffer cells in response to injury and carcinogen exposure, whereas higher levels of IL-6 in males have been demonstrated to promote tumour formation[44]. Furthermore, the estrogen receptor alpha ($ER\alpha$), which is expressed more widely in females, has been shown to have repressive effects on viral mRNA transcription by limiting HNF4 α binding to replication and enhancer sites in the HBV genome[45]. Activity of oestrogen through the $ER\alpha$ has also been shown to down-regulate the Na⁺/Taurocholate Co-transporting Polypeptide (NTCP) cell surface protein, an essential means by which HBV internalisation occurs through high-affinity interactions of NTCP with the preS1 region of the large surface protein of HBV[46]. Furthermore, females are more likely to have stronger innate and humoral responses to infection compared with males[47]. Oestrogens are well-characterised as ‘immunostimulatory’ which could help clear HBV and HCV and may help explain why women have lower rates of risk-factors which predispose to both liver disease and HCC. However, there is a lack of evidence around whether sex-divergencies in immunity could contribute to the clearance of early-stage cancer cells and a lack of clear evidence around the impact of sex on efficacy of cancer immunotherapies.

1.4.5.3 Cirrhosis

Progression of chronic liver disease to cirrhosis and subsequent end-stage liver disease is driven by sustained inflammation and hepatocyte injury (figure 1.3). Although the mechanisms underpinning sources of damage and inflammation vary, most causes of liver disease will cause progression to cirrhosis if untreated.

Figure 1.3: Progression of liver disease from healthy liver to end-stage liver disease.



Hepatic inflammation is triggered in response to hepatocyte death caused by metabolic disturbances and ROS generated by alcohol or high levels of fat, or immunological injury in response to viral infection[23, 48, 49]. As hepatocytes die they release gut and liver derived pathogen-associated molecular patterns (PAMPs) from immune cells in the liver and damage-associated molecular patterns (DAMPs) further exacerbating levels of inflammation and injury. In addition to this, in many causes of chronic liver disease, particularly in alcoholic liver disease and non-alcoholic fatty liver disease, gut flora may favour the generation of pro-inflammatory PAMP molecules, further worsening inflammation. These PAMP/DAMPs are recognised by sets of Toll-like receptors (TLRs) and NOD-like receptors (NLRs) expressed on both immune and liver cells. This then initiates the production of pro-inflammatory cytokines and an influx of cytotoxic and ROS generating immune cells, which serve to initiate repair and wound healing, but may also further exacerbate inflammatory injury.

Cirrhosis is scarring and fibrosis of the liver caused by long-term chronic liver disease. Repeat cycles of wound healing in response to sustained injury, leads to increasing amounts of collagen and subsequent fibrosis[23, 48, 49]. Furthermore, ROS and continued exposure to injury can stimulate other liver cells, including stellate cells, to release pro-fibrogenic signalling molecules, leading to greater levels of collagen deposition and scar tissue. When the liver reaches a critical mass of fibrous tissue, the elasticity of the liver is lost and vessels within the liver parenchyma become strictured, giving rise to portal hypertension. Throughout this period extensive remodelling of the liver and repeated attempts at wound healing lead to the progression of fibrosis and nodular appearance of the liver as fibrotic bands surround remaining clusters of functional hepatocytes. With persistent and severe injury, normal hepatocyte capacity to repair and regenerate is impaired due to incessant damage and subsequent growth arrest. In response to this, reserve progenitor cells from the biliary tree are activated to support regeneration in a process known as ductular reaction. These diverse repair and healing processes give rise to a wide variety of different stressors and a diverse, highly inflamed microenvironment. This microenvironment also exerts high selective pressure for genetic mutations or epigenetic alterations that can allow cells to survive these stresses and the presence of mutations can be both detrimental in initiating HCC, but also beneficial in promoting cell fitness[50].

As this process continues, there reaches a point where the liver can no longer adequately provide the synthetic or detoxifying functions for the body. At this point extra hepatic manifestations occur, including ascites (accumulation of fluid within the abdominal cavity resulting from low albumin production and salt retention), encephalopathy (cerebral dysfunction resulting from a complex multifactorial process, including the accumulation of ammonia), synthetic liver dysfunction (impaired protein synthesis) and portal hypertension[23, 49]. Cirrhosis is potentially reversible but most patients are unable to achieve this due to persistent disease. The only curative therapy for liver failure in cirrhosis is liver transplantation[51].

This severe liver dysfunction, which often co-occurs in patients with HCC, can make

administering effective anti-cancer therapy challenging and many patients are very frail with their extensive liver disease. Unlike other cancer types where death is caused by metastases or invasion of other structures, HCC patients are far more likely to die of liver failure[8].

1.4.5.4 Protective factors

Drinking coffee and taking low-dose aspirin have been proposed to reduce the chance of developing HCC in people with chronic liver disease. Both interventions have been found to be associated with a reduced cumulative incidence of HCC in observational cohort studies [52, 53]. These observational studies propose that both agents have anti-inflammatory properties and slow the progression of liver disease. However, neither agent has been tested in large-scale randomised clinical trials and there are unanswered questions about residual confounding. For example, people who drink coffee are more likely to come higher income socioeconomic groups and have markedly different healthcare outcomes compared with lower groups[54]. Similarly, these studies are likely to be at a high-risk of selection bias, as people with severe liver disease are unlikely to take aspirin due to perceived bleeding risk and are likely to develop HCC or die before those with milder disease who do take aspirin.

1.5 Clinical management

1.5.1 Diagnosis and surveillance

As people who develop HCC almost invariably have pre-existing chronic liver disease, there is a clear at-risk population. Therefore, in people living with chronic liver disease, routine screening (termed ‘surveillance’) for liver cancer is recommended in clinical practice guidelines. In people living with chronic liver disease, the annual incidence rate of malignant transformation to HCC is quoted at between 0.5 to 1.0% but in some populations is as high as 5%[12–14].

Surveillance in people living with chronic liver disease consists of 6 to 12 monthly ultrasonography of the liver, with serum alpha-fetoprotein (AFP) testing[55]. For people with long-term health conditions, such surveillance programmes can present a large burden on the

individual with chronic liver disease and as a result, non-adherence rates are high. Furthermore, the effectiveness of surveillance is hampered by the low sensitivity of ultrasonography and serum AFP measurement. In people with a high body mass index, visualisation of the liver parenchyma can be technically challenging, thus further limiting its diagnostic utility. Use of surveillance has been found to not improve HCC-related mortality and consequently many people with chronic liver disease present with intermediate-advanced or terminal stage disease[56, 57].

Diagnosis of HCC is made primarily through cross-sectional imaging using either contrast-enhanced computed tomography (CT), or magnetic resonance imaging (MRI)[6, 8]. On CT, HCC is seen as an enhancing lesion in the arterial phase, followed by rapid washout and subsequent hypoattenuation in the portal venous phase. MRI is useful in early disease and in the context of liver cirrhosis for distinguishing small HCC from dysplastic or regenerative nodules. On MRI, HCC is also seen as a lesion with arterial enhancement with rapid washout following gadolinium contrast administration. Arterial enhancement is observed across both modalities as HCC tumours derive their main blood supply from the hepatic artery rather than the portal vein. Given these distinct diagnostic features, HCC can be diagnosed to a high level of accuracy and specificity on imaging alone in the cirrhotic liver.

The Liver Imaging Reporting and Data System (LI-RADS) standardises the diagnosis and classification of HCC on cross sectional imaging, and aims to decrease the variability of diagnosis in people with chronic liver disease and communicate levels of risk clearly to clinicians[58]. Levels LR-1 and LR-2 indicate benign disease, whereas LR-3 describes intermediate risk lesions, LR-4 probable HCC and LR-5 definite HCC. Using this criteria, LR-3 lesions are typically managed through repeat imaging and LR-4 lesions can be biopsied for histological confirmation.

1.5.2 Classification, staging and treatment

Hepatocellular carcinoma is staged according to both the unified TNM and Barcelona Clinic Liver Cancer (BCLC) systems. The Union for International Cancer Control (UICC) and American Joint Committee on Cancer (AJCC) TNM 8th Edition classifies HCC according to

tumour size, nodal and metastatic spread[59].

Table 1.1: TNM staging of HCC

Tumour stage (T)		Nodal stage (N)		Metastasis stage (M)	
TX	Primary tumour cannot be assessed	NX	Regional lymph nodes cannot be assessed	M0	No distant metastasis
T0	No evidence of primary tumour	N0	No regional lymph node metastasis	M1	Distant metastasis
T1a	Solitary tumour 2 cm or less in greatest dimension with or without vascular invasion	pN0	Histological examination of a regional lymphadenectomy specimen will ordinarily include 3 or more lymph nodes If the lymph nodes are negative, but the number ordinarily examined is not met, classify as pN0		
T1b	Solitary tumour more than 2 cm in greatest dimension without vascular invasion	N1	Regional lymph node metastasis		
T2	Solitary tumour with vascular invasion more than 2 cm dimension or multiple tumours, none more than 5 cm in greatest dimension				
T3	Multiple tumours any more than 5 cm in greatest dimension				
T4	Tumour(s) involving a major branch of the portal or hepatic vein or with direct invasion of adjacent organs (including the diaphragm), other than the gallbladder or with perforation of visceral peritoneum				

The Barcelona Clinic system supplements this by incorporating measures of liver disease and functional status using the Child-Turcotte-Pugh score alongside performance status[60]. By incorporating these, the BCLC system helps to guide the use of therapies suitable for people with concurrent liver disease and identify groups where curative therapies such as resection and transplant would be most effective (and least harmful).

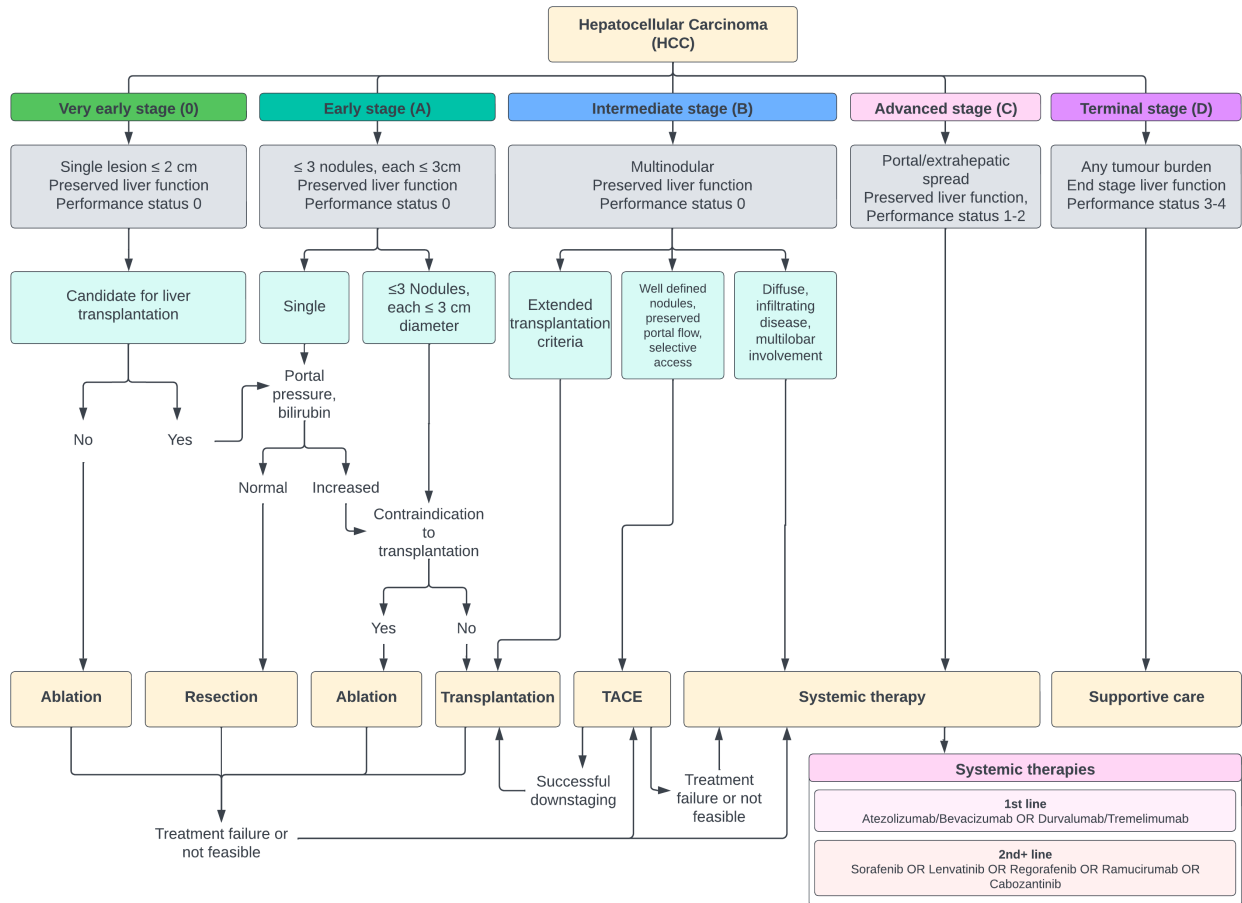
Both systems use similar descriptions of HCC disease characteristics (table 1.1 TNM, figure 1.4 BCLC). The regional lymph node drainage of the liver includes the hilar, hepatic, periportal, inferior phrenic and caval groups.

Within these criteria, downstaging to curative surgery is possible using transarterial chemoembolization and ablative therapies, so long as disease is confined to the liver, liver function is preserved, and performance status is good. Most people with HCC present with intermediate-advanced or terminal stage disease, where transarterial chemoembolization (TACE), systemic therapy and supportive care are the only options.

Transarterial chemoembolization (TACE) delivers chemotherapy directly to tumours in the liver and surrounding tissue in a locoregional manner via a radiologically guided arterial catheter. Chemotherapy is typically doxorubicin mixed with the contrast agent Lipiodol or

delivering using drug eluting microspheres which get trapped in the tumour vasculature, slowly releasing drug and occluding vessels leading to tumour hypoxia.

Figure 1.4: Barcelona Clinic Liver Cancer staging system. This takes into account multiple factors including background liver disease and performance status in addition to tumour stage. This shows there are many different therapy options for HCC, which increases with further lines of therapy.



1.5.3 Systemic therapy

The mainstay of systemic therapy for HCC over the past decade has been with tyrosine kinase inhibition. In 2008 the placebo-controlled, phase 3 SHARP trial found Sorafenib modestly improved survival of patients with previously untreated advanced HCC (median overall survival Sorafenib 10.7 months versus 7.9 months in placebo, HR 0.69 95% CI 0.55 to 0.87)[41]. Sorafenib subsequently became the standard of care for patients with advanced disease who could tolerate systemic therapy. In 2017, the RESOURCE trial found that for people with HCC who progressed on Sorafenib therapy, sequential treatment with the VEGFR2-TIE2 tyrosine kinase inhibitor Regorafenib extended survival for a further 10.6

months versus 7.8 months for those on placebo (HR 0.63 95% CI 0.50 to 0.79), thereby establishing Regorafenib as a second-line therapy option[61].

Randomised evidence for additional first- and second-line systemic therapy options was published in 2018. The REFLECT trial, a randomised phase 3 non-inferiority trial comparing Sorafenib with Lenvatinib, a multi-VEGFR tyrosine kinase inhibitor, demonstrated non-inferiority of first line Lenvatinib (median overall survival Lenvatinib 13.6 months versus 12.3 months with Sorafenib, HR 0.92 95% CI 0.79 to 1.06)[62]. Cabozantinib was also identified as a viable second-line therapy in people who had progressed on Sorafenib following the randomised phase 3 placebo-controlled CELESTIAL trial (median overall survival cabozantinib 10.2 months versus 8.0 months in placebo, HR 0.76 95% CI 0.63 to 0.92)[63].

Despite these clinical trials identifying therapies which can improve overall survival in advanced HCC, tyrosine kinase inhibition does not produce long-term durable responses and is not a potent cytotoxic therapy which can be used to effectively downstage disease.

1.5.3.1 Immune checkpoint therapy for HCC

Immune checkpoint inhibitors target immune checkpoints, which are cell-surface molecules that provide co-inhibitory signals to immune cells which limit cytotoxic response (figure 1.6). There are a wide range of known immune checkpoints, and cancer cells express these molecules to promote evasion from the immune system. These therapies most frequently target the inhibitory PD-1/PD-L1 or CTLA-4 immune checkpoints and were initially discovered using mouse models. Since their discovery, these therapies have been successfully translated, transforming the treatment of many solid tumour types, with markedly improved response rates and even durable control. Expression of these immune checkpoints has been demonstrated in people with HCC and preclinical studies have demonstrated efficacy of immune checkpoint inhibition *in-vivo*[60, 64].

The first reported study of immune checkpoint inhibition in HCC was the CheckMate 040 trial. CheckMate 040 was an open-label, non-comparative, phase 1/2 dose escalation study of the PD-1 immune checkpoint inhibitor Nivolumab in people with HCC with Child Pugh

A liver disease[65]. CheckMate 040 showed Nivolumab had an acceptable toxicity profile in this study population, with objective response rates of around 20%, thus paving the way for further trials of immune checkpoint inhibitors in HCC. Later evolution of the CheckMate 040 trial tested the addition of the CTLA-4 checkpoint inhibitor Ipilimumab to Nivolumab, again using a non-comparative design. This combination of Ipilimumab and Nivolumab was shown to have a manageable toxicity profile, thus opening-up dual checkpoint inhibition as a second-line therapy[60].

Following the initial CheckMate 040 study, the phase 2 KEYNOTE-224 study also demonstrated manageable toxicity of the PD-1 inhibitor Pembrolizumab[66]. The first phase 3 randomised trial of anti-PD-1 therapy in HCC was KEYNOTE-240[67]. In this trial, people with HCC who had previously received Sorafenib were randomised to receive Pembrolizumab or placebo. Although KEYNOTE-240 did not meet its prespecified one-sided endpoints, Pembrolizumab monotherapy demonstrated promising signs of efficacy toward modestly improved overall survival. The CheckMate 459 trial later published similar data, showing little difference in response rates with Nivolumab monotherapy compared to Sorafenib alone[68].

In 2020, the IMBrave150 trial, which combined Bevacizumab with Atezolizumab was the first phase 3 randomised controlled trial (RCT) to show superiority of PD-L1 immune checkpoint therapy over Sorafenib in the first line setting (HR 0.58, 95% CI 0.42 to 0.79)[69]. Shortly after this trial, the HIMALAYA trial, showed superiority of the PD-L1 inhibitor Durvalumab in combination with Tremelimumab, compared to Sorafenib alone in the first line setting (HR 0.78, 95%CI 0.65 to 0.93). This trial also showed the non-inferiority of Durvalumab monotherapy to Sorafenib in line with the KEYNOTE-240 and CheckMate 459 studies (HR 0.86, 0.73 to 1.03, noninferiority prespecified HR 1.08)[70]. Taken together, these trials demonstrate that unlike some solid tumours in other organs, immune checkpoint inhibition in HCC shows promise, but is not a radical game-changer as has been the case for melanoma and lung cancer. Addition of other agents, such as anti-VEGF therapy and combination immune checkpoint blockade is required for benefit over tyrosine kinase inhibitor

monotherapy.

Immune checkpoint inhibitor therapy, both alone and in combination with other agents, can be associated with substantial immune-mediated toxicities. Common side-effects include skin rashes, colitis, myocarditis, hepatitis, thyroiditis, and adrenal insufficiency[63, 65, 66, 69, 70]. These toxicities are mostly manageable with supportive measures, including glucocorticoid administration, immunosuppression and use of monoclonal antibodies such as infliximab[71]. Treatment with dual immune checkpoint inhibitor therapy raises risks of these immune-mediated toxicities further. Similarly, combination therapy with other agents such as Bevacizumab exposes patients to elevated risks of side effects including hypertension and stroke. In the HCC population where many patients are frail or have diminished liver function, these side-effects can lead to significant treatment harms and deciding on a suitable therapy needs to be tailored to each patient.

Based on these findings, the first line systemic therapy at the time of writing is combination therapy with either Atezolizumab and Bevacizumab, or the Durvalumab and Tremelimumab. For those who fail to respond to first line therapy, or who cannot tolerate immune checkpoint inhibitor therapy, tyrosine kinase inhibition with Sorafenib, Lenvatinib, Regorafenib or Cabozantinib is the next choice, immune checkpoint inhibitor monotherapy can be considered here if tyrosine kinase inhibition is contraindicated. In those with an alpha fetoprotein level of >400 ng/ml, ramucirumab may also be a valid second line option, in line with findings from the REACH-2 trial. Subsequent options after multiple lines of therapy include clinical trials or best supportive care, which aims to best manage symptoms and maximise quality of life[8, 60].

Immune checkpoint inhibition is currently under investigation for a broader range of applications within HCC, including in the neoadjuvant setting with the objective of reducing recurrence rates following resection, and with Nivolumab in combination with TACE. Initial reports from phase 2 trials of neoadjuvant anti-PD1 appear to show it is feasible, but with most (98.2%) participants reporting some form of adverse event over the treatment period[72].

1.6 Biology of hepatocellular carcinoma

The advent of high-throughput, untargeted molecular profiling technologies has allowed the study of cancer in unprecedented detail. By combining results from multiple profiling technologies using statistical techniques, it is possible to classify tumours according to their molecular features and interrogate how specific genetic drivers are associated with changes across multiple biological levels (e.g. epigenome, transcriptome, proteome, metabolome).

Several large initiatives, including The Cancer Genome Atlas (TCGA)[20] and the International Cancer Genome Consortium (ICGC)[21] have sought to generate molecular subclassifications of different tumour types, which has transformed how cancer therapies are developed. These subclassifications are useful for both clinical practice to underpin more personalised approaches and for research, to help guide molecularly targeted agents and develop preclinical model systems that more accurately recapitulate human disease. Clinically, molecular subclassifications are increasingly being incorporated to guide more personalised, subtype specific cancer therapy. An example of this is colorectal cancer, where MMR deficient disease responds nearly completely to anti-PD1 therapy, thus preventing the necessity for surgery in this subgroup of patients[73].

Although molecular classification studies have been performed in people with HCC, there currently are no randomised trials which have integrated molecular testing widely within their designs. Nor any molecularly targeted agents used for specific vulnerabilities. However, molecular subclassifications can still be retrospectively applied to clinical trial and observational treatment data to explore treatment resistance[74]. Furthermore, by using HCC molecular subclassifications, preclinical model systems can be developed to phenocopy human disease by incorporating the same genetic alterations and amplifications. Using this approach, treatments can be developed in a range of immunocompetent disease subtypes *in-vivo* and mechanisms of likely resistance identified in the preclinical development phase[75].

1.6.1 Molecular subclassification of HCC

Several studies have used exome or whole-genome sequencing of tumours to identify somatic alterations that are likely drivers of HCC. However, many of these were descriptive and summarised the frequency of alterations, rather than using dimensionality reduction to infer useful subclasses or combining with multiomic data sources. All these studies have selection bias towards patients with early disease, where tissue can be easily obtained following liver transplantation or resection[20, 21, 76–78].

The first integrative analysis of HCC molecular profiling data was published in 2009, where *Hoshida et al.*, profiled gene expression in 603 patients using microarrays and performed subclass mapping using hierarchical clustering, k-means clustering and non-negative matrix factorisation[78]. In this study, 3 major HCC subclasses were identified – Hoshida S1, Hoshida S2 and Hoshida S3. Hoshida S2 was the most common class, characterised by MYC and AKT activation, with inactivation of TP53.

Hoshida S1 was next most common, and had aberrant activation of the canonical WNT signalling pathway and the highest risk of recurrence after one year. Hoshida S3 was also found to have mutations in CTNNB1, but had a different phenotype to S1 tumours and tended to be more well-differentiated than both S1 and S2, suggesting a more nuanced role for CTNNB1 mutations.

In 2017, the Cancer Genome Atlas published an integrated analysis of 363 HCC tumours, using a range of platforms to profile whole-exome, copy number alteration, DNA methylation, RNA, micro RNA and proteomic Reverse Phase Protein Array (RPPA) data[20]. Joint multivariate regression was used to simultaneously cluster data from all platforms together to produce 3 integrated iClusters. The first cluster was associated with higher tumour grades, and specific alteration of microRNAs responsible for lipid metabolism including high expression of miR-181a and silencing of miR-122. iCluster 2 and 3 had high frequency of CDKN2A silencing by DNA hypermethylation, frequent TERT promoter mutation and CTNNB1 mutation. iCluster 3, compared with iCluster 2 had higher levels of chromosomal

instability, frequent TP53 mutation and hypomethylation of CpG islands. These iClusters were found to associate with prognosis in cohorts of HCC patients, with iCluster 1 patients having the worst long-term prognosis, although it is unclear if staging and other confounding factors were accounted for.

Whilst these molecular classifications distinguish groups of HCC within in the research setting, they have not been able to predict responses to therapy for any of the treatment modalities currently used in this disease and are not routinely used clinically.

1.6.2 Tumour microenvironment

The tumour microenvironment (TME) is a complex milieu of multiple different cell types and conditions which have developed to supply and support cancer cells. *Weinberg and Hanahan* describe eight hallmarks of cancer; sustained proliferative signalling, evasion of growth suppressors, resisting cell death, replicative immortality, angiogenesis, evasion, reprogramming of energy metabolism, evading immune destruction, and invasion and metastasis[79]. The tumour microenvironment supports cancer cells throughout development and progression, promoting many of these hallmarks.

Cancer cells have markedly different metabolic requirements from normal cells, due to a high rate of nutrient utilisation and high rates of glycolysis. Tumour cells and supporting cells in the TME secrete growth factors and vascular mediators to recruit new blood vessels to help meet these increased requirements[79–81]. These new blood vessels have major functional and structural inadequacies, preventing adequate tissue perfusion and resulting in a hypoxic, hypoglycaemic and theoretically acidotic TME, which in turn has implications for the correct function of cells not adapted to these conditions.

The TME alters profoundly over the course of tumour development and its composition is dictated in a large part by the genetic drivers present in cancer cells. These genetic drivers coordinate direct cell-cell interactions, paracrine and endocrine signals that cancer cells utilise to recruit or exclude specific cell-types to the TME or their proliferation within it, to support and sustain further growth and survival. In HCC, this can include both recruited cells from

the systemic circulation (lymphocytes, monocytes, macrophages, neutrophils, natural killer cells, myeloid derived suppressor cells [MDSCs]) and liver resident cells (hepatic stellate cells [HSCs], Kupffer cells, fibroblasts, endothelial cells, liver sinusoidal endothelial cells [LSECs])[64, 82]. Immune cells found within the TME can play a diverse range of roles, including anti-tumour, pro-tumour and mixed roles. Many of these cell lineages are unique to the liver, behave differently to similar lineage cells in other tumours, and express molecules which are known to dampen anti-cancer immunity. Furthermore, these unique liver resident populations are poorly characterised in the context of HCC, so may have a profound and liver-specific effect on shaping the TME[8].

1.6.3 Immune surveillance and anti-tumour immunity

Successful immune evasion is a key hallmark of cancer, and one which is essential for tumour cell survival[83]. This is particularly important given many mutations in genetic drivers and passenger mutations in the cancer genome can produce neoantigens that are likely to induce anti-tumour immune responses. The exact mechanisms behind cancer immunosurveillance are debated and knowledge continues to rapidly evolve. The general model for cancer immunosurveillance is that patrolling antigen presenting cells monitor cellular compartment to identify cancer cells which are presenting new, ‘non-self’ antigens and initiate cytotoxic responses to eliminate these cells. In the context of T-cell mediated cytotoxicity, APCs will identify new ‘non-self’ antigens and provide resting lymphocytes with two activation signals, the first being the tumour antigen and the second through CD28. Without this second signal through CD28, T-cell anergy occurs. Some NK subsets may also recognise very low levels of MHC class I molecule expression, known as ‘missing-self’, resulting in a cytotoxic immune response against cells which fail to express adequate levels of MHC class I, although evidence for this occurring in tumours *in-vivo* is currently lacking[84].

This general concept of immunosurveillance is supported by empirical evidence that immunodeficient preclinical models and patients on immunosuppressive therapies are predisposed to cancer versus immunocompetent comparators[85].

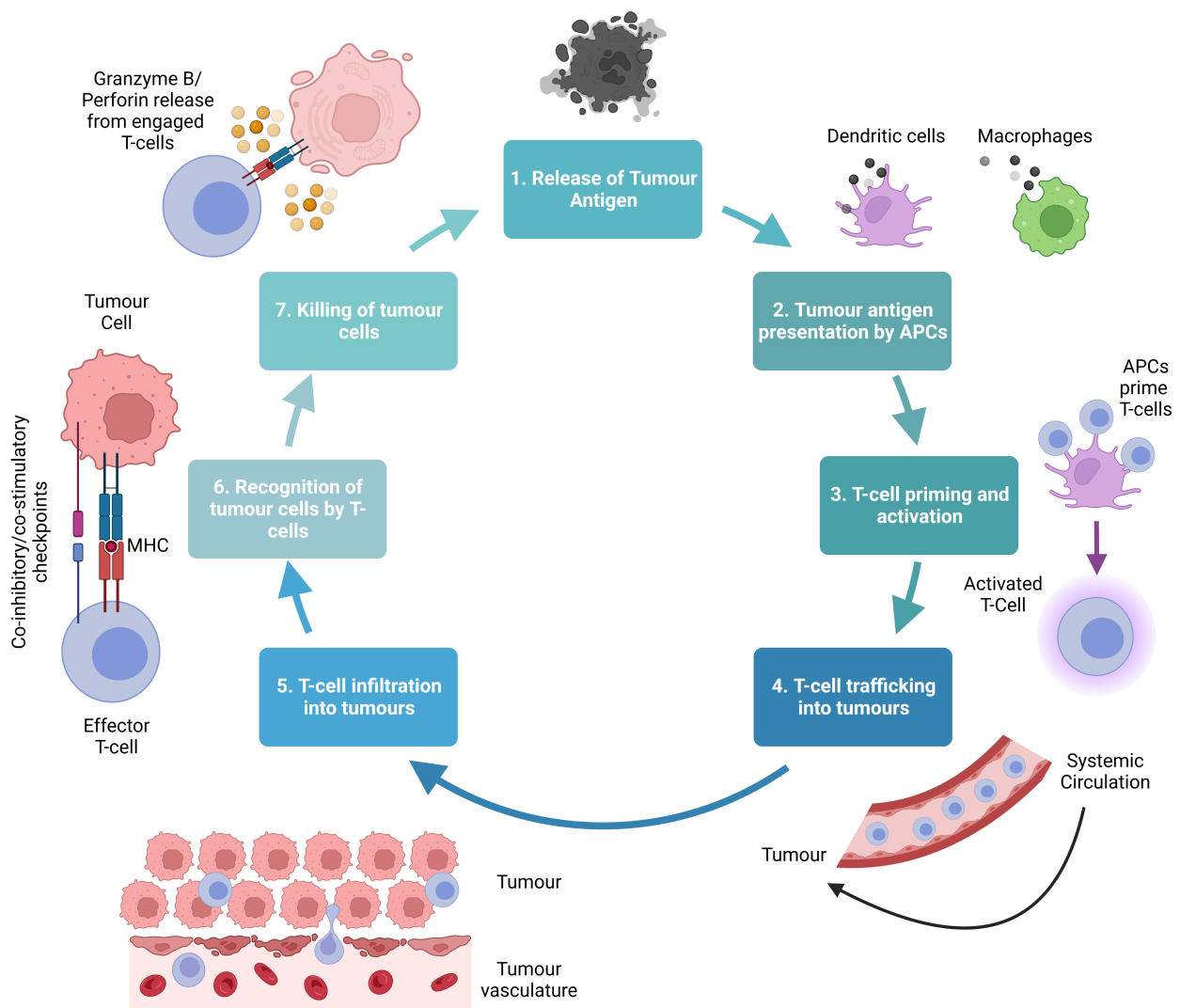
Immunosurveillance becomes progressively more difficult as tumours become more advanced and acquire increased ability to evade immune detection[86]. For tumour cell killing to occur in multicellular tumours, tumour antigen must be released and subsequently presented to antigen presenting cells (APCs, figure 1.5). These APCs then prime effector T-cells with the target antigen and activate them. T-cells then need to travel to the tumour site (trafficking) and infiltrate these tumours through often abnormal tumour endothelium. Once in the antigen restricted effector cells then engage tumour cells expressing the target antigen. This results in cytotoxicity, cell death and release of further quantities of tumour antigen.

1.6.4 Evasion of anti-tumour immunity and resistance to immunotherapy

Tumour cells can evade detection by the immune system in a variety of ways. First, they can down-regulate MHC class I expression or suppress pathways that result in generation of neoantigens, thereby reducing the levels of new ‘non-self’ antigens presented[83]. Second, cancer cells can induce the expression of inhibitory cell-surface molecules (including immune checkpoints) that limit effector cell activation and subsequently prevent elimination by the immune system. This can be in a cancer cell intrinsic manner, or through co-opting other cells in the TME (i.e. macrophages) to express these inhibitory molecules, thus favouring tolerogenic immune responses[8, 79, 86, 87]. Third, cancer cells exert control over cytokine and chemokine expression within the TME. This can be through a variety of mechanisms including suppressing DNA damage responses, or adaptation to cope with high levels of cell stress which may otherwise trigger the expression of cytokines and chemokines to attract cytotoxic immune cells[79, 88]. Again, this can be done in a cell intrinsic or extrinsic manner. In addition to controlling cell trafficking and infiltration of immune cells into tumours, cytokines may also dictate whether antigen processing and recognition is likely to result in tolerance or promote anti-tumour immunity.

These processes can occur at early and late stages of tumour evolution. The pressure of immune surveillance favours the selection of non-immunogenic tumour cell clones, leading to the outgrowth of clones with low neoantigen burdens. Throughout development and acquisition of additional driver mutations, this immunoselection (termed immunoediting) favours cells which can acquire mutations that enhance immune evasion[83]. As tumours become advanced, the TME plays an increasing role in shaping immune responses and can lead to the selection of cancer cells which can actively suppress immune responses in an antigen independent manner, known as immunosubversion. This can happen in numerous ways, including through production of immune mediators which limit antigen presenting cell (APC) and effector cell function, for example through the production of nitric oxide, ammonia species, lactate and depletion of essential metabolites required to support anti-tumour immune responses (i.e. depletion of

Figure 1.5: Cancer immunity cycle. This shows the steps required to mount a successful anti-tumour immune response. Cancer cells may disrupt this process in one or more places, leading to immune evasion or resistance to immune checkpoint therapies.



arginine through arginase-1 and production of urea)[80].

Cell-killing mediated by cytotoxic CD8+ T-cells is one of the key means of mounting anti-tumour immune responses. Although other cell-types contribute toward anti-tumour immunity, the CD8+ cytotoxic response is the best characterised and T-cells are key targets of immune checkpoint inhibitors. Therefore, characterising this response and the infiltration of T-cells into tumours will be a key focus of my thesis.

Immune checkpoints have received significant attention as therapeutic targets over the past decade. Humanised monoclonal antibodies are now widely used against the PD-1, PD-L1 and CTLA-4 co-inhibitory immune checkpoints and have notable therapeutic success (figure 1.6)[65, 67, 69, 70, 73]. Immune checkpoint inhibition disrupts both upon tumour-immune cell interactions but also APC-T-cell interactions, preventing co-inhibitory signals from immune checkpoints, thus attenuating anergic signals[89]. This skews anti-tumour effector cells to an activated phenotype which can then engage and kill tumour cells. In health, co-inhibitory checkpoints are crucial for self-tolerance and preventing autoimmunity, which gives rise to the immune mediated toxicities common whilst patients are receiving immune checkpoint therapies. Many of the ligands of immune checkpoints are yet to be discovered or fully characterised and thus this is a rapidly moving field.

There are also stimulatory immune checkpoints including OX-40, CD27, CD137, ICOS, GITR, CD40/CD154 and CD28[89]. Tumour cells may use immune checkpoints to evade the immune system through either upregulation of co-inhibitory checkpoints, suppression of co-stimulatory checkpoints or a combination of the two. A clinical trial of a CD28 super agonist TGN1412 has been attempted, ending in hospitalisation of six volunteers in a phase I study at Northwick Park Hospital, highlighting the issues around selectively activating T-cells to engage cancer cells[90].

1.6.5 Factors influencing immunotherapy response

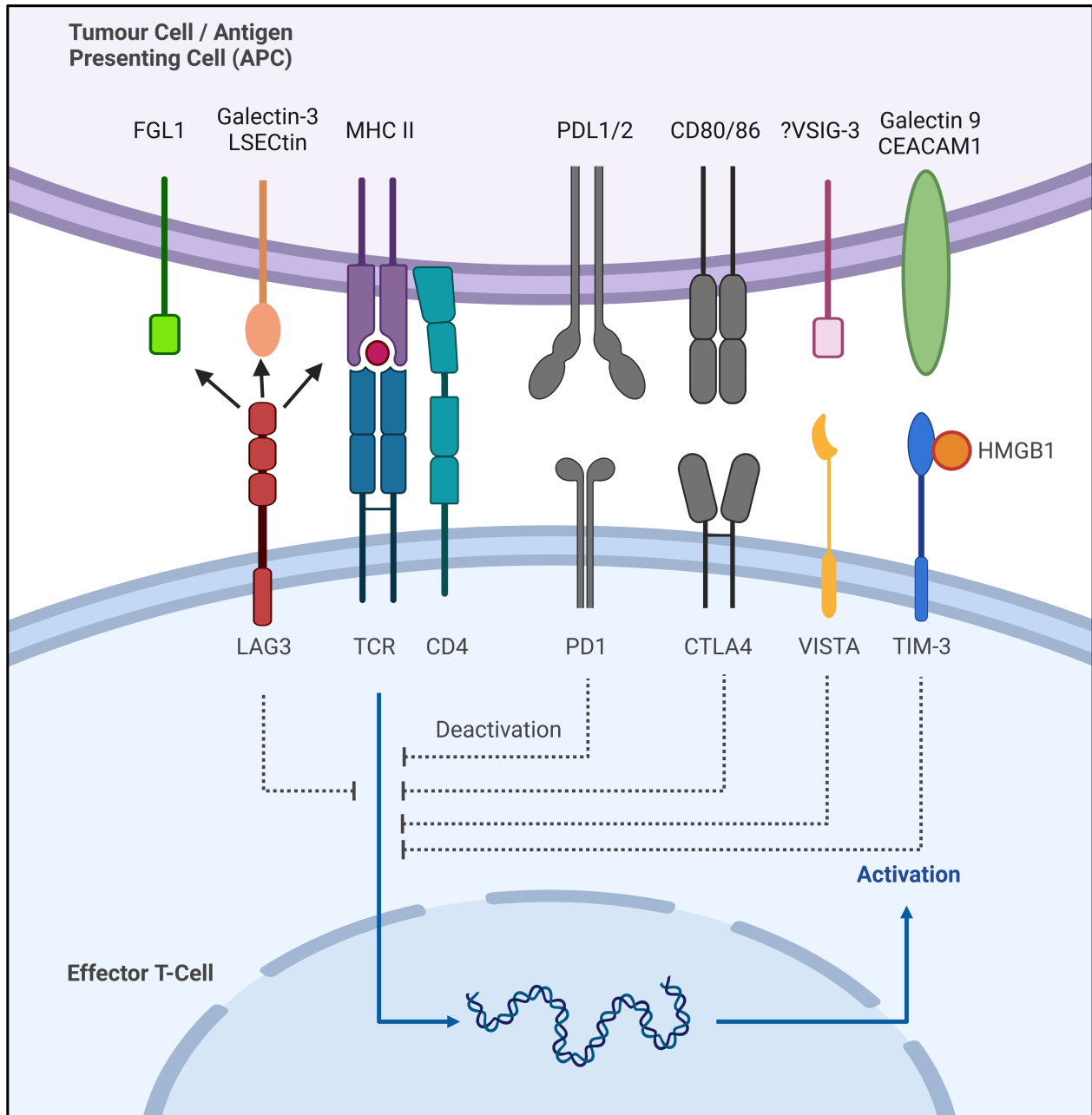
Several factors have been closely associated with response to immunotherapy in HCC including T-cell infiltration, tumour genotype and aetiology of liver disease. Immune-rich subclasses of HCC have been identified through NGS analysis of multiple cohorts of HCC patients[74, 87].

In 2017, an analysis by *Sia et al.*, identified up to a quarter of HCC tumours have inflammatory TME gene signatures, with high PD-1 and PD-L1 expression[87]. The immune-rich subclass was associated with high levels of interferon signalling and absence of activating CTNNB1 or other canonical WNT pathway mutations. Interestingly, there appeared to be little differences in neoantigen levels across immune subtypes. High levels of lymphocyte, macrophage and immune-cell associated infiltrate were also observed, which corresponds with evidence from other studies that high levels of CD8+ infiltration are associated with improved immunotherapy responses. Interestingly, patients with HCV were most likely to have an inflamed immune microenvironment compared with patients who had HCC due to other aetiologies. In other preclinical studies, supported by limited evidence in human disease, there is a suggestion that people with NASH/NAFLD HCC may also have resistance to immune checkpoint therapies[38]. It is suggested that NASH leads to aberrant T-cell activation that causes further tissue damage and supports a pro-tumorigenic immune microenvironment. Although there is scant evidence of the clinical relevance of this from randomised controlled trials of immunotherapy, the suggestion that an immune-enriched subclass of HCC expressing markers of exhaustion may be responsive to immune checkpoint inhibitors is further supported by evidence from other solid tumour types.

1.7 Mouse models of hepatocellular carcinoma

Existing mouse models of HCC can be divided into three main categories; genetically engineered mouse models (GEMMs), carcinogen-induced models and diet-induced models[91]. These different approaches can also be combined, for example using a GEMM in combination

Figure 1.6: Overview of inhibitory immune checkpoints with therapies currently under clinical development or approved for clinical use. PD-1, CTLA-4, PD-L1 and PD-L2 currently have a range of indications and their use has been transformative in many solid tumour types, however, given a wide range of immune checkpoints can be expressed, combinations of therapy may be explored to increase response rates. Suppression of stimulatory immune checkpoints may also play a vital role in evading the immune system (stimulatory checkpoints not shown), but have not yet been used in clinical practice.



with altered diets. Transplantation models of HCC also exist and are typically subcutaneous or orthotopic models using syngeneic murine cells (Hepa1-6 or Hep53.4) or human xenografts in immunodeficient mouse strains[92, 93]. A comparison of these different approaches to disease modelling can be found in table 1.2.

Dietary and carcinogen-induced models have formed the bulk of most preclinical HCC research up until very recently. As outlined in table 1.2, although these are straightforward to use in experiments, their relevance to human disease is limited. In response to this, genetically engineered preclinical models (GEMMs) have become increasingly common[91]. These GEMMs contain specific genetic elements which permits the model to be engineered to more accurately reflect the genetic alterations found in human disease. A unique complexity in studying HCC is that human disease almost invariably occurs on a background of chronic liver disease. Mutations in HCC are likely to be driven by the presence of chronic liver disease, and disease and vary across different aetiologies[16, 20, 21]. Therefore, introducing genetic drivers into healthy mouse livers may not fully recapitulate disease. However, use of GEMMs permits dietary or inflammation stimuli to be used in combination with genetics to model human disease more closely.

Genetically engineered mouse models of HCC can be further subcategorised into two main groups; those with endogenous drivers that are present within the germline genome and those which use exogenous drivers introduced through viral or plasmid DNA-based hydrodynamic tail vein injection[94]. Hydrodynamic tail vein injections rapidly deliver DNA in large volumes of fluid (up to 15% of mouse body weight) over the course of just a few seconds[91, 95, 96]. This is thought to then overload the right atrium temporarily, leading to increased inferior vena cava pressure and subsequent back flow of DNA solution from hepatic vein into liver parenchyma. The liver parenchyma is thought to be disrupted by these forces, leading to uptake of the DNA into hepatocytes.

Both endogenous and exogenous approaches have specific advantages and disadvantages. With endogenous systems that utilise site-specific recombination technology, precise genetic deletions can be conditionally introduced in a tissue-specific manner. Alternatively, by

introducing stop signals preceding expression cassettes into ‘safe harbours’ in the mouse genome, most commonly the Rosa26 locus, stop signals can be selectively excised to allow the overexpression of specific genes[97]. The gene dosage can be altered through breeding the mice to wild-type, heterozygosity or homozygosity at the loci of the given drivers of interest. As every cell contains these engineered drivers, the chance a driver is present in any given cell is likely to be more consistent than in exogenously delivered DNA. In conditional models, such as those which use site-specific Cre-lox or flippase-FRT technologies, recombinases can be introduced through either endogenous expression using engineered promoters or packaged into gene-delivery systems such as viruses[98, 99]. Commonly used approaches include the albumin-Cre system, which expresses Cre recombinase under control of the albumin promoter[91]. As hepatocytes are a major source of albumin, this specifically targets these cells and its progenitors, but is also found to have activity in cholangiocytes[100]. Furthermore, this widely used system is also active during embryogenesis and development, therefore inducing genetic alterations in early life, whereas HCC is a disease of adulthood.

Delivery of exogenous DNA has a higher chance of delivering multiple copies (particularly at high doses) or no copies (particularly at low doses) for a given cell. If vectors are not rationally designed, for example, if one strand of DNA encoded guides for one CRISPR target, rather than all targets, there is a risk of introducing genetic alterations to different populations in a heterogenous fashion (only a few cells would contain all the intended alterations).

These different approaches to genetic modelling all have different advantages and disadvantages. Ultimately, by using multiple models which can address the specific drawbacks of each other, more reliable data can be generated in a timely manner to address clinical needs.

1.7.1 Genetically engineered HCC models for studying immunotherapy response and resistance

Most studies studying the preclinical effectiveness of anti-PD1 therapy have used transplantation models (subcutaneous or orthotopic)[91, 107]. There have been several

Table 1.2: Comparison of different *in-vivo* modelling approaches

	Advantages	Disadvantages	Example
Genetically engineered mouse models (endogenous)	Single/multiple driver models can be produced to reflect the drivers found in human disease	Requires extensive breeding	Cre-lox/Flp-FRT recombination[98]:
	Can be combined with dietary or carcinogen exposure to more accurately model the effects of environmental exposures Genetic drivers can be conditionally or temporally controlled using techniques such as Cre-lox recombination, ER fusion or tetracycline controlled systems Causal effects of different drivers can be studied through titrating gene dosage (wild-type/heterozygous/homozygous)	Adding new drivers and development of new models takes many months or years Long intervals between administration and development of HCC May not have full penetrance of HCC Promoter-driven systems can drive expression of genetic drivers from embryonic stages, increasing the risk of modelling developmental cancers (i.e. hepatoblastoma) Does not take into account environmental exposures or background liver disease Non-conditional drivers can have off-target effects in other tissues and may be embryonically lethal Somatic mutations in murine genome do not necessarily have homologous roles in human disease (i.e. TERT)	Albumin promoter driven Cre-recombinase[91] Trp53 conditional knock-out[91]
Genetically engineered mouse models (exogenous delivery)	Does not require breeding of different genotype mice	Unclear mechanism of delivery	c-MYC[101]
	Liver tissue specific and can be used to introduce disease-relevant genetic drivers Genetic alterations can be produced <i>in-vitro</i> and be tested <i>in-vivo</i> in a matter of days Can be used to 'knock-in' genes (i.e. sleeping beauty transposon system) or 'knock-out' genes (i.e. CRISPR-Cas9)	Gene dosage per cell variable Requires skilled operator to deliver hydrodynamic tail vein injection	NRAS[95] Cyclin D1 and c-MET[96, 102]
Carcinogen induced models	Does not require breeding of different genotype mice Experiments are easily reproduced in different laboratories	May not be representative of human disease Wide ranging mutations across entire genome Acutely toxic to animals and those administering substances Long intervals between administration and development of HCC May not have full penetrance after a single dose	Diethylnitrosamine (DEN)[103] 9,10-dimethyl-1,2-benzanthracene (DMBA)[91, 104]
Diet/inflammation induced models	Simple administration	May not be representative of human disease	Choline deficient diet
	Does not require breeding of different genotype mice Can model environmental/inflammation associated aspects of liver disease	Long intervals between administration and development of HCC May not have full penetrance of HCC Some inflammation inducing agents are hazardous to human operators May not engraft in all animals	Western Diet/Modified Western Diet[105] American Lifestyle Induced Obesity Syndrome diet (ALIOS)[106] Carbon Tetrachloride
Transplantation models	Human disease can be directly studied in-vivo Does not require breeding of different genotype mice Tumours can be precisely delivered and controlled Cells can be manipulated <i>in-vitro</i> prior to being implanted <i>in-vivo</i>	Subcutaneous models do not recapitulate liver micro-environment Requires high levels of technical skill to perform orthotopic surgery Selects for cells which have the ability to engraft Syngeneic mouse lines originate from spontaneous or carcinogen induced models, thereby limiting human disease relevance Requires syngeneic, immunocompromised or humanised strains which can be costly and difficult to maintain	<i>Human cells:</i> - Huh6 - Huh7 - HepG2 <i>Mouse cells:</i> - Hepa1-6[93] - Hep53.4[92]

studies which have employed genetically engineered mouse models of HCC and studied immunotherapy response to checkpoint inhibitors. Although they typically take longer to develop cancer GEMMs are likely to provide a more in-depth model system which permits study of immunotherapy response as tumours develop and evolve, in a genetically defined context.

The most notable example of HCC GEMMs used to study responses to anti-PD1 therapy was published in 2019 by *de Galarreta et al.*, where a hydrodynamic system was used to delete TP53 using CRISPR-Cas9, in combination with strong MYC overexpression driven by the EF1 α core promoter[101]. Some TP53^{-/-} and MYC overexpressing mice responded to anti-PD1 therapy and were found to have immune-rich tumour microenvironments. This effect was particularly pronounced in mice which overexpressed three model antigens (collectively known as OS; SIYRYYGL, SIINFEKL (OVA I) and OVA II). The authors also overexpressed a mutant form of β -Catenin, which led to a reduction in infiltrating CD8+ T-cells and resulted in resistance to anti-PD1 immunotherapy. Having identified CCL5 suppression in β -Catenin mutant cancer, overexpression of CCL5 restored immunotherapy responses in this model, however, the authors only showed this in antigen expressing OS mice, which limits the applicability of this – particularly given β -Catenin mutation is associated with low levels of immunogenic epitopes[108]. Nonetheless, this study demonstrated the feasibility to model immunotherapy responsive (‘immune hot’) and immunotherapy resistant (‘immune cold’) HCC in GEMMs.

Chapter 2

Hypothesis and aims

2.1 Hypothesis and aims

Given the relatively low response rates and poor outcomes there is a clear need to identify new, more effective therapies for people with HCC. In a subset of patients, immunotherapies can lead to durable and even complete responses. Unlike other therapies, immunotherapies hold promise of durable cures and could even play a role in downstaging advanced disease prior to curative surgery.

To identify new therapies which can increase the number of people who benefit from immunotherapy, understanding mechanisms of immunotherapy resistance and how these differ across different genetic drivers of HCC is essential. Preclinical mouse models of HCC provide a useful means to study resistance mechanisms across different molecular subtypes and allow new therapies to be tested in-vivo in a much faster manner than in humans. Using a range of mouse models, in this thesis I will explore underlying mechanisms of immunotherapy resistance and explore how these can be targeted.

2.1.1 Hypotheses

To systematically understand the mechanisms underpinning immunotherapy resistance in different molecular subtypes of HCC, I propose the following hypotheses for my project:

1. Different aetiologies and molecular drivers of HCC shape the tumour microenvironment leading to the development of immunotherapy resistance, either by excluding immune cells, or by driving immune-exhaustion programmes.
2. Drivers such as canonical WNT/ β -Catenin promote immune exclusion through suppression of inflammatory signalling, including cytokine signalling.
3. Comparing pathways present in immune excluded to immune infiltrated tumours will allow me to identify approaches to restore cytokine and proinflammatory signalling.

2.1.2 Aims

To investigate these hypotheses, I will:

1. Establish an autochthonous, genetically engineered mouse model of HCC which is responsive to therapy with immune checkpoint blockade ('immunotherapy sensitive').
2. Systematically compare an immunotherapy sensitive model with a canonical WNT/ β -Catenin-driven model of HCC, using a range of multiomic technologies and identify signalling pathways which could plausibly drive resistance in WNT/ β -Catenin-driven tumours.
3. Test whether targeting signalling pathways present or absent in canonical WNT/ β -Catenin-driven tumours can alter inflammatory signalling and identify potential mechanisms to promote immune infiltration.
4. Develop new genetically engineered mouse models of HCC and immunity which can be used to casually examine how cancer drivers contribute to immune evasion.

Chapter 3

Materials and methods

3.1 Mouse models

3.1.1 Adeno-associated virus preparation

Adeno-associated virus (AAV) vectors were purchased from Addgene (AAV8-TBG-Cre, Addgene 107787 or AAV8-TBG-Null, Addgene 105536) and were provided by the University of Pennsylvania vector core (Penn Vector Core). The thyroxine binding globulin (TBG) promoter was used to drive hepatocyte specific expression of the Cre-recombinase. All constructs were packaged into virus by Penn Vector Core, with the AAV8 serotype selected due to its high liver tropism. Packaged virus stocks were stored at $-80\text{ }^{\circ}\text{C}$ until subsequent use.

When required, virus stocks were thawed on ice and a working solution for injection into mice was prepared in sterile phosphate buffered saline (PBS) according to a calculated dilution in a class II microbiological safety cabinet. Working solutions were then frozen on dry ice and stored at $-20\text{ }^{\circ}\text{C}$ prior to administration to mice by intravenous tail vein injection. The dose was defined as the number of genomic copies (GC) delivered in $100\text{ }\mu\text{l}$ of sterile PBS. Further information on timings and dosages can be found in the results chapters. Low-dose was defined as 6.4×10^8 GC, medium dose 5×10^9 GC, medium-high dose 5×10^{10} GC and high dose 2×10^{11} GC.

3.1.2 Mouse husbandry

All experimental mice were adults aged 8 to 15 weeks at the time of first intervention. Mice were housed in cages of up to 5 mice in a Home Office licensed, specific pathogen-free facility with 12-hour day-night cycles. All animals had *ad-libitum* access to food (irradiated normal chow unless otherwise specified) and drinking water. Environmental enrichment was provided in the form of irradiated nesting materials, plastic tunnels, and wooden gnawing sticks. Experiments were performed under Home Office project license numbers 70/8891 or PP0604995. In humans, males are more likely to develop HCC. Therefore, due to these sex specific differences, and to save costs and time, male mice were used for all experiments unless otherwise stated. All

Table 3.1: Clinical signs and grading for determining endpoints in mouse models

	Mild	Moderate	Substantial
1a	Weight loss	Weight loss of up to 20%	Weight loss 20%
1b	Body Condition Score Normal	loss of body conditioning (BCS 2*)	Poor body conditioning (BCS 1*)
2	Partial piloerection	Staring coat	Marked piloerection
3	Subdued but responsive Animal shows normal behaviour	Subdued Animal shows subdued behaviour with little peer interaction May show aggression	Animal unresponsive to extraneous activity and provocation
4	Transient hunched posture, especially after dosing Normal mobility	Hunched intermittently Reduced mobility	Hunched, persistently frozen No spontaneous mobility
5	Normal appearance of mucous membranes	Pallor/jaundice of eyes, nose, ears and feet	Pallor Animal feels cold when handled
6	Normal respiratory rate	Altered respiration Temporary or intermittent abnormal breathing pattern Intermittent ‘chattering’	Laboured respiration Prolonged ‘chattering’
7	No abdominal distension	Abdominal distension	Abdominal distension affecting movement or breathing
8	No diarrhoea or transient diarrhoea	Intermittent or continuous (>72h) diarrhoea No dehydration	Continuous diarrhoea (>72h) with faecal soiling of perineum and/or dehydration
9	No observable tumour mass	Tumour mass <1.5cm	Tumour mass >1.5cm Tumour restricts animal movement Tumour ulceration

experiments had ethical approval from the Animal Welfare and Ethical Review Body (AWERB) at the University of Glasgow and complied with the ARRIVE guidelines[109].

Monitoring to establish the genetic background was performed on ear notch or tail samples. Samples were sent to either Taconic or Transnetyx where DNA was extracted, and single nucleotide polymorphism (SNP) arrays used to determine the background strain genotype. For experiments in this thesis, the background strain genotype was 99% C57BL/6 or greater. Genetic drift was minimised by periodically refreshing mouse colonies by crossing mice onto commercial C57BL/6J (JAX) mice obtained from Charles River.

Mice were monitored daily and those on experimental protocols were subject to enhanced model-specific checks at least 3 times per week for any clinical signs. As mice reached expected endpoint the frequency of checks increased to enhanced daily monitoring. Mice were killed when they reached three or more moderate signs, or one substantial sign described in table 3.1. Mice displaying 1 or more moderate signs received enhanced daily monitoring.

Mice were euthanised by inhalation of rising concentration of carbon dioxide for 4 minutes

and death confirmed with cervical dislocation as the secondary method. Immediately after euthanasia, mice were weighed and blood was obtained by cardiac puncture using a transthoracic anterolateral approach with a 25-gauge needle and 1 ml syringe. Blood was divided into an EDTA coated tube (Starstedt) and a lithium-heparin tube (Starstedt). Tubes were inverted 3 times and placed on wet ice. Plasma was subsequently obtained by centrifugation of the lithium-heparin tube at 10,000 rpm for 10 minutes at 4 °C. Blood from the EDTA coated tube was run through the IDEXX ProCyte Dx haematology analyser to obtain blood count data (IDEXX Laboratories, Maine, USA).

Where appropriate, the macroscopic appearance of the liver was photographed using a Canon PowerShot G5 mark II (Canon, Japan). Tumours were counted and measured in one dimension for spherical tumours or three perpendicular dimensions for ellipsoid tumours using digital vernier callipers. Tumours were judged to be spherical if they had a similar radius in the X, Y and Z planes. To calculate tumour volume in mm³ the following equation was used for spherical tumours where r is the radius:

$$V = \frac{4}{3}\pi r^3$$

The following equation was used for ellipsoid tumours where a, b and c are half the measurements in the X, Y and Z planes:

$$V = \frac{4}{3}\pi abc$$

3.1.3 Orthotopic transplantation

For subcutaneous transplant models, cells were cultured as described below and tested for mycoplasma contamination prior to transplantation (Minerva Biolabs 11-91025). Cells were made up to the required concentration in Matrigel (Corning 354230) and kept on ice until the procedure. Mice receiving cells had their flanks shaved and received a subcutaneous injection of 100 μ l cells and Matrigel. Mice were monitored daily and received enhanced checks 3 times

per week. Mice were sampled when there were visible tumours present 5mm in diameter or displayed clinical signs as outlined in table 3.1.

For orthotopic transplantation models, cells were cultured as described below and tested for contamination prior to transplantation. Cells were made up to the required concentration in Matrigel (Corning 354230) and kept on ice until the procedure. Mice were weighed and abdomens shaved. General anaesthesia was induced using 5% Sevoflurane (Animalcare XVD015) with oxygen as the carrier gas at 2L per minute.

Once adequate depth of anaesthesia was achieved, mice were transferred to a heated table with nose cone and maintained at 2 to 4% Sevoflurane carried in oxygen at 2L per minute. To provide some degree of fluid replacement, 100 μ l of sterile PBS was given subcutaneously, along with 0.1 mg/kg of buprenorphine. Prior to incision, skin was prepared with alcoholic 0.5% chlorhexidine. Once the skin was dry, a sterile drape was placed over the surgical site. A sterile surgical field was maintained throughout the procedure. All instruments were steam autoclaved beforehand.

A 5 to 10 mm horizontal incision in the skin was made perpendicular to the xiphisternum using a pair of sterile sharp dissecting scissors. The skin layer was bluntly dissected to create a plane between the skin and fascia covering the abdominal muscles. Next, a vertical 5 mm incision was made in the midline to access the intraperitoneal cavity, initially through a small incision, followed by more blunt dissection to avoid damage to underlying structures. The liver was subsequently manipulated so one or more lobes were externalised. Lobes of the liver were stabilised using a sterile, damp swab on a stick prior to injection with 10 μ l of cells in Matrigel.

Cells were drawn up using a 100 μ l gas-tight syringe (Hamilton 1710LT) with a 25-gauge needle attached, prior to injection cells were mixed and any air bubbles expelled. Cells were slowly injected to allow Matrigel to solidify and form a subcapsular bleb of cells in the liver. This also reduced the chance of embolism from Matrigel and cells. After injection, the needle was carefully removed, and a small patch of Surgicel regenerated oxidised cellulose mesh placed over the puncture site (Ethicon 1903).

Once adequate haemostasis had been achieved, the liver was replaced into the intraperitoneal cavity and the muscle layer closed with a continuous layer of 4-0 Vicryl (Ethicon W9074). Topical 0.1% bupivacaine in PBS was applied to the wound and the skin layer subsequently closed with 2 to 4 Clay-Adams autoclips (VetTech IN015A).

Mice were then transferred to a warming cabinet and were supplied with 0.5% Carprofen drinking water, mashed chow, and DietGel Recovery supplement packs (ClearH₂O 72-06-5022). Mice were monitored closely during the postoperative period and when they were adequately recovered transferred to normal cage racks from the warming cabinet. Mice received daily checks and enhanced daily monitoring for the first 2 postoperative days, which then decreased to three times per week. Mice were sampled at 30 days as described above.

3.1.4 Alleles

3.1.4.1 Conditional β -Catenin exon 3 deletion

Constitutive activation of β -Catenin was achieved through conditional deletion of the third exon of the *Ctnnb1* gene using the *Ctnnb1*^{tm1Mmt} allele (MGI: 1858008)[110]. This allele contains two loxP sites flanking the third exon of *Ctnnb1*, which encodes serine/threonine phosphorylation sites which enables the degradation of β -Catenin through the Adenomatous Polyposis Coli (APC) β -Catenin destruction complex. In the presence of Cre-recombinase, the third exon is deleted and a constitutively active, ‘un-degradable’ β -Catenin protein is produced. Experimental mice were bred to heterozygosity for this allele, unless otherwise specified.

3.1.4.2 Conditional Trp53 deletion

To model deletions and loss-of-function mutations in the TP53 gene, the *Trp53*^{tm1Brn} conditional allele (MGI: 1931011) was used to knock-out *Trp53* *in-vivo*[111]. This allele has loxP sites flanking exons 2 and 10 of the *Trp53* gene. In the presence of Cre-recombinase exons 2 to 10 are excised, leading to a loss of p53 expression. Mice with this allele were bred to homozygosity and used for experiments unless otherwise stated.

3.1.4.3 Conditional c-MYC expression

Mice with the $Gt(ROSA)26Sor^{tm1(MYC)Djmy}$ allele were used to generate models of cancer with conditional overexpression of human c-MYC[112]. This allele encodes the endogenous locus Rosa26 promoter, followed by a lox-stop-lox cassette and a full-length human c-MYC cDNA. In the presence of Cre-recombinase, the lox-stop-lox, expression of human c-MYC is driven by the moderate-strength endogenous Rosa26 promoter. Experimental mice were bred to homozygosity for this allele, unless stated otherwise.

3.1.4.4 TetO- Δ N89 β -Catenin expression

To develop a genetically engineered mouse model where expression of constitutively active β -Catenin could be controlled temporally and in a tissue-specific manner, we obtained mice with the $Col1a1^{tm1(tetO-CTNNB1)Tcd}$ allele (MGI: 5469323, gift from Trevor Dale, Cardiff University)[113]. These mice have a TetO-TRE driven human N-terminal myc-tagged Δ N89 β -catenin gene at the *Col1a1* locus. Δ N89 β -catenin is a truncated version of human β -catenin with the first (N-terminus) 89 amino acids (including those encoded by the third exon) deleted. These amino acids encode serine-threonine residues which when phosphorylated, mediate the degradation of β -Catenin through E3 Ubiquitin Ligase (β -TrCP), thus resulting in the production of an ‘un-degradable’ constitutively active form of human β -Catenin.

3.1.4.5 Tetracycline controlled systems

Expression of tetracycline responsive genes driven by promoters containing Tetracycline response elements (TRE; TetO) *in-vivo* was controlled by an enhanced version of the tetracycline-controlled transactivator (tTA2) protein as a ‘Tet-Off’ system. In the presence of Doxycycline (Melford D43020), the tTA2 protein binds doxycycline, which blocks tTA2 binding to the TRE elements of the promoter, therefore preventing target gene transcription.

To establish a conditional tetracycline controlled mouse model of Δ N89 β -Catenin expression, mice with the $Igs2^{tm5(CAG-tTA2-TagBFP)Luo}$ allele (MGI: 6119574) were obtained from JAX (Strain 031776)[114]. These mice have a CAG promoter, followed by a lox-stop-lox

cassette upstream of tTA2-T2A-H2B-TagBFP-3xMyc-WPRE sequence at the intergenic site 2 (Igs2) locus. In the presence of Cre-recombinase, the lox-stop-lox cassette is excised, driving the expression of tTA2 and H2B-TagBFP. As Cre-recombinase expression can be targeted in a tissue-specific manner, this system allows control over the expression of TetO-TRE driven transgenes with the addition of tetracycline.

For whole-body ‘Tet-On’, to confirm expression of Δ N89 β -Catenin and its response to doxycycline, mice with the Gt(ROSA)26Sor^{tm1(rtTA*M2)Jae} transgene were crossed to mice with the Δ N89 β -Catenin allele. The Gt(ROSA)26Sor^{tm1(rtTA*M2)Jae} allele (MGI: 3702294) encodes a non-conditional, optimised reverse tetracycline controlled transactivator (rtTA-M2) at the Rosa26 locus[115]. In this ‘Tet-On’ system, the rtTA-M2 is only capable of binding the TetO-TRE element in the presence of tetracycline, therefore driving transcription. This allele is not tissue specific, conflicts with other transgenes at the Rosa26 locus, and requires administration of doxycycline, which limits its use in long-term mouse models of cancer.

3.1.4.6 Generation of the NeoTAP mouse model of conditional antigen expression

The mCherry-Ovalbumin construct gifted by Dr Edward Roberts (CRUK Beatson Institute) was used as a basis to develop a genetically engineered mouse model which permitted tissue-specific and temporally controllable neoantigen expression. To do this, the construct was first sanger sequenced using an mCherry specific forwards primer and primers subsequently ‘walked’ along the construct according to the sequencing results. Finally, full contigs were assembled in SnapGene version 6.0 (GSL Biotech, California, USA) and aligned to publicly available sequences of *Gallus gallus* ovalbumin sequences and the mCherry fluorescent protein.

Following verification of the sequences, the ovalbumin protein was truncated by deletion of the first 48 amino acid sequences to restrain expression to the cytosol. The sequences encoding the truncated cytosolic ovalbumin and mCherry were then combined with a porcine *teschovirus-1* 2A (P2A) self-cleaving peptide sequence to produce a bicistronic OVA-P2A-mCherry coding sequence.

The design of the final construct was developed in conjunction with Arielle Bryan at

Ingenious Targeting laboratories (Ronkonkoma, New York, USA) and the mouse was produced by Ingenious using C57BL/6 embryonic stem cells, prior to shipping and rederivation at the CRUK Beatson Institute using *in-vitro* fertilisation. The native allele was annotated as C57BL/6N-Polr2a^{tm1(CAG-OVAL,-mCherry,tetO-rtTA)Itl} MGI:7282145 and the recombined allele C57BL/6N-Polr2a^{tm1.1(tetO-OVAL,-mCherry,CAG-rtTA)Itl} MGI:7282253. Genetic monitoring was performed to establish mice had a 99.5% C57BL/6 genetic background, prior to commencing experiments. Further information on the allele is available in the results chapters. This was named the NEOantigen expression in Time And sPace (NeoTAP) model.

3.1.5 Diethylnitrosamine american lifestyle-induced obesity syndrome model of NASH-HCC

To study the tumour microenvironment in the context of non-alcoholic fatty liver disease (NAFLD) and non-alcohol related steatohepatitis (NASH), diethylnitrosamine in combination with the american lifestyle-induced obesity syndrome (ALIOS) diet was used.

Diethylnitrosamine (DEN) is a widely established chemical carcinogen model, promoting the development of liver tumours. Mice on a C57BL/6 genetic background were injected with a single 80mg/kg dose of intraperitoneal DEN at 14 days of age. Mice were then started on the American lifestyle-induced obesity syndrome (ALIOS) diet, which consisted of an irradiated chow diet containing high levels of trans-fats (22% hydrogenated vegetable fat, Envigo TD.110201) with the addition of sugar water (23.1 g/L fructose and 18.9 g/L glucose). The diet and sugar water were kindly supplied by Thomas Jamieson and Dr. Ee Hong Tan at the CRUK Beatson Institute.

3.1.6 Drug administration

For administration of putative therapeutic compounds, the dosing schedules, concentrations and vehicles can be found in table 3.2. Briefly, standardised vehicles were used whenever possible. Orally bioavailable compounds were administered as a suspension in 0.5% Hydroxypropyl Methylcellulose (HPMC, Merck 09963) and 0.1% Tween 80 (Merck P1754).

Anti-PD1 (Biolegend RMP1-14) and IgG isotype (Biolegend RTK2758) antibody were obtained from Biolegend and diluted to a concentration of 1 mg/ml in sterile PBS. Mice were administered 200 μ g of antibody via intraperitoneal injection twice weekly. This was kindly coordinated by Thomas Jamieson and Dr. Saadia Karim. AZD5069 was provided as a gift by AstraZeneca (Cambridge, UK).

Table 3.2: Drug dosing and administration

Compound name	Target	Vehicle	Dose	Frequency	Route
AZD5069	CXCR2	HPMC 0.5%, Tween 80 0.1%	100 mg/kg	Twice daily	Oral gavage
anti-PD1	PD1	Sterile PBS	200 μ g/dose	Twice weekly	Intraperitoneal
IgG Isotype	Not applicable	Sterile PBS	200 μ g/dose	Twice weekly	Intraperitoneal

3.2 Histology

3.2.1 Tissue processing

Liver tissue, including for those with liver tumour, was fixed in 10% neutral buffered formalin for 24 to 48 hours at room temperature. After this, the formalin was removed and replaced with 70% ethanol 30% ultrapure water to dehydrate the fixed tissues.

Following tissue fixation and dehydration in ethanol, tissue samples were trimmed and embedded into paraffin blocks by the core histology service at the CRUK Beatson Institute. 4 μ m sections were cut from paraffin blocks, mounted onto glass slides and baked at 60°C for 1 hour. Haematoxylin and Eosin (H&E) staining was performed on tissue sections according to standard protocols by the CRUK Beatson Institute core histology facility.

3.2.2 Immunohistochemistry

For mouse samples, the majority of single 3,3'-Diaminobenzidine chromogen (DAB) immunohistochemistry was performed by the CRUK Beatson Institute core histology facility using Leica Bond Autostainers. The antibodies used can be found in table 3.3.

For single chromogen staining, 4 μ m sections were dewaxed using xylene, graded ethanol and water, and heat mediated epitope retrieval performed by boiling sections in a water bath in either a pH6 Sodium Citrate Buffer for 20 minutes or pH9 Tris-EDTA buffer for 40 minutes. Endogenous peroxidases were blocked with 0.3% hydrogen peroxide in methanol for 20 minutes, sections washed in distilled water and mounted in a ThermoFisher Sequenza staining rack. Mounted slides were washed with Tris Buffered Saline with Tween 20 (TBST), then incubated

with an avidin-biotin block as per the manufacturer's instructions for a total of 1 hour. To reduce non-specific antibody binding, a non-animal protein block was applied for at least 2 hours. Slides were then incubated overnight at 4°C with primary antibody in diluent (ThermoFisher 003218).

The following day, sections were washed with TBST and incubated with either a biotinylated secondary (1:200, Vector Laboratories) against the species of the primary antibody, or with 2 drops per slide of a HRP conjugated secondary antibody polymer for 1 hour (Agilent). Slides were then washed with TBST and if a biotinylated secondary was used, slides were incubated with 2 drops of avidin conjugated horseradish peroxidase (HRP, Vector Laboratories PK-6100) for 30 minutes before being washed again with TBST. Following thorough washing with TBST, DAB substrate (Agilent) was freshly prepared and incubated with the slides for 5 minutes.

For human samples, ethical approval for access to anonymised lesional HCC and non-lesional adjacent liver tissue was first sought from the National Health Service Research Scotland (NRS) Lothian Biorepository. Ethical approval was given under the reference number SR1159. Slides were sent to the Newcastle University histology service who stained for CD3, and CXCR2 using Roche Ventana autostainers. The antibodies used can be found in table 3.3.

Counterstaining was performed using Haematoxylin and slides mounted using Dibutylphthalate Polystyrene Xylene mountant (DPX, CellPath SEA-1300-00A).

3.2.3 RNA in-situ hybridisation

In-situ hybridisation (ISH) staining was performed by the CRUK Beatson Institute histology service on 4 μ m formalin fixed paraffin embedded sections (FFPE) which had previously been baked in an oven at 60 °C for 2 hours.

ISH detection for, Ccl5 (469608), Cxcl10 (408928), Lag3 (420418), Cd274 (PD-L1, 420508), Tnfrsf4 (811958), Vsr (439468), Ppib (313918) and Dapb (312038) (Bio-Techne) mRNA was

performed using RNAScope 2.5 LSx (Brown) detection kit (Bio-Techne 322700) on a Leica Bond Rx autostainer strictly according to the manufacturer's instructions.

To complete the ISH staining sections were rinsed in tap water, dehydrated through graded ethanol's and placed in xylene. The stained sections were coverslipped in xylene using DPX mountant (CellPath SEA-1300-00A).

Table 3.3: Antibody list

Antigen	Product number	Company	Retrieval	Dilution
β -Catenin	610154	BD Transduction	Vector Citrate pH6	1/500
CD3	ab16669	AbCam	ER2 20 mins	1/100
CD66b	305102	Biolegend	Citrate pH6	1/200
CD8a	14-0808-82	eBioscience	ER2 20 mins	1/500
CXCR2	HPA031999	Merck	Citrate pH6	1/1000
F4/80	ab6640	AbCam	ENZ1 10min	1/100
GS	HPA007316	Merck	Tris Low	1/800
Keratin 19	ab133496	AbCam	Tris High	1/1000
OAT	ab137679	Abcam	ER2 20mins	1/200
pan-CD45	ab10558	AbCam	ER2 20mins	1/2500
RFP	600-401-379	Rockland	Tris High	1/1000
SOX-9	AB5535	Millipore	Tris High	1/500
Sting	13647	Cell Signalling	ER2 20mins	1/200

3.2.4 Tissue analysis

Microscope slides were scanned using the Leica Aperio AT2 slide scanner at x20 magnification. For RNA in-situ hybridisation, slides were scanned at x40 magnification. Automated quantification of positively stained cells or regions was performed using HALO version 3.6.4134 (Indica Labs, New Mexico, USA) or QuPath version 0.4.3 (University of Edinburgh, UK) image analysis software using custom analysis scripts.

3.2.5 Computer vision for slide labelling

To allow for the high-throughput analysis and archiving of scanned slide micrograph images, a computer-vision classifier system was developed to read microscope slide labels. Briefly, using R version 4.2.0, microscope labels in portable network graphics (PNG) format were sent to the Google Cloud Vision (Google, Palo Alto, USA) Application Programming Interface (API). The API returned read strings, which were then passed to a string cleaning algorithm which coerced strings to alphanumeric characters only ($[A-z,0-9]$, no special characters). These were then matched to known identifiers of the mouse identifier, organ on the slide and the antigen(s) stained for using immunohistochemical techniques. File names were then renamed according

to the mouse identifier, timestamp of file generation, organ and antigen.

3.3 Protein and molecular assays

3.3.1 Cytokine assays

Protein was extracted from homogenised fine powder obtained by grinding liver or tumour using the Cryocooler mortar pestle system, cooled with liquid nitrogen (Ops Diagnostics, New Jersey, USA). A 20 mM Tris HCl (pH 7.5), 0.5% Tween 20 (Merck P1379), 150 mM NaCl extraction buffer with EDTA-free protease inhibitors (ThermoFisher A32955) was added to each sample, and each sample passed a minimum of ten times through a 26-gauge needle. Samples were then incubated on ice for 30 minutes, vortexed vigorously and then spun at 13,200 x g for 10 minutes at 4°C. The cleared lysates were then aliquoted into lo-bind protein tubes and stored at -80. Stored lysates were then sent to Eve Technologies, who performed automated 44-plex testing, with the addition of IFN- α and IFN- β tests.

3.3.2 Nucleic acid extraction from tissue

Samples of snap frozen tissue, stored previously at -80 °C, were homogenised into a fine powder using the Cryocooler mortar and pestle system cooled with liquid nitrogen. Tissue powder was divided into LoBind eppendorf 1.5 ml precooled tubes and stored at -80°C until further analysis.

From the aliquoted tissue powder, RNA was extracted with the Qiagen RNeasy mini kit with a DNase treatment step according to the manufacturer's instructions (Qiagen 74104). The resulting RNA was cleaned and further purified using the Zymo RNA clean and concentrator kit (Zymo Research R1016). RNA integrity was assessed using an Agilent RNA ScreenTape on a Tapestation 2200 (Agilent) and quantified using the high sensitivity Qubit RNA assay (ThermoFisher). DNA samples were treated with RNaseA and proteinase K, then run on a D5000 screen tape or 1% agarose gel to check integrity.

RNA samples with an RNA integrity (RIN) score of 6.8 and above were taken forward to library preparation. DNA samples without any RNA smearing and a single large band at 5000 to 10000 bp were taken forward to library preparation.

3.3.3 Whole exome library preparation and sequencing

Whole exome sequencing (WES) was performed on genomic DNA extracted with the NEB gDNA extraction kit with RNase A treatment according to the manufacturer's instructions (NEB T3010L). DNA was subsequently quantified and quality checked on a D5000 DNA screen tape. Whole exome capture was performed with mouse specific Agilent SureSelect XT or Twist Mouse exome panel kits according to the manufacturer's instructions by Graeme Clark at the CRUK Beatson Institute core facility. Prepared libraries were subsequently sequenced on a Novaseq 6000 at 2x150 bp with coverage of between x50 and x100.

3.3.4 Whole exome sequencing analysis

Nextflow Sarek version version 3.0.2 (nf-core/sarek) was used to process whole exome sequencing data according to the Genome Analysis Toolkit 4 best practice guidelines[116]. Fastq files were downloaded over Secure File Transfer Protocol to a virtual machine and quality controlled using FastQC and Fastp. Reads were subsequently mapped to the GRCh38 (Ensembl) reference genome, duplicates marked and depth calculated with mosdepth. Variants were called with Mutect2[117] and the subsequent effect predicted using Ensembl Variant Effect Predictor version 102[118]. The R package ExomeDepth was used to perform copy number variation analysis[119].

3.3.5 mRNA stranded library preparation and sequencing

For mRNA sequencing from tissue and cGAMP treated organoids, 1 μ g of total RNA was input into a poly-A magnetic bead enrichment step and libraries subsequently prepared using the Qiagen Qiaseq mRNA stranded with unique dual indexing as per the manufacturer's instructions (Qiagen 180440). A dual sided size selection step of library fragments between 150 to 800 bp was subsequently performed using AMPure Agencourt XP beads (Beckman Coulter

A63880). Libraries were checked and quantified using the hsDNA screen tape then pooled at a concentration of 4nM in nuclease free water. Pooled libraries were then sent to Novogene for paired end sequencing on a Novaseq 6000 at 2x150 bp, with a minimum depth of 20 million reads per sample.

3.3.6 RNA sequencing analysis

Fastq files were downloaded over Secure File Transfer Protocol to a virtual machine in the CRUK Beatson Institute (48 Intel Xeon CPU E5-2698 v4 Cores and 148 Gb RAM). Following MD5 checksum verification, raw fastq files were staged for subsequent quality control, sequence alignment and analysis. The Nextflow (RNASeq version 3.9, nf-core/rnaseq) workflow manager was used to coordinate sequencing analysis pipelines using singularity containers on the CRUK Beatson High Performance Computing Infrastructure. This pipeline and its dependencies are described in detail in Nextflow documentation and allows reproducible and scalable analyses to be conducted.

RNA sequencing data were first concatenated and initial quality control (QC) performed using FastQC. Quality control with FastQC was deemed acceptable so long as the average per-base sequencing quality was over Q30 for the entire length of sequence. Sequences were then trimmed using Trim Galore! and quality control performed on the trimmed sequences with FastQC. Next, genome contaminants were removed with BBSplit and any remaining ribosomal RNA reads were removed with SortMeRNA. The cleaned and trimmed sequencing reads were subsequently aligned to the GRCm38 (Ensembl) genome using STAR alignment with Salmon quantification. STAR was configured to enable alignment which was aware to splice variants. SAMtools were subsequently used to sort and generate indexed alignments, before transcript assembly and quantification using StringTie and Ballgown. Ballgown was also used to estimate gene-level counts. Finally, post processing was performed with RSeQC, Preseq, Qualimap and Dupradar and all QC steps were summarised using MultiQC.

Using R version 4.2.0, RNA sequencing counts were filtered to retain the top 60% most variable genes across all samples and library sizes normalised using trimmed mean of M values

(TMM) with singleton pairing. Differential expression analyses were then performed using DESeq2. Differentially expressed genes (DEGs) were then aligned to the Kyoto Encyclopedia of Genes and Genomes (KEGG) or Gene Ontology (GO) pathways corresponding to a given gene and enrichment analyses performed to identify sets of pathways that were significantly enriched across different experimental conditions. Statistical significance was taken at the adjusted level of $P < 0.05$. The R packages tidyverse, DESeq2, clusterProfiler and bioMart were used to perform these analyses.

To validate my findings in human data, I used STAR RNASeq counts from the Cancer Genome Atlas (TCGA) for the LIHC cohort to perform analysis using DESeq2 in the same way described above. TCGA data were accessed via TCGAbiolinks and the National Cancer Institute's Genomic Data Commons. These data were annotated using the GRCh38 (hg38) assembly.

3.3.7 Assay for transposase-accessible chromatin library preparation and sequencing

Libraries for Assay for Transposase-Accessible Chromatin using sequencing (ATAC-seq) were prepared using the Active Motif ATAC-seq library preparation kit with 80,000 nuclei per reaction (Active Motif 53150). Libraries were quantified by quantitative polymerase chain reaction (PCR) using the Collibri Library Quantification kit (ThermoFisher A38524100) using a QuantStudio 3 quantitative PCR machine (Applied Biosystems), pooled at 4nM and sequenced on a NextSeq 2000 at 2x100 bp with at least 75 million reads per sample.

3.3.8 ATAC sequencing analysis

Fastq files were downloaded over Secure File Transfer Protocol to a virtual machine in the CRUK Beatson Institute, MD5 checksums verified and staged to the High-Performance Computing infrastructure. Using the Nextflow ATACSeq version 1.2.2 workflow (nf-core/atacseq), raw sequencing data was quality controlled using FastQC and adapters trimmed using Trim Galore!, before reads were aligned to the GRCm38 (Ensembl) reference genome with Burrows-Wheeler Aligner (BWA) software[116, 120].

Following alignment, duplicates were marked with Picard prior to filtering. Filtering was applied to remove duplicate reads, blacklisted regions, non-primary alignments, mitochondrial DNA, one-to-many alignments, large insert sizes ($>2\text{Kb}$), soft-clipped and unmapped reads. Filtered reads were then subjected to quality control with FastQC and library complexity estimated with Picard and Preseq. Normalised bigwig files were generated that were scaled to 1 million mapped reads from the filtered data. Genome-wide enrichment was calculated using deepTools. Peaks were then called using MACS2, in narrow-peak mode[121].

Differential accessibility analysis was performed in R using the ChIPQC, ChIPseeker and DESeq2 packages. PCA was used to visualise the variance across different experimental conditions. This step was also used as a check to ensure that biological replicates of different cancer models and their respective controls clustered together as expected. Reads within each genotype were pooled together to generate consensus peaksets and increase power for transcription factor footprinting analyses with the HMM-based IdeNtification of Transcription factor footprints (HINT) functions in the Regulatory Genomics Toolbox (RGT)[122].

Further quality control was performed post-alignment using SAMtools, BEDtools, picard, ataqv and Preseq. Pipeline QC reports were then compiled using MultiQC.

3.3.9 Single cell RNA library preparation and sequencing

Mice on a C57BL/6 genetic background were injected with a single 80mg/kg dose of intraperitoneal DEN at 14 days of age and were then started on the american lifestyle-induced obesity syndrome (ALIOS) diet 42 days later. At day 200 post DEN, mice received either vehicle (0.5% Hydroxypropyl Methylcellulose (HPMC) and 0.1% Tween 80) by oral gavage, CXCR2 inhibitor (CXCR2i, AZD5069) by oral gavage, intraperitoneal anti-PD1, or combination CXCR2i with anti-PD1 as a combination therapy. At day 235 post DEN, mice were killed and fresh tumour tissue was obtained. Tumour tissue was dissociated into a single-cell suspension before being loaded onto 10X chromium controller chips. Cells were barcoded using the 10X Single Cell 3' reagent v3.1 kit and sequencing libraries prepared as per the manufacturer's instructions. Prepared libraries were quality controlled and pooled.

Sequencing was performed by Glasgow Polyomics on an Illumina NextSeq 2000 as per the single cell library manufacturer's recommendations. These experiments were performed by Thomas Jamieson, Dr. Rachel Ridgway, Dr. Amanda McFarlane, Dr. Ximena L Raffo Iraolagoitia, Dr. John Mackey, and Dr. Ya-Ching Hsieh.

3.3.10 Single cell RNA sequencing analysis

Fastq files were downloaded over Secure File Transfer Protocol to a virtual machine in the CRUK Beatson Institute (48 Intel Xeon CPU E5-2698 v4 Cores and 148 Gb RAM). Following MD5 checksum verification, raw fastq files were staged for subsequent quality control, sequence alignment and analysis. The Nextflow (scrnaseq version 2.1.0, nf-core/scrnaseq) workflow manager was used to coordinate sequencing analysis pipelines using singularity containers on the CRUK Beatson High Performance Computing Infrastructure. This pipeline and its dependencies are described in detail in Nextflow documentation and allows reproducible and scalable analyses to be conducted[116].

Fastq files were aligned using the Cell Ranger workflow (10X Genomics, California, USA) against the GRCm38 (Ensembl) reference genome to generate sparse expression matrices for each barcoded cell. To analyse RNA velocity, the aligned bam files generated by Cell Ranger were processed using VeloCyto 1.7 to identify which reads were likely to be from unspliced (immature) and spliced (mature) transcripts[123].

These data were then imported into R, where it was processed using a standard Seurat workflow. During the workflow, dimension reduction using Principal Component Analysis was performed and unsupervised clustering performed using the Uniform Manifold Approximation and Projection (UMAP) functions. Trajectory analysis was performed using monocle 3[124]. The UMAP embeddings were then exported into Python version 3.7.9 and using scVelo, merged with the RNA velocities calculated by VeloCyto[123]. The velocity streams were then plotted for each cluster using scVelo.

3.4 Cell culture

3.4.1 2-D Cell culture

Two-dimensional cell culture was used to grow Trp53^{fl/fl} Rosa26^{c-MYC/c-MYC} tumour cells as a monolayer culture. Tissue-culture treated vented T75 or T175 flask culture vessels (Corning and Starstedt) were used to grow cells in 37.5°C, 5% CO₂ incubators. ‘Advanced liver media’ was used, comprising per 500 ml of Advanced DMEM/F12 (ThermoFisher 12634010): 5 ml FCS, 500 µl B27 supplement without vitamin A (ThermoFisher 17504044), 500 µl N2 supplement (ThermoFisher 17502048), 500 µl 1mM Forskolin in ethanol (HelloBio HB1348), 500 µl 1mM Y27632 in ultrapure water (HelloBio HB2297, 0.2 µm filtered), 50 µl 5mM A83.01 in DMSO (HelloBio HB3218) and 500 µl Cultrex Type 2 Reduced Growth Factor BME (BioTechne 3533-010-02). The advanced liver media was then sterile filtered using a 0.2 µm vacuum filter unit. Media was sterile filtered using 0.2 µm syringe filter units at the start of each cell culture session. Antibiotics or antifungal agents were not used. Cultures were routinely tested for mycoplasma by PCR, every 3-4 passages after derivation, prior to first injection into mouse models or just before extraction of nucleic acids for sequencing experiments.

To dissociate monolayer cultures, cells were washed with sterile phosphate buffered saline (PBS) and TrypLE Express dissociation enzyme added (ThermoFisher 12604013). Cells were incubated at 37.5°C for 5 minutes before being aspirated, washed in PBS, counted and plated at the appropriate concentration.

For cryopreservation, 1 million dissociated cells were centrifuged at 500 x g for 7 minutes, supernatant aspirated and the cell pellet resuspended in 1 ml of Recovery freezing medium (ThermoFisher 12648010). The cell suspension was transferred into 1 ml cryovial tubes (Starstedt) and placed in a Corning CoolCell insulated container. The container was placed into a -80°C freezer for 24 hours before tubes were removed and stored at -80°C for short-term storage or liquid nitrogen for long-term storage.

3.4.2 3-D Cell culture

Three-dimensional cell culture (tumour organoid culture) was performed based on previously published protocols by *Broutier et al.*[125]. Tumour organoids were derived from liver tumour tissue taken from $Cttnb1^{\text{exon3/Wt}}$ $Rosa26^{\text{c-MYC/c-MYC}}$ and $Trp53^{\text{fl/fl}}$ $Rosa26^{\text{c-MYC/c-MYC}}$. Tumour tissue was dipped briefly in 70% ethanol, then placed in ice-cold PBS. The tumour tissue was then cut into small 1-2mm chunks using a sterile scalpel (Swann-Morton) in a class II microbiological safety cabinet. Tissue chunks were washed in ice-cold PBS containing 1% Penicillin-Streptomycin (ThermoFisher 15140122), before being dissociated using the Tumour Dissociation Kit, Mouse (Miltenyi Biotec 130-096-730) diluted in Roswell Park Memorial Institute Medium 1640 (RPMI 1640) in gentleMACS C-tubes. The ‘Mouse-LIDK’ protocol was used (with heating). The resulting single-cell suspension was then diluted in RPMI 1640 with 5% FCS and 10mM EDTA to a total volume of 50 ml. Cells were counted and the corresponding volume to give a final concentration of 10,000 cells per well was measured and centrifuged at 500 x g for 7 minutes.

The resulting pellet was resuspended in 30 μl per well of ice cold Cultrex Type 2 Reduced Growth Factor BME (BioTechne 3533-010-02) and mixed gently with a pipette tip. The resulting cell:BME suspension was then gently pipetted onto pre-warmed 24 well plates (Corning) to form domes of extracellular matrix containing cells. Plates were prewarmed for at least 24 hours at 37.5°C. After plating cells, plates were incubated in a 37.5°C, 5% CO₂ incubator for 10 minutes to allow the extracellular matrix to solidify.

Once solidified, 500 μl of ADTT++ media was applied. The composition of this media per 10 ml of Advanced DMEM/F12 (ThermoFisher 12634010) was: 200 μl B27 supplement without vitamin A (ThermoFisher 17504044), 100 μl N2 supplement (ThermoFisher 17502048), 100 μl 1mM Forskolin in ethanol (HelloBio HB1348), 100 μl 1M Nicotinamide in ultrapure water (Merck N0636-100G, 0.2 μm filtered), 100 μl FGF-10 10 $\mu\text{g/ml}$ in 0.1% BSA/PBS (PeproTech 100-26), 100 μl 1mM Y27632 in ultrapure water (HelloBio HB2297, 0.2 μm filtered), 20 μl 500mM n-Acetylcysteine in ultrapure water (Merck A9165-5G), 20 μl murine EGF 50 $\mu\text{g/ml}$

in 0.1% BSA/PBS (ThermoFisher PMG8041, 0.2 μm filtered), 10 μl 5mM A83.01 in DMSO (HelloBio HB3218) and 2.5 μl HGF 10 $\mu\text{g}/\text{ml}$ in 0.1% BSA/PBS (PeproTech 100-39). In the first 7 days whilst deriving cultures, 20 μl of murine Noggin 50 $\mu\text{g}/\text{ml}$ in 0.1% BSA/PBS (PeproTech 250-38) was added for every 10 ml of ADTT++ media.

Media was sterile filtered using 0.2 μm syringe filter units at the start of each cell culture session. Antibiotics or antifungal agents were not used. Cultures were routinely tested for mycoplasma by PCR, every 3-4 passages, prior to first injection into mouse models or just before extraction of nucleic acids for sequencing experiments. All experiments were performed on cells at passage numbers no greater than 12. No contamination was found, but if it was all contaminated cultures and non-contaminated cultures within that experiment would be discarded.

For 2'3' cGAMP stimulation experiments, cells were plated at a density of 5000 cells per well and grown for 6 days. At day 6, media was aspirated, and fresh media applied. 24 hours later, media was removed and 2'3'cGAMP (InvivoGen tlrl-nacga23) in PBS to a final concentration of 10 $\mu\text{g}/\text{ml}$ or PBS vehicle, both in fresh media were applied. 48 hours after treatment, nucleic acids were extracted as detailed above. The volume of 2'3'cGAMP or PBS vehicle was kept constant across all conditions.

3.5 Statistical analyses

All statistical analyses were performed in R version 4.2.0 (Vigorous Calisthenics, R Foundation for Statistical Computing, Vienna, Austria), using the RStudio Server integrated development environment (community version 2023.03.0 build 386). For categorical data, data were summarised using counts and percentages. Differences in categorical variables were tested for using the Chi-square or Fisher's exact test (where any cross-tabulation cell counts were under 5).

For continuous data, the distribution of the data was plotted using histograms and density plots. Where continuous data followed a normal (Gaussian) distribution, data were summarised

using the arithmetic mean and standard deviation as measure of central tendency. Where continuous data did not follow a normal distribution, data were summarised using the median, alongside the 25th and 75th centiles. Differences between groups of continuous data, following the normal distribution were tested for using either a Student's T-Test (2 group comparisons), or a one-way Analysis of Variance (ANOVA, 2 or more groups). Where there was a large amount of data (>50 data points per group) and continuous data were distributed in a unimodal distribution, a Student's T-Test was used to test for differences across two groups (central limit theorem). For non-normal continuous data, Wilcoxon rank sum or Kruskal-Wallis tests were used. Where paired testing of continuous variables took place, either the Student's T-test (normally distributed data) or Wilcoxon signed rank (non-normal data) were used. The 95% confidence interval using centile methods (2.5th and 97.5th) was used as the measure of central tendency for comparative analyses.

For survival (time-to-event) analyses, data were first plotted using a Kaplan-Meier plot alongside numbers-at-risk tables. Survival time was presented as median survival time in days and difference in survival time tested using the log-rank test.

Statistical significance was taken at the two-tailed level of $P < 0.05$ for comparisons of less than 200 observations per group. For larger datasets and where multiple testing occurred statistical significance was taken at the two-tailed level of $P < 0.01$. Where P-value adjustments occurred, the Benjamini and Hochberg method was used. For general statistical analysis and data manipulation the R packages Tidyverse, ggplot2, ggsci, Finalfit, scales, purrr, Hmisc, survival and survminer were used.

Chapter 4

Development of immunotherapy
resistant and immunotherapy
responsive genetically engineered
mouse models of hepatocellular
carcinoma

4.1 Introduction

Inflammation plays a multifaceted role in the development of HCC and within the tumour microenvironment. This multifaceted role is intricately linked to immunotherapy response. Primary resistance to immunotherapy is understood to be mediated through either tumour epithelium intrinsic mechanisms, such as the expression of high levels of regulatory signalling molecules such as immune checkpoints, absence of antigenic peptides through either promoting genome stability or suppression of presentation machinery, immune exclusion, or resistance to effector immune cell responses (such as interferon gamma or granzyme B). Tumour cells may also directly or indirectly recruit immunosuppressive lineages to the microenvironment.

The latter is a major contributor to immunotherapy resistance in the inflamed HCC microenvironment along with expression of immune checkpoint molecules and presence of regulatory T-cells[74]. In inflamed HCC, sustained inflammation from aetiologies such as viral hepatitis infection or non-alcoholic steatohepatitis can promote oxidative stress, leading to recruitment of immune cell subsets (including neutrophils and autoaggressive CD8+ T-cells) which in turn exacerbate damage, leading to further PAMP/DAMP release thus triggering wound healing responses. Regulatory cells, including myeloid subsets, such as monocytes and M2-like polarised macrophages respond to these cues and are recruited to areas of inflammation to promote wound-healing. This is typically orchestrated by NF- κ B.

Continued, non-resolving cycles of oxidative damage then leads to immune cell exhaustion, where effector cells cannot mount effective cytotoxic responses toward cancer cells, thus leading to impaired function and promoting tumour formation. However, in the non-inflamed HCC microenvironment, absence of antigenic peptide presentation and immune exclusion through tumour-cell intrinsic genetics is proposed as the most likely mechanism of impaired anti-tumour immunity. These mechanisms of evading the immune system may also be acquired in response to immunotherapy, for example by acquiring a mutation that promotes immune exclusion[101]. Therefore, these mechanisms not only have major implications for increasing the efficacy of first-line therapies, but also for combination agents in both the first- and second-line setting.

Molecular studies of human HCC suggest high levels of canonical WNT/ β -Catenin signalling is associated with exclusion of T-cells from the tumour microenvironment[87]. To understand which signalling pathways may be contributing to this immune excluded phenotype, it would be useful to compare this immune-excluded model to one with an inflamed, immune infiltrated tumour microenvironment.

4.2 Hypothesis

- Lower numbers of infiltrating T-cells are likely to be present in subtypes of HCC which have genetic drivers associated with immunotherapy resistance ('immune exclusion').
- Combining genetic drivers of human HCC together, which are not members of the canonical WNT/ β -Catenin signalling pathway, will lead to the development of HCC models with inflamed tumour microenvironments which are sensitive to immune checkpoint inhibition.

4.3 Model development

4.3.1 Overview of Cre mediated recombination

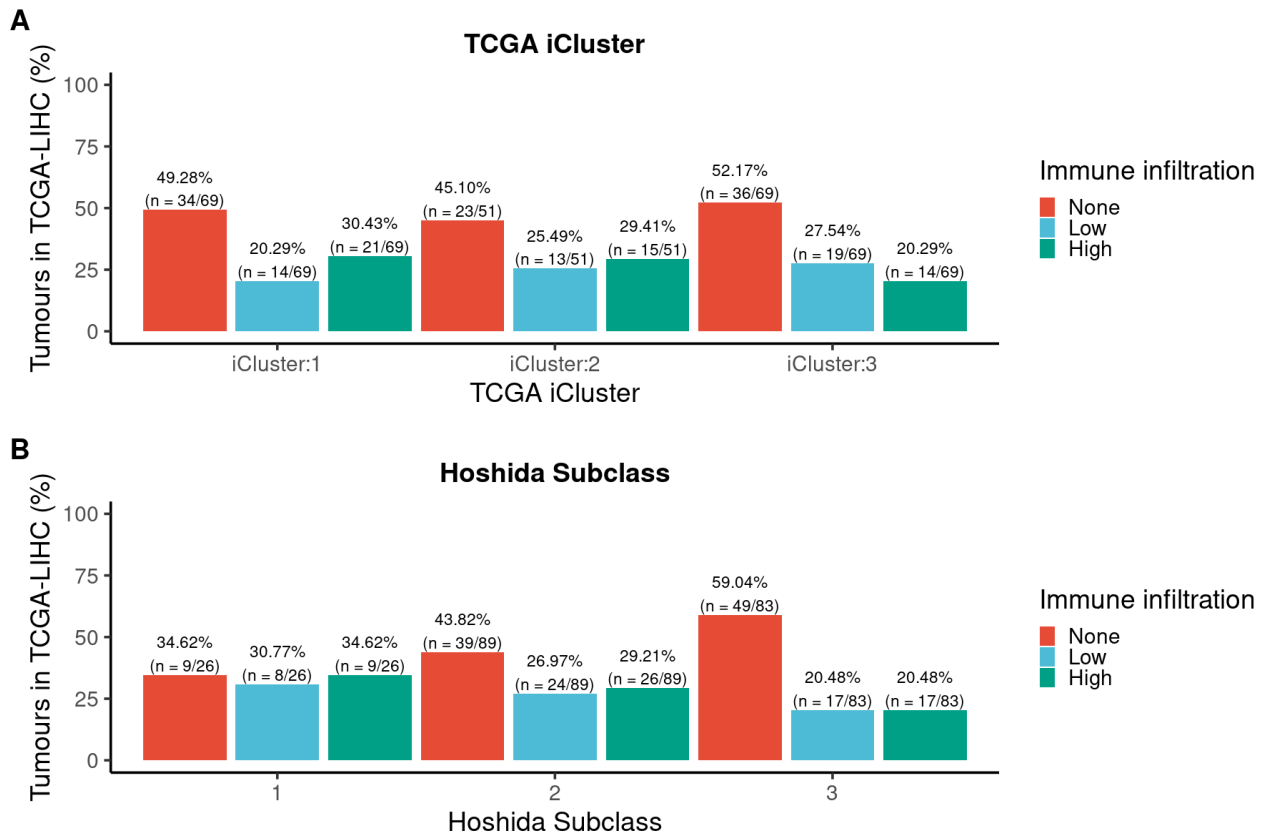
The conditional Cre-lox recombination system allows tissue-specific genetic engineering based upon two genetic elements derived from bacteriophage P1[98]. The first element is a Cre recombinase enzyme, which recognises hydroxyl group of the tyrosine residue on LoxP sites, allowing the recombinase to bind to targeted inserts known as 'LoxP' sequences. The recombinase then cuts the DNA at the specific LoxP sites and depending on the sequence and orientation of LoxP pairs, leads to the excision or inversion of the target sequence. By combining this approach with other genetic elements (such as overexpression, inducible promoters or 'STOP' cassettes) genes can be edited, mutated or overexpressed in a tissue-specific and even temporal manner in-vivo. This approach has been widely applied in murine experimental models particularly in cancer[97].

Although the HCC cell of origin is subject to ongoing scientific debate, it is broadly accepted that HCC can arise from hepatocyte lineages. To selectively induce transgene expression in hepatocytes, I used an adeno-associated virus serotype 8 vector, containing a thyroglobulin promoter driven Cre-recombinase payload (AAV8-TBG-Cre) to recombine these alleles in hepatocytes alone.

Adeno-associated viruses (AAV) are small viruses belonging to the *Parvoviridae* family. They are largely deemed to have limited pathogenicity, and with engineering of the virus to remove the *rep* and *cap* from the viral genome, can persist in an extrachromosomal state without integration into the host genome[126]. They are also able to infect both dividing and non-dividing cells. A further advantage of using AAV vectors is that they are replication deficient, minimally immunogenic, allowing repeat dosing of vector and avoiding vector-associated inflammation which may confound results[127].

The AAV8 serotype has a high tissue tropism to the liver, and the thyroglobulin expression has been well-characterised as nearly exclusively found in hepatocytes[126]. Combined, these two genetic elements provided a high level of specificity to target genetic recombination in hepatocytes[127]. In contrast to germline Cre promoters such as albumin Cre or albumin CreER, AAV8-TBG-Cre can be administered at any age so target alleles can be recombined in either adult or juvenile tissues. Furthermore, using a viral vector avoids toxicity or off-target 'leakiness' associated with chemical induced Cre expression (e.g. tetracyclines or tamoxifen in 'tet-on' or CreERT2 respectively), and can be titrated in such a way that delivers a specific number of particles per mouse to generate single-cell or whole-organ recombination. Previous work within the Bird laboratory has found that delivery of 6.4×10^8 genomic copies (GC) of AAV8-TBG-Cre results in clonal induction of hepatocytes across the liver (termed 'low dose') whereas delivery of 2×10^{11} GC results in recombination in most hepatocytes (termed 'high dose'). Both doses are highly liver and hepatocyte specific and are associated with minimal off target effects[127].

Figure 4.1: Immune infiltration in HCC patients in the Cancer Genome Atlas. Haematoxylin and Eosin-stained sections were reviewed by a consultant histopathologist (Dr Tim Kendall) and classified according to the amount of immune infiltrate present within them. Data is presented as percent (%) of each subtype by immune infiltration. TCGA iCluster 3 and Hoshida subclass S3 are found to be enriched for canonical WNT/ β -Catenin activation[20, 78]



The presence of anti-tumour immune cells, such as cytotoxic T-cells, within the tumour microenvironment is a well described prognostic factor and a key marker of response to immunotherapy. Exclusion of immune cells from the tumour microenvironment is also a key mechanism underpinning primary immunotherapy resistance. To identify which groups of patients were least likely to have immune infiltrated tumours, I compared levels of immune infiltrate present in different molecular subclasses of tumours within the Cancer Genome Atlas. Immune infiltrates were quantified by a consultant histopathologist (Dr Tim Kendall) who studied tumour haematoxylin and eosin sections and scored these. Figure 4.1 shows these findings, where the lowest levels of immune infiltration are present in patients who have disease characterised by activated canonical WNT/ β -Catenin signalling.

Given these findings, the strong association between activating CTNNB1 mutations and immune exclusion, and lack of immunotherapy response described in the literature, I opted to model the effects of activating β -Catenin mutations in a human-relevant model of immunotherapy resistant HCC.

Previous work in the Bird laboratory has established a conditional $Ctnnb1^{\text{exon3/Wt}}$ $Rosa26^{\text{c-MYC/c-MYC}}$ model of HCC using the Cre-lox recombination technique as described in the preceding section. Briefly, $Ctnnb1^{\text{exon3/Wt}}$ $Rosa26^{\text{c-MYC/c-MYC}}$ mice aged between 8 to 12 weeks of age are given 6.4×10^8 GC of AAV8-TBG-Cre via intravenous tail vein injection. This leads to allele recombination in a small proportion of hepatocytes throughout the liver. This clonal induction of hepatocytes then leads to the development of macroscopic tumours within 90 to 120 days of induction[75].

To confirm these tumours were immune excluded, sections from mice sampled at 140 days post induction were stained for the leukocyte marker CD45, the monocyte/macrophage marker F4/80, the lymphocyte marker CD3 and cytotoxic lymphocyte marker CD8 (figure 4.2). Besides some CD45 F4/80 positivity, there was a lack of immune infiltrate.

4.3.1.1 Function of β -Catenin and the canonical WNT signalling pathway

The WNT signalling pathways control a wide variety of cellular processes[128]. The canonical pathway controls gene transcription, the non-canonical planar cell polarity pathway regulates the cell cytoskeleton and mobility and the non-canonical calcium pathway controls calcium release from the endoplasmic reticulum. There is cross-talk across these pathways, however, the canonical pathway is the only pathway to involve β -Catenin as the main effector of gene transcription.

In HCC, up to 40% of people are found to have activating somatic mutation in β -Catenin and other members of the canonical WNT signalling pathway[20]. In health, the canonical WNT signalling pathway responds to extracellular signals from WNT proteins. These WNTs bind the lipoprotein receptor-related protein (LRP) and frizzled (FRZ) WNT receptor complex, which

leads to the receptor complex binding Axin through Dishevelled (DSH)[128, 129]. In the ‘WNT-off’ state, Axin forms a key component of the β -Catenin destruction complex. This complex phosphorylates serine motifs on β -Catenin, through Glycogen synthase kinase 3β which then allows the E3 ubiquitin ligase β -TrCP to tag β -Catenin for proteosomal degradation. These serine motifs are found in the 3rd exon and are frequently mutated in HCC. Therefore, these mutations render β -Catenin ‘undegradable’. Similar activation can occur upstream, in members of the β -Catenin destruction complex, such as AXIN1 mutations.

Accumulation of β -Catenin, either through WNT ligand signals or activating mutation, then allows increasing quantities to translocate into the nucleus and bind to β -Catenin co-factors such as TCF/LEF and BCL9/BCL9L which form complexes to activate transcription of target genes[128, 129]. This includes regulating cell cycle checkpoints and driving cell proliferation. The canonical WNT signalling pathway plays important roles in controlling gene expression and response to a variety of external stimuli. It has a major role in development, embryonic patterning, and maintenance of stem cell populations.

4.3.1.2 Function of c-MYC

The MYC family encompasses several basic helix-loop-helix (bHLH) and leucine zipper transcription factors, including c-MYC, n-MYC and l-MYC. c-MYC was the first to be discovered and is found to be frequently upregulated or amplified across a wide range of cancer types[130].

In health, c-MYC has major roles in regulating a wide range of cellular functions, including cell proliferation, maintaining stem-cell populations, response to injury and metabolism. c-MYC binds to enhancer (E-box) regions across the entire genome to regulate gene transcription. In cancer, c-MYC drives proliferation but also cooperates with a range of other oncogenes to enhance gene transcription governing other key cancer hallmarks, including immune evasion[112, 131].

4.3.2 Selection of genetic drivers for inflamed HCC model

As the Bird laboratory lacked a model of inflamed, immune checkpoint responsive HCC, a major objective of my PhD fellowship was to generate such a model to allow comparison of immunotherapy resistant and immunotherapy sensitive disease to help identify tractable therapeutic targets.

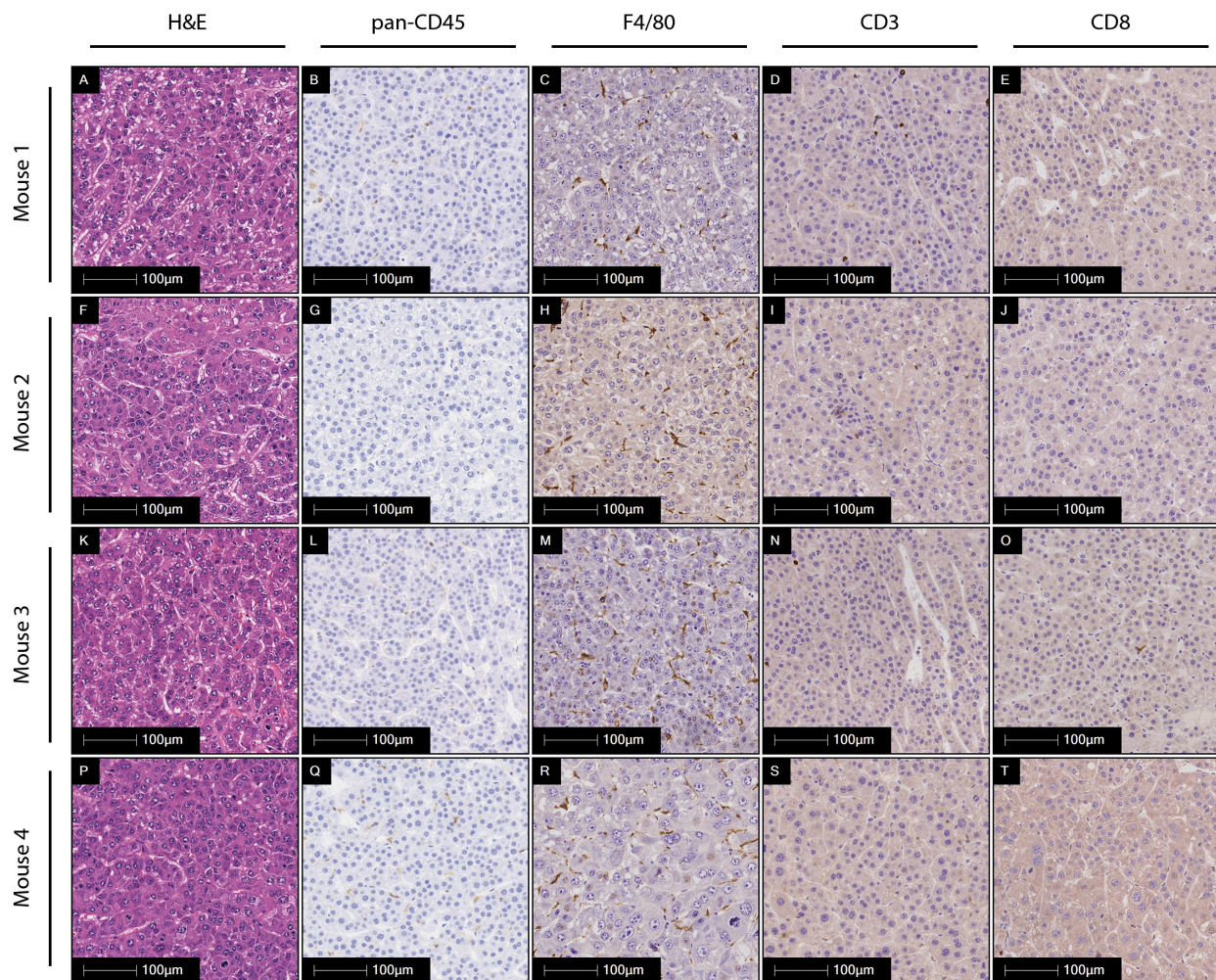
To identify the best strategy for establishing a model of HCC with an inflamed tumour microenvironment, I performed a literature review to find genetic drivers of HCC associated with inflamed tumour microenvironment in somatic human whole-exome and whole-genome HCC sequencing studies. I used data from patients with HCC in The Cancer Genome Atlas to identify the most frequent mutations.

To ensure an inflamed mouse model of HCC was of maximal relevance to human disease, the following criteria needed to be satisfied:

- Over 5% of people with HCC should have somatic mutation of this gene(s) or pathway.
- Conditional mouse models with this driver(s) or driver pathway should be readily available for study.
- Is associated with sensitivity to immune checkpoint blockade in human disease.
- Preferably be available on an inbred (C57BL/6J) background, to allow for syngeneic transplantation studies to be conducted.
- Reach endpoint disease within 200 days, so survival studies are feasible during a PhD fellowship.

Dietary and carcinogen induced models were not considered for two reasons. First, many of these models have been shown to induce a wide range of mutations, many of which are in putative cancer driver genes not usually found in human HCC. Second, by not relying on dietary models, this allows future studies of the interactions between tumour genetics and diet.

Figure 4.2: Overview of key immune populations in tumour regions of $Ctnnb1^{\text{exon3/Wt}}$ $Rosa26^{\text{c-MYC/c-MYC}}$ tumours. Haematoxylin and Eosin (H&E) alongside, pan-leukocyte CD45, F4/80 (monocyte/macrophage), pan-lymphocyte CD3 and CD8 immunohistochemical stains. All images acquired on Leica Aperio AT-2 at 20x magnification. Representative images from $n = 6$ mice at day 140 timepoint post AAV8-TBG-Cre.



Given there is no clear evidence that specific mutations are found in specific aetiologies of HCC, besides the relationship between TERT and TP53 in viral hepatitis (figure 4.3), dietary modification could be used in conjunction with a GEMM model to see how this may alter treatment responses in future experiments.

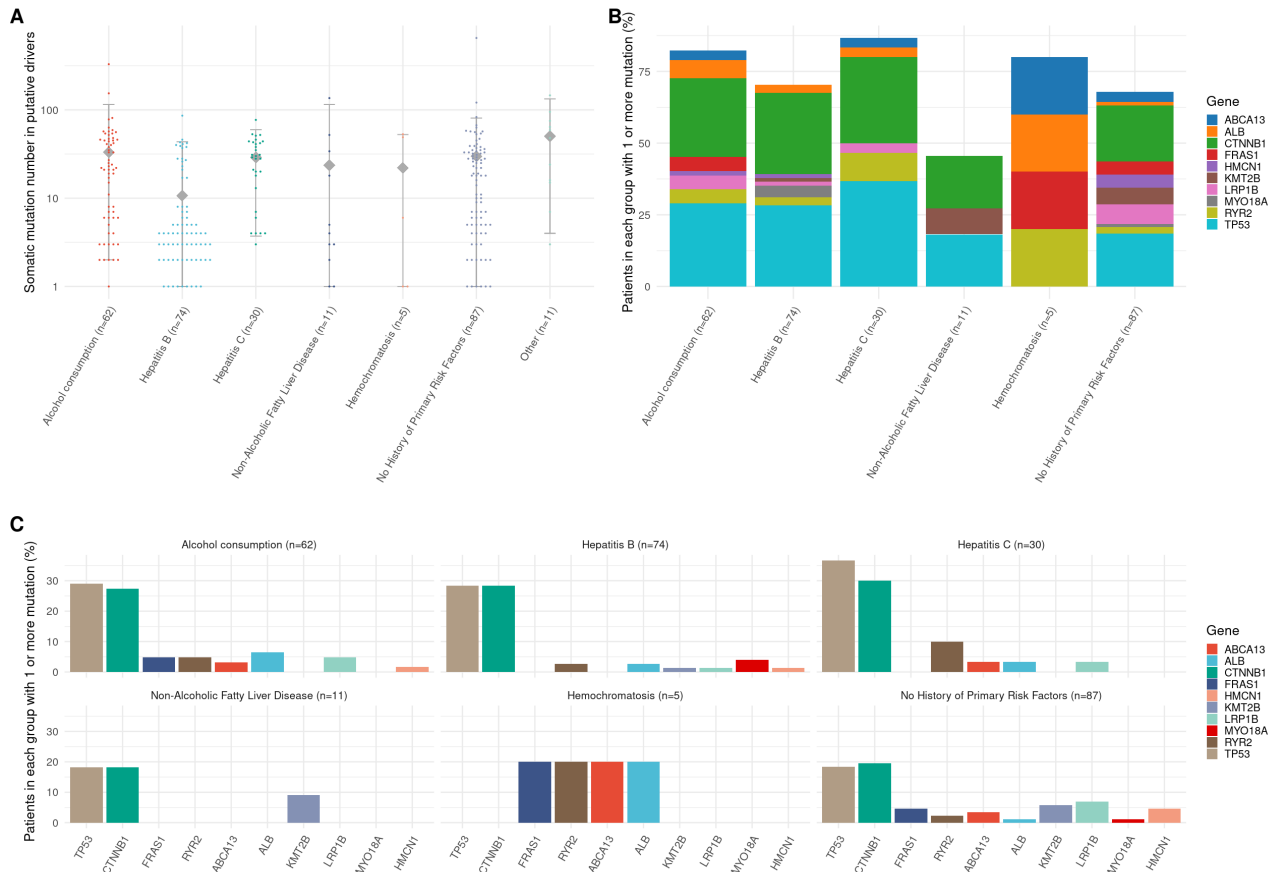
Table 4.1 below outlines the genes which met the above criteria and describes the feasibility of incorporating these into a mouse model of inflamed HCC.

From the identified list of candidate drivers and most frequent mutations present in TCGA-LIHC (figure 4.3), TP53 was one of the most frequently mutated genes. The TP53 tumour suppressor is the most frequently mutated gene in human cancers[132]. It plays a major role in regulating cell cycle progression, detection of DNA damage, directing DNA repair and subsequent apoptosis. In health, functional TP53 maintains genome stability and will promote apoptosis if DNA damage is irreparable, thereby eliminating potentially cancerous cells[133].

Loss of function or gain of deleterious mutations lead to TP53 dysfunction. This can range from deep deletion, thus removing a cells ability to detect potentially harmful mutations through to gain of function, where oncogenic TP53 isoforms can increase cancer cell fitness and help tumour cells adapt to their local microenvironment[32, 99].

Evidence from other solid tumours suggests TP53 mutations drive genome instability, generation of tumour neoantigens and an inflammatory tumour microenvironment. Different TP53 mutations have often disparate effects from one another and lead to both loss and gain of function of TP53[99]. Given the lack of available alleles for the most frequently mutated version of TP53 in human HCC, TP53^{R249S}, using a model of TP53 loss of function such as a conditional Trp53^{fl/fl} was the most appropriate choice. Mice with point mutations are available, including TP53^{R175H} (synonymous murine allele Trp53^{R172H}) or TP53^{R273H} (synonymous murine allele Trp53^{R270H}). However, given these point mutations are rarely found in human HCC and these alleles have been shown to have very different biological effects compared to TP53^{R249S}, these were deemed less appropriate choices[20].

Figure 4.3: Frequency of somatic mutations in TCGA-LIHC patient cohort by aetiology of liver disease. Panel A – Number of mutations found per putative driver gene. Panel B – Patients with one or more mutations in top 10 putative drivers by aetiology of liver disease. Panel C – Percentage of people within each aetiology group with mutations in top 10 putative driver genes as a side-by-side comparison.



Models which use homozygous Trp53 deletion have been reported to develop HCC with varied penetrance, or develop fully penetrant HCC in long timescales (up to 30 months)[104]. Heterozygous deletion of Trp53 has also been reported to not lead to tumourigenesis in the liver[104]. As a 30-month timeframe is not feasible for characterising a model of HCC and using it for future experiments within my PhD fellowship, it was clear conditional Trp53 deletion would need to be combined with a further genetic driver. Amplification of *c-MYC* or upregulation of *MYC* associated pathways commonly co-occurred with TP53 mutation[20]. Given a model of HCC with an inflamed tumour microenvironment would be compared to the immune excluded $Cttnb1^{exon3/Wt} Rosa26^{c-MYC/c-MYC}$ model, using *c-MYC* overexpression in a $Trp53^{fl/fl} Rosa26^{c-MYC/c-MYC}$ model would allow me to directly examine the effects of

Table 4.1: Selection of alleles for development of an immunotherapy responsive mouse model of HCC.

Genetic driver	Relevance of mutation in human HCC	Notes on disease modelling
TERT	Very high – Many HCC patients (up to 60%) are found to have somatic TERT promoter mutations or amplification[20, 21, 76, 77]	Murine and human TERT have alternative roles and regulatory sequences are not homologous[134] Would have to develop a conditional hybrid mouse/human TERT gene and develop a mouse model from this
TP53	High – Around 33% of HCC patients have somatic TP53 deletions or truncating mutations[20, 21] Other patients have a range of mutations, most commonly R249S point mutation	A wide range of mutant, including conditional Trp53 mouse models have already been developed, therefore allele would be readily available Some evidence these tumours are sensitive to anti-PD1 in-vivo[101] Trp53 ^{fl/fl} model results in deletion of exons 2 to 10, with minimal toxicity in non-recombined cells[111] Trp53 ^{R172H} are whole body mutants, which therefore affects all tissues, including immune cell lineages This mutant is rare in human HCC Trp53 ^{R270H} are available as conditional models but are rare in human HCC[20, 135] Trp53 ^{R246S} (synonymous to human R249S) are described as whole-body mutants This model is not readily available in commercial repositories or local research institutes Highly relevant to human disease as this is the most common TP53 mutation found in human disease and would require a new conditional mouse model to be made
RAS pathway	High – the RAS/ERK pathway is activated in over 50% of human HCC[20]	Mutations are spread along genes within this pathway, with few mutational hotspots, thus making it likely that these will respond to therapies in a heterogenous manner
Hepatitis B virus expression	Moderate – HBV infection causes large numbers of HCC cases worldwide Effective vaccine programme is in place, leading to this as a declining cause of HCC	Mutation of NRAS, HRAS or KRAS alone is relatively rare[20, 21] Likely to have an inflamed tumour microenvironment[136] Vaccination is a successful preventative measure already and is less relevant to emerging disease drivers i.e. NASH/NAFLD Major human health risks as some of these models express HBV DNA or require viral vectors, which can lead to hepatitis B virus infection in unvaccinated humans, making these animals high risk to handle
PTEN	Moderate – PTEN is found in 7% of human HCC[20, 21]	Conditional PTEN ^{fl/fl} mice are available commercially and within the research institute
RB1	Moderate – RB1 is found in around 10% of human HCC[20, 21]	PTEN loss has been shown to correlate with immune exclusion in human disease and therefore may not be the best choice to produce an immune infiltrated tumour model[137, 138] Conditional Rb ^{fl/fl} mice are commercially available It is unclear which genetic background they are available on, which risks the need for extensive backcrossing[111]
CDKN2A	High – silencing or deletion of CDKN2A is found in over 50% of human HCC[20, 139]	Loss of function of CDKN2A has been shown in other cancers to be associated with poor response to immunotherapy, which may suggest it is less likely to generate immune infiltrated tumours[140] Allele available within institute is CDKN2A/p16 constitutive knock-out affecting the whole-body CDKN2A is essential for normal immune cell function and mice have abnormal extramedullary haematopoiesis and develop lymphoma Therefore, for long-term modelling this would be unsuitable[141]

$Ctnnb1^{\text{exon3/Wt}}$, as both models would share identical c-MYC driver overexpression. An overview of the conditional strategy used to introduce liver-specific drivers is shown in figure 4.4.

4.3.3 Optimising the $\text{Trp53}^{\text{fl/fl}}$ $\text{Rosa26}^{\text{c-MYC/c-MYC}}$ mouse model

I crossed C57BL/6J mice with the $\text{Trp53}^{\text{fl/fl}}$ and $\text{Rosa26}^{\text{c-MYC/c-MYC}}$ alleles together and bred both alleles to homozygosity to generate experimental mice to test whether the $\text{Trp53}^{\text{fl/fl}}$ $\text{Rosa26}^{\text{c-MYC/c-MYC}}$ combination would firstly produce tumours and secondly to identify the optimal timeframe for this model.

To establish the optimal dose of AAV8-TBG-Cre, I conducted a series of experiments where $\text{Trp53}^{\text{fl/fl}}$ $\text{Rosa26}^{\text{c-MYC/c-MYC}}$ mice aged between 8 to 12 weeks were given either 6.4×10^8 GC (low), 5×10^9 GC (medium), 5×10^{10} GC (medium-high) or 2×10^{11} GC (high) of AAV8-TBG-Cre via IV tail vein injection. An overview of these experiments is shown in figure 4.5A. These doses were already used in the laboratory and were chosen so they would be comparable to other experiments in future. Mice were aged to 160 days post induction and were sampled to check for the presence of tumours. The optimal dose was selected according to the following criteria:

- 100% tumour penetrance at 160 days.
- Non-lesional liver tissue appears microscopically normal.
- Discrete, easily measurable macroscopic tumours to ensure reliable measurements for timepoint experiments.

Figure 4.4: Overview of conditional strategy used genetically engineered mouse model of hepatocellular carcinoma to introduce targeted mutations in hepatocytes. Here, the source of Cre-recombinase is an AAV8-TBG-Cre vector. Adeno-associated virus (AAV) serotype 8 has tropism for the liver. Cre recombinase is expressed under control of the thyroxine binding globulin (TBG) promoter, which increases hepatocyte-specificity. This AAV8-TBG-Cre also has an empty vector control, where the Cre recombinase is removed. This empty vector control is termed AAV8-TBG-Null. The $Trp53^{fl/fl}$ $Rosa26^{c-MYC/c-MYC}$ model is introduced later in this chapter.

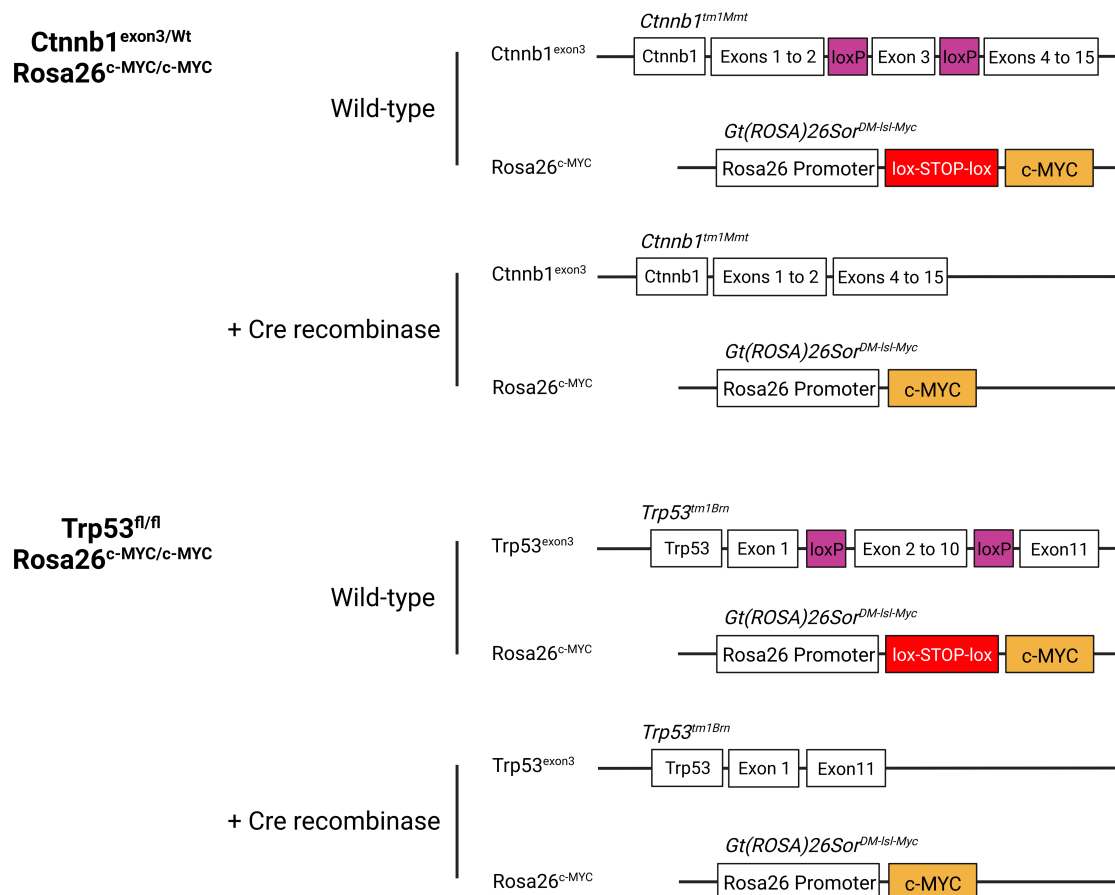


Figure 4.5 shows an overview of the experiments conducted to find the optimal AAV8-TBG-Cre dose, the penetrance of tumours in each dose group and the macroscopic appearance of the liver in the three highest penetrance doses. There was a clear dose response relationship, with the low dose (6.4×10^8 GC) resulting in tumours in only one mouse out of eight (12.5%) by 160 days and the high dose (2×10^{11} GC) leading to 100% penetrance ($n = 11$). Mice who received the highest dose were noted to have a macroscopically abnormal adjacent liver, compared with mice who received lower doses (figure 4.5C).

Microscopically, $\text{Trp53}^{\text{fl/fl}}$ $\text{Rosa26}^{\text{c-MYC/c-MYC}}$ tumours varied in histological, depending on the dose of AAV8-TBG-Cre vector received (figure 4.6). Low doses produced relatively well-differentiated tumours on H&E staining, whereas medium doses produced poorly differentiated tumours which were basophilic and did not readily resemble either epithelial morphology or adenocarcinoma. In the high and medium-high doses on H&E staining, tumours resembled moderately to poorly differentiated HCC. Compared with normal mouse liver and tumour from $\text{Ctnnb1}^{\text{exon3/Wt}}$ $\text{Rosa26}^{\text{c-MYC/c-MYC}}$ mice, $\text{Trp53}^{\text{fl/fl}}$ $\text{Rosa26}^{\text{c-MYC/c-MYC}}$ tumours tended to be arranged in a macrotrabecular pattern, with bizarre nuclei featuring marked pleomorphism and polyploidy. Tumour stroma content was more frequent than in $\text{Ctnnb1}^{\text{exon3/Wt}}$ $\text{Rosa26}^{\text{c-MYC/c-MYC}}$ tumours, and infiltration of leukocytes was also observed (figure 4.6 and figure 4.8). Heterogeneity in the microscopic appearance of tumours was clearly seen, even between separate tumours within the same mouse.

Next, to identify whether these tumours resembled HCC, rather than intrahepatic cholangiocarcinoma (iCCA), the markers SOX9 (progenitor-like marker), Keratin-19, Glutamine Synthetase (GS) and Ornithine Aminotransferase were stained for (OAT, figure 4.7). Both GS and OAT are canonical WNT/ β -Catenin target genes in the liver, therefore these could serve as markers of canonical WNT/ β -Catenin activity in these tumours. The majority of $\text{Trp53}^{\text{fl/fl}}$ $\text{Rosa26}^{\text{c-MYC/c-MYC}}$ tumours had high levels of expression of SOX9 and Keratin-19 staining was confined to normal ductal regions. Interestingly, there were several tumours in the medium-high group, across all the mice sampled, which had tumours that did stain positively for Keratin-19 and had a more glandular appearance in keeping with either

Figure 4.5: Optimising dose of AAV8-TBG-Cre vector in $Trp53^{fl/fl}$ $Rosa26^{c-MYC/c-MYC}$ model. Panel A – Experimental overview. Panel B – Tumour penetrance by dose. Panel C – Macroscopic images of medium (5×10^9 GC), medium-high (5×10^{10} GC) and high dose (2×10^{11} GC) – low dose (6.4×10^8 GC) not shown due to low penetrance. Representative macroscopic images from $n = 6$ in medium-high and high groups, medium dose $n = 2$.

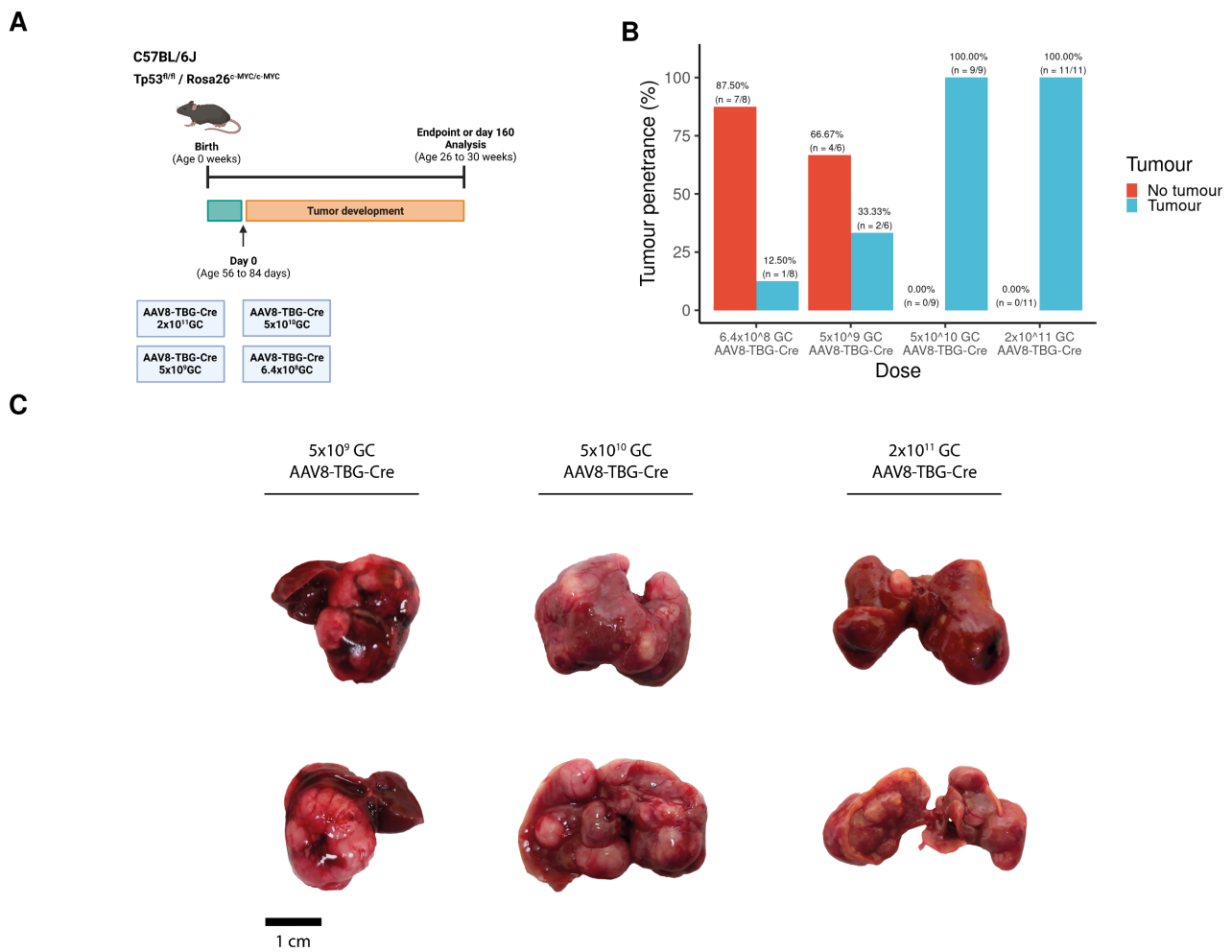


Figure 4.6: Haematoxylin and Eosin (H&E) stained sections from tumour and adjacent non-tumour regions in $\text{Trp53}^{\text{fl/fl}}$ $\text{Rosa26}^{\text{c-MYC/c-MYC}}$ mice induced with different doses of AAV8-TBG-Cre vector. Tumour penetrance increased with the number of genomic copies administered. Higher viral titres were accompanied by increasingly frequent abnormalities in non-tumour regions. Representative images from a minimum $n = 2$ mice per dose group at day 160 timepoint or clinical endpoint post AAV8-TBG-Cre.

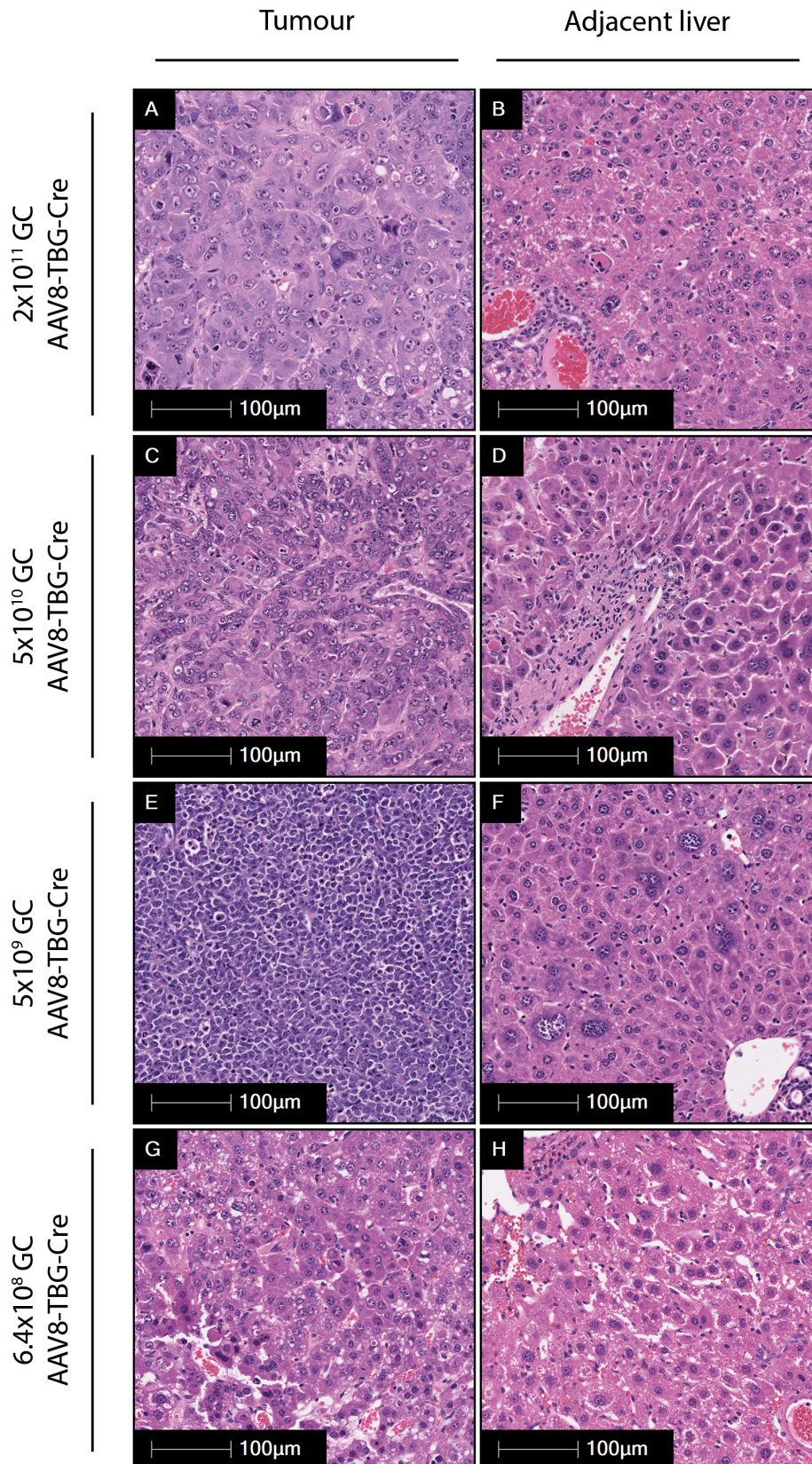
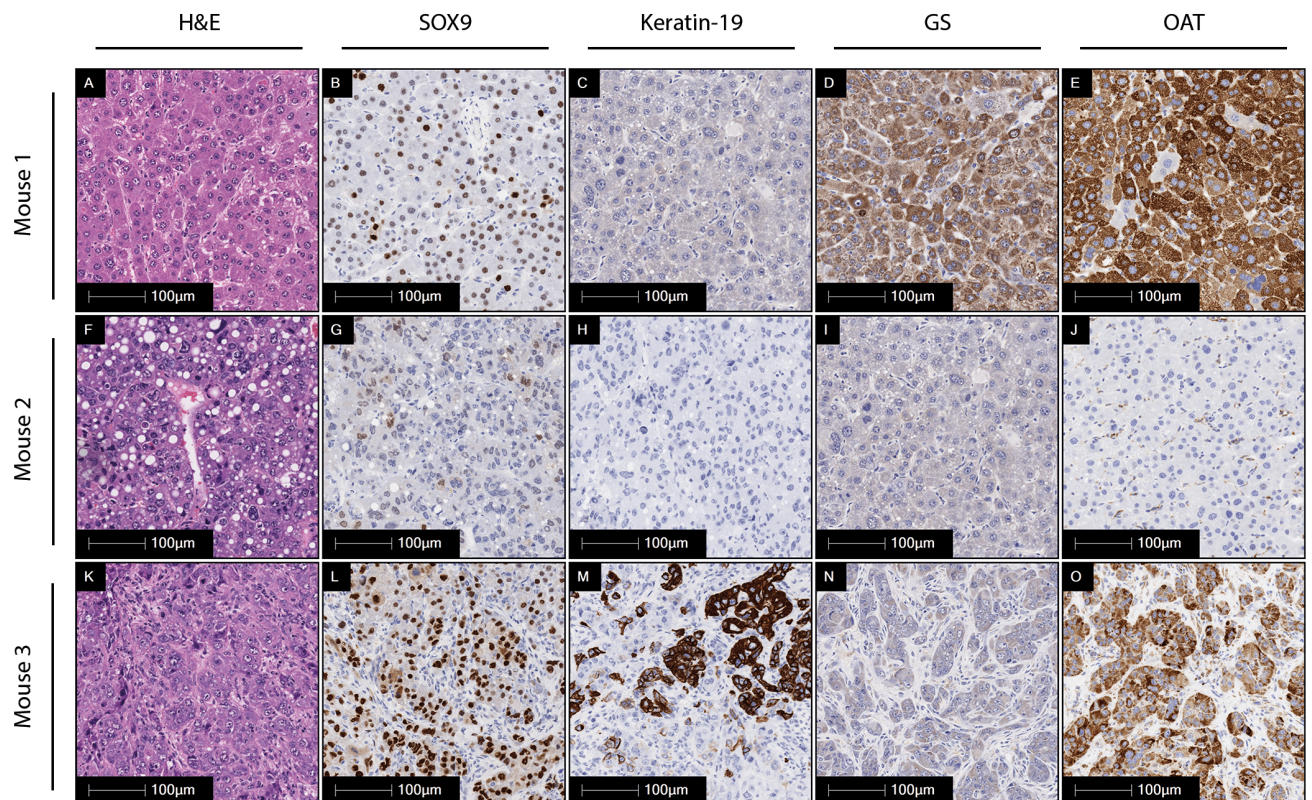


Figure 4.7: Overview of phenotypic biomarkers in tumour regions of $Trp53^{fl/fl}$ $Rosa26^{c-MYC/c-MYC}$ tumours. Haematoxylin and Eosin (H&E) alongside, SOX9, Keratin-19, Glutamine Synthetase (GS) and Ornithine Aminotransferase (OAT) immunohistochemical stains. All images acquired on Leica Aperio AT-2 at 20x magnification. Representative images from $n = 6$ mice at day 160 timepoint post AAV8-TBG-Cre.



combined HCC-iCCA or iCCA (figure 4.7, panel M). This may suggest a degree of cellular plasticity, either with hepatocytes differentiating into iCCA-like tumour cells or hepatocytes differentiating into cholangiocyte-like cells and subsequently into form tumours. Staining for GS and OAT revealed heterogeneity which was present both across mice and within the same mouse. Tumour cells which stained strongly positive for GS also stained strongly positive for OAT and had more well-differentiated appearance (figure 4.7, panel D and E). Some tumours did stain moderately or weakly positive for OAT, but negative for GS, suggesting varied degrees of canonical WNT/ β -Catenin pathway activation (figure 4.7, panel N and O). These tumours also appeared less well differentiated.

To assess immune infiltrate, slides were stained for the pan-leukocyte marker CD45, the monocyte/macrophage marker F4/80, the pan-lymphocyte marker CD3 and cytotoxic lymphocyte marker CD8 (figure 4.8). $\text{Trp53}^{\text{fl/fl}}$ $\text{Rosa26}^{\text{c-MYC/c-MYC}}$ tumours had pan-CD45 positive cells found throughout tumours, with strong staining in multiple areas for F4/80. In contrast to $\text{Ctnnb1}^{\text{exon3/Wt}}$ $\text{Rosa26}^{\text{c-MYC/c-MYC}}$ tumours, CD3+ cells were identified throughout $\text{Trp53}^{\text{fl/fl}}$ $\text{Rosa26}^{\text{c-MYC/c-MYC}}$ tumours, as were CD8+ cells.

As this experiment was staggered, with cohorts of mice receiving different AAV8-TBG-Cre doses as they became available for experiments, the high dose of AAV8-TBG-Cre (2×10^{11} GC) was first identified as producing fully penetrant tumours with immune infiltrate present. Therefore, this dose was selected for use in the subsequent experiments presented in this chapter. The medium-high (5×10^{10} GC) dose preserved more adjacent liver tissue and is therefore more optimal for future studies.

As these tumours had increased levels of T-cell infiltration and given that there is evidence in humans that systemic inflammatory markers are raised in inflammatory HCC, I studied the peripheral white-cell counts of these mice.

Figure 4.9 shows blood counts for white cells and relevant subpopulations from age and litter matched $\text{Trp53}^{\text{fl/fl}}$ $\text{Rosa26}^{\text{c-MYC/c-MYC}}$ mice who received either AAV8-TBG-Null (control) or AAV8-TBG-Cre (tumour bearing, both 2×10^{11} GC). Normal ranges from Jackson Laboratory physiological data summaries for the C57BL/6J strain were used to interpret the counts[142]. Tumour bearing $\text{Trp53}^{\text{fl/fl}}$ $\text{Rosa26}^{\text{c-MYC/c-MYC}}$ mice had significantly higher overall white cell counts (mean control 9.78 vs. tumour 16.91, $p = 0.029$), neutrophil counts (mean control 1.41 vs. tumour 3.60, $p = 0.012$) and monocyte counts (mean control 0.34 vs. tumour 1.26, $p = 0.019$). The neutrophil:lymphocyte ratio (NLR) has been shown in human disease to be negatively associated with response to immunotherapy[143], which may be interesting to investigate whether NLR has predictive power in this $\text{Trp53}^{\text{fl/fl}}$ $\text{Rosa26}^{\text{c-MYC/c-MYC}}$ model too.

Figure 4.8: Overview of key immune populations in tumour regions of $\text{Trp53}^{\text{fl/fl}}$ $\text{Rosa26}^{\text{c-MYC/c-MYC}}$ tumours. Haematoxylin and Eosin (H&E) alongside, pan-leukocyte CD45, F4/80 (monocyte/macrophage), pan-lymphocyte CD3 and CD8 immunohistochemical stains. All images acquired on Leica Aperio AT-2 at 20x magnification. Representative images from $n = 6$ mice at day 160 timepoint post AAV8-TBG-Cre.

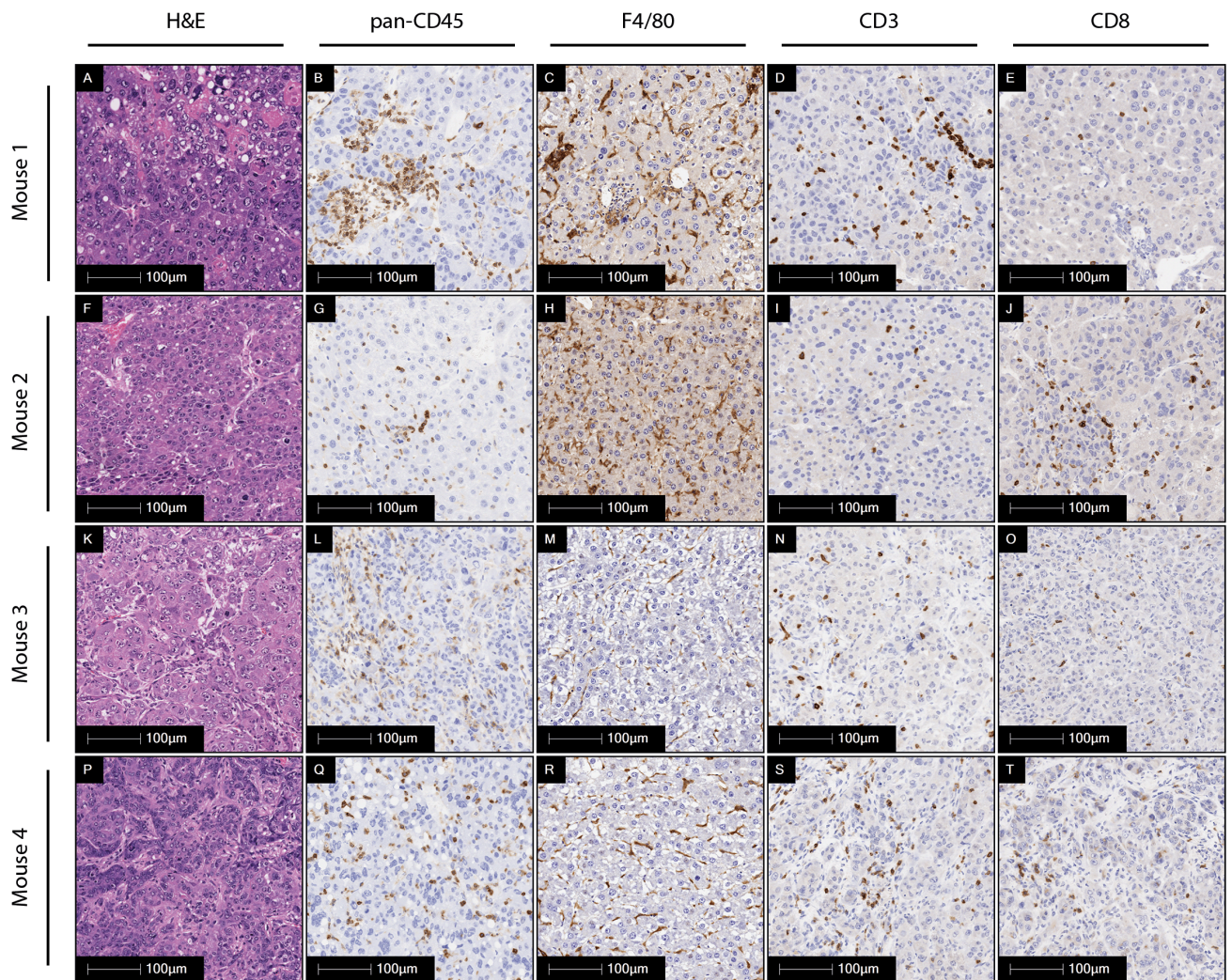


Figure 4.10 shows blood counts for white cells and relevant subpopulations from either $Ctnnb1^{\text{exon3/Wt}} Rosa26^{\text{c-MYC/c-MYC}}$ or $Trp53^{\text{fl/fl}} Rosa26^{\text{c-MYC/c-MYC}}$ tumour bearing mice. Compared with $Ctnnb1^{\text{exon3/Wt}} Rosa26^{\text{c-MYC/c-MYC}}$, $Trp53^{\text{fl/fl}} Rosa26^{\text{c-MYC/c-MYC}}$ tumour mice had significantly higher white cell counts (mean $Ctnnb1^{\text{exon3/Wt}} Rosa26^{\text{c-MYC/c-MYC}}$ 9.78 vs. $Trp53^{\text{fl/fl}} Rosa26^{\text{c-MYC/c-MYC}}$ 16.91, $p < 0.001$), lymphocyte counts (mean $Ctnnb1^{\text{exon3/Wt}} Rosa26^{\text{c-MYC/c-MYC}}$ 3.77 vs. $Trp53^{\text{fl/fl}} Rosa26^{\text{c-MYC/c-MYC}}$ 11.90, $p = 0.0014$), neutrophil counts (mean $Ctnnb1^{\text{exon3/Wt}} Rosa26^{\text{c-MYC/c-MYC}}$ 1.40 vs. $Trp53^{\text{fl/fl}} Rosa26^{\text{c-MYC/c-MYC}}$ 3.60, $p = 0.0013$) and monocyte counts (mean $Ctnnb1^{\text{exon3/Wt}} Rosa26^{\text{c-MYC/c-MYC}}$ 0.22 vs. $Trp53^{\text{fl/fl}} Rosa26^{\text{c-MYC/c-MYC}}$ 1.26, $p < 0.001$). This suggests that in addition to higher numbers of immune cells within tumour tissue in $Trp53^{\text{fl/fl}} Rosa26^{\text{c-MYC/c-MYC}}$ mice, there may be a systemic inflammatory response occurring in $Trp53^{\text{fl/fl}} Rosa26^{\text{c-MYC/c-MYC}}$ mice compared with $Ctnnb1^{\text{exon3/Wt}} Rosa26^{\text{c-MYC/c-MYC}}$ mice and in mice without tumours.

4.3.4 Response to immune checkpoint inhibition of $Trp53^{\text{fl/fl}} Rosa26^{\text{c-MYC/c-MYC}}$ mouse model

As $Trp53^{\text{fl/fl}} Rosa26^{\text{c-MYC/c-MYC}}$ tumours were found to be infiltrated with CD3+ and CD8+ T-cells, I next hypothesised that as these lymphocyte subsets were present in relative abundance these tumours would respond to immune checkpoint inhibition. Clinically, immune checkpoint inhibitors targeting PD1/PD-L1 interactions (i.e., Nivolumab and Pembrolizumab) are the most widely investigated for use in HCC[67, 69]. As this was at the time the most clinically relevant immune checkpoint therapy, I opted to examine whether anti-PD1 therapy would increase overall survival in mice with $Ctnnb1^{\text{exon3/Wt}} Rosa26^{\text{c-MYC/c-MYC}}$ or $Trp53^{\text{fl/fl}} Rosa26^{\text{c-MYC/c-MYC}}$ tumours. I hypothesised that due to the absence of immune infiltrate, $Ctnnb1^{\text{exon3/Wt}} Rosa26^{\text{c-MYC/c-MYC}}$ mice would not respond to therapy, whereas survival would be extended in mice with $Trp53^{\text{fl/fl}} Rosa26^{\text{c-MYC/c-MYC}}$ tumours.

Figure 4.9: Comparison of systemic blood counts from tumour bearing $\text{Trp53}^{\text{fl/fl}}$ $\text{Rosa26}^{\text{c-MYC/c-MYC}}$ mice ($n = 9$) versus age matched empty vector (AAV8-TBG-Null) controls ($n = 5$). $\text{Trp53}^{\text{fl/fl}}$ $\text{Rosa26}^{\text{c-MYC/c-MYC}}$ mice had significantly higher white cell counts (panel A), neutrophil counts (panel C) and monocyte counts (panel D) and non-significantly higher lymphocyte counts (panel B), compared to age matched empty vector controls. Normal reference white cell count for 26-week-old male C57BL/6J mouse is $5.2 \text{ K}/\mu\text{l}$, lymphocyte count $4.39 \text{ K}/\mu\text{l}$, neutrophil count $0.47 \text{ K}/\mu\text{l}$ and monocyte count $0.25 \text{ K}/\mu\text{l}$ [142]. Tests are Wilcoxon rank sum. Black diamond is arithmetic mean average. Error bars are mean \pm 95% confidence interval.

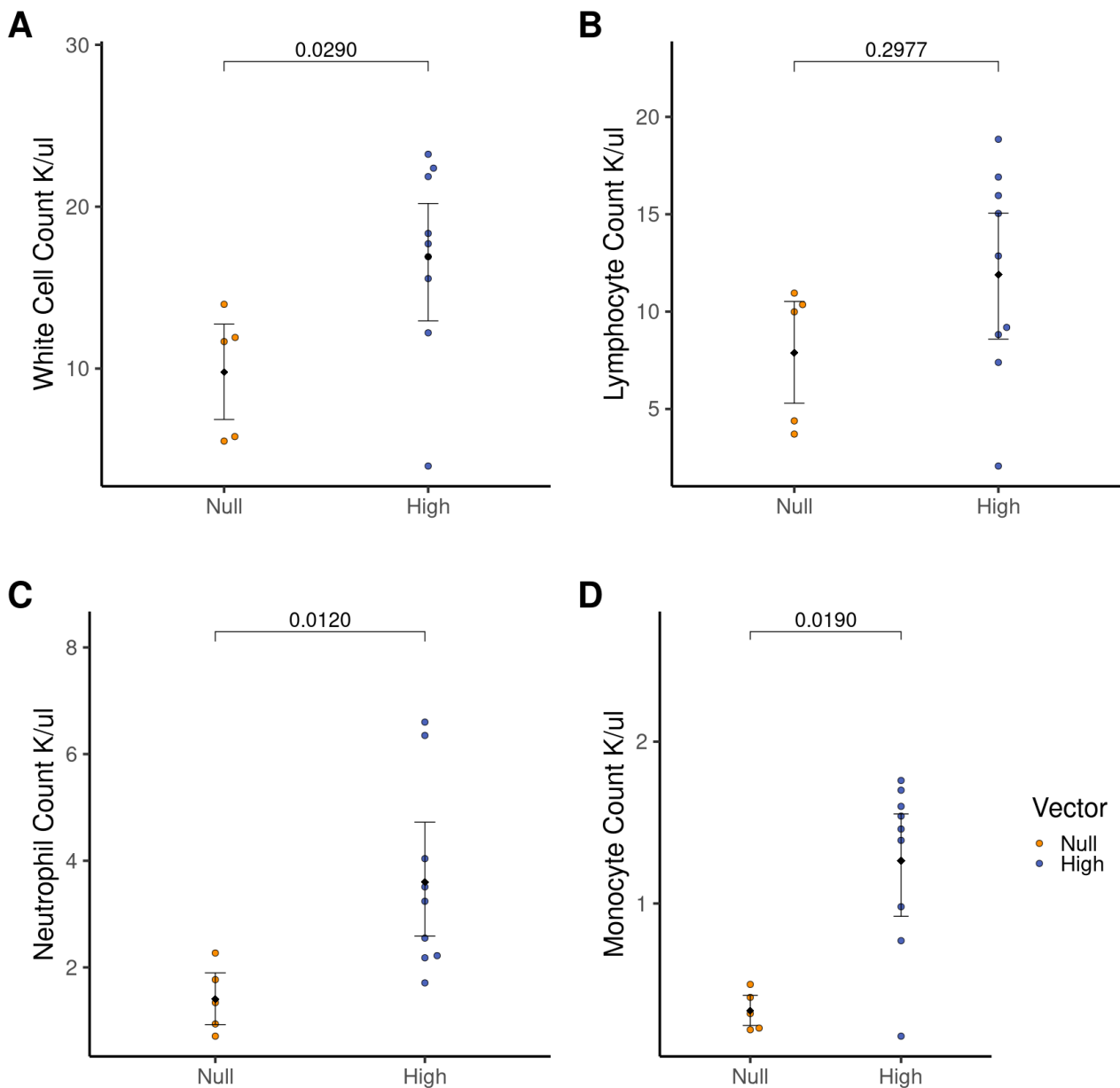


Figure 4.10: Comparison of systemic blood counts from tumour bearing $Cttnb1^{exon3/Wt}$ $Rosa26^{c-MYC/c-MYC}$ ($n = 13$) and $Trp53^{fl/fl}$ $Rosa26^{c-MYC/c-MYC}$ mice ($n = 9$). Blood sampled by intracardiac puncture using same technique and needle size. $Trp53^{fl/fl}$ $Rosa26^{c-MYC/c-MYC}$ mice had significantly higher white cell counts (panel A), lymphocyte counts (panel B), neutrophil counts (panel C) and monocyte counts (panel D) compared to $Cttnb1^{exon3/Wt}$ $Rosa26^{c-MYC/c-MYC}$ mice. Normal reference white cell count for 26-week-old male C57BL/6J mouse is 5.2 $K/\mu l$, lymphocyte count 4.39 $K/\mu l$, neutrophil count 0.47 $K/\mu l$ and monocyte count 0.25 $K/\mu l$ [142]. Tests are Wilcoxon rank sum. Black diamond is arithmetic mean average. Error bars are mean \pm 95% confidence interval.

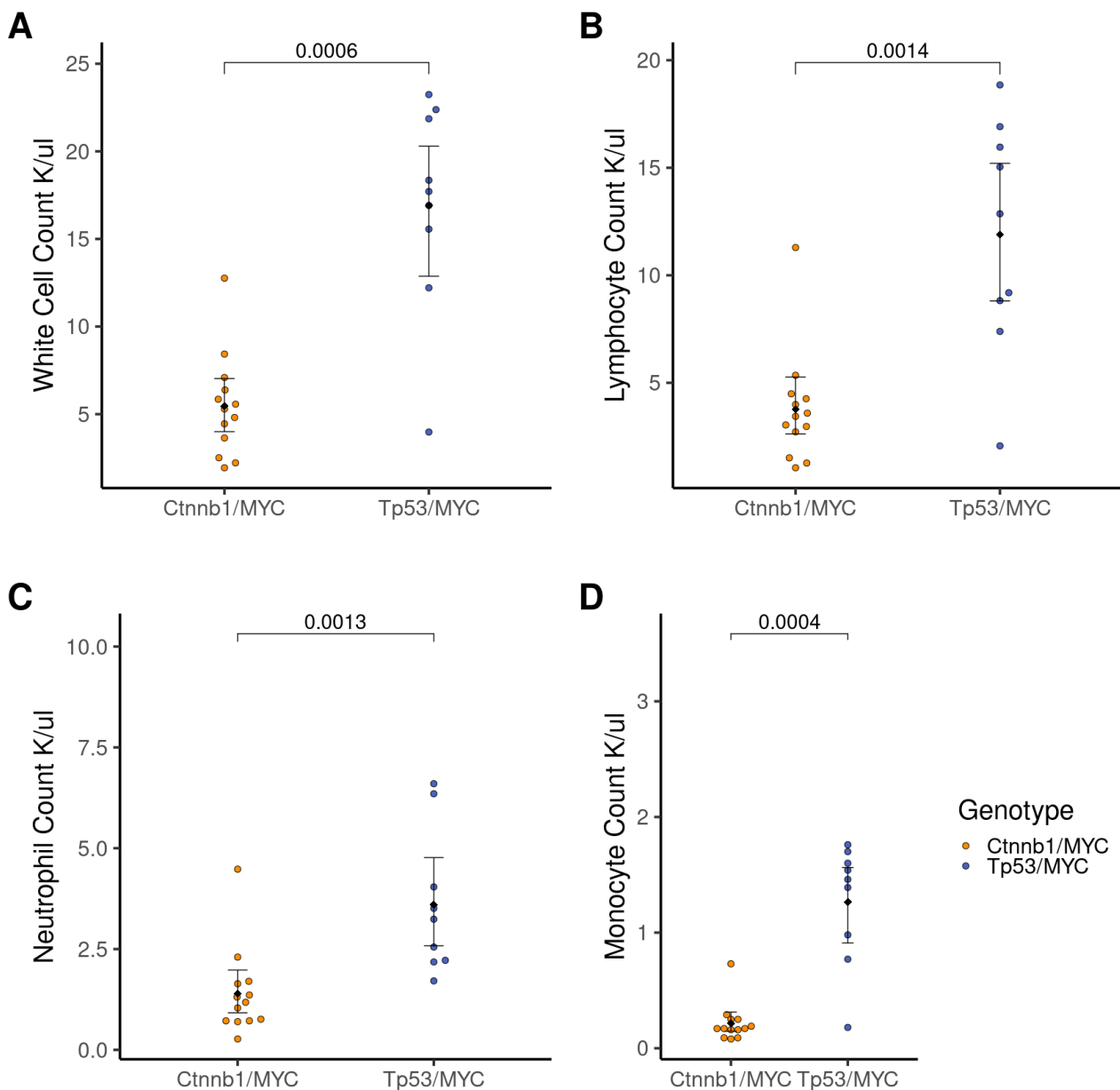
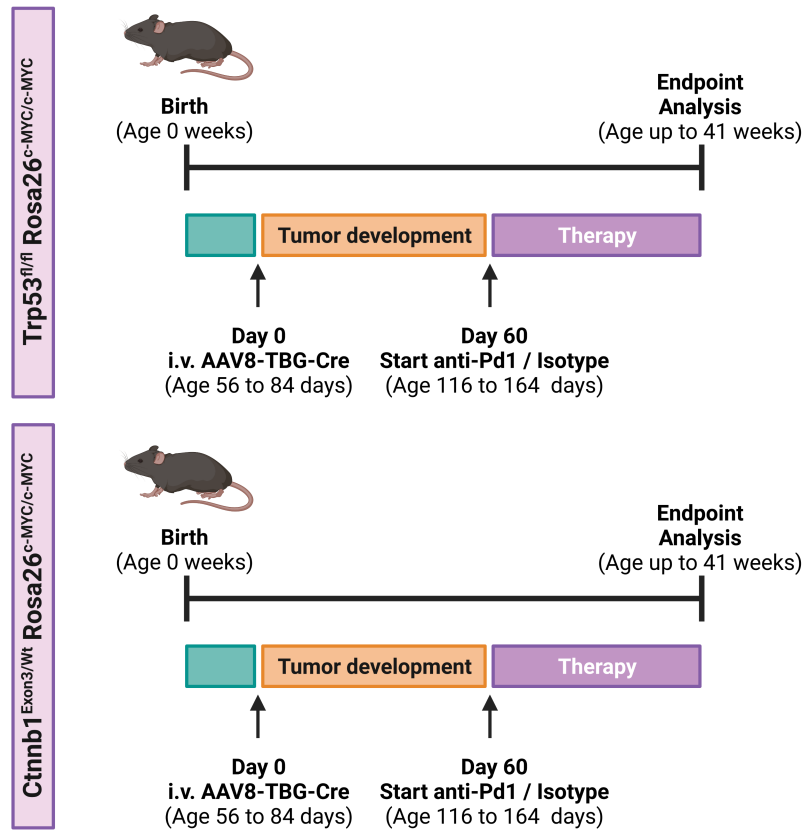


Figure 4.11: Overview of anti-PD1 experiment. $Cttnb1^{\text{exon3/Wt}} \text{ Rosa26}^{\text{c-MYC/c-MYC}}$ ($n = 16$) and $\text{Trp53}^{\text{fl/fl}} \text{ Rosa26}^{\text{c-MYC/c-MYC}}$ mice ($n = 17$) mice were induced with AAV8-TBG-Cre (6.4×10^8 GC for $Cttnb1^{\text{exon3/Wt}} \text{ Rosa26}^{\text{c-MYC/c-MYC}}$ mice and 2×10^{11} GC for $\text{Trp53}^{\text{fl/fl}} \text{ Rosa26}^{\text{c-MYC/c-MYC}}$ mice) and subsequently randomised within litter and cage to receive anti-PD1 or IgG Isotype control from day 60 post induction. Mice were killed when they reached clinical endpoint defined by conditions in Home Office license.

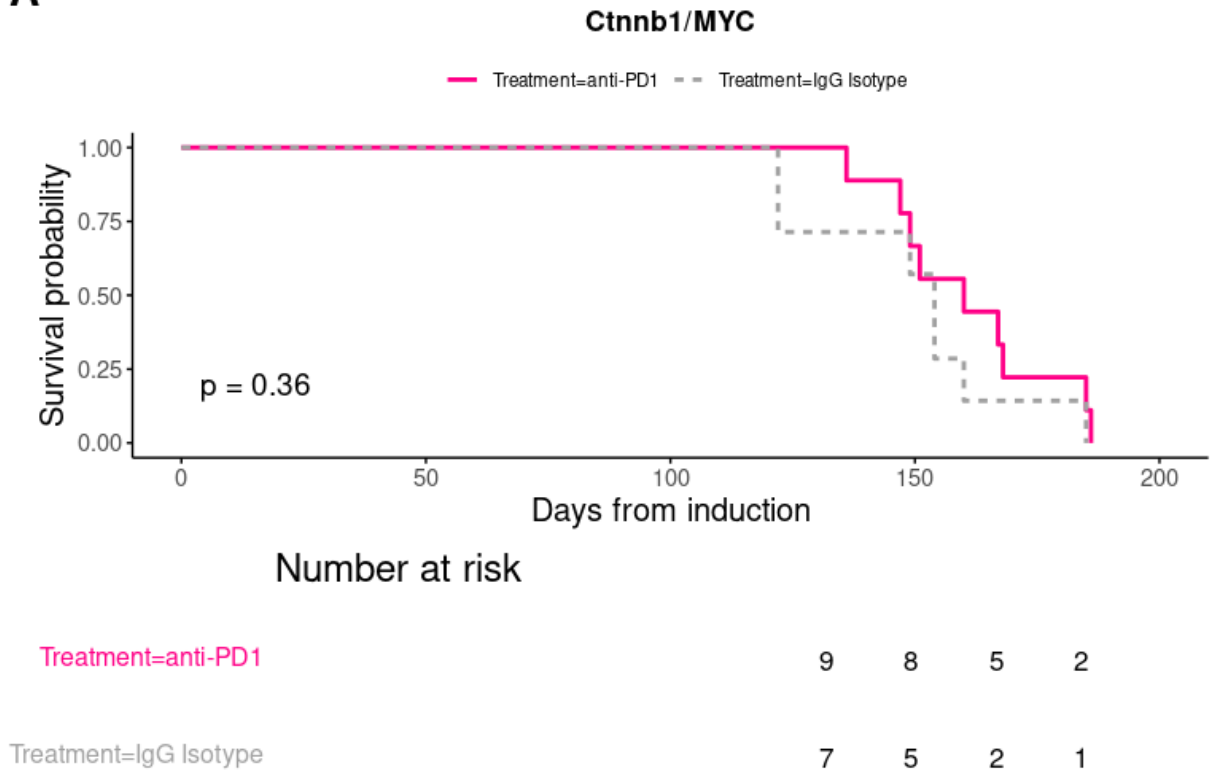


Mice who had received the appropriate dose of AAV8-TBG-Cre (6.4×10^8 GC for $Cttnb1^{\text{exon3/Wt}} \text{ Rosa26}^{\text{c-MYC/c-MYC}}$ or 2×10^{11} GC for $\text{Trp53}^{\text{fl/fl}} \text{ Rosa26}^{\text{c-MYC/c-MYC}}$) were randomised within litters to receive either 200 μg of anti-PD1 (Biologend RMP1-14 clone) or 200 μg of IgG2a isotype control (Biologend RTK2758 clone) twice weekly via intraperitoneal (i.p.) injection, starting 60 days after AAV8-TBG-Cre administration. Isotype control was used to control for any non-specific effects of anti-PD1 antibody therapy. Mice were sampled at endpoint where they displayed signs of being unwell which included reduced mobility, piloerection, any sign of distress, feet palor or signs of internal bleeding as defined within the Home Office project license. An overview of this experiment is shown in figure 4.11.

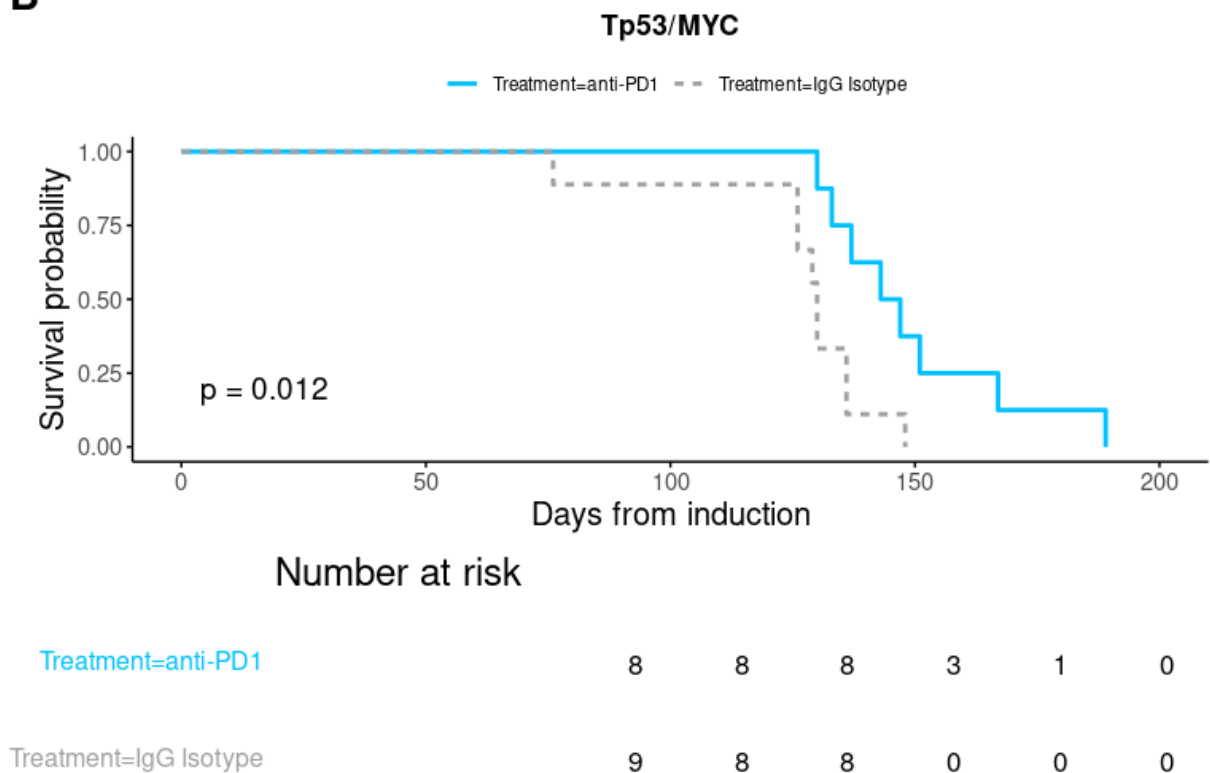
Treatment with anti-PD1 did not significantly extend overall survival in $Cttnb1^{\text{exon3/Wt}}$

Figure 4.12: Overall survival for endpoint anti-PD1 study in *Ctnnb1^{exon3/Wt} Rosa26^{c-MYC/c-MYC}* (n = 16, median overall survival anti-PD1; 160 days, isotype; 154 days, panel A) compared with *Trp53^{fl/fl} Rosa26^{c-MYC/c-MYC}* (n = 17, median overall survival anti-PD1; 145 days, isotype; 130 days, panel B) mouse models. Mice were killed when they reached clinical endpoint defined by conditions in Home Office license. Statistical tests are log-rank.

A



B



Rosa26^{c-MYC/c-MYC} mice (figure 4.12). However, in Trp53^{fl/fl} Rosa26^{c-MYC/c-MYC} mice, anti-PD1 therapy significantly increased overall survival by just over 2 weeks compared to isotype control. Although this is suggestive of response, it was not durable and did not result in complete responses. However, this provides an opportunity to use to model acquired immunotherapy resistance and identify how tumours evolve in response to anti-PD1 therapy.

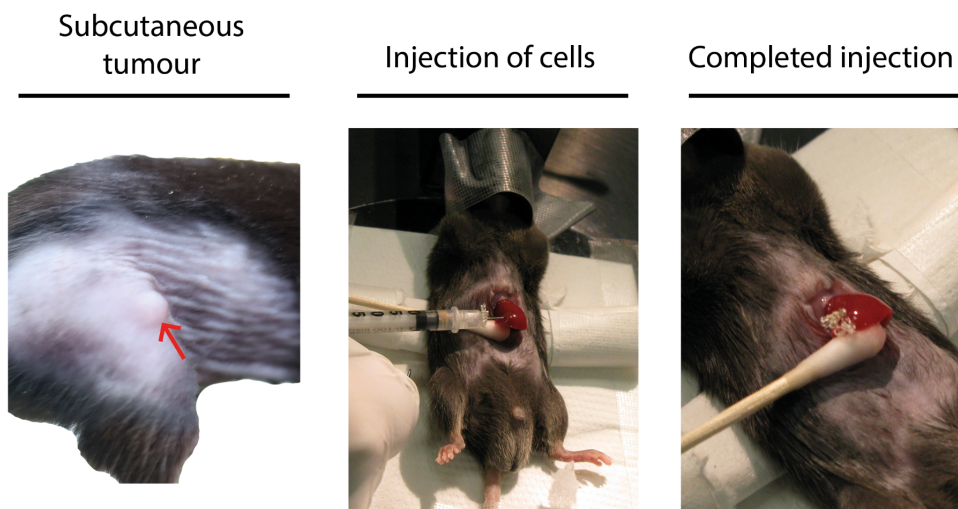
4.3.5 Generating a genetically defined orthotopic transplantation model

Given Trp53^{fl/fl} Rosa26^{c-MYC/c-MYC} tumours are sensitive to immunotherapy, I aimed to leverage this model system to identify new therapeutic combinations which enhance the effectiveness of anti-PD1 immune checkpoint blockade. As Trp53^{fl/fl} Rosa26^{c-MYC/c-MYC} tumours take at least 120 days to develop and require genetically modified mice, orthotopic transplantation may be a more rapid approach to testing new therapies *in-vivo*.

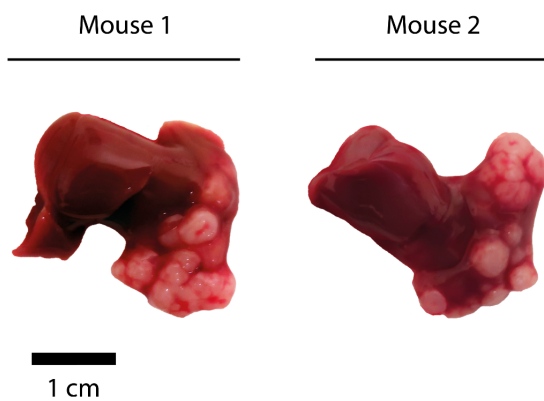
The common murine syngeneic orthotopic HCC transplantation models are the Hepa1-6 and Hep53.4 cell lines. Both are derived from C57 strains and allow unifocal HCC to be produced by orthotopic injection of cells into the liver of C57 inbred strains. Transplantation models allow experiments to be performed rapidly, without the requirement for time consuming breeding and backcrossing. These models also have a major advantage of permitting cell-line manipulation *in-vitro* prior to transplantation.

Figure 4.13: Generating an immunotherapy responsive orthotopic transplantation model from $\text{Trp53}^{\text{fl/fl}}$ $\text{Rosa26}^{\text{c-MYC/c-MYC}}$ tumours. Panel A – Using subcutaneous and orthotopic injection to ‘passage’ cells in-vivo to increase engraftment rates. Panel B – macroscopic appearance of tumours 30 days after orthotopic injection. Panel C – This model retains sensitivity to anti-PD1 therapy. Mice were injected with 1 million cells in 10 μl Matrigel, then 2 weeks later randomised to receive IgG isotype or anti-PD1. Mice were sampled 2 weeks after commencing anti-PD1 therapy.

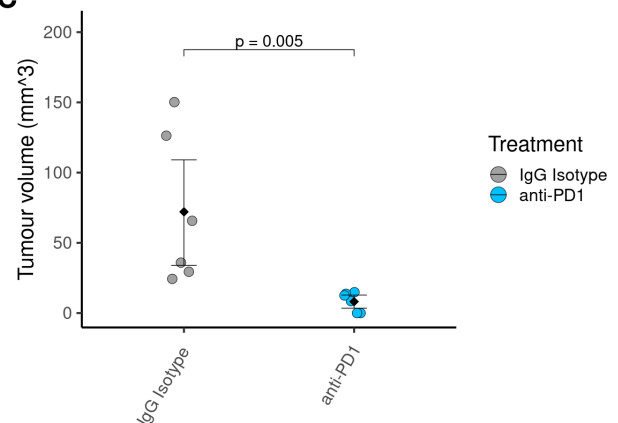
A



B



C

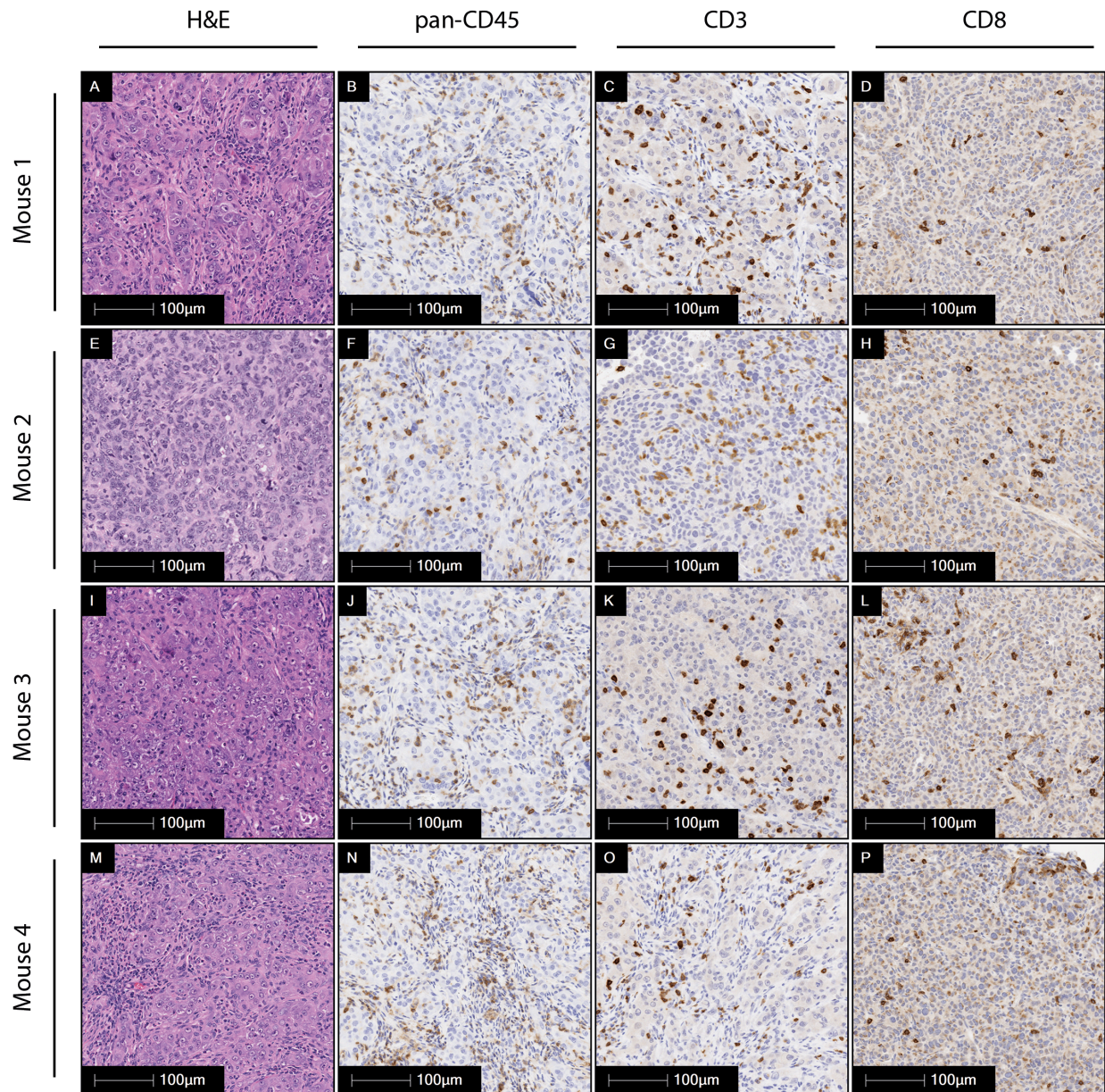


Hepa1-6 lines were originally reported in 1980, isolated from a serially transplantable BW7756 mouse hepatoma tumour which arose spontaneously in C57L/J mice[93]. The mutational burden of this line is poorly characterised in the literature and, therefore, it is unknown whether Hepa1-6 lines have shared genetic drivers with human HCC[144]. A further drawback of this line is the relatively low engraftment rate. This is poorly reported in the literature but may be as low as 0% 30 days after injection[144]. With poor engraftment rates comes the requirement to transplant large numbers of animals and use imaging to confirm the presence of tumours prior to commencing therapeutic studies. Therefore, application as a useful transplant model of HCC is limited due to uncharacterised genetic drivers, ethical considerations for animal welfare and impractical requirements for therapeutic testing.

The Hep53.4 line has a much higher engraftment rate, reported in the literature at around 100%, addressing the practical and ethical shortcomings of the Hepa1-6 line. Hep53.4 originates from a liver tumour arising in a C57BL/6J mouse who received a single dose of the chemical carcinogen Diethylnitrosamine (DEN) at 15 days of age[92]. The original publication reported Hep53.4 to be a Trp53 wild-type cell line. Besides this original publication there is a paucity of evidence describing the driven mutations contained in this line. The Hep53.4 line along with other DEN induced HCC models have high levels of genomic instability and mutations in putative HCC driver genes which are not usually found to be mutated in humans[103].

Given HCC is a global health problem, I opted to produce an in-vitro model which could be cultured relatively inexpensively and would be more accessible for investigators to use in lower resource settings. To do this, I isolated tumour cells from a male Trp53^{fl/fl} Rosa26^{c-MYC/c-MYC} mouse 100 days post induction and attempted to grow them in monolayer cell culture, as organoid culture is not readily compatible with high-throughput culture and depends on the availability of expensive reagents. These cells grew well in a defined low-serum medium as described in the methods section. 5 million cells were then injected subcutaneously into the flanks of C57BL/6J wild-type mice and given 6 weeks to engraft. Of these mice, one (25%, n= 1/4) developed a tumour. Tumour cells were expanded from this tumour in-vitro and were injected into the livers of 5 C57BL/6J wild-type mice (1 million cells per mouse). Three (60%,

Figure 4.14: Overview of key immune populations in tumour regions of orthotopic transplant model, derived from $\text{Trp53}^{\text{fl/fl}}$ $\text{Rosa26}^{\text{c-MYC/c-MYC}}$ tumours. Haematoxylin and Eosin (H&E) alongside pan CD45, CD3, and CD8 immunohistochemical stains. All images acquired on Leica Aperio AT-2 at 20x magnification. Representative images from $n = 4$ mice at day 30 timepoint post injection.



n= 3/5) developed a tumour and cells from one of these tumours was again expanded in-vitro to give a cell line with a 100% orthotopic engraftment rate (n = 12/12).

At 30 days after transplantation of 1 million cells from this optimised line (figure 4.13), macroscopically visible, discrete liver tumours were present. These tumours shared some of the histological features of the autochthonous $\text{Trp53}^{\text{fl/fl}}$ $\text{Rosa26}^{\text{c-MYC/c-MYC}}$ GEMM, with a degree of trabecular structure and bizarre nuclei. In keeping with the autochthonous model, these tumours were found to be infiltrated with immune cells, including the presence of CD3+ and CD8+ T-cells (figure 4.14). This immune infiltrate was more homogenous and more frequent than in the autochthonous GEMM. To verify the orthotopic model recapitulated sensitivity to anti-PD1 therapy, I randomised 12 mice to receive 2 weeks of anti-PD1 or IgG isotype 2 weeks after orthotopic injection of 1 million cells. Anti-PD1 was at an identical dose, route, and schedule to anti-PD1 in the autochthonous model. Figure 4.13C demonstrates that following anti-PD1, tumour volume was significantly reduced using this GEMM derived line in the immunocompetent orthotopic setting compared to isotype treated control mice.

4.4 Summary

Guided by molecular characterisation studies of human disease, I have developed a model of HCC with a T-cell infiltrated tumour microenvironment. At a high and medium-high dose of AAV8-TBG-Cre vector, tumour penetrance was 100% within 160 days, which allows for experiments to be performed in adult mice within a practical timeframe. Full penetrance also negates the requirement to guided therapy commencement by preclinical imaging. The $\text{Trp53}^{\text{fl/fl}}$ $\text{Rosa26}^{\text{c-MYC/c-MYC}}$ model has features of systemic inflammation as demonstrated by raised peripheral white cell counts, which are not found in age-matched $\text{Trp53}^{\text{fl/fl}}$ $\text{Rosa26}^{\text{c-MYC/c-MYC}}$ empty vector control (AAV8-TBG-Null) or in $\text{Ctnnb1}^{\text{exon3/Wt}}$ $\text{Rosa26}^{\text{c-MYC/c-MYC}}$ tumour bearing mice. Using the high dose model, which has intratumoural immune infiltration, I demonstrate that anti-PD1 therapy significantly extends survival in tumour bearing $\text{Trp53}^{\text{fl/fl}}$ $\text{Rosa26}^{\text{c-MYC/c-MYC}}$ mice.

Sensitivity of this model to anti-PD1 therapy is in line with previous reports in the literature.

Ruiz de Galarreta et al. have described a Trp53^{-/-} MYC model, where Trp53 was deleted using a CRISPR-Cas9 and c-MYC overexpressed using transposase-based expression using a hydrodynamic tail vein injection system (HDTV). In this study they identified that Trp53^{-/-} MYC models responded to anti-PD1 therapy, but this led to the selection of tumour cells with activated β -Catenin which were then able to escape the effects of immune checkpoint blockade. In contrast to this HDTV model, my Trp53^{fl/fl} Rosa26^{c-MYC/c-MYC} model has a genetically defined dosage of Trp53 and c-MYC, and does not rely on delivery via HDTV, a process that can be highly varied. This variable level of overexpression often results in extremely high and non-physiological levels of gene expression[94]. Furthermore, the system utilised by *de Galarreta et al.*[101] simultaneously expressed three model antigens to achieve sensitivity to anti-PD1 therapy (SIYRYYGL (SIY), SIINFEKL (SIN; OVA257-264), and OVA323-339), in addition to luciferase which is also immunogenic[145]. Therefore, this system may have more limited relevance to clinical disease, where such model neoantigens are absent. Although the effect of anti-PD1 in my Trp53^{fl/fl} Rosa26^{c-MYC/c-MYC} model was relatively modest (median 15 days additional survival with treatment) it provides a strong basis to test combination therapies which can be tested to extend overall survival further. In humans, TP53 mutation has also been associated with infiltration of T-cells and high expression of immune checkpoints.

To maximise the utility of this model and allow in-vitro manipulation of these cells for applications such as high-throughput screens, I successfully developed an orthotopic Trp53^{fl/fl} Rosa26^{c-MYC/c-MYC} transplantation model. This model recapitulated the histological appearance and responsiveness to anti-PD1 therapy observed in the autochthonous GEMM. This is also the first genetically defined, immunocompetent murine transplantation model of HCC, which could be replicated across different HCC molecular subtypes to build a more comprehensive and rapid means of testing novel therapies in-vitro and in-vivo. By using the same process used to derive this line, it would be possible to treat Trp53^{fl/fl} Rosa26^{c-MYC/c-MYC} mice with anti-PD1 and sample cells from a resistant tumour and produce models of acquired immunotherapy resistance. This would also help to recapitulate the more heterogeneous anti-PD1 responses seen in the GEMM, rather than the homogenous near complete responses seen in the Trp53^{fl/fl} Rosa26^{c-MYC/c-MYC} orthotopic model.

There are several limitations of the genetically engineered models presented in this chapter which must be considered. First, these models do not have any background of liver disease. Liver disease is present in nearly every patient with HCC and is the single biggest risk-factor for the development of HCC. Different aetiologies are likely to impact the arising tumour immune microenvironment and studying these comprehensively would be out of the scope of this thesis. Second, I opted to compare the $Ctnnb1^{\text{exon3/Wt}}$ $Rosa26^{\text{c-MYC/c-MYC}}$ model with the $Trp53^{\text{fl/fl}}$ $Rosa26^{\text{c-MYC/c-MYC}}$ model. An alternative comparison would have been to compare $Ctnnb1^{\text{exon3/Wt}}$ $Trp53^{\text{fl/fl}}$ $Rosa26^{\text{c-MYC/c-MYC}}$ with the $Trp53^{\text{fl/fl}}$ $Rosa26^{\text{c-MYC/c-MYC}}$ model. This latter comparison would strengthen my comparisons by allowing me to study the effect of adding in $Ctnnb1^{\text{exon3/Wt}}$, and how this alters the $Trp53^{\text{fl/fl}}$ $Rosa26^{\text{c-MYC/c-MYC}}$ phenotype. In previous experiments in the Bird laboratory, $Ctnnb1^{\text{exon3/Wt}}$ $Trp53^{\text{fl/fl}}$ $Rosa26^{\text{c-MYC/c-MYC}}$ mice have a rapid onset of tumour burden with the lower dose of AAV-Cre. Direct comparison with the $Trp53^{\text{fl/fl}}$ $Rosa26^{\text{c-MYC/c-MYC}}$ model would therefore be challenging and would require comparison at different timepoints. Furthermore, $Ctnnb1^{\text{exon3/Wt}}$ may act as a more 'dominant' driver of carcinogenesis, producing a different tumour microenvironment to one found in $Trp53^{\text{fl/fl}}$ $Rosa26^{\text{c-MYC/c-MYC}}$ entirely, thus limiting this comparison. A better experiment would be to 'add-in' mutant β -Catenin into established $Trp53^{\text{fl/fl}}$ $Rosa26^{\text{c-MYC/c-MYC}}$ tumours. A tetracycline controlled system for doing this is shown in chapter 7. Finally, the conditional genetics present in these systems combines human c-MYC with endogenous human mutations. There may be specific interactions between human c-MYC, human β -Catenin and human TP53 mutations which cannot be recapitulated in these systems due to incompatibility across species.

4.5 Future directions

- In contrast to clonal induction models used previously within the Bird laboratory, the $Trp53^{\text{fl/fl}}$ $Rosa26^{\text{c-MYC/c-MYC}}$ model had a low penetrance of tumours using a low-dose AAV8-TBG-Cre clonal induction strategy. Increasing doses of AAV8-TBG-Cre resulted in higher levels of tumour penetrance, suggesting that cells with $Trp53$ deletion and c-MYC overexpression, may require further genetic 'hits' to drive tumour formation.

Whole exome and transcriptome sequencing may help to identify additional mutations or signalling pathways which may be implicated in the malignant transformation of these cells.

- Given the higher AAV8-TBG-Cre doses required to induce reliable tumour formation, it would be interesting to see whether other microenvironment modifications affect this. This could be done by modifying the liver microenvironment using agents such as carbon tetrachloride to induce fibrosis, or high-fat diets to induce a NASH-style phenotype (american lifestyle induced obesity diet[106] or modified western diet[105]). If higher tumour penetrance rates are seen, or fully penetrant tumour models are accelerated, it may suggest that these exposures predispose cells to developing further tumorigenic mutations or support the survival of cancer initiating $\text{Trp53}^{\text{fl/fl}}$ $\text{Rosa26}^{\text{c-MYC/c-MYC}}$ cells.
- Given the effect of age on immune response and sexual dimorphism, it would be interesting to see whether anti-PD1 therapy response was maintained in older mice or in females[146, 147]. Ensuring experimental design includes both sexes is important, not only for reducing cancer inequalities but also to identify whether sex can act as a response biomarker or identify new aspects of biology.
- Although tumour penetrance was equivalent in mice receiving high and medium high dose of AAV8-TBG-Cre vector, animals who received medium-high dose had more healthy-looking adjacent background liver. As the medium-high model took longer to develop than the high model, I did not have time to test whether the medium-high model is also sensitive to anti-PD1 therapy. It would be interesting to establish whether a higher proportion of normal epithelium improves responses or if this extends survival. This is important as in humans HCC is unifocal or multifocal and does not result in almost 100% of the liver parenchyma being comprised of tumour tissue, which is a disadvantage of these GEMMs. Given the use of anti-angiogenic therapies and evidence that normal and tumour tissues are different in how they permit immune cell trafficking across endothelium, this is likely to be an important aspect of disease to model.

- Having developed a transplantable Trp53^{fl/fl} Rosa26^{c-MYC/c-MYC} model, it would be interesting to know whether addition of drivers known to be associated with immune checkpoint resistance reverses sensitivity of these lines to anti-PD1. This would provide a means to identify mechanisms of how RAS/RTK or canonical Wnt/ β -Catenin pathway activity may lead to therapy resistance and identify novel immunotherapeutic targets. To do this, whole exome and transcriptome sequencing could be used to comprehensively characterise the model and compare it to other GEMMs and transplantable cell lines.
- I have shown it is possible to directly use genetically engineered mouse models to generate cell lines which subsequently recapitulate the microscopic appearance and immunotherapeutic sensitivity of the parent model. It would, therefore, be useful to generate orthotopic transplant models from a variety of other genetically engineered models, including immunotherapy resistant models. This would allow subtype-specific responses to therapy to be investigated.
- As orthotopic cells can be manipulated in-vivo and injected into a defined area of the liver, it would be useful to introduce non-invasive reporters into these lines to monitor response to therapy or target gene activity. This could include near-infrared fluorescent proteins or luminescent reporters (i.e. firefly luciferase).

Chapter 5

Multimic analysis of hepatocellular carcinoma models to identify pathways associated with immune exclusion

5.1 Introduction

Multiple tumour-cell intrinsic signalling pathways have been associated with immune exclusion in the tumour microenvironment. Several studies across a range of cancer types including colorectal, melanoma, hepatocellular carcinoma and pancreatic cancer have shown specific tumour-cell intrinsic genetic drivers promote an immune excluded phenotype. These genetic drivers primarily include KRAS, PTEN and mutations in the Wnt/ β -Catenin signalling pathway[88, 137, 148]. Mutations in these pathways have been broadly shown to act, at least in part, through impairing cytokine expression in tumour cells, thus preventing the recruitment of effector cell populations, antigen-presenting cells or skewing intratumoural immune cell populations toward a tolerogenic axis. These pathways typically suppress cytokine signalling either directly or through pathways including PI3K, TGF β , NF- κ B and MAPK, which can be in turn modulated using small molecule agonists or antagonists to promote immune cell recruitment to the tumour microenvironment[149–151].

The mouse models of HCC which I have developed in chapter 4 allow comparison between immune excluded and immune infiltrated form of the tumour. These models are based upon commonly found genetic drivers of human disease and demonstrated differential response to anti-PD1 immune checkpoint therapy. Therefore, I set about comprehensively characterising the molecular differences and similarities across these models. By signalling pathways using multiple ‘omic’ technologies, it is possible to use computational methods to identify potential mechanisms responsible for orchestrating immunity within the tumour microenvironment.

I opted to focus on using approaches to understand how gene expression is regulated from DNA. Therefore, I decided to combine exome sequencing, RNA sequencing and ATAC sequencing, as these were most likely to provide me with information on how gene expression was regulated and potential drug targets. Undertaking this at the single-cell level would have allowed me to capture information around heterogeneity and focus my analysis on different cell populations, however this comes at very high cost, so I opted to perform these experiments using bulk material in the first instance. This would allow me to identify whether

there were major differences and follow up my findings using single-cell technologies in future.

5.2 Hypothesis

- Immune infiltrated tumours display increased expression of pathways known to be associated with inflammatory responses compared with immune excluded tumours.
- These pathways will include immune checkpoints and cytokine pathways, some of which may be tractable therapeutic targets in immune-cold tumours.

5.3 Whole exome sequencing

I have shown combinations of $Ctnnb1^{\text{exon3/Wt}}$, $Trp53^{\text{fl/fl}}$ and $Rosa26^{\text{c-MYC/c-MYC}}$ lead to the development of HCC in mice in chapter 4, however, it is unclear whether these genes are solely responsible for initiation of cancer, or if acquired mutations also help to promote tumorigenesis. Acquired mutations may have a profound impact on the tumour immune microenvironment, promoting immune exclusion or inflammation. Similarly, acquired mutations could arise at random, or be related to the underlying genetic drivers present.

To understand this, I performed an experiment where mice with $Ctnnb1^{\text{exon3/Wt}}$ $Rosa26^{\text{c-MYC/c-MYC}}$ or $Trp53^{\text{fl/fl}}$ $Rosa26^{\text{c-MYC/c-MYC}}$ genotypes were block randomised to receive model optimised doses of AAV8-TBG-Cre or AAV8-TBG-Null via intravenous tail vein injection at between 8 to 12 weeks of age (defined as day 0, 5.1A). Mice were randomised within litters and returned to the same cages after administration of virus, so each treatment group had litter and cage mate controls. At 125 days after induction mice were sampled. This time point was selected as across discrete, macroscopic tumours are present in both $Ctnnb1^{\text{exon3/Wt}}$ $Rosa26^{\text{c-MYC/c-MYC}}$ and $Trp53^{\text{fl/fl}}$ $Rosa26^{\text{c-MYC/c-MYC}}$ at this timepoint, with adequate tissue to be frozen for downstream assays. Fresh frozen tissue was snap frozen on dry ice within 5 minutes of death. Mice in tumour (AAV8-TBG-Cre) and normal tissue (AAV8-TBG-Null) groups were sampled alternately to avoid potential confounding from time of day.

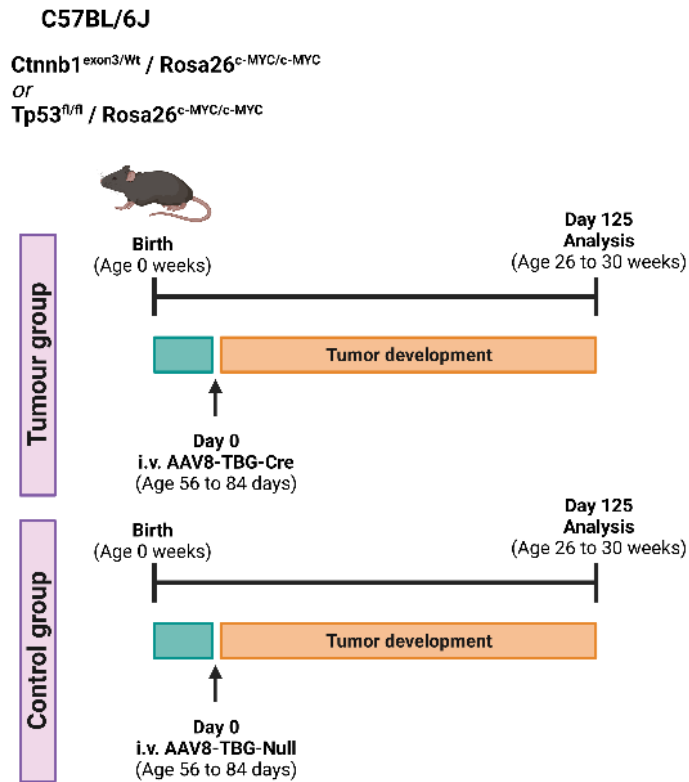
Tissue from tumour or normal liver was then homogenised on liquid nitrogen to create a fine powder and genomic DNA extracted (figure 5.1B). All analyses in this chapter are from the same samples of tissue processed in this manner. Whole-exome libraries were prepared from this DNA in a single batch and deep sequenced at a coverage of around 1000X. Sequences were then aligned to the Ensembl v102 GRCm38 mouse genome with a Burrows-Wheeler Aligner, SNPs identified by Mutect2, and copy-number variants called using ExonDepth[117, 119, 120]. All experiments described in this chapter were performed on tissue that was extracted in the same way, to ensure the multiple ‘omics’ captured the same part of the whole tumour, rather than different samples within it.

For exome sequencing, I sequenced a total of 22 tumours and 6 normal matched livers from 20 individual mice. All mice used were male as HCC in humans has a male preponderance, but also that within the PhD resources and timeframe, repeating the experiment in females would be challenging. Ensuring equality across sexes is important, particularly in biological research, therefore this work should be repeated in females and results across both sexes compared. 5 were $Ctnnb1^{\text{exon3/Wt}} \text{ Rosa26}^{\text{c-MYC/c-MYC}}$ who received AAV8-TBG-Cre, 3 were $Ctnnb1^{\text{exon3/Wt}} \text{ Rosa26}^{\text{c-MYC/c-MYC}}$ who received AAV8-TBG-Null, 17 were $\text{Trp53}^{\text{fl/fl}} \text{ Rosa26}^{\text{c-MYC/c-MYC}}$ who received AAV8-TBG-Cre and 3 were $\text{Trp53}^{\text{fl/fl}} \text{ Rosa26}^{\text{c-MYC/c-MYC}}$ who received AAV8-TBG-Null. The 17 $\text{Trp53}^{\text{fl/fl}} \text{ Rosa26}^{\text{c-MYC/c-MYC}}$ tumours were obtained from 9 individual mice, to enable characterisation of tumour heterogeneity in this model. In the following analysis, the data is analysed per tumour, rather than per mouse to demonstrate any potential tumour heterogeneity. Analysing one tumour per mouse would result in discarding data and having to select which tumour is deemed to be the most representative, or pooling tumours from the same mouse together, both of which may hide useful information.

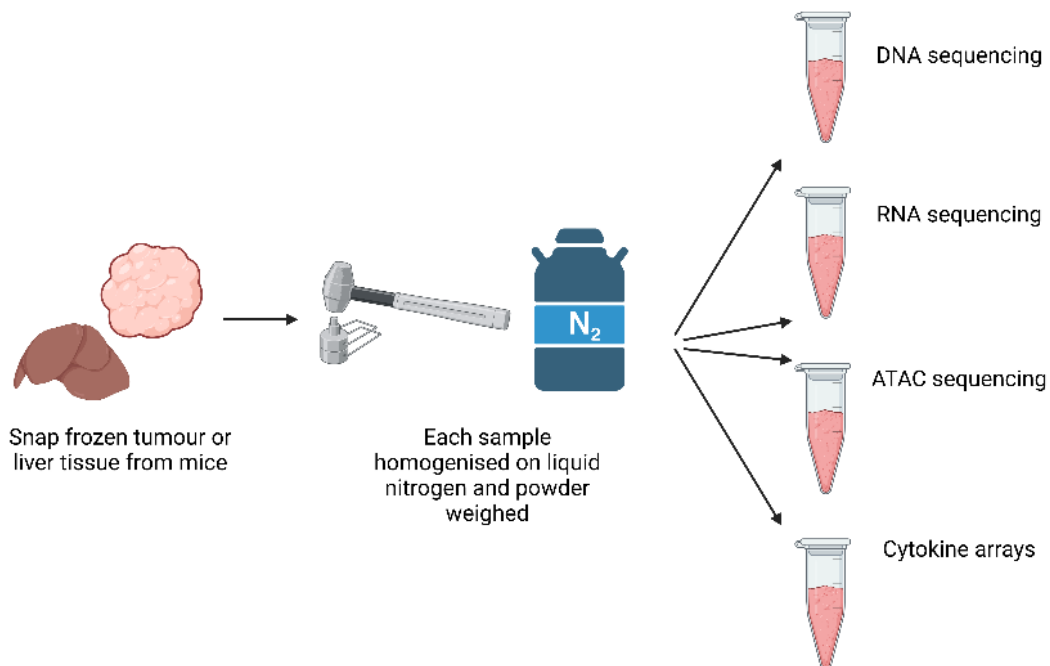
The predicted impact of mutations on the genome was assessed using the Ensembl Variant Effect Predictor (VEP 102)[118]. VEP determines the variant consequences and localises these by comparing these to large, annotated databases of information generated from large genomics studies to allow the effect of alterations to be interpreted. As many mutations, including those in cancer driver genes may have no deleterious effects, the following analysis was performed

Figure 5.1: Overview of experimental design used to generate data in this chapter. Panel A – Experimental overview of mouse timepoint sampling. Panel B – Homogenisation of tissue specimens to generate powdered tissues, allowing multiple analyses to be performed without sampling bias.

A



B



on selected mutations deemed by VEP to have ‘moderate’ or ‘high’ impact. In the figures throughout this chapter, $Cttnb1^{\text{exon3/Wt}} \text{ Rosa26}^{\text{c-MYC/c-MYC}}$ are described as ‘ $Cttnb1/\text{MYC}$ ’ and $\text{Trp53}^{\text{fl/fl}} \text{ Rosa26}^{\text{c-MYC/c-MYC}}$ as ‘ $\text{Tp53}/\text{MYC}$ ’ for brevity.

5.3.1 Comparison of whole exome sequencing in $Cttnb1^{\text{exon3/Wt}} \text{ Rosa26}^{\text{c-MYC/c-MYC}}$ and $\text{Trp53}^{\text{fl/fl}} \text{ Rosa26}^{\text{c-MYC/c-MYC}}$ tumours

SNPs were the most frequent genetic alteration (figure 5.2 and figure 5.3), followed by deletions. There were similar numbers of mutations found in each tumour, across both genotypes. Although less frequent, deletions were present in a higher proportion of samples than SNPs were. SNPs were most commonly present in chromosomes 1, 4, 10 and 17 in $Cttnb1^{\text{exon3/Wt}} \text{ Rosa26}^{\text{c-MYC/c-MYC}}$ tumours and 1, 4, 11 and 17 in $\text{Trp53}^{\text{fl/fl}} \text{ Rosa26}^{\text{c-MYC/c-MYC}}$ tumours. $\text{Trp53}^{\text{fl/fl}} \text{ Rosa26}^{\text{c-MYC/c-MYC}}$ tumours had a higher number of mutations overall, but the proportion of mutation by type (SNP, DEL, DNP, INS, TNP, ONP) was similar across both $Cttnb1^{\text{exon3/Wt}} \text{ Rosa26}^{\text{c-MYC/c-MYC}}$ and $\text{Trp53}^{\text{fl/fl}} \text{ Rosa26}^{\text{c-MYC/c-MYC}}$ tumour genotypes (figure 5.3A). T>G and A>C SNPs were more commonly observed in $\text{Trp53}^{\text{fl/fl}} \text{ Rosa26}^{\text{c-MYC/c-MYC}}$ tumours, with G>A and C>T more common in $Cttnb1^{\text{exon3/Wt}} \text{ Rosa26}^{\text{c-MYC/c-MYC}}$ tumours (figure 5.3B). As allele recombination involves deletion of large regions, rather than point mutations as found in human disease, short read sequencing may not be suited to the sensitive detection of these, hence a lack of apparent mutation in these driver regions.

Figure 5.3C shows tumour mutational burden (TMB) across $Cttnb1^{\text{exon3/Wt}} \text{ Rosa26}^{\text{c-MYC/c-MYC}}$ and $\text{Trp53}^{\text{fl/fl}} \text{ Rosa26}^{\text{c-MYC/c-MYC}}$ tumour genotypes. TMB in the $\text{Trp53}^{\text{fl/fl}} \text{ Rosa26}^{\text{c-MYC/c-MYC}}$ group was more variable, but overall, there were no significant differences across the two genotypes, suggesting TMB cannot account for the differences in immune microenvironment and immunotherapy response. A high tumour mutational burden was thought enhance response to immunotherapy. This is thought to be mediated by increased inflammatory gene expression and increasing the burden of tumour neoantigens. However, this has not been shown to be the case in clinical studies[152]. TMB was calculated as

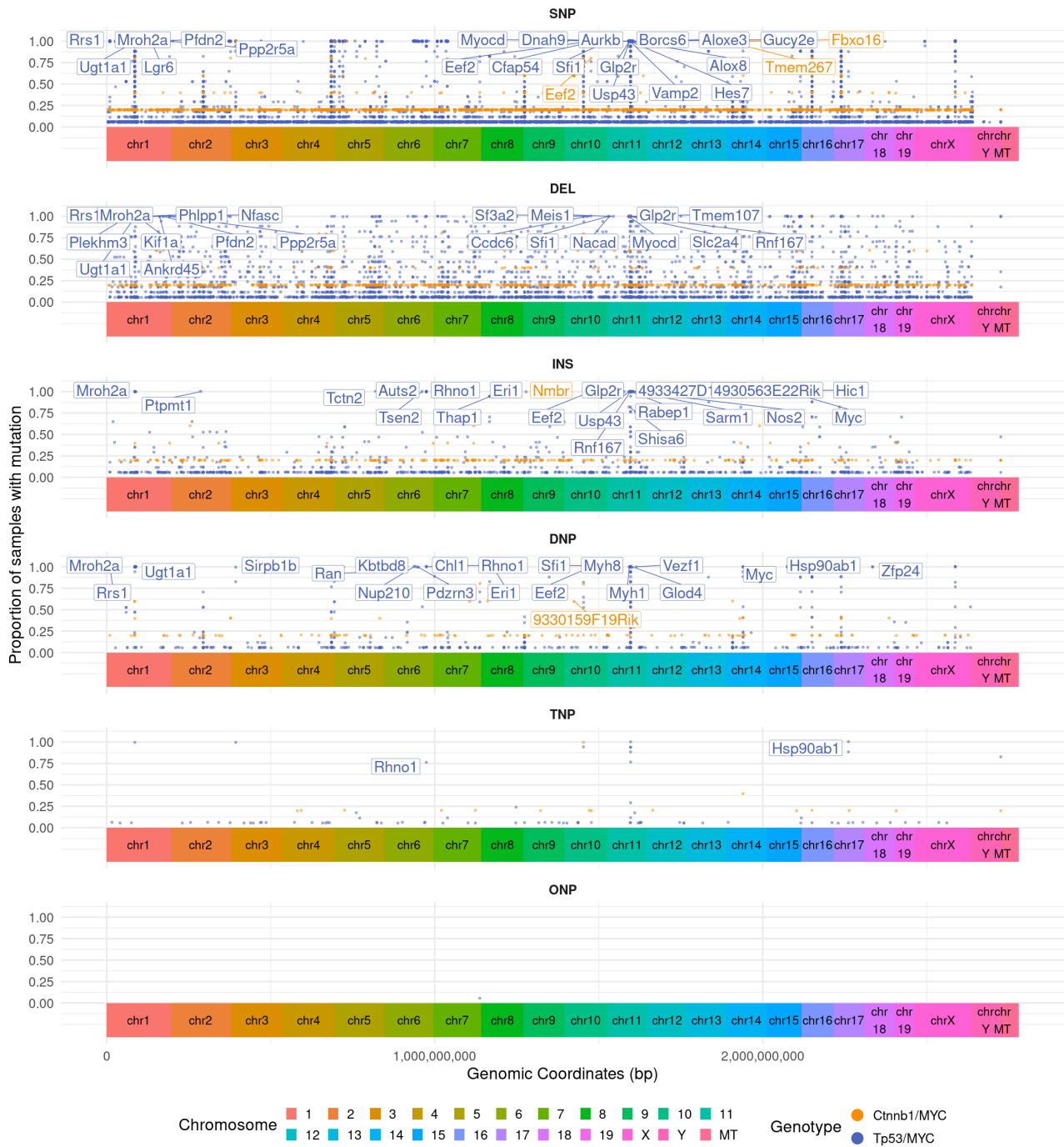
number of all mutations per kilobase per million reads, to account for the increased likelihood of detecting with higher sequencing depths.

Several large genes were expectedly mutated, including *Muc4*, *Vmp2* and its receptors. Most of the highly mutated genes are rodent-specific vomeronasal receptors which humans lack and are therefore not relevant to human disease. The most frequently mutated genes in *Ctnnb1^{exon3/Wt} Rosa26^{c-MYC/c-MYC}* were shared with *Trp53^{fl/fl} Rosa26^{c-MYC/c-MYC}* tumours (*Muc4*, *Duxf3*, *Mroh2a*, *Sp110*), except for *Nlrp1a* and *Nlrp1b* in *Trp53^{fl/fl} Rosa26^{c-MYC/c-MYC}* tumours – which play a key role in inflammasome activation. None of the SNPs found in *Nlrp1a* or *Nlrp1a* were alleles associated with aberrant inflammasome activation (i.e. *Nlrp1a^{Q593P}*).

Extending the analysis in figures 5.2, 5.3A and 5.3B, to identify whether tumours from these mouse models had human-relevant mutations, beyond that of the genetically engineered driver mutations, I performed mouse-human homology mapping using Ensembl annotations. I first identified all homologous mouse-human gene pairs and then selected genes found in the Catalogue of Somatic Mutations in Cancer (COSMIC) database which were relevant to HCC. Figure 5.3D shows the most frequently mutated genes (this time adjusted for gene length) present in $Cttnb1^{\text{exon3/Wt}} \text{ Rosa26}^{\text{c-MYC/c-MYC}}$ and $Trp53^{\text{fl/fl}} \text{ Rosa26}^{\text{c-MYC/c-MYC}}$ tumour genotypes. The most mutated genes which were also present in HCC-related Catalogue of Somatic Mutations in Cancer (COSMIC) gene lists were *Mroh2a*, *Sfi1* and *Rrs1* (figure 5.3D)[153]. These were the most common in both $Cttnb1^{\text{exon3/Wt}} \text{ Rosa26}^{\text{c-MYC/c-MYC}}$ and $Trp53^{\text{fl/fl}} \text{ Rosa26}^{\text{c-MYC/c-MYC}}$ tumour genotypes and are found to be rarely mutated, if at all, in any human cancer[132, 154, 155]. This suggests that, at least at the gene level beyond the genetically engineered drivers, these mouse models do not share similar genetics with human disease.

Considering this lack of homologous variants found in human disease, I next considered whether there were alterations at the pathway level which may be relevant to human disease. $Cttnb1^{\text{exon3/Wt}} \text{ Rosa26}^{\text{c-MYC/c-MYC}}$ tumours were found to have alterations most frequently in the *Myc*, *Hippo*, *Notch*, *Wnt* and *Rtk-Ras* pathways which affected all tumours (figure 5.3E). $Trp53^{\text{fl/fl}} \text{ Rosa26}^{\text{c-MYC/c-MYC}}$ tumours had proportionally more of these pathways affected (figure 5.3F), most commonly in the *TP53*, *HIPPO*, *RTK-RAS*, *NOTCH* and *WNT* pathways. These pathways are commonly found to be mutated in human HCC, suggesting the same gene pathways in humans and mice are likely to be affected; albeit without sharing homologous gene variants. At the exome level, it is important to appreciate these models do not fully recapitulate the genetics of human HCC and that findings from these models is supplemented with data from human model systems.

Figure 5.2: Exome mutations by type and location across genome in tumours from *Trp53^{fl/fl} Rosa26^{c-MYC/c-MYC}* (blue dots) and *Ctnnb1^{exon3/Wt} Rosa26^{c-MYC/c-MYC}* (orange dots). Labelled genes are mouse genes where all samples contain mutations and genes have high confidence homology to human genes present in COSMIC drivers from human HCC. BP – Base pairs, CHR – Chromosome, SNP – Single Nucleotide Polymorphism, MT - mitochondrial, DEL – Deletion, INS – Insertion, DNP - Diucleotide Polymorphism, TNP - Trinucleotide Polymorphism, ONP - Oligonucleotide Polymorphism.



To compare whether $Ctnnb1^{\text{exon3/Wt}} \text{ Rosa26}^{\text{c-MYC/c-MYC}}$ and $\text{Trp53}^{\text{fl/fl}} \text{ Rosa26}^{\text{c-MYC/c-MYC}}$ had shared mutational features, I performed dimensionality reduction with sparse PCA, followed by UMAP and plotted the projection in 2 dimensions (figure 5.4A). $Ctnnb1^{\text{exon3/Wt}} \text{ Rosa26}^{\text{c-MYC/c-MYC}}$ were tightly clustered together, at the extreme of both UMAP dimensions from the $\text{Trp53}^{\text{fl/fl}} \text{ Rosa26}^{\text{c-MYC/c-MYC}}$ tumours. The $\text{Trp53}^{\text{fl/fl}} \text{ Rosa26}^{\text{c-MYC/c-MYC}}$ cluster was more spread than the $Ctnnb1^{\text{exon3/Wt}} \text{ Rosa26}^{\text{c-MYC/c-MYC}}$ cluster, suggesting there was more variation across tumours of this genotype than in the $Ctnnb1^{\text{exon3/Wt}} \text{ Rosa26}^{\text{c-MYC/c-MYC}}$ tumours (figure 5.4A). To confirm this, I sampled different tumours from the same $\text{Trp53}^{\text{fl/fl}} \text{ Rosa26}^{\text{c-MYC/c-MYC}}$ mice and included these in the analysis. Samples of different tumours from the same mouse did not cluster close to other tumour samples from the same mouse (figure 5.4B), making it likely they arose separately and spontaneously, rather than from intrahepatic spread. This suggests that $\text{Trp53}^{\text{fl/fl}} \text{ Rosa26}^{\text{c-MYC/c-MYC}}$ tumours contain heterogenous mutation patterns across tumours from the same mouse and between individual mice. Further phylogenetic analysis would help to confirm this.

Figure 5.3: Variant types, tumour mutational burden (TMB), variants in coding regions and homologous human oncogene pathways by tumour genotype. Panel A – Total variants per tumour by variant type and tumour genotype. Panel B – Base SNP alterations by genotype. Panel C – Tumour mutational burden by genotype. Panel D – Most frequently mutated (per sample per KB) COSMIC HCC genes with human homologs by variant classification. Panel E – Mutations found within homologous oncogenic pathways in *Cttnb1*^{exon3/Wt} *Rosa26*^{c-MYC/c-MYC} tumours. Panel F – Mutations found within homologous oncogenic pathways in *Trp53*^{fl/fl} *Rosa26*^{c-MYC/c-MYC} tumours. SNP – Single Nucleotide Polymorphism, DEL – Deletion, INS – Insertion, DNP - Dinucleotide Polymorphism, TNP - Trinucleotide Polymorphism, ONP - Oligonucleotide Polymorphism, KB – Kilobases.

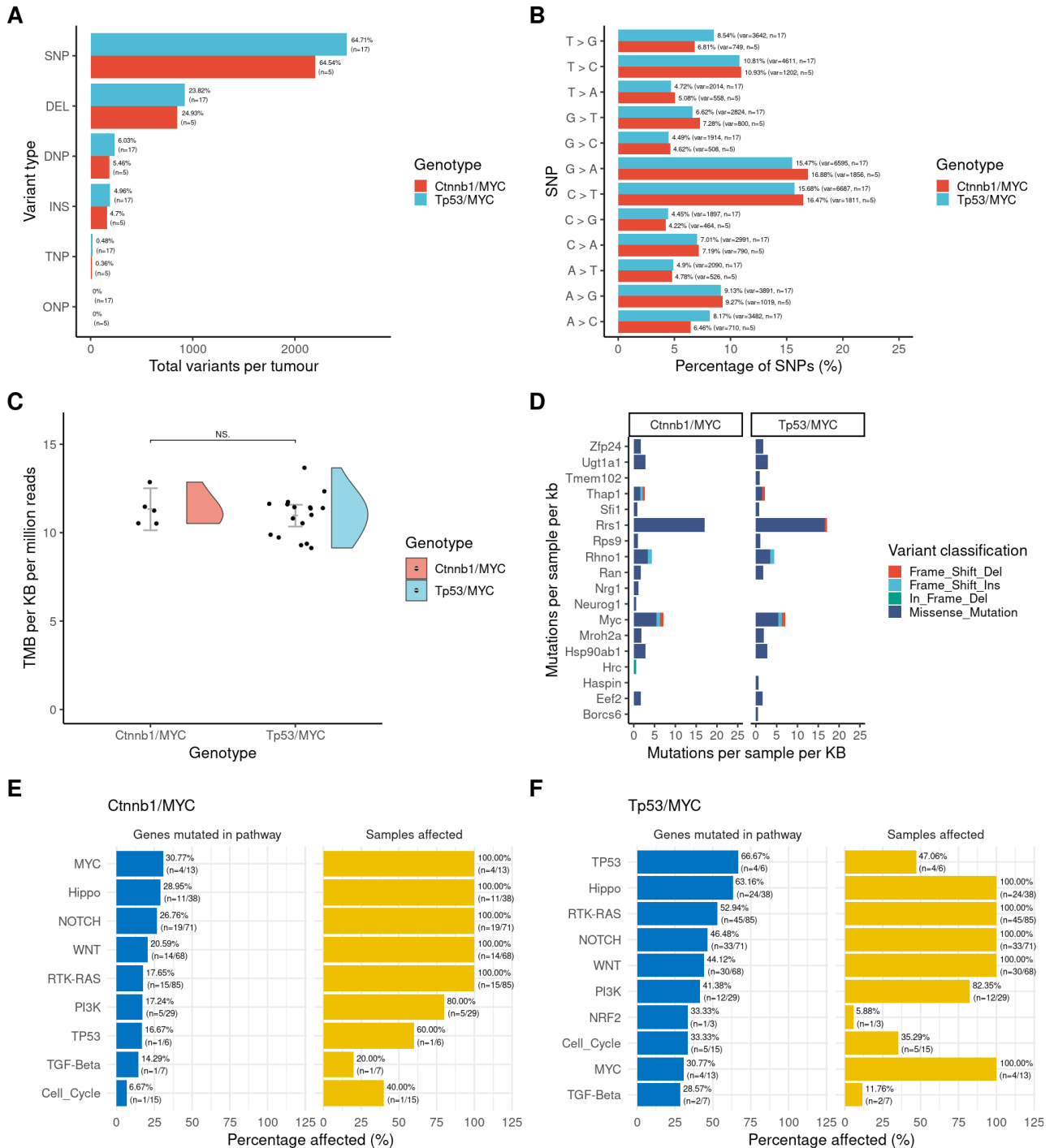
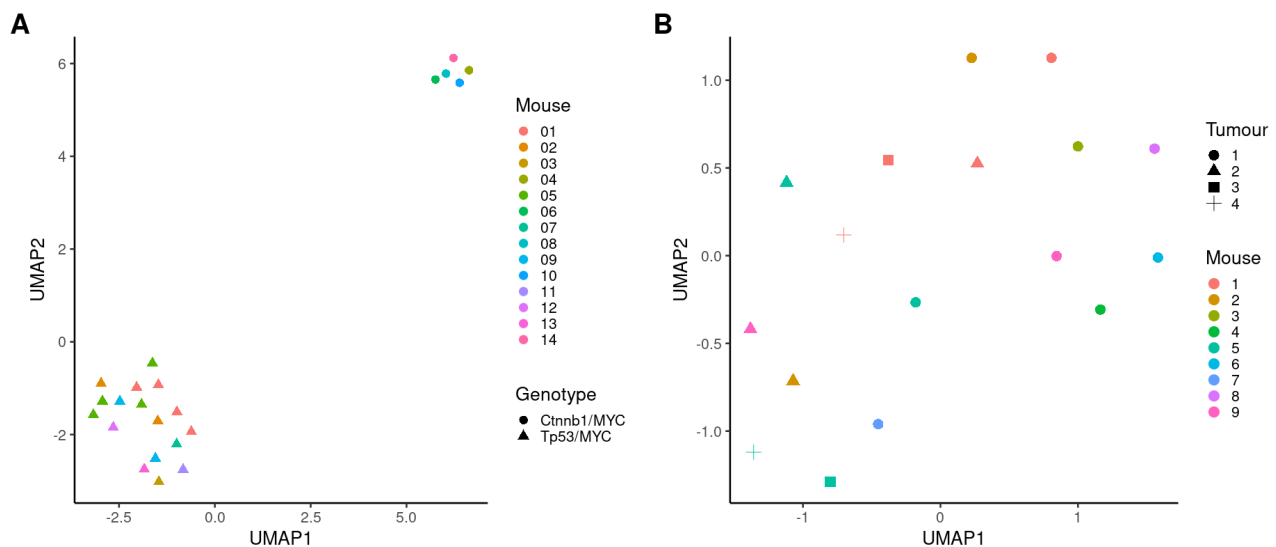


Figure 5.4: Uniform Manifold Approximation Projection (UMAP) plot of mutations from whole exome sequencing of $Cttnb1^{\text{exon3}/\text{Wt}}$ $Rosa26^{\text{c-MYC}/\text{c-MYC}}$ and $Trp53^{\text{fl/fl}}$ $Rosa26^{\text{c-MYC}/\text{c-MYC}}$ tumours. Panel A – There are distinct clusters of mutations which form by genotype, suggesting genotypes have very different mutations to each other. Panel B – shows re-clustering of $Trp53^{\text{fl/fl}}$ $Rosa26^{\text{c-MYC}/\text{c-MYC}}$ exomes, with samples taken from different tumours in the same mice. This shows that there is considerable heterogeneity between tumours within the same mouse, suggesting these are not intrahepatic metastases and are more likely to be synchronous tumours.



5.3.2 Comparison of copy number variation in $Cttnb1^{\text{exon3}/\text{Wt}}$ $Rosa26^{\text{c-MYC}/\text{c-MYC}}$ and $Trp53^{\text{fl/fl}}$ $Rosa26^{\text{c-MYC}/\text{c-MYC}}$ tumours

Copy number variations (CNVs) are genomic alterations where sections of DNA are deleted or duplicated, leading to change in gene dosage. CNVs can arise from chromosomal instability and are common across many cancer types[154, 155]. Hepatocytes are frequently polyploid, therefore can tolerate loss or gain in genes which may otherwise be lethal, as multiple copies of genes exist, providing a degree of redundancy. As HCC tumours arise from hepatocytes, these too can also be polyploid, making CNVs a common feature of HCC[20]. Therefore, to understand this and whether it is likely to be implicated in immune evasion, I called and compared CNVs in the $Cttnb1^{\text{exon3}/\text{Wt}}$ $Rosa26^{\text{c-MYC}/\text{c-MYC}}$ and $Trp53^{\text{fl/fl}}$ $Rosa26^{\text{c-MYC}/\text{c-MYC}}$ models using ExomeDepth. To account for polyploidy in healthy hepatocytes, I used CNV calls from normal healthy litter and cage-mate matched liver tissue as a baseline to calculate the likelihood of CNVs. All exome samples were processed at the

same time using a robotic liquid handling system to reduce the risk of amplification artefact.

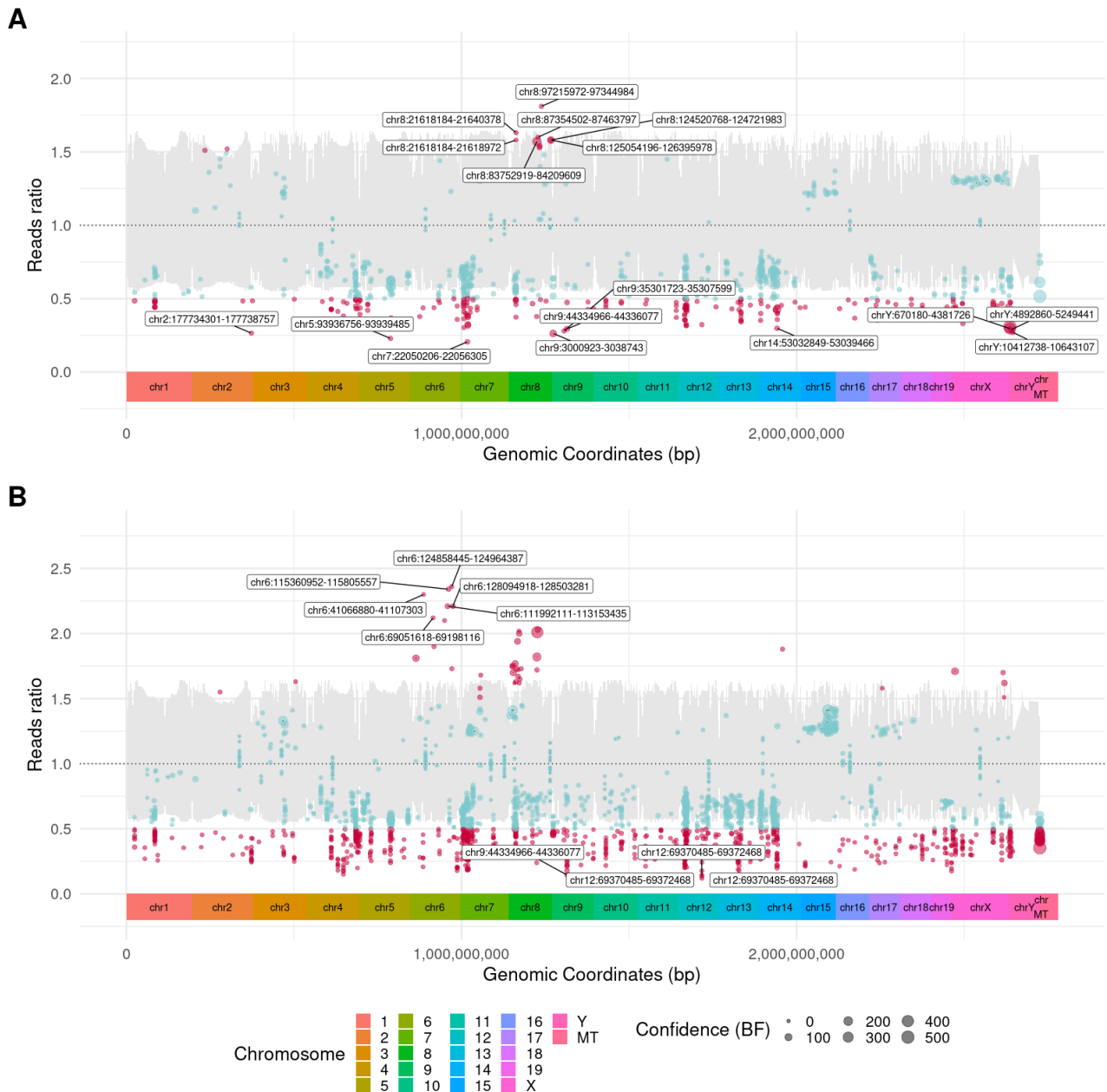
The plot in figure 5.5 shows copy number alteration as a ratio of the reads observed across exome regions, compared to the number which were expected. A ratio of greater than one suggests amplification or duplication and less than one suggests deletion. Each point represents one CNV and the size of the point is relative to the Bayes Factor, which expresses the likelihood or confidence in the CNV. The higher the bayes factor the greater the likelihood of the beta-binomial model accurately identifying a ‘true’ CNV. The grey shaded trace in the plot background represents the binomial 95% confidence interval. Points outwith the 95% confidence interval can be considered as significantly amplified or deleted relative to normal liver tissue.

The majority of CNVs in both tumour genotypes were deletions. CNVs were more frequent in the $\text{Trp53}^{\text{fl/fl}}$ $\text{Rosa26}^{\text{c-MYC/c-MYC}}$ tumour genotype, which is plausible given the key role of wild-type p53 in maintaining chromosomal and genomic stability.

In $\text{Ctnnb1}^{\text{exon3/Wt}}$ $\text{Rosa26}^{\text{c-MYC/c-MYC}}$ tumours, deletions were the most common form of CNV. CNV deletions were most common in chromosomes 4, 7 and 14. Deletions in predicted genes were most common (C130026I21Rik, 1700001F09Rik, 1700010N08Rik), followed by cytokine genes (Ccl19 and Ccl21a) and Ddx3y. Cytokine gene deletions are notable for their association with a reduction in infiltrating immune cells in this model, particularly given these are both chemoattractants for T-cells and dendritic cells through Ccr7[156–158].

The findings with $\text{Trp53}^{\text{fl/fl}}$ $\text{Rosa26}^{\text{c-MYC/c-MYC}}$ tumours were similar. In $\text{Trp53}^{\text{fl/fl}}$ $\text{Rosa26}^{\text{c-MYC/c-MYC}}$ tumours, deletions were also the most common form of CNV. CNV deletions were most common in chromosomes 7, 12 and 14. Deletions in pseudogenes were most common (Gm6740, Gm18191, Gm18200), followed by mitochondrial genes (mt-Atp6, mt-Atp8, mt-Co1). Ccl19 and Ccl21a were also found to have CNV deletions. Deletion of mitochondrial oxidation genes was less prominent in $\text{Ctnnb1}^{\text{exon3/Wt}}$ $\text{Rosa26}^{\text{c-MYC/c-MYC}}$ tumours which are immune excluded compared with $\text{Trp53}^{\text{fl/fl}}$ $\text{Rosa26}^{\text{c-MYC/c-MYC}}$ tumours.

Figure 5.5: Panel A – Copy Number Variations (CNVs) across genome in *Ctnnb1*^{exon3/Wt} *Rosa26*^{c-MYC/c-MYC}. Panel B – *Trp53*^{fl/fl} *Rosa26*^{c-MYC/c-MYC} tumour genotypes. The light grey banding indicates 95% confidence interval. Red dots are amplifications or deletions outwith or near the boundaries of the 95% confidence interval. Example regions are labelled. Not all regions labelled due to visual constraints. Size of the point represents the Bayes Factor likelihood of detection. A Bayes Factor of 20 or higher is deemed decisive. BP – Base pairs, BF – Bayes Factor, CHR – Chromosome.



Dysfunction of mitochondrial oxidation has been heavily implicated in ROS generation and triggering inflammation through cGAS/STING, RIG-I/MAVS and type I interferons[159–161].

Exons were mapped to the genomic ranges of the CNV to identify which homologous COSMIC HCC genes were affected by CNVs. There were comparatively few CNVs which were significantly different across tumours with $Ctnnb1^{\text{exon3/Wt}}$ $Rosa26^{\text{c-MYC/c-MYC}}$ and $Trp53^{\text{fl/fl}}$ $Rosa26^{\text{c-MYC/c-MYC}}$ genotypes (table 5.1 illustrates the top 20 most frequent CNVs from each genotype). There were 4 CNV deletions and no amplifications which were significantly different across tumour genotypes. These deletions affected the *Mid1*, *Ddx3y*, *Usp9y* and *Kdm5d* genes and only in the $Ctnnb1^{\text{exon3/Wt}}$ $Rosa26^{\text{c-MYC/c-MYC}}$. In the $Ctnnb1^{\text{exon3/Wt}}$ $Rosa26^{\text{c-MYC/c-MYC}}$ deletions most frequently occur on the Y chromosome. *Mid1* is found on the X chromosome and is implicated in embryonic development, ubiquitination and modulates mTORC pathways. *Ddx3y* is a putative Y-linked RNA helicase, with a homolog on the X chromosome and is implicated in spermatogenesis. *Usp9y* is also implicated in spermatogenesis and ubiquitination and is found on the Y chromosome. *Kdm5d* is an alpha-ketoglutarate-dependent hydroxylase and found on the Y chromosome. Of these 4 CNVs, 3 have putative roles in inflammatory responses, most notably *Kdm5d*, which contains H-Y minor histocompatibility antigen regions in humans which acts as both a source of potential antigen and regulates expression of several inflammation associated genes[162]. Similarly, *Mid1* has been shown to mediate the effect of TNF-related apoptosis-inducing ligand (TRAIL)[163] and *Ddx3* has been shown to be essential for RIG/MAVs and type I interferon responses[164, 165]. Therefore, it is plausible that these deletions at the CNV level in $Ctnnb1^{\text{exon3/Wt}}$ $Rosa26^{\text{c-MYC/c-MYC}}$ mice could affect immune infiltration into the tumour microenvironment, either through suppression of type I IFN responses, or through reduced expression of tumour neoantigen.

Despite this finding, as with the mutations, CNVs observed in these mice were not commonly found in human disease. This could be for several reasons. First, although these mice are model organisms, they are not humans and do not necessarily share identical processes which lead to chromosomal instability and there are differences in genome regulation across species. The

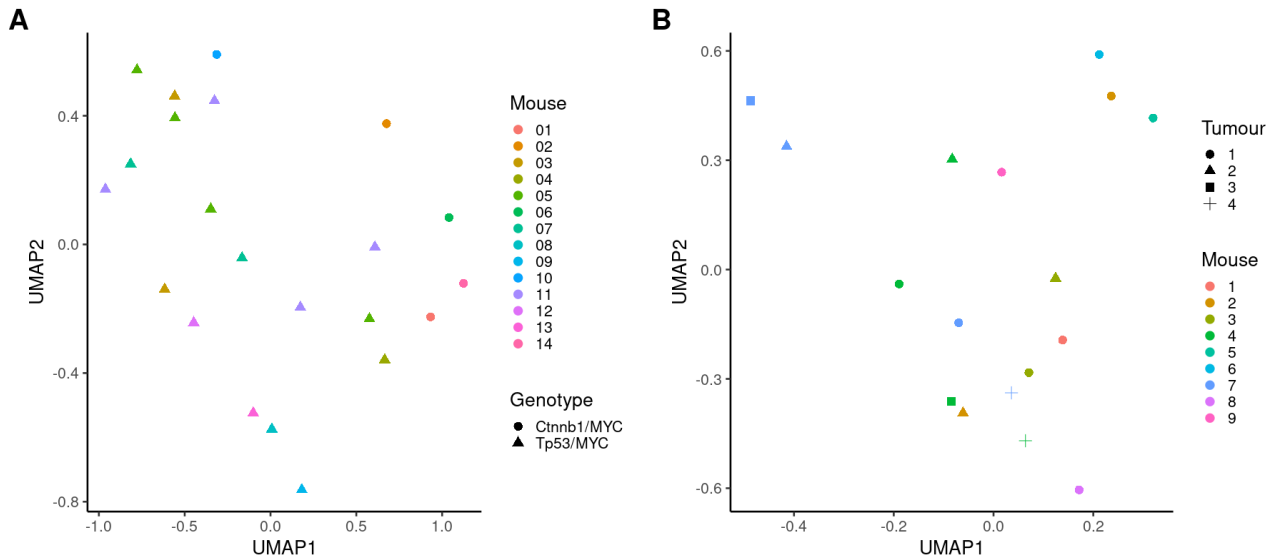
Table 5.1: Tables of top 20 most affected genes by CNVs in in (left side) $\text{Trp53}^{\text{fl/fl}}$ $\text{Rosa26}^{\text{c-MYC/c-MYC}}$ genotypes and $\text{Ctnnb1}^{\text{exon3/Wt}}$ $\text{Rosa26}^{\text{c-MYC/c-MYC}}$ (right side). P-values are from two-sided binomial tests comparing frequency in $\text{Trp53}^{\text{fl/fl}}$ $\text{Rosa26}^{\text{c-MYC/c-MYC}}$ with $\text{Ctnnb1}^{\text{exon3/Wt}}$ $\text{Rosa26}^{\text{c-MYC/c-MYC}}$.

$\text{Trp53}^{\text{fl/fl}}$ $\text{Rosa26}^{\text{c-MYC/c-MYC}}$			$\text{Ctnnb1}^{\text{exon3/Wt}}$ $\text{Rosa26}^{\text{c-MYC/c-MYC}}$		
Gene	CNV	Number of samples (P-value)	Gene	CNV	Number of samples (P-value)
Arf6	Deletion	11/17 (p=0.6381)	Ddx3y	Deletion	4/5 (p=0.0370)
Ccdc177	Deletion	11/17 (p=0.6381)	Kdm5d	Deletion	4/5 (p=0.0370)
Cda	Deletion	11/17 (p=0.6381)	Usp9y	Deletion	4/5 (p=0.0370)
Fam43b	Deletion	11/17 (p=0.6381)	Tmem181a	Deletion	4/5 (p=0.4298)
Nudt19	Deletion	11/17 (p=0.6381)	Mid1	Deletion	3/5 (p=0.0070)
Pink1	Deletion	11/17 (p=0.6381)	Jund	Deletion	3/5 (p=1.0000)
Tpbgl	Deletion	11/17 (p=0.6381)	Clcn4	Deletion	2/5 (p=0.0643)
Gcat	Duplication	10/17 (p=0.0701)	Gm3435	Deletion	2/5 (p=0.0643)
Gas1	Deletion	10/17 (p=0.3089)	Gm13693	Duplication	2/5 (p=0.2252)
Rgs9bp	Deletion	10/17 (p=0.8164)	Ncald	Duplication	2/5 (p=0.2252)
Jund	Deletion	9/17 (p=1.0000)	Sox8	Deletion	2/5 (p=0.2252)
Dmrta2	Deletion	9/17 (p=1.0000)	Borcs6	Deletion	2/5 (p=0.4357)
Frat1	Deletion	9/17 (p=1.0000)	Arf6	Deletion	2/5 (p=0.6381)
Frat2	Deletion	9/17 (p=1.0000)	Ccdc177	Deletion	2/5 (p=0.6381)
Tmem181a	Deletion	8/17 (p=0.4298)	Cda	Deletion	2/5 (p=0.6381)
Nanos1	Deletion	8/17 (p=0.5725)	Fam43b	Deletion	2/5 (p=0.6381)
Hnrnpf	Deletion	8/17 (p=1.0000)	Nudt19	Deletion	2/5 (p=0.6381)
Pde3a	Deletion	8/17 (p=1.0000)	Pink1	Deletion	2/5 (p=0.6381)
Map6d1	Deletion	7/17 (p=0.2334)	Tpbgl	Deletion	2/5 (p=0.6381)
Zfp367	Deletion	7/17 (p=0.2334)	Ccdc184	Duplication	2/5 (p=0.6589)

genetic alterations seen in humans are as a result of years of cumulative liver disease, whereas these models have genetic drivers introduced in an otherwise healthy liver. Second, HCC in these mice was induced in the absence of liver disease. Liver disease is known to affect ploidy, which alters CNV detection in both human and mouse tissue. Finally, most statistical methods for identifying CNVs were primarily developed for use with cytogenetic arrays in humans and not exome sequencing. The Genomic Identification of Significant Targets in Cancer (GISTIC) algorithm is commonly used to call CNVs but lacks relevant compatibility with different species and is over a decade old at the time of writing[166]. Larger sample sizes, particularly in the $\text{Ctnnb1}^{\text{exon3/Wt}}$ $\text{Rosa26}^{\text{c-MYC/c-MYC}}$ group may also help to enhance CNV detection.

To extend this comparison further, I next considered whether there was between genotype, between mouse and between tumour similarities or heterogeneity. To do this I performed dimensionality reduction of the chromosomal CNV windows with PCA, followed by UMAP and plotted the projection in 2 dimensions. Unlike the mutation data, which were different depending on tumour genotype, $\text{Ctnnb1}^{\text{exon3/Wt}}$ $\text{Rosa26}^{\text{c-MYC/c-MYC}}$ and $\text{Trp53}^{\text{fl/fl}}$

Figure 5.6: Uniform Manifold Approximation Projection (UMAP) plot of copy number variations (CNVs) from whole exome sequencing of $Cttnb1^{\text{exon3/Wt}}$ $Rosa26^{\text{c-MYC/c-MYC}}$ and $Trp53^{\text{fl/fl}}$ $Rosa26^{\text{c-MYC/c-MYC}}$ tumours. Panel A – UMAP of both $Cttnb1^{\text{exon3/Wt}}$ $Rosa26^{\text{c-MYC/c-MYC}}$ and $Trp53^{\text{fl/fl}}$ $Rosa26^{\text{c-MYC/c-MYC}}$. Panel B – UMAP after re-clustering of $Trp53^{\text{fl/fl}}$ $Rosa26^{\text{c-MYC/c-MYC}}$, including samples from different tumours within the same mice demonstrating the presence of intra-tumour heterogeneity within mice.



$Rosa26^{\text{c-MYC/c-MYC}}$ did not form mutually exclusive genotype clusters (figure 5.6A). However, like the mutations found in $Trp53^{\text{fl/fl}}$ $Rosa26^{\text{c-MYC/c-MYC}}$ mice, there was considerable heterogeneity in CNVs across tumours from the same $Trp53^{\text{fl/fl}}$ $Rosa26^{\text{c-MYC/c-MYC}}$ mice (figure 5.6B).

5.4 Transcriptomic comparison of *Ctnnb1*^{exon3/Wt} *Rosa26*^{c-MYC/c-MYC} and *Trp53*^{fl/fl} *Rosa26*^{c-MYC/c-MYC} mouse models

Although genomic analysis can provide useful insight into tumour biology, analysing gene expression allows the behaviour and signalling taking place within cancer cells to be studied. To study differences in global gene expression across *Ctnnb1*^{exon3/Wt} *Rosa26*^{c-MYC/c-MYC} and *Trp53*^{fl/fl} *Rosa26*^{c-MYC/c-MYC} tumours, I extracted RNA from homogenised tissue extracts, enriched for polyadenylated messenger RNAs, and constructed stranded cDNA sequencing libraries. Libraries were sequenced at a minimum depth of 40 million reads per sample. In this analysis I included samples of tumour and normal liver from 24 mice sampled at day 125 post-induction with AAV8-TBG-Cre or AAV8-TBG-Null. Of these 24 mice, 6 were *Ctnnb1*^{exon3/Wt} *Rosa26*^{c-MYC/c-MYC} who received AAV8-TBG-Cre, 6 were *Ctnnb1*^{exon3/Wt} *Rosa26*^{c-MYC/c-MYC} who received AAV8-TBG-Null, 7 were *Trp53*^{fl/fl} *Rosa26*^{c-MYC/c-MYC} who received AAV8-TBG-Cre and 5 were *Trp53*^{fl/fl} *Rosa26*^{c-MYC/c-MYC} who received AAV8-TBG-Null. These samples were from the same homogenised tumour tissue as used for the genomic and ATAC sequencing experiments described in this chapter (figure 5.1).

5.4.1 Comparison of transcriptome sequencing in *Ctnnb1*^{exon3/Wt} *Rosa26*^{c-MYC/c-MYC} and *Trp53*^{fl/fl} *Rosa26*^{c-MYC/c-MYC} tumours

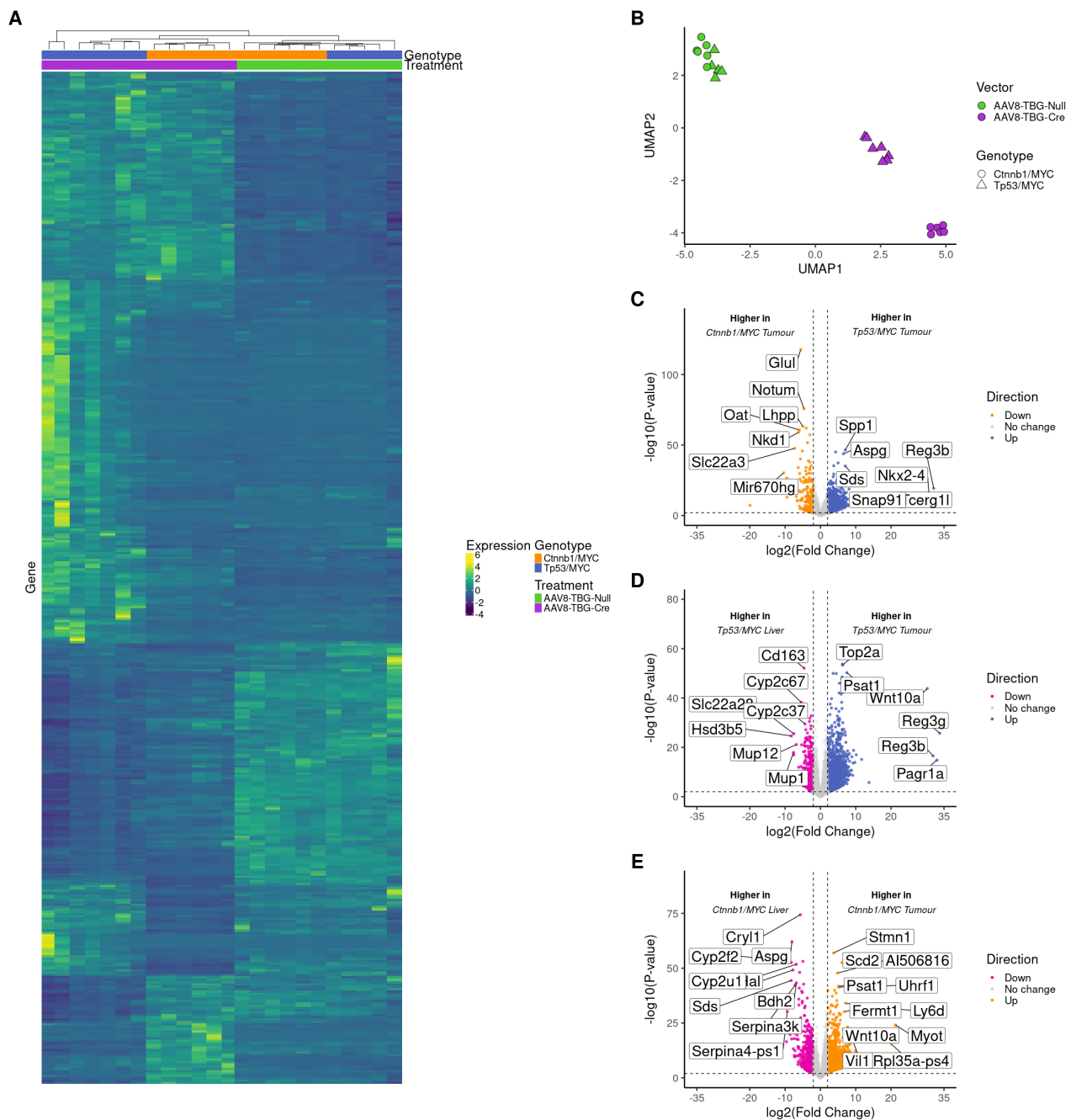
Figure 5.7 summarises the overall transcriptomic differences between *Ctnnb1*^{exon3/Wt} *Rosa26*^{c-MYC/c-MYC} and *Trp53*^{fl/fl} *Rosa26*^{c-MYC/c-MYC} mice. Unsupervised hierarchical clustering accurately classified mice according to their genotype and the AAV8 vector received, indicating each group had distinct transcriptomic differences (figure 5.7A). Figure 5.7B shows the UMAP plot for the 24 samples included in this experiment. The matched control (AAV8-TBG-Null) induced tissue from both genotypes clustered together, suggesting there is no difference in gene expression in the absence of Cre recombinase. In the mice which received AAV8-TBG-Cre vector, distinct clusters formed for each genotype, with individual

points within each cluster close together. This suggests both the $Ctnnb1^{\text{exon3/Wt}}$ $Rosa26^{\text{c-MYC/c-MYC}}$ and $Trp53^{\text{fl/fl}}$ $Rosa26^{\text{c-MYC/c-MYC}}$ tumours have markedly different transcriptomic features from one another and from normal liver tissue.

Many genes in $Ctnnb1^{\text{exon3/Wt}}$ $Rosa26^{\text{c-MYC/c-MYC}}$ and $Trp53^{\text{fl/fl}}$ $Rosa26^{\text{c-MYC/c-MYC}}$ were differentially expressed (figure 5.7C to 5.7E). Genes associated with canonical Wnt/ β -Catenin signalling including *Glul* (Glutamine synthetase), *Notum* and *Oat* (Ornithine aminotransferase) were upregulated in $Ctnnb1^{\text{exon3/Wt}}$ $Rosa26^{\text{c-MYC/c-MYC}}$ tumours. In $Trp53^{\text{fl/fl}}$ $Rosa26^{\text{c-MYC/c-MYC}}$ tumours, genes involved in metabolism and transcription were significantly upregulated. These included *Spp1* (Osteopontin), *Aspg* (Asparaginase), *Sds* (Serine Dehydratase) and *Tcerg1l* (Transcription elongation regulator 1 like).

Although there were major transcriptomic differences, some differentially expressed genes were shared between $Ctnnb1^{\text{exon3/Wt}}$ $Rosa26^{\text{c-MYC/c-MYC}}$ and $Trp53^{\text{fl/fl}}$ $Rosa26^{\text{c-MYC/c-MYC}}$. Most notably *Wnt10a* and *Psat1* were significantly upregulated in both tumour genotypes compared with normal matched liver control. *Wnt10a* is a member of the wider WNT family and acts through frizzled receptor (thought to be mainly frizzled 10) to activate canonical Wnt/ β -Catenin signalling[167]. Given $Ctnnb1^{\text{exon3/Wt}}$ $Rosa26^{\text{c-MYC/c-MYC}}$ tumours have constitutively activated canonical Wnt/ β -Catenin, *Wnt10a* is likely to have less of an effect on tumour epithelium in this model. However, its presence in the context of $Trp53^{\text{fl/fl}}$ $Rosa26^{\text{c-MYC/c-MYC}}$ tumours suggests *Wnt10a* and the canonical Wnt/ β -Catenin signalling pathway may play an important role in tumour behaviour even in the context of wild-type *Ctnnb1*. It would be interesting to examine this further and identify whether *Wnt10a* overexpression affects the immune microenvironment, both in $Ctnnb1^{\text{Wt/Wt}}$ cells (i.e. macrophages, mesenchymal cells) within $Ctnnb1^{\text{exon3/Wt}}$ $Rosa26^{\text{c-MYC/c-MYC}}$ tumours, but also in the context of $Trp53^{\text{fl/fl}}$ $Rosa26^{\text{c-MYC/c-MYC}}$ tumours. *Psat1* was also significantly upregulated in both tumour genotypes. This gene encodes phosphoserine aminotransferase, a key component of the phosphorylated serine synthesis pathway. Phosphoserine aminotransferase catalyses the formation of 3-phospho-L-serine, which is later converted to L-serine. L-serine is a key substrate within the cell and is required for several key processes

Figure 5.7: Overview of transcriptomic differences in immune excluded $Cttnb1^{exon3/Wt}$ $Rosa26^{c-MYC/c-MYC}$ tumour model compared with immune infiltrated $Trp53^{fl/fl}$ $Rosa26^{c-MYC/c-MYC}$ model. Panel A – shows heatmap and unsupervised hierarchical clustering for all genes by genotype and vector received. Panel B – shows UMAP plot by genotype and vector received. Panel C – Volcano plot shows differentially expressed genes across tumour genotypes, indicating canonical Wnt/ β -Catenin signalling is higher in $Cttnb1^{exon3/Wt}$ $Rosa26^{c-MYC/c-MYC}$ tumours. Panel D – shows comparison between $Trp53^{fl/fl}$ $Rosa26^{c-MYC/c-MYC}$ tumour and normal matched liver tissue. Panel E – shows comparison between $Cttnb1^{exon3/Wt}$ $Rosa26^{c-MYC/c-MYC}$ tumour and normal matched liver tissue. Total n individual mice = 24, 6 $Cttnb1^{exon3/Wt}$ $Rosa26^{c-MYC/c-MYC}$ with Cre, 6 $Cttnb1^{exon3/Wt}$ $Rosa26^{c-MYC/c-MYC}$ with null, 7 $Trp53^{fl/fl}$ $Rosa26^{c-MYC/c-MYC}$ with Cre and 5 $Trp53^{fl/fl}$ $Rosa26^{c-MYC/c-MYC}$ with null.

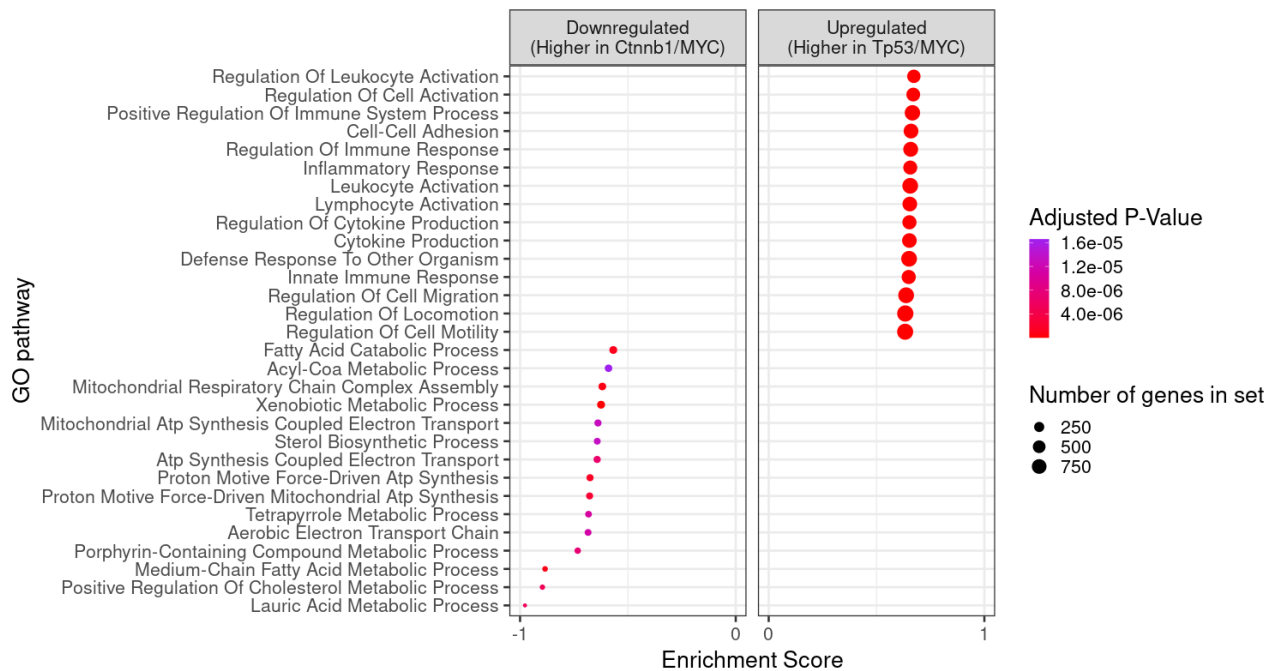


including purine nucleotide synthesis, itself required for continued proliferation and cell survival[168]. This suggests that $Ctnnb1^{\text{exon3/Wt}}$ $Rosa26^{\text{c-MYC/c-MYC}}$ and $Trp53^{\text{fl/fl}}$ $Rosa26^{\text{c-MYC/c-MYC}}$ may share similarities in how they fuel and maintain tumour growth.

Vast numbers of genes (4,553 in total across both genotypes) were differentially expressed in immune infiltrated $Trp53^{\text{fl/fl}}$ $Rosa26^{\text{c-MYC/c-MYC}}$ compared with immune excluded $Ctnnb1^{\text{exon3/Wt}}$ $Rosa26^{\text{c-MYC/c-MYC}}$ tumours (figure 5.7). Therefore, to understand how these differences may affect immune response to these different tumours, and which signalling pathways were likely to be implicated, I performed a Gene Set Enrichment Analysis (GSEA). In $Trp53^{\text{fl/fl}}$ $Rosa26^{\text{c-MYC/c-MYC}}$ tumours, leukocyte activation and cytokine production were the most significantly enriched pathways (figure 5.8). This included lymphocyte activation and cell-killing, both critical pathways for effective anti-tumour immunity. Pathways associated with mitochondrial oxidation, cholesterol and fatty-acid metabolism were upregulated in $Ctnnb1^{\text{exon3/Wt}}$ $Rosa26^{\text{c-MYC/c-MYC}}$ tumours. Although it is clear from these results that $Trp53^{\text{fl/fl}}$ $Rosa26^{\text{c-MYC/c-MYC}}$ tumours are far more inflammatory, the role of mitochondrial and metabolic pathways in $Ctnnb1^{\text{exon3/Wt}}$ $Rosa26^{\text{c-MYC/c-MYC}}$ tumours may also be important to maintain metabolic homeostasis and suppress inflammatory signals, particularly given the increased burden of mt-DNA mutations found in $Trp53^{\text{fl/fl}}$ $Rosa26^{\text{c-MYC/c-MYC}}$ tumours[159].

Next, I focussed on identifying pathways which may explain why these cytokines in $Trp53^{\text{fl/fl}}$ $Rosa26^{\text{c-MYC/c-MYC}}$ tumours are more highly expressed than in $Ctnnb1^{\text{exon3/Wt}}$ $Rosa26^{\text{c-MYC/c-MYC}}$ tumours. In the GSEA analysis, I noticed defence responses, NOD-like receptor (NLR), Toll-like receptor (TLR), receptor for advanced glycation end products (RAGE), and anti-viral response pathways (including cGAS STING) were significantly upregulated in $Trp53^{\text{fl/fl}}$ $Rosa26^{\text{c-MYC/c-MYC}}$ tumours. Figure 5.9 shows these pathways were enriched only in the $Trp53^{\text{fl/fl}}$ $Rosa26^{\text{c-MYC/c-MYC}}$ tumours. These signalling pathways are complex, and activation can occur through a range of different signalling molecules. Despite the complexity, the overarching function of these pathways is to sense damage or pathogen associated patterns (DAMP/PAMPs) and subsequently generate an immune response. The

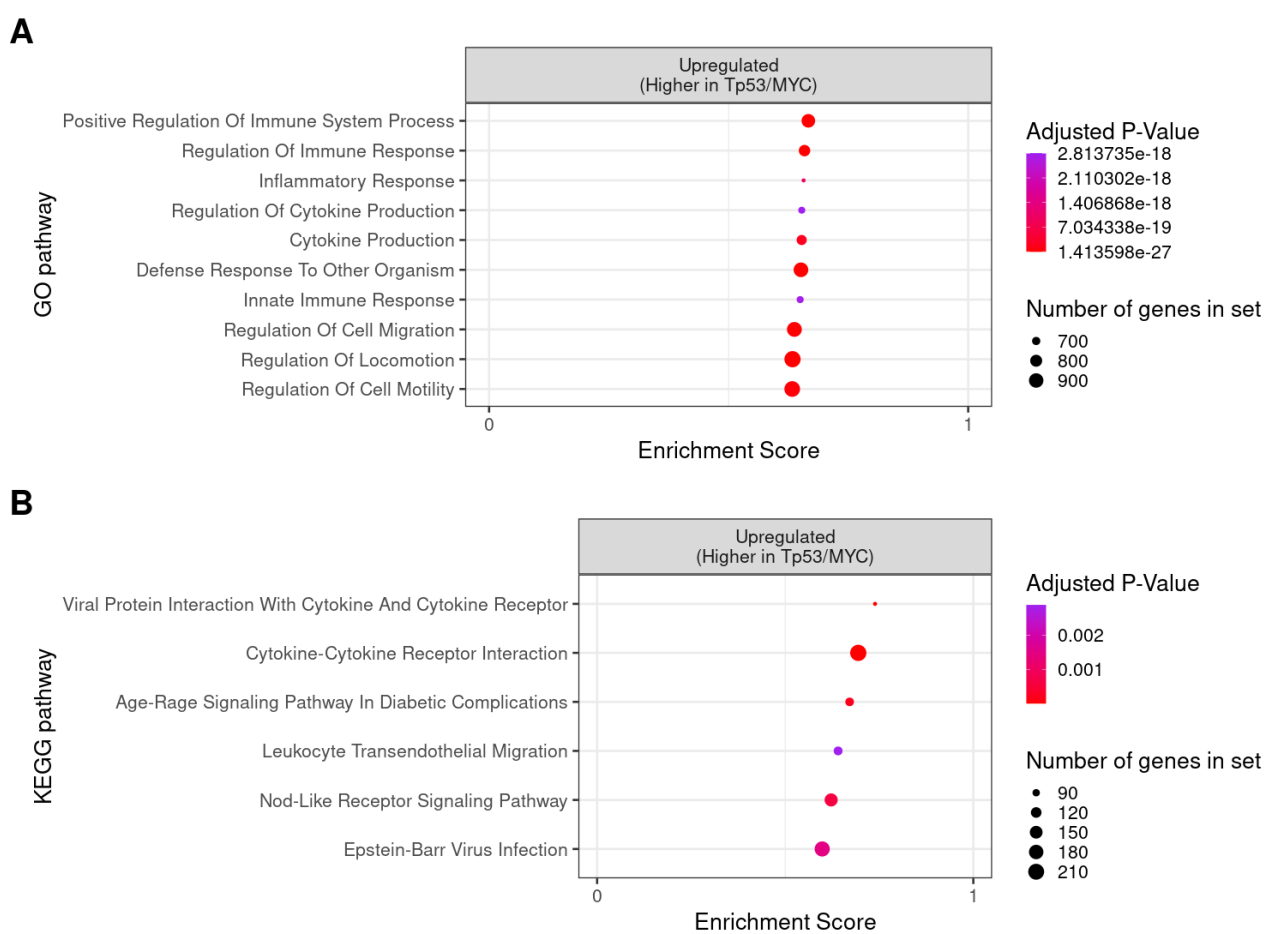
Figure 5.8: Gene Set Enrichment Analysis (GSEA) for Gene Ontology Biological Process Terms in $\text{Trp53}^{\text{fl/fl}}$ $\text{Rosa26}^{\text{c-MYC/c-MYC}}$ tumours compared to $\text{Ctnnb1}^{\text{exon3/Wt}}$ $\text{Rosa26}^{\text{c-MYC/c-MYC}}$ tumours.



response that can be generated is typically context dependent. For example, evoking a cytotoxic immune response is detrimental to maintaining tissue health and could be fatal in certain tissues – for example in the intestine, liver, or skin, where exposure to DAMP/PAMPs from food and skin contact is constant. On the other hand, triggering a cytotoxic immune response may be advantageous where a cell becomes infected with a pathogenic virus or undergoes malignant transformation. This will be discussed further later in later chapters.

As cytokines are major regulators of immune cell trafficking into tumours, I sought to identify which were differentially expressed across immune infiltrated $\text{Trp53}^{\text{fl/fl}}$ $\text{Rosa26}^{\text{c-MYC/c-MYC}}$ and immune excluded $\text{Ctnnb1}^{\text{exon3/Wt}}$ $\text{Rosa26}^{\text{c-MYC/c-MYC}}$ tumours. Figure 5.10 shows normalised read counts from individual mice for a range of cytokine genes implicated in immune cell trafficking. Nearly all the cytokines which were significantly upregulated were present in $\text{Trp53}^{\text{fl/fl}}$ $\text{Rosa26}^{\text{c-MYC/c-MYC}}$ tumours compared with $\text{Ctnnb1}^{\text{exon3/Wt}}$ $\text{Rosa26}^{\text{c-MYC/c-MYC}}$ tumours and normal liver tissue. In $\text{Ctnnb1}^{\text{exon3/Wt}}$ $\text{Rosa26}^{\text{c-MYC/c-MYC}}$ tumours if cytokines were differentially expressed, they were typically

Figure 5.9: Gene Set Enrichment Analysis (GSEA) of specific anti-viral or PAMP/DAMP associated pathways significantly enriched in $\text{Trp53}^{\text{fl/fl}}$ $\text{Rosa26}^{\text{c-MYC/c-MYC}}$ tumours compared to $\text{Ctnnb1}^{\text{exon3/Wt}}$ $\text{Rosa26}^{\text{c-MYC/c-MYC}}$ tumours. Panel A – Gene Ontology (GO) terms. Panel B – Kyoto Encyclopedia of Genes and Genomes (KEGG) terms.



downregulated compared with $\text{Trp53}^{\text{fl/fl}}$ $\text{Rosa26}^{\text{c-MYC/c-MYC}}$ tumours. $\text{Ctnnb1}^{\text{exon3/Wt}}$ $\text{Rosa26}^{\text{c-MYC/c-MYC}}$ tumours often had lower or the same expression of cytokines than normal liver. In $\text{Trp53}^{\text{fl/fl}}$ $\text{Rosa26}^{\text{c-MYC/c-MYC}}$ tumours, many of the cytokines which were significantly upregulated were involved in dendritic cell and T-cell chemotaxis, including *Ccl20*, *Cxcl13*, *Ccl22*, *Ccl11*, *Ccl8*, *Ccl5* and *Cxcl10*. Given the GSEA findings, this suggests that $\text{Trp53}^{\text{fl/fl}}$ $\text{Rosa26}^{\text{c-MYC/c-MYC}}$ tumours produce higher amounts of cytokines which attract anti-tumour immune cells into the tumour microenvironment and could explain why anti-PD1 therapy extended survival in these mice. The venn diagrams in figure 5.11 summarise the total number of genes and the number of cytokines differentially expressed.

5.4.2 Expression of immune checkpoint genes

Immune checkpoints mediate the balance between immune tolerance and immune response. In the previous chapter, I demonstrated that treatment of $\text{Trp53}^{\text{fl/fl}}$ $\text{Rosa26}^{\text{c-MYC/c-MYC}}$ mice with anti-PD1 extends overall survival and no effect in $\text{Ctnnb1}^{\text{exon3/Wt}}$ $\text{Rosa26}^{\text{c-MYC/c-MYC}}$ mice. Therefore, it would be expected that these $\text{Trp53}^{\text{fl/fl}}$ $\text{Rosa26}^{\text{c-MYC/c-MYC}}$ tumours express greater levels of PD-L1 (*Cd274*) and PD1 (*Pdcd1*). Figure 5.12 shows normalised read counts from individual mice for known inhibitory and stimulatory immune checkpoints. As expected, $\text{Trp53}^{\text{fl/fl}}$ $\text{Rosa26}^{\text{c-MYC/c-MYC}}$ tumours expressed higher levels of PD-L1 (*Cd274*) and PD1 (*Pdcd1*). $\text{Trp53}^{\text{fl/fl}}$ $\text{Rosa26}^{\text{c-MYC/c-MYC}}$ tumours also had much higher expression of both inhibitory and stimulatory immune checkpoints overall. $\text{Ctnnb1}^{\text{exon3/Wt}}$ $\text{Rosa26}^{\text{c-MYC/c-MYC}}$ tumours expressed slightly more Icos ligand, which has been implicated with endothelial senescence and clearance of cells via the senescence-associated secretory phenotype[169]. Taken together, if it is assumed immune checkpoint blockade works best in tumours with high immune checkpoint expression, immune checkpoint blockade is unlikely to work in $\text{Ctnnb1}^{\text{exon3/Wt}}$ $\text{Rosa26}^{\text{c-MYC/c-MYC}}$ without adjuvant therapies to enhance checkpoint expression.

Interestingly, PD1 PD-L1 expression was not the most highly or consistently expressed checkpoint across samples (figure 5.12). There have been several clinical trials investigating dual targeting of CTLA-4 and PD-1/PD-L1[68]. In these models CTLA-4 was not frequently

Figure 5.10: Expression of cytokine genes across tumour and control liver tissue. Cytokine expression was highest in the $\text{Trp53}^{\text{fl/fl}}$ $\text{Rosa26}^{\text{c-MYC/c-MYC}}$ immune infiltrated tumours, with little difference across the normal control tissue. Yellow is high expression, dark blue is low expression. Total n individual mice = 24, 6 $\text{Ctnnb1}^{\text{exon3/Wt}}$ $\text{Rosa26}^{\text{c-MYC/c-MYC}}$ with Cre, 6 $\text{Ctnnb1}^{\text{exon3/Wt}}$ $\text{Rosa26}^{\text{c-MYC/c-MYC}}$ with null, 7 $\text{Trp53}^{\text{fl/fl}}$ $\text{Rosa26}^{\text{c-MYC/c-MYC}}$ with Cre and 5 $\text{Trp53}^{\text{fl/fl}}$ $\text{Rosa26}^{\text{c-MYC/c-MYC}}$ with null.

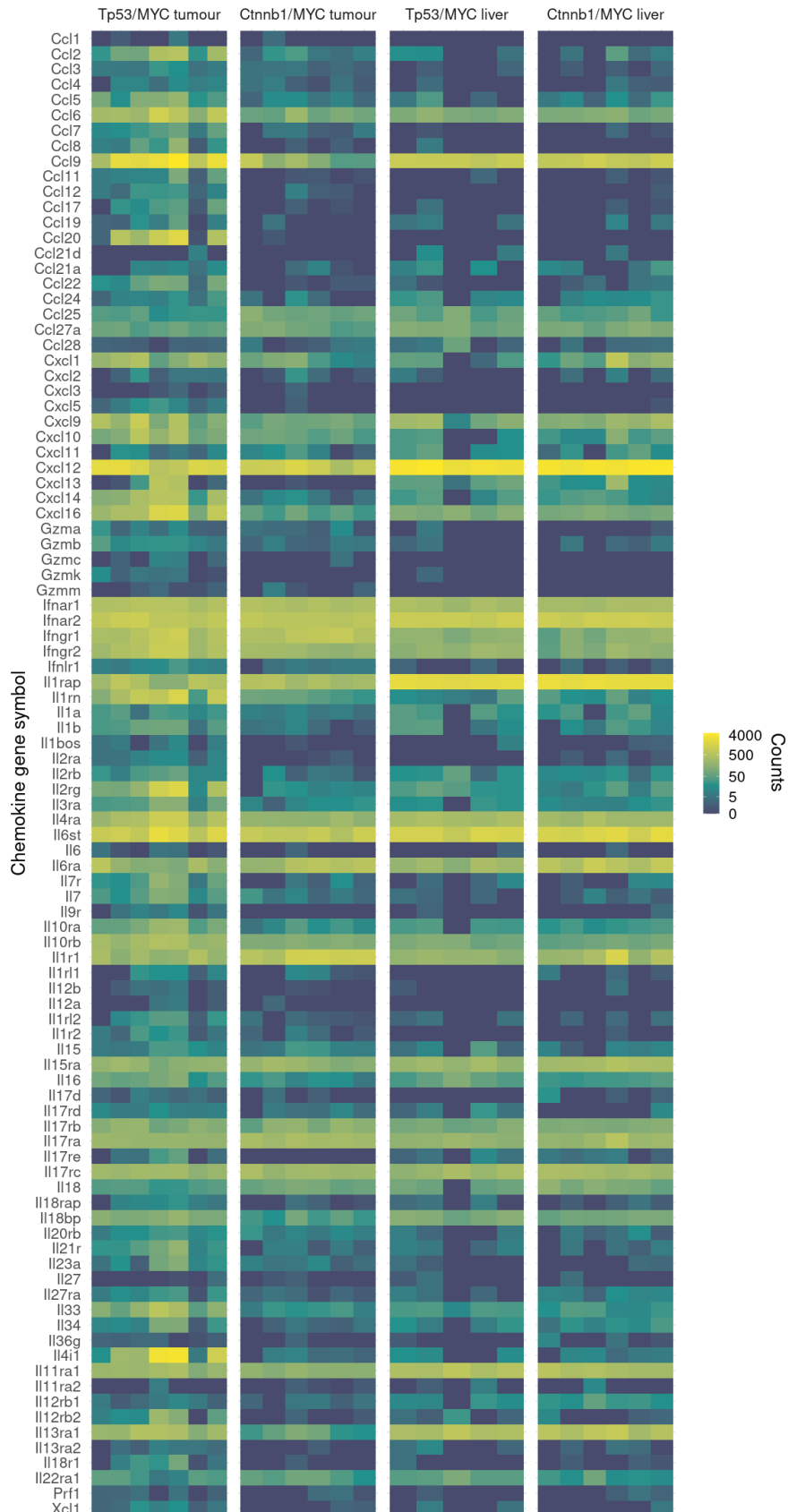


Figure 5.11: Venn diagrams summarising differential gene expression in $\text{Trp53}^{\text{fl/fl}}$ $\text{Rosa26}^{\text{c-MYC/c-MYC}}$ tumours compared with $\text{Ctnnb1}^{\text{exon3/Wt}}$ $\text{Rosa26}^{\text{c-MYC/c-MYC}}$ tumours. Panel A – Significantly upregulated genes. Panel B – Significantly downregulated genes. Panel C – Significantly upregulated cytokine genes only. Panel D – Significantly downregulated cytokine genes only. The comparison for each genotype is to normal matched liver tissue (AAV8-TBG-Null). Total n individual mice = 24, 6 $\text{Ctnnb1}^{\text{exon3/Wt}}$ $\text{Rosa26}^{\text{c-MYC/c-MYC}}$ with Cre, 6 $\text{Ctnnb1}^{\text{exon3/Wt}}$ $\text{Rosa26}^{\text{c-MYC/c-MYC}}$ with null, 7 $\text{Trp53}^{\text{fl/fl}}$ $\text{Rosa26}^{\text{c-MYC/c-MYC}}$ with Cre and 5 $\text{Trp53}^{\text{fl/fl}}$ $\text{Rosa26}^{\text{c-MYC/c-MYC}}$ with null.

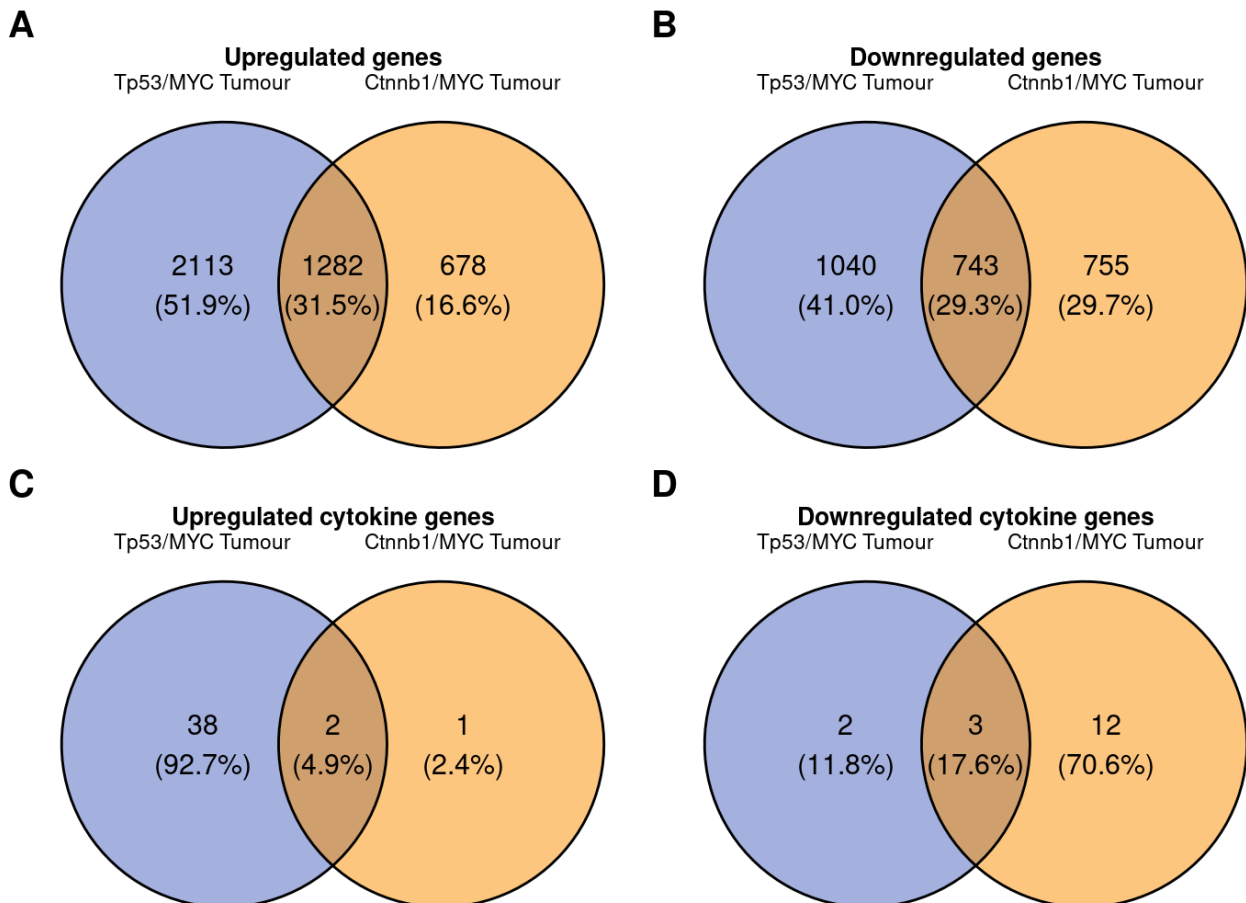
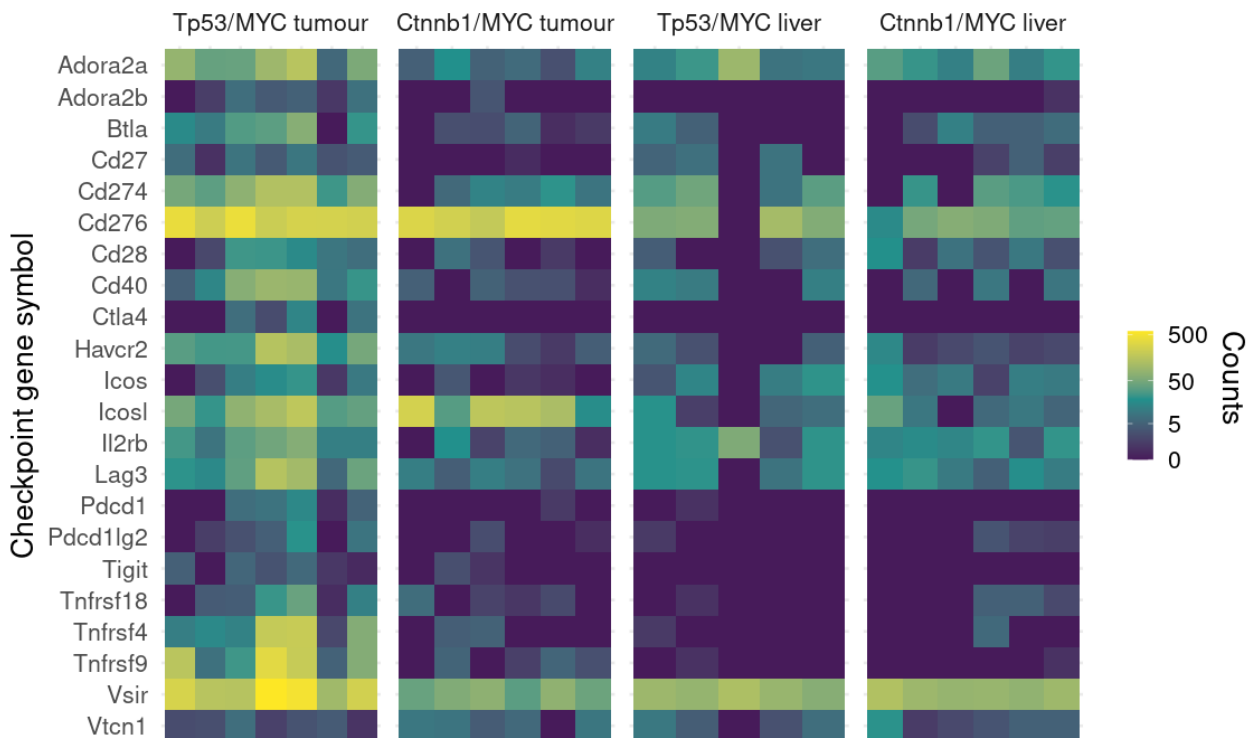


Figure 5.12: Expression of inhibitory and stimulatory immune checkpoint genes across tumour and control liver tissue. Checkpoint expression was highest in the $\text{Trp53}^{\text{fl/fl}}$ $\text{Rosa26}^{\text{c-MYC/c-MYC}}$ immune infiltrated tumours, with little difference across the normal control tissue. Yellow is high expression, dark blue is low expression. Total n individual mice = 24, 6 $\text{Ctnnb1}^{\text{exon3/Wt}}$ $\text{Rosa26}^{\text{c-MYC/c-MYC}}$ with Cre, 6 $\text{Ctnnb1}^{\text{exon3/Wt}}$ $\text{Rosa26}^{\text{c-MYC/c-MYC}}$ with null, 7 $\text{Trp53}^{\text{fl/fl}}$ $\text{Rosa26}^{\text{c-MYC/c-MYC}}$ with Cre and 5 $\text{Trp53}^{\text{fl/fl}}$ $\text{Rosa26}^{\text{c-MYC/c-MYC}}$ with null.



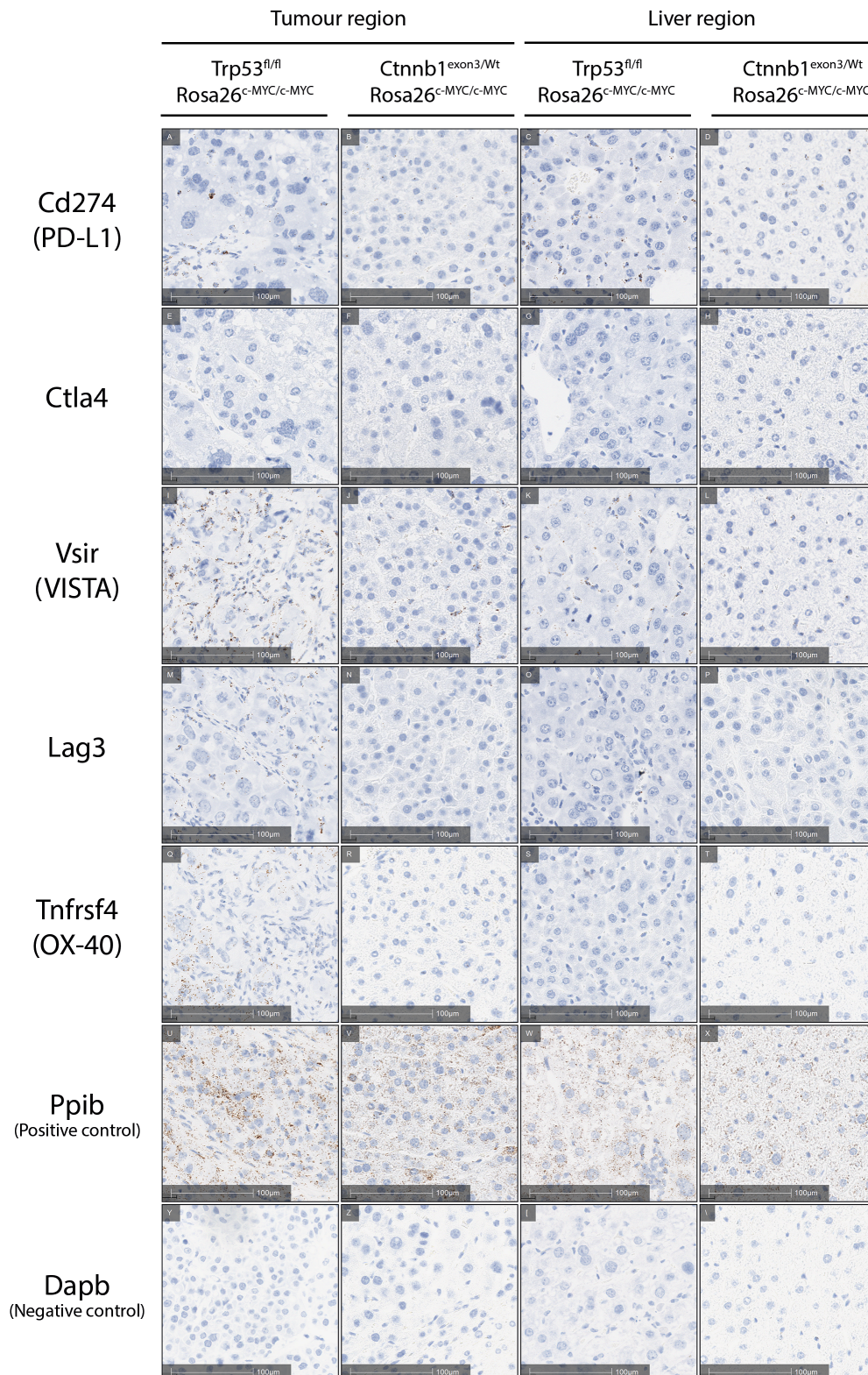
expressed, even in $\text{Trp53}^{\text{fl/fl}}$ $\text{Rosa26}^{\text{c-MYC/c-MYC}}$ tumours. Therefore, these models may not be the ideal system to test the effects of dual CTLA-4 and PD-1/PD-L1 blockade but might be very useful to identify other effective immune checkpoint inhibition or stimulation. For example, combining VISTA blockade with anti-PD-1/PD-L1 appears attractive, given these are both highly expressed in $\text{Trp53}^{\text{fl/fl}}$ $\text{Rosa26}^{\text{c-MYC/c-MYC}}$ tumours.

5.4.3 Spatial validation of RNA sequencing results

With adequate power, RNA sequencing is an extremely sensitive technique and does not necessarily need validation with real-time quantitative PCR, particularly where multiple biological replicates have been used[170]. However, it is important to ensure bulk RNA sequencing results can be attributed to the tissue of interest. Similarly, as bulk RNA sequencing lacks spatial resolution, validating where gene expression is occurring provides useful information that the correct area was sampled and may help to suggest in which cell-types expression is occurring. To spatially validate my RNA-sequencing results, the Beatson Core Histology facility performed RNAScope for Cd274 (PD-L1), Ctla4, Vsir (VISTA), Lag3 and Tnfrsf4 (OX-40) immune checkpoints on tissue from $\text{Ctnnb1}^{\text{exon3/Wt}}$ $\text{Rosa26}^{\text{c-MYC/c-MYC}}$ and $\text{Trp53}^{\text{fl/fl}}$ $\text{Rosa26}^{\text{c-MYC/c-MYC}}$ samples.

In keeping with the RNA-sequencing, immune checkpoint RNA was expressed almost exclusively in $\text{Trp53}^{\text{fl/fl}}$ $\text{Rosa26}^{\text{c-MYC/c-MYC}}$ tumour tissue (figure 5.13). Lag3, Vsir and Tnfrsf4 had the strongest expression. Non-tumoural adjacent liver in both genotypes had little immune checkpoint expression.

Figure 5.13: Spatial validation of immune checkpoints in $\text{Trp53}^{\text{fl/fl}}$ $\text{Rosa26}^{\text{c-MYC/c-MYC}}$ and $\text{Ctnnb1}^{\text{exon3/Wt}}$ $\text{Rosa26}^{\text{c-MYC/c-MYC}}$ tissue. All images acquired on Leica Aperio AT-2 at 40x magnification. Results are presented with Ppib and Dapb controls from the same sample. Images are representative of minimum $n = 2$ mice per region and genotype. Liver regions are from the same tumour bearing mouse, demonstrating tumour specificity expression of Cd274, Vsir, Lag3 and Tnfrsf4 immune checkpoints in $\text{Trp53}^{\text{fl/fl}}$ $\text{Rosa26}^{\text{c-MYC/c-MYC}}$ tumours, which is concordant with RNA-sequencing results. Given the pattern of expression in these micrographs, it is likely some of the immune checkpoints may be expressed by a range of cells and are not exclusive to tumour epithelium.



5.5 Comparison of chromatin accessibility and transcription factor footprints

Given the major transcriptomic differences in $Cttnb1^{\text{exon3/Wt}}$ $Rosa26^{\text{c-MYC/c-MYC}}$ and $Trp53^{\text{fl/fl}}$ $Rosa26^{\text{c-MYC/c-MYC}}$ tumours, identifying the processes which regulate different pathways may allow these to be targeted to reprogramme the $Cttnb1^{\text{exon3/Wt}}$ $Rosa26^{\text{c-MYC/c-MYC}}$ tumour microenvironment. These pathways are usually controlled by a series of master regulators, known as transcription factors (TFs), which regulate gene expression, activating or repressing transcription of specific genes. Assay for Transposase-Accessible Chromatin (ATAC) sequencing allows regions of open chromatin to be identified and crucially, can determine transcription factor footprints found in these regions to determine which transcription factors are controlling gene expression.

As immune excluded $Cttnb1^{\text{exon3/Wt}}$ $Rosa26^{\text{c-MYC/c-MYC}}$ tumours have lower expression of pro-inflammatory genes, identifying therapies to specifically agonise inflammatory signals in tumour cells may be very difficult. ATAC sequencing allows identification of the transcription factors repressing these pro-inflammatory pathways or activating immunosuppressive pathways. The identified factors, or regulatory pathways upstream, could then be targeted with selective therapies such as small molecule inhibitors to reprogramme the immune microenvironment.

To perform this assay, nuclei were isolated from homogenised tissue extracts, tagmented with a hyperactive Tn5 transposase and libraries prepared for sequencing. The ATAC-sequencing kit contained detergents to minimise the presence of mitochondrial DNA during library preparation. Libraries were sequenced at a minimum depth of 75M reads per library to provide adequate pooled coverage to perform transcription factor footprinting analysis.

5.5.1 Results of ATAC sequencing and differences in chromatin accessibility by genotype and tissue

Figure 5.14 shows genome wide accessibility of chromatin by genotype and tissue type (tumour or normal matched tissue). Mapped reads from biological replicates were merged to increase ATAC-seq resolution and provide more sensitive mapping of transcription factor footprints in later analyses. ATAC-sequencing fragment size analysis revealed clear nucleosome-free (below 100 bp), mono-nucleosome (180 to 250 bp) and poly-nucleosome (subsequent peaks at 250 bp and above) enriched fractions across all genotypes and tissue types, indicating the assay was successful (figure 5.14A). UMAP clustering demonstrated normal tissue from both genotypes was similar and clustered closely together (figure 5.14B). Separate clusters formed for $Ctnnb1^{\text{exon3/Wt}}$ $Rosa26^{\text{c-MYC/c-MYC}}$ and $Trp53^{\text{fl/fl}}$ $Rosa26^{\text{c-MYC/c-MYC}}$ tumours, suggesting these genotypes have very different chromatin accessibility profiles (figure 5.14B and 5.14C).

$Trp53^{\text{fl/fl}}$ $Rosa26^{\text{c-MYC/c-MYC}}$ tumours had greater numbers of genes with open chromatin around transcriptional start sites and intronic regions (figure 5.15). These open regions were distributed more broadly around the transcriptional start sites (TSSs) in $Trp53^{\text{fl/fl}}$ $Rosa26^{\text{c-MYC/c-MYC}}$ tumours, compared with more central peaks in $Ctnnb1^{\text{exon3/Wt}}$ $Rosa26^{\text{c-MYC/c-MYC}}$ tumours. Intronic regions frequently contain regulatory elements such as enhancers, suggesting transcription in $Trp53^{\text{fl/fl}}$ $Rosa26^{\text{c-MYC/c-MYC}}$ tumours is affected to a greater extent by activity in regulatory regions than $Ctnnb1^{\text{exon3/Wt}}$ $Rosa26^{\text{c-MYC/c-MYC}}$ tumours are. This was confirmed by annotating ATAC peaks to their corresponding genomic features (figure 5.16), which identified a higher proportion of intron regions in $Trp53^{\text{fl/fl}}$ $Rosa26^{\text{c-MYC/c-MYC}}$ tumours than other tissue types.

Next, I performed differential accessibility analysis to identify differences in open regions across tissue types. Figure 5.17A to 5.17C demonstrates the findings of this analysis. I focused my analysis on promoter regions and introns, as introns are most likely to contain regulatory elements such as enhancers. In $Trp53^{\text{fl/fl}}$ $Rosa26^{\text{c-MYC/c-MYC}}$ tumours regions associated with inflammatory response were significantly more likely to be open, whereas

Figure 5.14: Overview of ATAC sequencing results. Panel A – Fragment size plot indicating experiment was successful and produced clear peaks in nucleosome free (NFR), mono-nucleosome (M), di-nucleosome (D) and poly-nucleosome regions. Panel B – UMAP plot of the analysed samples, demonstrating tumour genotypes had markedly different chromatin accessibility profiles compared to each other and normal matched liver tissue. Normal matched liver tissue from each genotype clustered closely together whilst each GEMM clustered together independent of each other. Panel C – Genome wide plot of ATAC read counts.

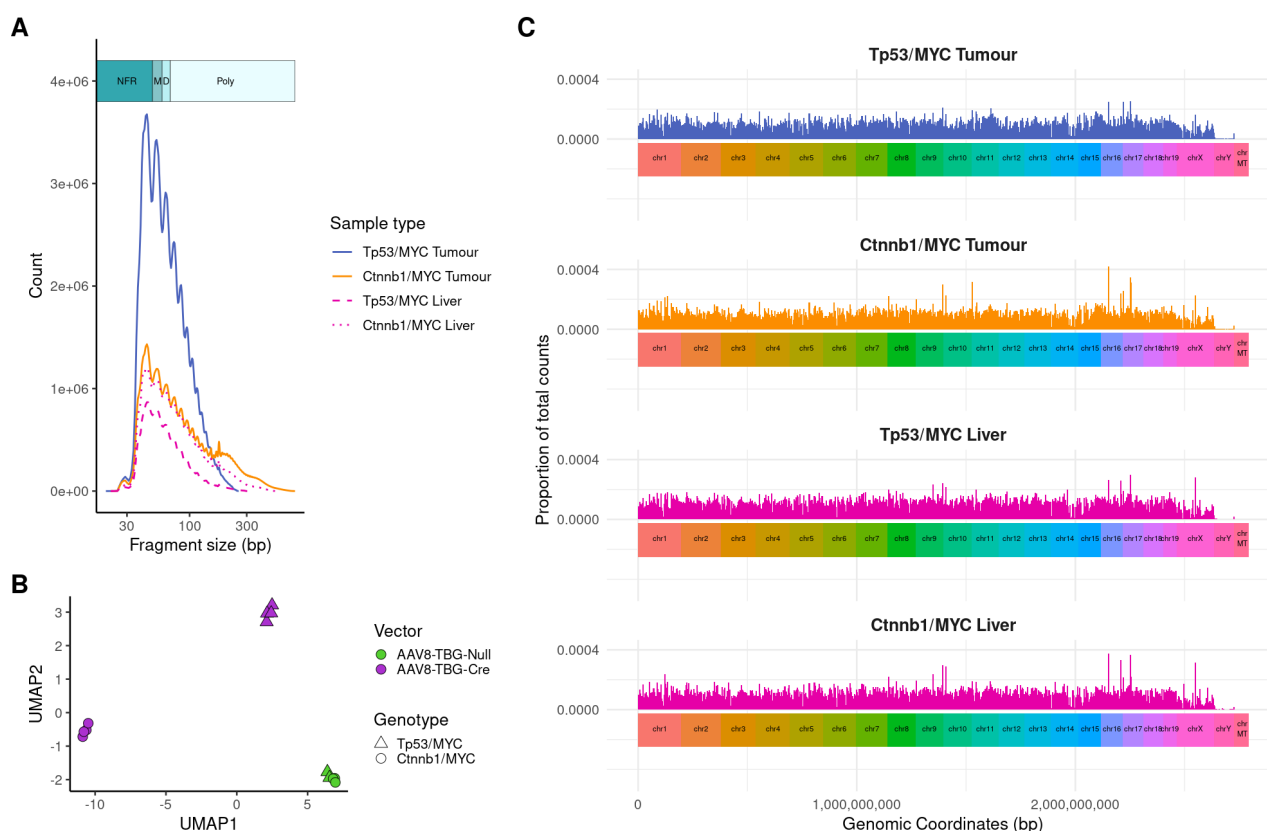


Figure 5.15: Overview of ATAC sequencing results by tissue type according to proximity to transcription start sites (TSS). The top panels are distribution of the proportion of read count around the TSS. Heatmaps indicate the read count and distance from the TSS for each gene, ranked by the total sum of the counts, weighted by centrality to the TSS. Panel A – $\text{Trp53}^{\text{fl/fl}}$ $\text{Rosa26}^{\text{c-MYC/c-MYC}}$ tumours have a broader distribution around the TSS than compared with other genotypes. Panel B – $\text{Ctnnb1}^{\text{exon3/Wt}}$ $\text{Rosa26}^{\text{c-MYC/c-MYC}}$, which are more comparable to normal liver (panel C and panel D). Results are resampled 3000 times for computational feasibility and account for sequencing depth.

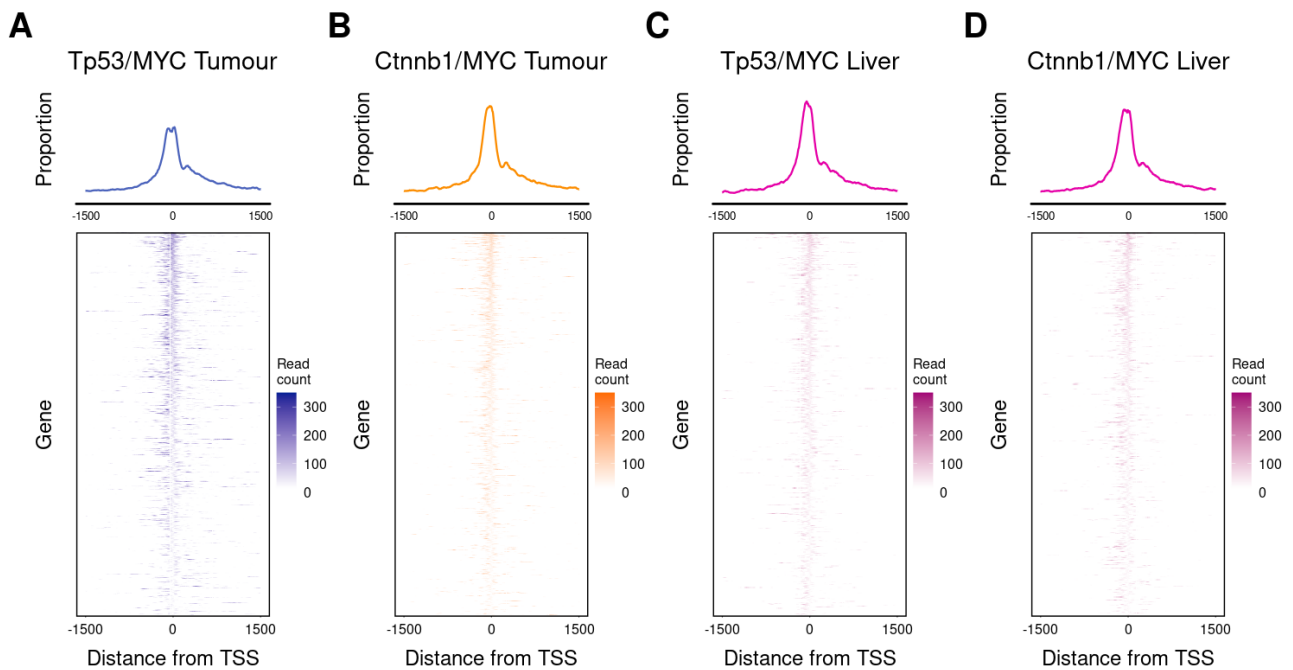
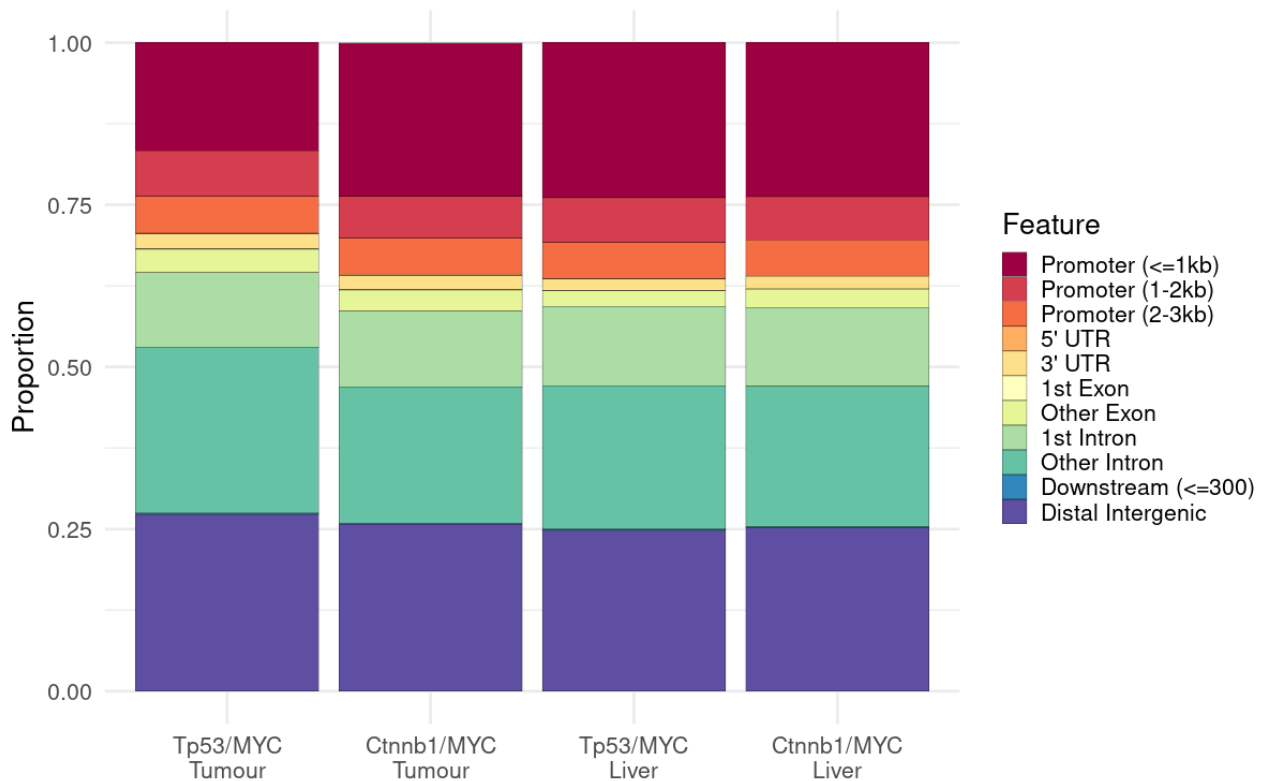


Figure 5.16: Annotated regions of open chromatin across different tissue types. $Trp53^{fl/fl}$ $Rosa26^{c-MYC/c-MYC}$ tumours more frequently had open intron regions than other tissues, which had similar open features to one another.



promoters and introns of one-carbon, glutamine and glutamate related metabolism were higher in $Ctnnb1^{exon3/Wt}$ $Rosa26^{c-MYC/c-MYC}$ tumours. KEGG pathway enrichment analysis identified that in immune infiltrated $Trp53^{fl/fl}$ $Rosa26^{c-MYC/c-MYC}$ tumours, there was a significantly higher activity in pathways associated with cytokine response and transendothelial migration of leukocytes (figure 5.17D). There was also enrichment for pathogen and viral associated pathways (Yersinia, Salmonella, HPV infection) in intron regions of $Trp53^{fl/fl}$ $Rosa26^{c-MYC/c-MYC}$ tumours (figure 5.17E). These factors are known to interact with key DNA damage sensing pathways, notably triggering the downstream cytokine targets of cGAS-STING[171]. Therefore, taken together and corroborated by the RNA sequencing results, it is possible that $Trp53^{fl/fl}$ $Rosa26^{c-MYC/c-MYC}$ tumours trigger cytokine responses through activation of these pathways which facilitates the migration of immune cells into the tumour microenvironment.

Figure 5.17: Overview of differentially accessible genomic features identified by ATAC sequencing of Trp53^{fl/fl} Rosa26^{c-MYC/c-MYC} tumours compared with Ctnnb1^{exon3/Wt} Rosa26^{c-MYC/c-MYC} tumours. Panel A – All features, showing higher accessibility of regions largely concordant with RNA-sequencing. Canonical WNT/ β -Catenin targets such as Glul were found in Ctnnb1^{exon3/Wt} Rosa26^{c-MYC/c-MYC} tumours. Panel B – Differentially accessible promoter regions. Panel C – Differentially accessible intron regions. Panel D – KEGG Pathway enrichment for differentially accessible promoter regions. Panel E – KEGG Pathway enrichment for differentially accessible intron regions.

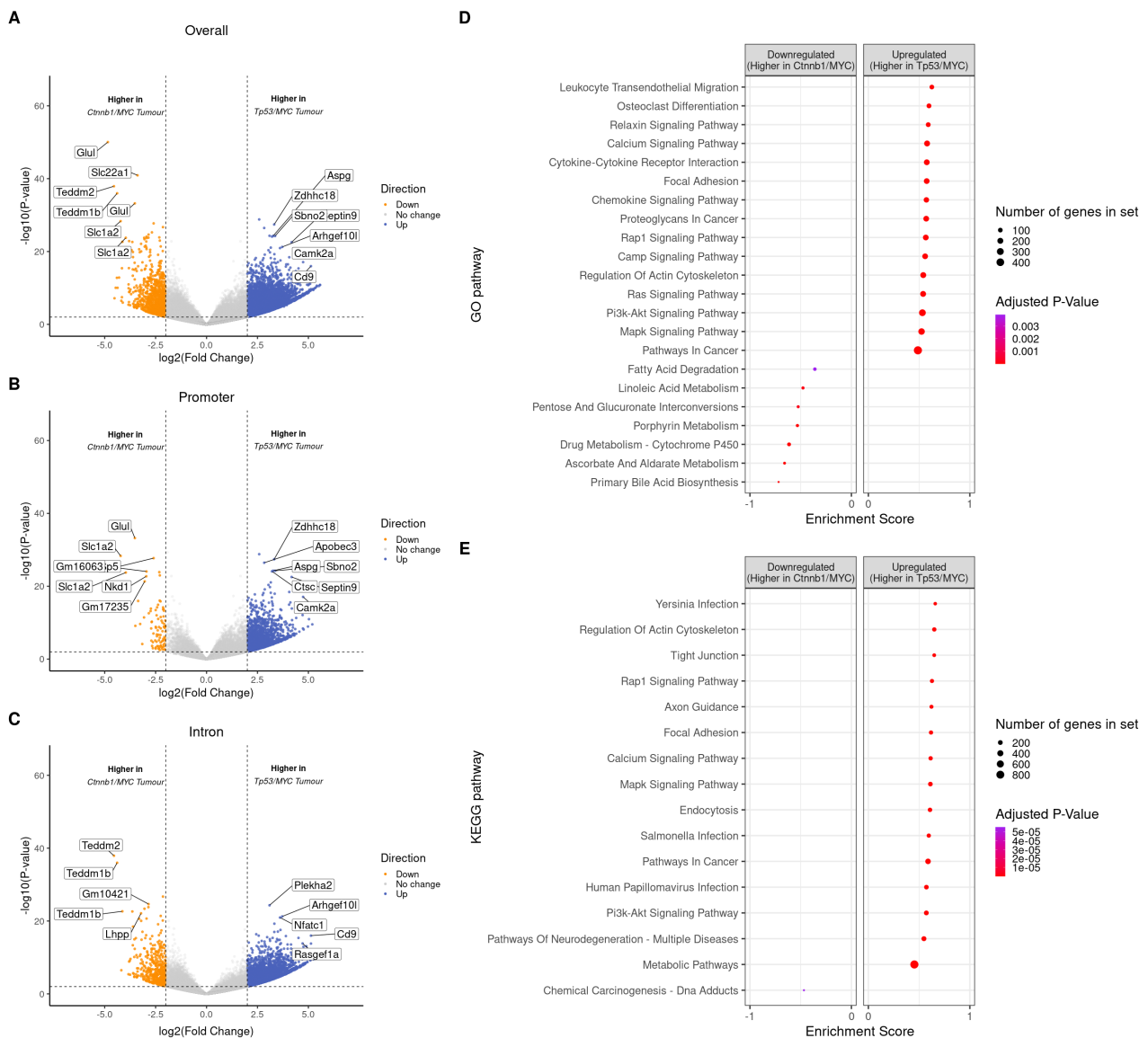


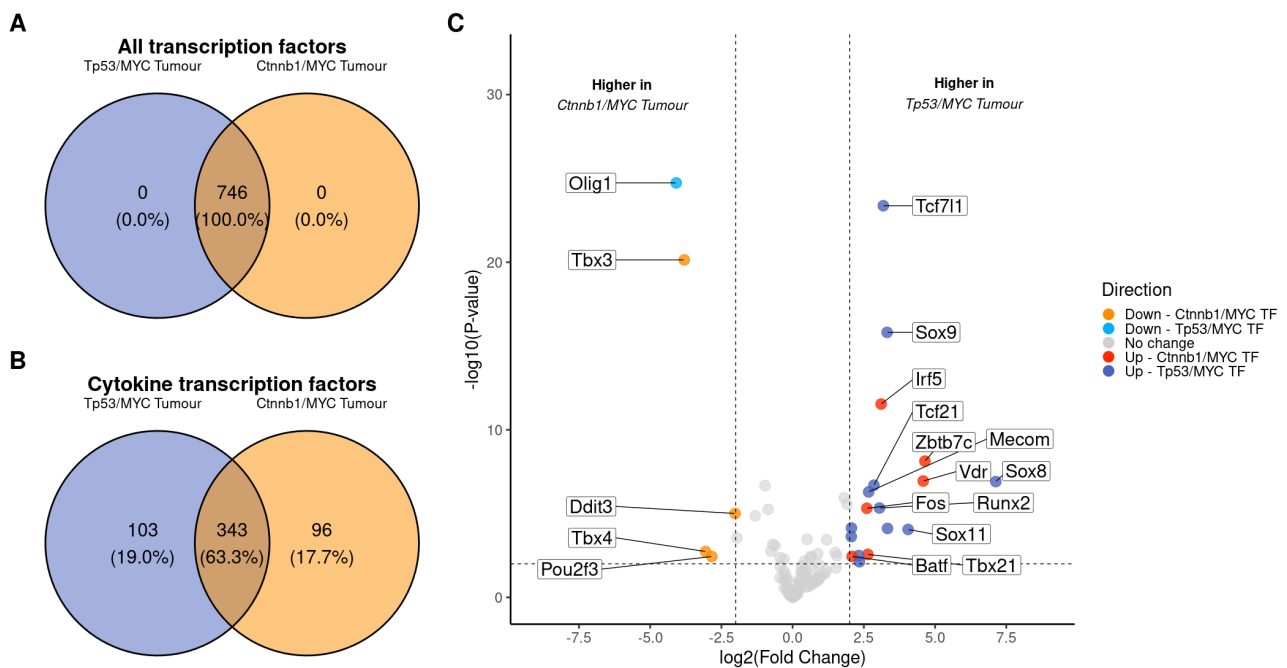
Table 5.2: Transcription factors in cytokine TSS regions found exclusively in either $\text{Trp53}^{\text{fl/fl}}$ $\text{Rosa26}^{\text{c-MYC/c-MYC}}$ or $\text{Ctnnb1}^{\text{exon3/Wt}}$ $\text{Rosa26}^{\text{c-MYC/c-MYC}}$ tumours. In the $\text{Ctnnb1}^{\text{exon3/Wt}}$ $\text{Rosa26}^{\text{c-MYC/c-MYC}}$ group many of these factors are associated with embryonic development and AP-1 mediated transcription.

Present only in $\text{Trp53}^{\text{fl/fl}}$ $\text{Rosa26}^{\text{c-MYC/c-MYC}}$ tumours	Present only in $\text{Ctnnb1}^{\text{exon3/Wt}}$ $\text{Rosa26}^{\text{c-MYC/c-MYC}}$ tumours
Alx4, Arid3b, Arnt, Arntl, Atf1, Bach2, Barhl1, Barhl2, Bcl6b, Bhlha15, Bhlhe22, Bhlhe23, Creb3l2, Dbp, Dmrt1, Foxa1, Foxb1, Foxc1, Foxe2, Foxd1, Foxf2, Foxh1, Foxi1, Foxj2, Foxj3, Foxk1, Foxl1, Foxl2, Foxn3, Foxo3, Foxo4, Foxo6, Foxp3, Gcm1, Gmeb2, Gsx2, Hes7, Hltf, Hoxa11, Hoxc13, Hoxd3, Hsf1, Hsf2, Irf6, Lin54, Maf, Mecom, Meis1, Mlx, Mnt, Msantd3, Myc, Myf6, Neurod2, Nfe2, Nkx2-2, Nkx2-3, Nkx6-1, Nkx6-2, Nkx6-3, Nr1h4, Nr2f1, Nr4a2, Olig1, Olig2, Olig3, Pax5, Pax6, Pbx2, Plagl2, Pou5f1, Pou6f1, Pou6f2, Prdm4, Rarb, Rarg, Rfx7, Runx2, Rxra, Rxb, Sox10, Sox11, Sox13, Sox15, Sox18, Sox2, Sox2, Sox21, Sox6, Sox8, Sox9, Srebf1, Tbp, Tcf21, Tcf7l1, Tef, Thrb, Tp53, Tp63, Tp73, Yy1, Zfp42, Zkscan1, Znf382, Znf384, Znf410	Atf3, Batf, Batf3, Cdx2, Cebpa, Ddit3, Dmrtc2, Dprx, E2f1, E2f2, E2f4, Eomes, Esrra, Esrrb, Esrrg, Fos, Fosl1, Foxd3, Foxq1, Glis1, Glis3, Hand1, Hes6, Hmbox1, Hoxa10, Hoxa13, Hoxb13, Hoxd13, Hsf4, Irf5, Jun, Junb, Jund, Maf, Mafa, Mga, Mitf, Mtf1, Myf5, Nkx2-5, Nkx3-2, Nr1d2, Nr1h3, Nr2e3, Nr2f1, Nr2f2, Nr2f6, Phox2a, Phox2b, Pitx1, Pitx2, Pitx3, Pou1f1, Pou2f2, Pou2f3, Pou3f1, Pou3f2, Pou3f3, Prdm15, Ptfla, Rara, Rfx1, Rora, Rxra, Rxrg, Scrt1, Scrt2, Smad2, Smad3, Tbr1, Tbx1, Tbx15, Tbx2, Tbx21, Tbx3, Tbx4, Tbx6, Tcf3, Thap1, Vdr, Xbp1, Zbtb12, Zbtb32, Zbtb7c, Zic1, Zic3, Zic4, Zic5, Znf136, Znf423, Zscan29, Zscan4

A key strength of ATAC sequencing is the ability to identify transcription factors regulating gene expression. Using HINT (HMM-based IdeNtification of Transcription factor footprints), I identified 746 transcription factors (TFs) were present across the genomes of $\text{Trp53}^{\text{fl/fl}}$ $\text{Rosa26}^{\text{c-MYC/c-MYC}}$ and $\text{Ctnnb1}^{\text{exon3/Wt}}$ $\text{Rosa26}^{\text{c-MYC/c-MYC}}$ tumours. Although the presence of these TFs was shared across both, different binding patterns were observed across tumour genotypes (figure 5.18), particularly in cytokine regions. Table 5.2 shows the TFs found exclusively in $\text{Trp53}^{\text{fl/fl}}$ $\text{Rosa26}^{\text{c-MYC/c-MYC}}$ and $\text{Ctnnb1}^{\text{exon3/Wt}}$ $\text{Rosa26}^{\text{c-MYC/c-MYC}}$ tumours respectively. In $\text{Ctnnb1}^{\text{exon3/Wt}}$ $\text{Rosa26}^{\text{c-MYC/c-MYC}}$ tumours, many of these TFs were related to embryonic development or cell stress and have been implicated in suppression of cytokine responses in tumours, most notably Atf3 and the T-box transcription factor family, both of which have been implicated in canonical WNT/ β -Catenin signalling[88, 110, 172].

Although transcription factor footprinting provides a useful overview of factors regulating

Figure 5.18: Overview of transcription factor footprints comparing immune infiltrated $Cttnb1^{exon3/Wt}$ $Rosa26^{c-MYC/c-MYC}$ tumours to $Trp53^{fl/fl}$ $Rosa26^{c-MYC/c-MYC}$ tumours. Panel A – Venn diagram of all transcription factor footprints. A total of 746 footprints were found across both tumour types. However, these were found in significantly different regions of the genome. Panel B – Venn diagram of transcription factor footprints found in cytokine gene regions (± 500 bp from TSS). Panel C – Volcano plot of differentially expressed TF RNAs found in cytokine gene regions (± 500 bp from TSS). This shows many of the TFs were upregulated in $Trp53^{fl/fl}$ $Rosa26^{c-MYC/c-MYC}$ tumours, including transcriptional activators largely. In $Cttnb1^{exon3/Wt}$ $Rosa26^{c-MYC/c-MYC}$ tumours, embryonic $Tbx3$ and $Tbx4$ factors and $Ddit3$ a stress response factor.



transcriptional control, it simply shows likelihood of binding, rather than the effect the transcription factor has on the genomic region it is bound to. By combining RNA sequencing with ATAC sequencing and TF footprinting analyses, it is possible to identify for a given TF, if transcription of the target gene is increased (activation) or decreased (repression). To do this, I selected a range of cytokine associated genes as I have done in previous cytokine analyses. I then looked to see which TF motifs were present within 500 bp of the TSSs for each given cytokine. For each cytokine, I then plotted normalised RNA counts of the cytokine gene against the RNA counts of the TF gene bound to it and calculated the Spearman's correlation coefficient (figure 5.19 and figure 5.20). These analyses demonstrate many known TF:cytokine interaction, including reliance on Stat4 and Stat5. Rarg, Wt1, Stat4 and Stat5 were generally associated with activation of cytokine expression, whereas Rxra and Foxo1 were associated with repression. Some of these TF:Cytokine combinations have not previously been described and may warrant further investigation.

Given the enrichment of viral and pathogen defence pathways in both ATAC and RNA sequencing data in immune infiltrated tumours, I hypothesised that there may be TFs present in $Ctnnb1^{\text{exon3/Wt}} \text{ Rosa26}^{\text{c-MYC/c-MYC}}$ tumours which repress transcription of these inflammatory pathways. To do this, I manually explored the TSS regions of *Sting1* and *Cxcl10*, which are major components of the cGAS-STING signalling pathway. Figure 5.21 shows the exon regions and where TFs bind within 500 bp of the TSS for both *Sting1* (figure 5.21A and 5.21B) and *Cxcl10* (figure 5.21C). In $Ctnnb1^{\text{exon3/Wt}} \text{ Rosa26}^{\text{c-MYC/c-MYC}}$ tumours, many of the transcription factor motifs present had well described repressive roles. These included MAZ (which enhances CTCF mediated transcription blockade)[173], E2F6 which is known to recruit the polycomb transcriptional repressor complex[174], and constituents of AP-1 including JDP2, JUN and FOS[175]. These constituents of AP-1 have been shown to form complexes with β -Catenin in response to genotoxic stress and may provide a direct link to β -Catenin mediated repression of these pathways [175, 176].

Figure 5.19: Selected plots of normalised counts of RNA for cytokine associated genes and transcription factors which are found within 500 bp of the TSS for the given cytokine. Test is Spearman's rank (coefficient R). Plots selected had an R of ± 0.75 or higher. Orange circular points are $Cttnb1^{exon3/Wt}$ $Rosa26^{c-MYC/c-MYC}$ and blue triangular $Trp53^{fl/fl}$ $Rosa26^{c-MYC/c-MYC}$ tumours. A positive R coefficient indicates the given transcription factor is associated with cytokine expression and a negative R coefficient indicates the factor is associated with repression.

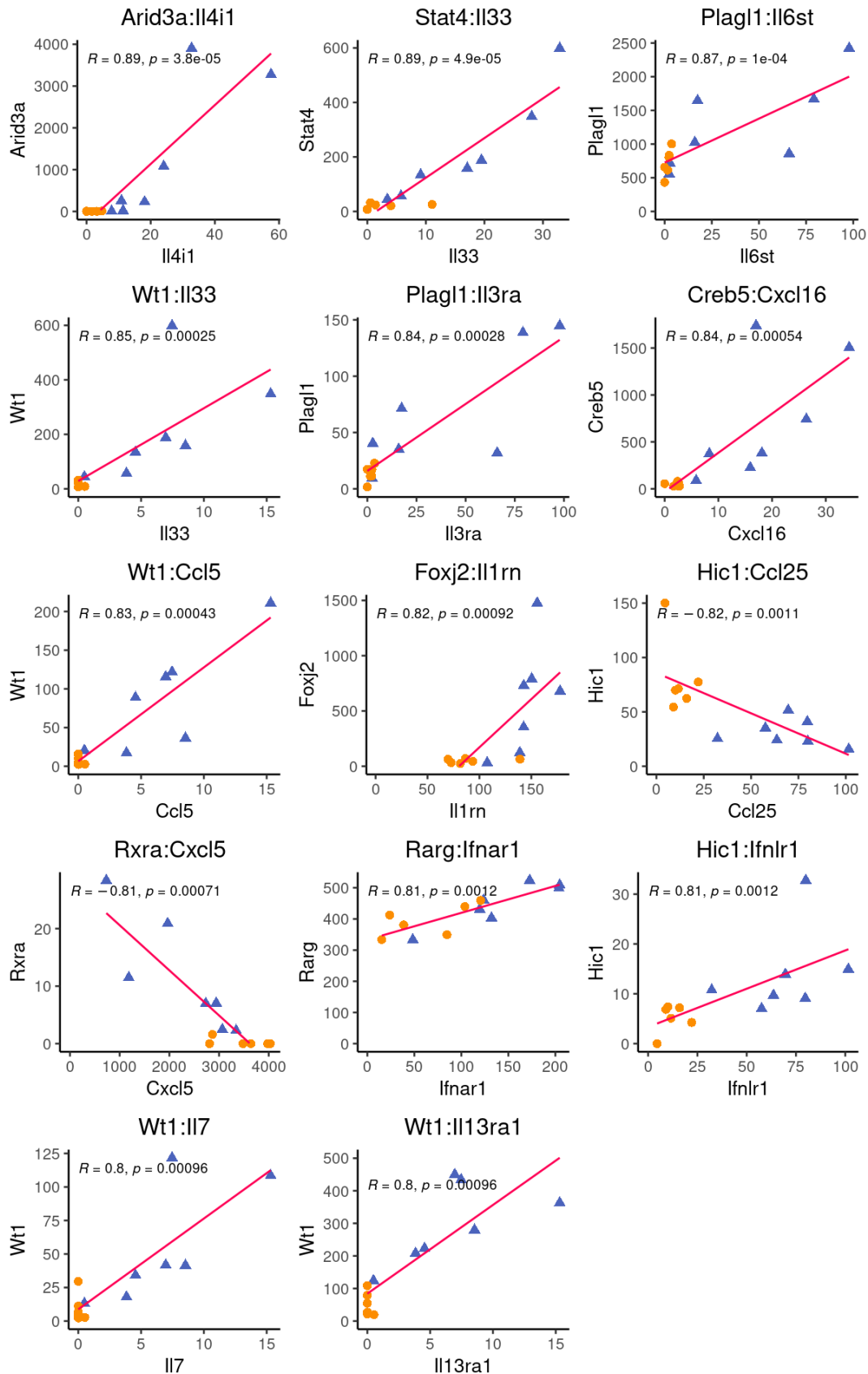


Figure 5.20: Selected plots of normalised counts of RNA for cytokine associated genes and transcription factors which are found within 500 bp of the TSS for the given cytokine (continued). Test is Spearman's rank (coefficient R). Plots selected had an R of ± 0.75 or higher. Orange circular points are $Cttnb1^{\text{exon3}/Wt}$ $Rosa26^{\text{c-MYC}/c-MYC}$ and blue triangular $Trp53^{\text{fl/fl}}$ $Rosa26^{\text{c-MYC}/c-MYC}$ tumours. A positive R coefficient indicates the given transcription factor is associated with cytokine expression and a negative R coefficient indicates the factor is associated with repression.

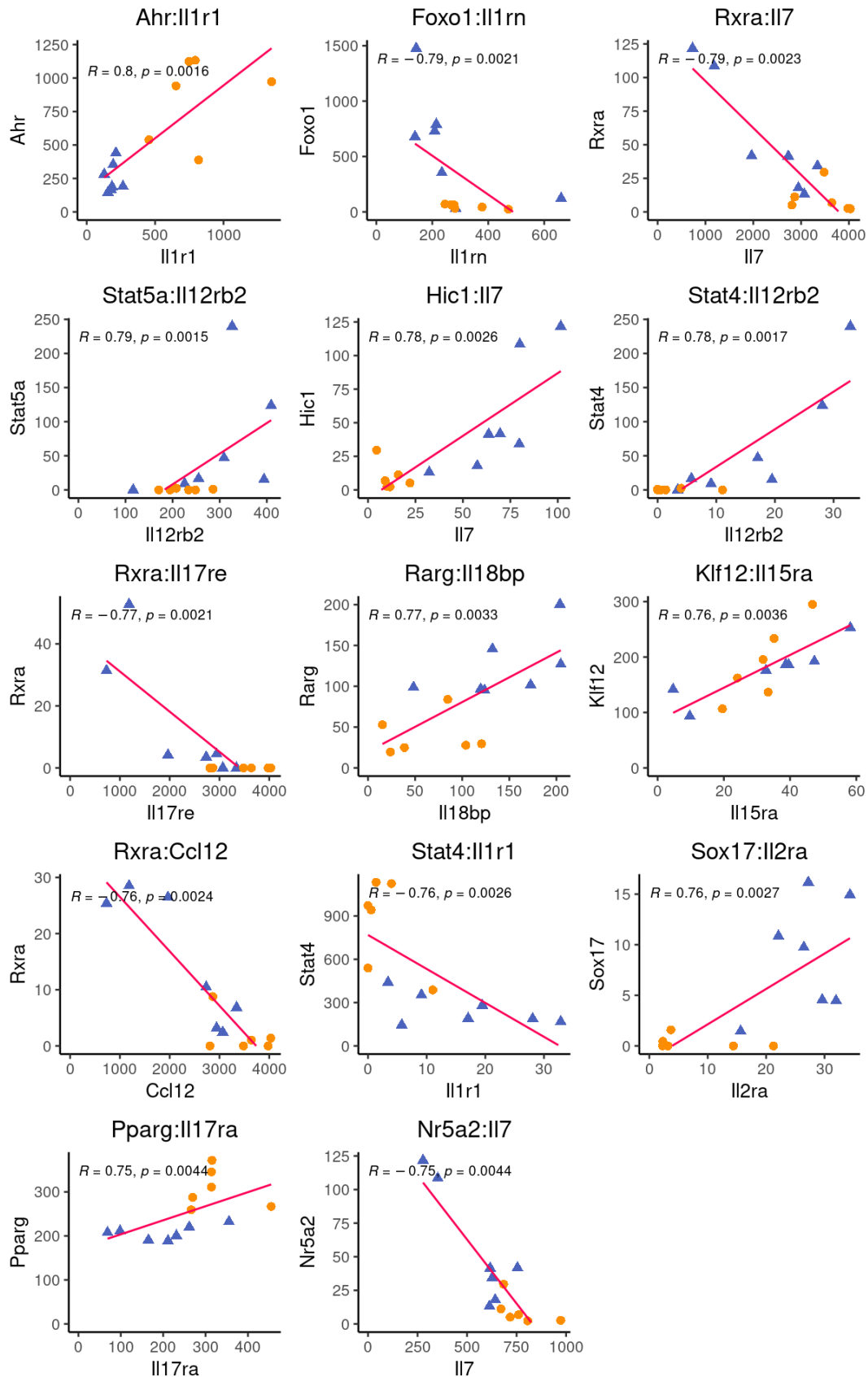
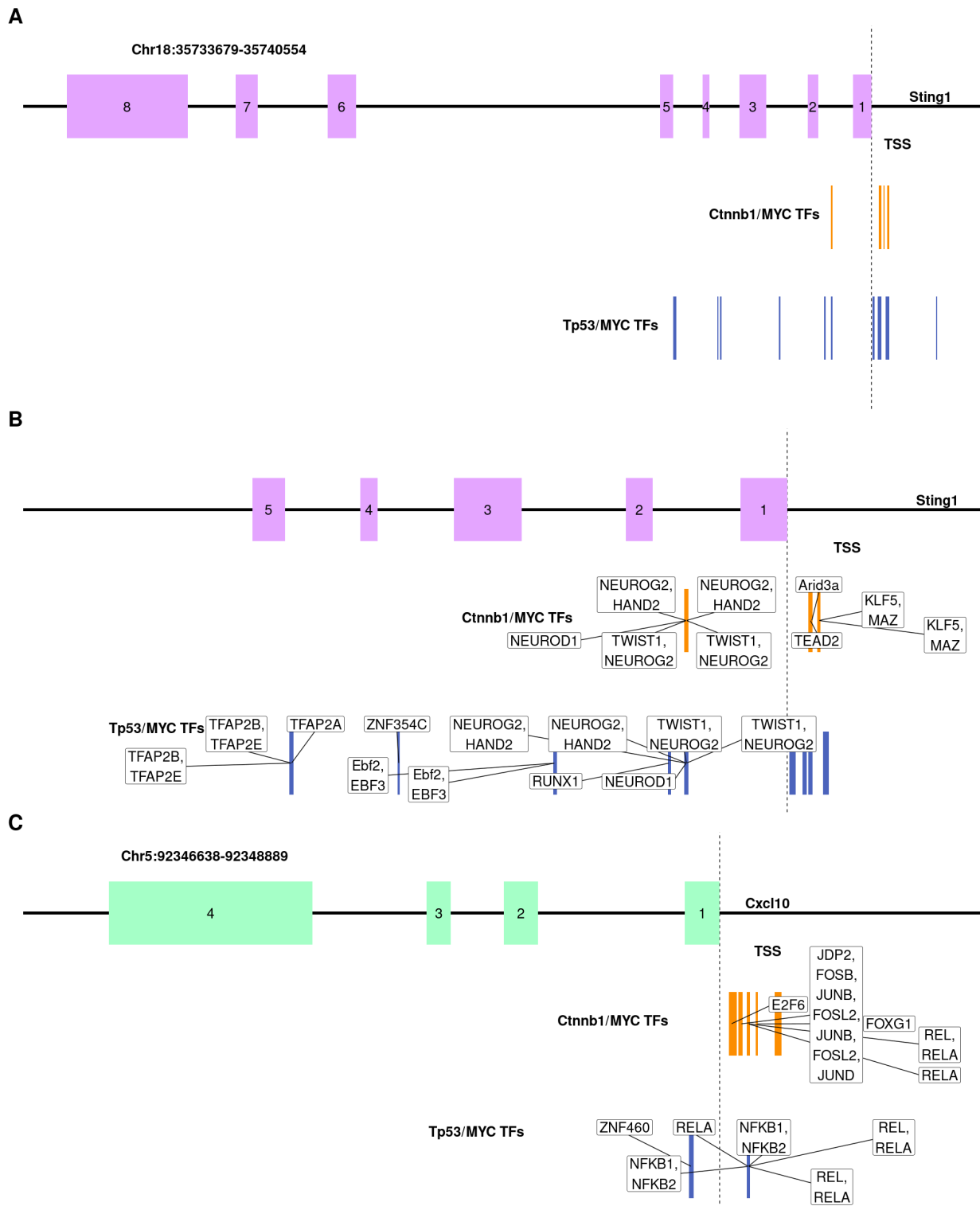


Figure 5.21: Examples of different transcription factors found in genomic regions of the pro-inflammatory STING signalling pathway (Sting1 and Cxcl10, a main STING cytokine target). Panel A – Overview of Sting1 region and transcription factors showing TFs in promoter and first intron regions. Panel B – Zoomed in view of panel A and annotation of key TFs in Sting1 promoter and intron regions comparing Ctnnb1^{exon3/Wt} Rosa26^{c-MYC/c-MYC} and Trp53^{fl/fl} Rosa26^{c-MYC/c-MYC} tumours. MYC and CTCF associated zinc finger transcription factors were identified in the Sting1 promoter region. These factors cooperate to block gene transcription. Panel C – Cxcl10 genomic region, showing presence of NF- κ B factor binding at both sites, but with AP-1 associated TF binding, which has known repressive roles. AP-1 constituents are repeated as these are found together in heteromeric complexes.



5.6 Protein-level quantification of cytokine expression in HCC mouse models

As cytokines play a major role in immune cell trafficking into tissues, I hypothesised that there would be lower levels of cytokines attracting T-cells and dendritic cells in the immune excluded $Ctnnb1^{\text{exon3/Wt}} Rosa26^{\text{c-MYC/c-MYC}}$ tumours, compared to $Trp53^{\text{fl/fl}} Rosa26^{\text{c-MYC/c-MYC}}$ tumours. Although RNA-sequencing can provide this information at the level of gene expression, post translational modifications and other events mean not all RNAs are expressed as proteins. Therefore, I used commercial cytokine array testing (Eve Technologies) to investigate cytokine expression at the protein level.

The multiplex array included the following cytokines; CCL2, CCL3, CCL4, CCL5, CCL12, CCL17, CCL19, CCL20, CCL21, CCL22, CSF1, CX3CL1, CXCL1, CXCL2, CXCL5, CXCL9, CXCL10, EOTAXIN (CCL11), EPO, G-CSF, GM-CSF, IFN- α , IFN- β , IFNG, IL-1 α , IL-1 β , IL-2, IL-3, IL-4, IL-5, IL-6, IL-7, IL-9, IL-10, IL-11, IL-13, IL-15, IL-16, IL-17, IL-20, IL-12P40, IL-12P70, LIF, TIMP-1, TNF α and VEGF.

5.6.1 Comparison of cytokine expression in $Ctnnb1^{\text{exon3/Wt}} Rosa26^{\text{c-MYC/c-MYC}}$ and $Trp53^{\text{fl/fl}} Rosa26^{\text{c-MYC/c-MYC}}$ HCC models

Results of the multiplex arrays can be seen in figure 5.22, figure 5.23 and figure 5.24. Results are presented by cytokine and tissue type. There were significant differences in cytokine concentration in $Ctnnb1^{\text{exon3/Wt}} Rosa26^{\text{c-MYC/c-MYC}}$ immune excluded tumours compared to normal liver and $Trp53^{\text{fl/fl}} Rosa26^{\text{c-MYC/c-MYC}}$ immune infiltrated tumours compared to normal liver. In $Ctnnb1^{\text{exon3/Wt}} Rosa26^{\text{c-MYC/c-MYC}}$ immune excluded tumours, where there were significant differences in cytokine concentration, cytokine levels tended to be lower in tumours compared to matched normal tissue (e.g., CXCL2, CCL4, CCL20, figure 5.22). In $Trp53^{\text{fl/fl}} Rosa26^{\text{c-MYC/c-MYC}}$ immune infiltrated tumours, compared with matched

normal tissue, cytokine levels were usually of a higher concentration (e.g., CCL2, CCL3, CXCL10, figure 5.22). This was largely in keeping with the RNA-sequencing gene expression results.

Next, I sought to address whether cytokine expression can explain the differences in immune infiltration between $Cttnb1^{\text{exon3/Wt}} Rosa26^{\text{c-MYC/c-MYC}}$ immune excluded tumours and $Trp53^{\text{fl/fl}} Rosa26^{\text{c-MYC/c-MYC}}$ immune infiltrated tumours. If a specific cytokine, or set of cytokines could explain this, it would be expected that the level of a given cytokine would be significantly higher (or lower if immunosuppressive) in the $Trp53^{\text{fl/fl}} Rosa26^{\text{c-MYC/c-MYC}}$ tumours, compared to both matched normal liver and $Cttnb1^{\text{exon3/Wt}} Rosa26^{\text{c-MYC/c-MYC}}$ tumours. Figure 5.25 summarises the findings of the multiplex array. Of the cytokines tested, levels of CCL12, CCL17, CCL22, CX3CL1, CXCL10, Eotaxin (CCL11), G-CSF and IL-16 were significantly higher in $Trp53^{\text{fl/fl}} Rosa26^{\text{c-MYC/c-MYC}}$ tumours compared with $Cttnb1^{\text{exon3/Wt}} Rosa26^{\text{c-MYC/c-MYC}}$ tumours or matched normal liver. CCL4, CCL17, CCL20, CCL22, CXCL2, Eotaxin (CCL11), IL-6 and IL12P40 were significantly lower in $Cttnb1^{\text{exon3/Wt}} Rosa26^{\text{c-MYC/c-MYC}}$ tumours than $Trp53^{\text{fl/fl}} Rosa26^{\text{c-MYC/c-MYC}}$ tumours or normal matched liver.

Of these cytokines upregulated in $Trp53^{\text{fl/fl}} Rosa26^{\text{c-MYC/c-MYC}}$ tumours, nearly all are involved in recruitment of T-cells or dendritic cells [5, 101, 171]. These cytokines primarily mediate their effects via the receptors CCR4, CX3CR1, CXCR3 and CD4. The exceptions being G-CSF and CCL11, which are implicated in the recruitment of granulocytes, and additionally having key roles in dendritic cell maturation and differentiation[177]. This suggests that $Cttnb1^{\text{exon3/Wt}} Rosa26^{\text{c-MYC/c-MYC}}$ may evade the immune system using a two-fold approach. First through preventing antigen presenting cells from infiltrating tumours, thereby preventing cytotoxic T-cell activation and second, through preventing T-cell trafficking into tumours. To confirm this, future experiments could be performed *in-vivo* to see whether deletion of CCR4, CX3CR1 and/or CXCR3 reverts $Trp53^{\text{fl/fl}} Rosa26^{\text{c-MYC/c-MYC}}$ tumours to an immune excluded phenotype.

Cytokines which were downregulated in $Cttnb1^{\text{exon3/Wt}} Rosa26^{\text{c-MYC/c-MYC}}$ tumours

Figure 5.22: Multiplex cytokine array results by cytokine and tissue type. Tests are independent samples, two-tailed Wilcoxon signed rank tests. In tumours from the immune infiltrated $\text{Trp53}^{\text{fl/fl}}$ $\text{Rosa26}^{\text{c-MYC/c-MYC}}$ genotype, levels of CCL4, CCL12, CCL17, CCL20, CCL22, CX3CL1, CXCL9, CXCL10, Eotaxin, G-CSF, IL-16 and IL-17 were significantly higher than in tumours from the immune excluded $\text{Ctnnb1}^{\text{exon3/Wt}}$ $\text{Rosa26}^{\text{c-MYC/c-MYC}}$ genotype.

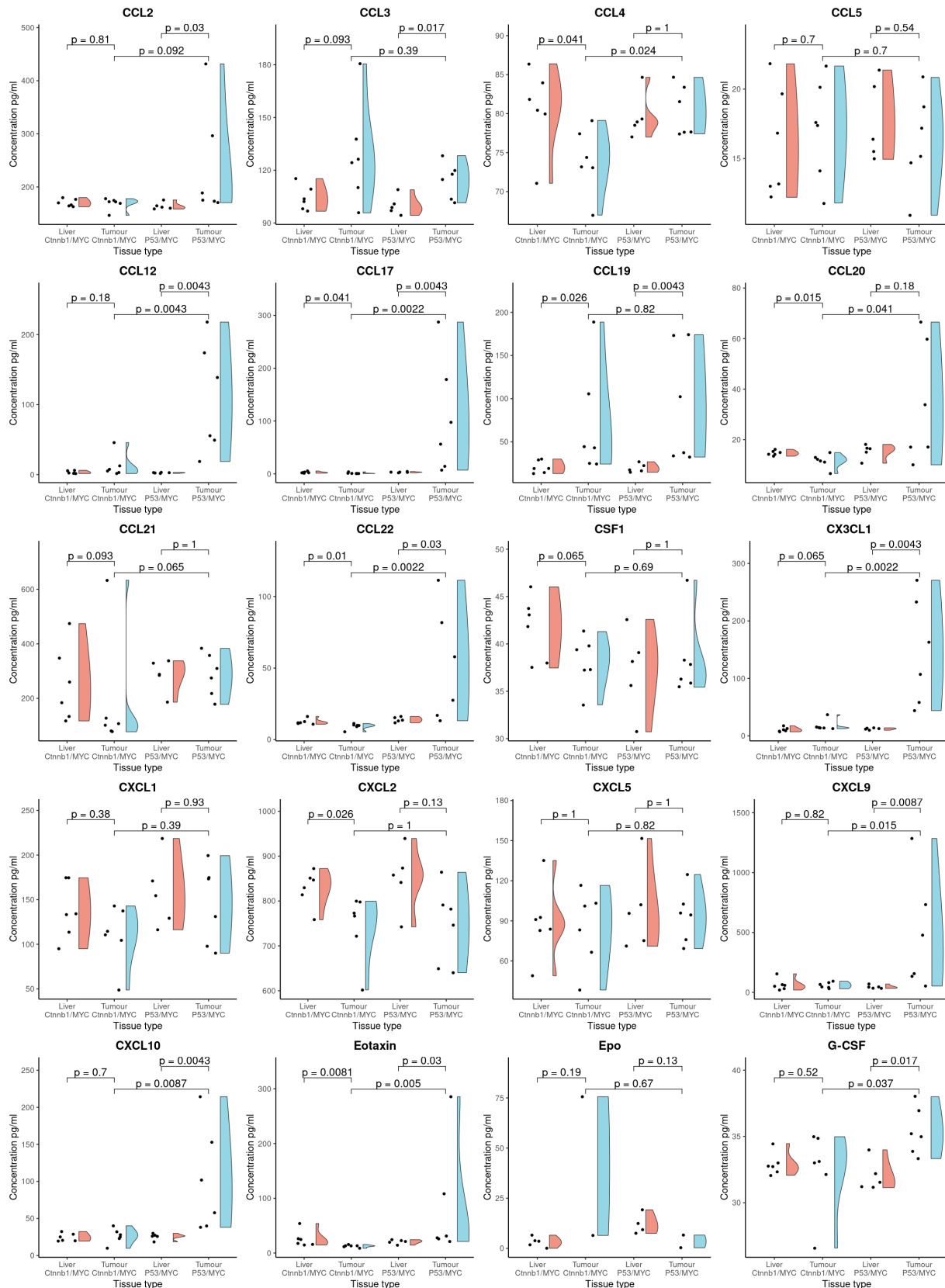
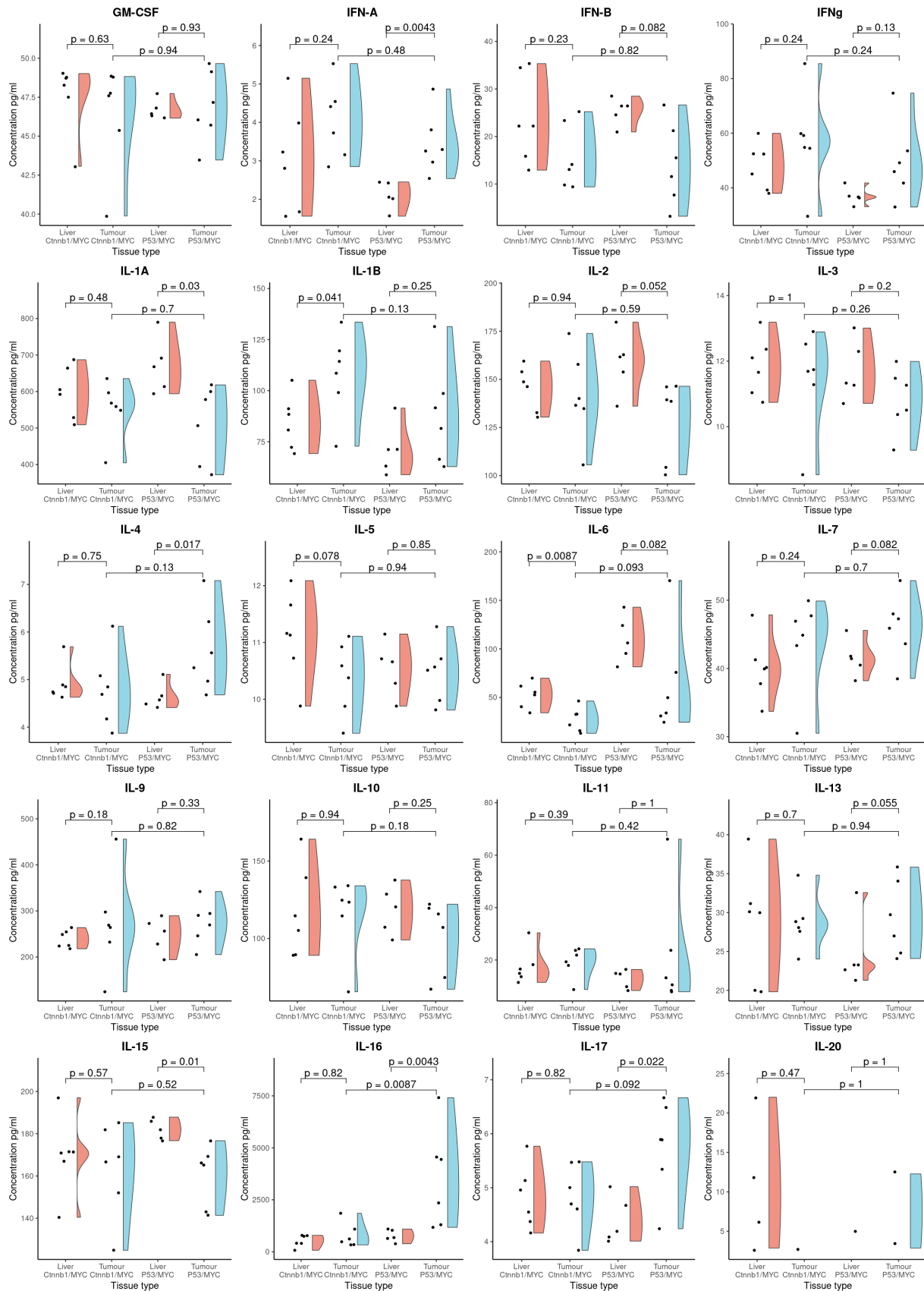


Figure 5.23: Multiplex cytokine array results by cytokine and tissue type (continued). Tests are independent samples, two-tailed Wilcoxon signed rank tests. In tumours from the immune infiltrated $\text{Trp53}^{\text{fl/fl}}$ $\text{Rosa26}^{\text{c-MYC/c-MYC}}$ genotype, levels of CCL4, CCL12, CCL17, CCL20, CCL22, CX3CL1, CXCL9, CXCL10, Eotaxin, G-CSF, IL-16 and IL-17 were significantly higher than in tumours from the immune excluded $\text{Ctnnb1}^{\text{exon3/Wt}}$ $\text{Rosa26}^{\text{c-MYC/c-MYC}}$ genotype.



compared with immune infiltrated Trp53^{fl/fl} Rosa26^{c-MYC/c-MYC} tumours and normal matched liver were not involved with T-cell and dendritic cell recruitment. Most of these cytokines (CCL17, CXCL2, CCL11, IL-6 and IL12p40) have been described most frequently as being produced by granulocytes and macrophages as part of innate immune responses to PAMP/DAMP signals from tissue damage[178]. The reduced expression of these in Ctnnb1^{exon3/Wt} Rosa26^{c-MYC/c-MYC} tumours suggests these tumours may either recruit fewer cell types which produce these cytokines or may be suppressing production of PAMP/DAMP signals to avoid immune cell recruitment to the tumour microenvironment.

5.7 Summary

Using integration of multiple high-throughput technologies, I have characterised differences across the genome, epigenome, transcriptome, and proteome which may contribute to the immune excluded phenotype seen in Ctnnb1^{exon3/Wt} Rosa26^{c-MYC/c-MYC} tumours. The findings of this chapter are summarised in table 5.3. As immune evasion is a complex and multifactorial process, this ‘multiomic’ approach allows an unbiased and synergistic assessment of which mechanisms are likely to be underpinning this.

In immune infiltrated Trp53^{fl/fl} Rosa26^{c-MYC/c-MYC} tumours, there were significantly elevated levels of cytokines which are known to potently attract immune cells, including those which mediate key anti-tumour responses. In addition to this immune checkpoint expression was significantly higher in Trp53^{fl/fl} Rosa26^{c-MYC/c-MYC} tumours, which may explain why this model is sensitive to anti-PD1 therapy. Interestingly, there was no difference in the tumour mutational burden between Ctnnb1^{exon3/Wt} Rosa26^{c-MYC/c-MYC} and Trp53^{fl/fl} Rosa26^{c-MYC/c-MYC} tumours, suggesting lack of cytokine expression in the Ctnnb1^{exon3/Wt} Rosa26^{c-MYC/c-MYC} model is due differences in how Ctnnb1^{exon3/Wt} or Trp53 deletion subsequently affect signalling pathways.

In Trp53^{fl/fl} Rosa26^{c-MYC/c-MYC} tumours I consistently observed enrichment of pathways associated with anti-viral or responses to pathogens in both RNA and ATAC sequencing data.

Table 5.3: Summary of findings of this chapter, establishing most likely mechanisms that may contribute to immune exclusion and therapy resistance in $Ctnnb1^{\text{exon3/Wt}}$ $Rosa26^{\text{c-MYC/c-MYC}}$ tumours.

Feature	Likelihood of causing immune exclusion or resistance
Lack of cytokine expression	Highly likely - $Ctnnb1^{\text{exon3/Wt}}$ $Rosa26^{\text{c-MYC/c-MYC}}$ tumours had very low levels of cytokine expression, particularly those known to attract T-cells and dendritic cells
Low levels of PAMP/DAMPs or DNA damage	Highly likely – activation of viral and defence associated pathways in RNA-sequencing, along with AP-1 associated footprints in ATAC-sequencing data Deletions are present in mt-DNA regions of immune infiltrated $Trp53^{\text{fl/fl}}$ $Rosa26^{\text{c-MYC/c-MYC}}$ tumours
Inhibitory immune checkpoint expression	Highly unlikely – immune checkpoints have lower expression than normal liver tissue in $Ctnnb1^{\text{exon3/Wt}}$ $Rosa26^{\text{c-MYC/c-MYC}}$ tumours
Low tumour mutational burden	Unlikely – both $Ctnnb1^{\text{exon3/Wt}}$ $Rosa26^{\text{c-MYC/c-MYC}}$ and $Trp53^{\text{fl/fl}}$ $Rosa26^{\text{c-MYC/c-MYC}}$ tumours have similar levels of mutations
Deletion or amplification of inflammatory or immunosuppressive genomic regions	Unlikely – both $Ctnnb1^{\text{exon3/Wt}}$ $Rosa26^{\text{c-MYC/c-MYC}}$ and $Trp53^{\text{fl/fl}}$ $Rosa26^{\text{c-MYC/c-MYC}}$ tumours have similar regions amplified or deleted
Presence of immunosuppressive cells	Unlikely – immunosuppressive cell types (most likely regulatory T-cells, neutrophils, or other myeloid populations) would likely produce mRNAs that would be identified in this analysis Furthermore, immunohistochemistry characterisation of $Ctnnb1^{\text{exon3/Wt}}$ $Rosa26^{\text{c-MYC/c-MYC}}$ tumours identifies a paucity of immune cells, which is not restricted to a particular lineage

This was further reinforced by evidence at the protein-level demonstrating increased expression of cytokines associated with PAMP/DAMP and cGAS-STING pathways (CXCL10 and $IFN\alpha$) in $Trp53^{\text{fl/fl}}$ $Rosa26^{\text{c-MYC/c-MYC}}$ tumours. This suggests that $Ctnnb1^{\text{exon3/Wt}}$ may be somehow suppressing these responses, either directly or through reducing sources of PAMP/DAMPs. Analysis of transcription factor footprints identified several embryonic development and stress response transcription factors which were exclusively present in $Ctnnb1^{\text{exon3/Wt}}$ $Rosa26^{\text{c-MYC/c-MYC}}$ tumours. Indeed, it is emerging that embryonic or stem-like cell states are found to have incredibly efficient DNA repair machinery and high replication fidelity. Based on these findings and the known role of canonical WNT/ β -Catenin signalling in stem cell development, it could be hypothesised that $Ctnnb1^{\text{exon3/Wt}}$ $Rosa26^{\text{c-MYC/c-MYC}}$ tumours suppress inflammatory responses through relying on ‘embryonic-like’ cell-cycle checkpoint fidelity and DNA-repair mechanisms.

An intriguing finding was the presence of different TF footprints around the sites of cytokine regions and inflammation promoting genes, such as *Sting1*. First, I found several potential targets which were associated with activation or repression cytokine expression. An

example of this is Rarg (Retinoic acid receptor-gamma), which was associated with higher expression of cytokine associated genes, namely *Ifnar1* and *Il18bp*. Many of these targets, including Rarg, have readily available agonists or antagonists which could be tested as adjuvant immunotherapies. Second, I found the presence of known ‘transcription blocking’ factors in cytokine regions of *Ctnnb1^{exon3/Wt} Rosa26^{c-MYC/c-MYC}* tumours[174]. These included CTCF, MAZ and AP-1. Interestingly, there are reports of many of these factors being activated or found to have altered function when in complex with β -Catenin[175]. Performing immunoprecipitation experiments to identify these proteins may help to elucidate how these TFs may suppress cytokine expression and discover druggable targets.

5.8 Future directions

- Although there was no significant difference in tumour mutational burden between *Ctnnb1^{exon3/Wt} Rosa26^{c-MYC/c-MYC}* and *Trp53^{fl/fl} Rosa26^{c-MYC/c-MYC}* tumours, this was assessed crudely by simply counting the number of alterations per kilobase per million reads. Tumour neoantigens may still be responsible for the differences observed and further work to use neoantigen prediction software to further refine this analysis may be useful. To definitively establish the role of tumour antigens in promoting anti-tumour immunity, it would be useful to test whether in the presence of a defined neoantigen *Ctnnb1^{exon3/Wt} Rosa26^{c-MYC/c-MYC}* tumours remain immune excluded. Until now there has not been a mouse model which would allow this. As discussed later in chapter 7, I have successfully developed a model which will allow expression of a defined neoantigen in a conditional manner.
- RNA sequencing analysis identified anti-viral and host defence pathways as highly enriched in *Trp53^{fl/fl} Rosa26^{c-MYC/c-MYC}* tumours. Further investigation of which pathways these are likely to be and whether they can be targeted to induce cytokine expression in immune excluded *Ctnnb1^{exon3/Wt} Rosa26^{c-MYC/c-MYC}* tumours to promote infiltration with T-cells and dendritic cells is warranted.
- Bulk RNA sequencing of *Ctnnb1^{exon3/Wt} Rosa26^{c-MYC/c-MYC}* and *Trp53^{fl/fl}*

Rosa26^{c-MYC/c-MYC} tumours identified profound differences in cytokine and immune checkpoint expression. However, it is unclear whether these are expressed by tumour epithelium, or other immune mesenchymal cells or a combination of both. The spatial patterns of immune checkpoint RNA molecule expression in Trp53^{fl/fl} Rosa26^{c-MYC/c-MYC} tumours suggested these may be expressed in a range of cells. Therefore, using high resolution spatial transcriptomics or single-cell RNA sequencing may help to identify which cell types cooperate to promote immune infiltration into tumours.

- Pathways and gene targets identified in this molecular characterisation should also be studied at the protein level. Transcription of RNA does not equate to production of protein, and the amino acid products of many genes undergo post-translational modifications which alter function. Similarly, much pathway activity is mediated by biological processes which cannot be detected at the gene-level, such as phosphorylation. By using protein level measurement such as western-blot, ELISAs and imaging techniques, the activity of gene pathways can be validated at the protein level and localised to the cell-type in which they are produced.
- Further work should be undertaken to identify therapeutic targets in pathways which control cytokine production in tumour cells. Understanding this will allow these pathways to be targeted using selective tools such as small molecules or antisense oligonucleotides and generate chemotactic gradients that allow immune cells to be trafficked into tumours. Approaches such as intratumoural delivery may have benefits in selected cases, but are unlikely to be useful in many patients, particularly those with disseminated disease or disease that is not anatomically amenable to intratumoural delivery. Targets could be identified systematically by using high throughput drug or genetic screening techniques such as CRISPR-Cas9 libraries. These libraries could be combined with fluorescent reporter constructs to allow screening of large numbers of cells and could be multiplexed to measure several different cytokines. Based on this work, I have designed Ccl5-mNeonGreen and Cxcl10-mRuby2 reporter constructs to identify new immunotherapeutic targets in high-throughput screens (data not shown,

but under current validation).

Chapter 6

Targeting the cGAS-STING pathway
to induce cytokine expression in
models of immune excluded
hepatocellular carcinoma

6.1 Introduction

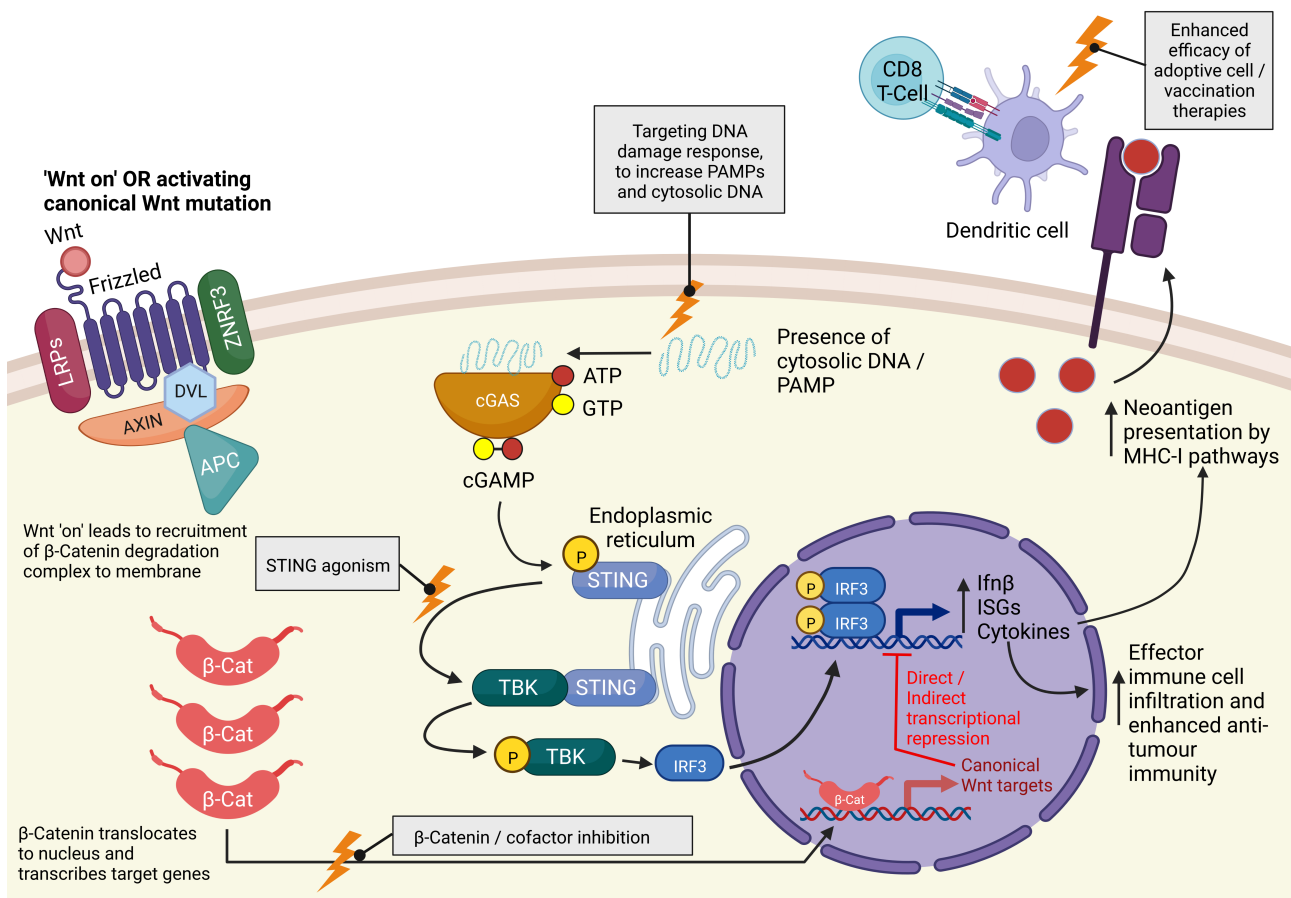
To promote immune cell infiltration into the tumour microenvironment, understanding how these cytokines are produced is essential. As the cytokines which promote anti-tumour immune responses are absent in $Ctnnb1^{\text{exon3/Wt}}$ $Rosa26^{\text{c-MYC/c-MYC}}$ tumours, they are very difficult to target. Recruitment of immune cells into tissue microenvironments is complex and requires chemokine/cytokine (termed cytokine onwards) gradients. Therefore, approaches such as systemic agonism of cytokine receptors or administration of recombinant cytokine is unlikely to work.

Most literature on how tumour epithelial cells control cytokine signalling and production is relatively sparse. However, there are a handful of pathways which have been studied which are well known to promote production of some of the cytokines I have identified as being highly expressed in immune infiltrated $Trp53^{\text{fl/fl}}$ $Rosa26^{\text{c-MYC/c-MYC}}$ tumours. These include CXCL10 and CCL5[179, 180]. CXCL10 is secreted by several cell-types, including epithelial and endothelial cells. It acts through its receptor CXCR3 and has been shown to attract a wide variety of immune cells, including macrophages, monocytes, and dendritic cells. Crucially, it potently attracts CD8+ T-cells and promotes anti-tumour immune responses[181]. CCL5 is a proinflammatory cytokine, which can be secreted by epithelial cells and promotes the recruitment of immune subsets which contribute to anti-tumour immunity[182]. This includes T-cells, natural killer cells and dendritic cells. It exerts its effects through its receptors CCR1, CCR3, CCR4 and CCR5.

Both CXCL10 and CCL5 can be produced by epithelial cells, making them well suited as a specific means to induce pro-inflammatory cytokine signalling in tumour epithelium[180]. In both genes, there are interferon stimulated response elements (ISRE) found in the promoter regions. This feature allows epithelial-specific cytokine production of CXCL10 and CCL5 to arise when upstream pathways are targeted to induce Type-I interferon responses. These type-I interferon (IFNs) responses detect cell stress, such as viral infection, or DNA damage, which then stimulates a response causing specific interferon regulatory factors (IRF) to bind to ISRE

sites across the genome. Binding of these IRFs to ISREs leads to the transcription of these genes and cytokine production. These responses attract the immune system and can promote both immune responses and antigen presentation facilitating immune cytotoxicity against cells producing type-I IFNs in order to remove a potential hazard to the rest of the organism (i.e. an infected cell).

Figure 6.1: Overview of the cGAS-STING pathway and potential interactions with canonical WNT/ β -Catenin signalling which may prevent adequate activation and subsequent cytokine production.



The cGAS-STING pathway senses the presence of cytosolic DNA and triggers expression of inflammation in response to this (figure 6.1). This is a key component of the innate immune system, as the presence of DNA within the cytosol often arises from potentially harmful sources, including viral infection, intracellular bacteria, or carcinogenesis[179, 180]. Activation of the cGAS-STING pathway in response to cytosolic DNA allows clearance of these cells by the immune system and is implicated in both immunosurveillance and the senescence associated secretory phenotype which promotes the recruitment of immune cells[183]. Cyclic GMP-AMP synthase (cGAS) binds to cytosolic dsDNA, which conformationally alters cGAS to permit the formation of 2'3' cyclic GMP-AMP (cGAMP) from Adenosine triphosphate (ATP) and Guanosine-5'-triphosphate (GTP). 2'3'cGAMP is a potent Stimulator of Interferon Genes (STING) agonist. When cGAS binds dsDNA, it forms spatially distributed complexes along the length of the dsDNA strand and activation is

therefore proportional to the length and quantity of dsDNA present. This prevents aberrant activation of cGAS in response to physiological levels of cytosolic dsDNA. The increased level of 2'3'cGAMP is detected by STING at the endoplasmic reticulum, which in turn leads to phosphorylation of TANK-binding kinase 1 (TBK1), which then phosphorylates STING itself. There may also be some activation of the RELA and RELB NF- κ B subunits, but this is poorly characterised. The phosphorylated STING/TBK1 complex can then phosphorylate IRF3, allowing its dimerization and subsequent translocation into the nucleus where it then activates a range of interferon type I target genes. This activation is tissue and context specific but is known to include CXCL10 and CCL5[179, 180].

In the previous chapter, I identified that $Ctnnb1^{\text{exon3/Wt}} \text{ Rosa26}^{\text{c-MYC/c-MYC}}$ had low levels of expression of the cytokines Ccl5 and Cxcl10, which are both direct targets of the cGAS-STING signalling pathway. Pathway enrichment analysis also identified activation of viral and intracellular bacteria (salmonella and yersinia) defence pathways were upregulated in the immune infiltrated $\text{Trp53}^{\text{fl/fl}} \text{ Rosa26}^{\text{c-MYC/c-MYC}}$ model. Furthermore, ATAC sequencing data identified motifs around promoter regions of *Sting1* and *Cxcl10* which were associated with transcriptional repression in immune excluded $Ctnnb1^{\text{exon3/Wt}} \text{ Rosa26}^{\text{c-MYC/c-MYC}}$ tumours. Therefore, targeting this pathway may allow cytokine signalling to be induced in a selective manner.

6.2 Hypothesis

- Activation of the cGAS-STING pathway in $Ctnnb1^{\text{exon3/Wt}} \text{ Rosa26}^{\text{c-MYC/c-MYC}}$ tumour cells will induce expression of cytokines to attract immune cell populations with anti-tumour functions (including Ccl5 and Cxcl10).

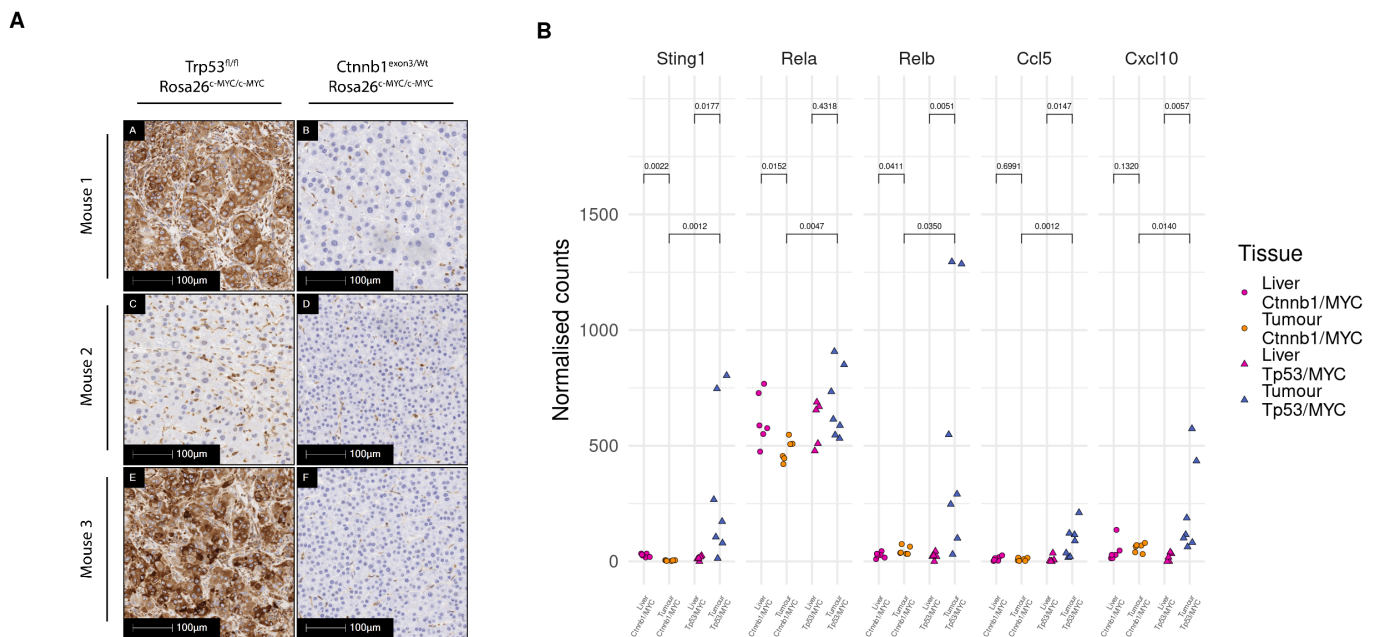
6.3 Targeting the cGAS-STING pathway

To establish whether $\text{Trp53}^{\text{fl/fl}} \text{ Rosa26}^{\text{c-MYC/c-MYC}}$ tumours had higher expression of STING, sections from $Ctnnb1^{\text{exon3/Wt}} \text{ Rosa26}^{\text{c-MYC/c-MYC}}$ and $\text{Trp53}^{\text{fl/fl}} \text{ Rosa26}^{\text{c-MYC/c-MYC}}$ tumours were

stained (figure 6.2) for the protein. In $\text{Trp53}^{\text{fl/fl}}$ $\text{Rosa26}^{\text{c-MYC/c-MYC}}$, STING expression was much higher, albeit varied between tumours. Some tumours had a very strong cytoplasmic stain, whereas others had no cytoplasmic staining but did have some mild to moderate nuclear staining. STING can reside within the cytoplasm or in the nuclear envelope, but both forms appear to activate similar target genes[184]. $\text{Ctnnb1}^{\text{exon3/Wt}}$ $\text{Rosa26}^{\text{c-MYC/c-MYC}}$ tumours had no expression of STING at all. In both genotypes STING was also expressed in cells with macrophage/Kupffer cell morphology and in mononuclear cells (figure 6.2).

Next, to test whether STING target genes are expressed in $\text{Trp53}^{\text{fl/fl}}$ $\text{Rosa26}^{\text{c-MYC/c-MYC}}$ tumours as suggested by the mouse models, I looked at the differences in normalised RNA counts from the RNA-sequencing timepoint I performed in the previous chapter. This analysis is shown in figure 6.2B. All the STING effector genes studied (*Rela*, *Relb*, *Ccl5*, *Cxcl10*) had significantly greater expression in $\text{Trp53}^{\text{fl/fl}}$ $\text{Rosa26}^{\text{c-MYC/c-MYC}}$ compared to $\text{Ctnnb1}^{\text{exon3/Wt}}$ $\text{Rosa26}^{\text{c-MYC/c-MYC}}$ tumours and all genes tested besides *Rela* were significantly higher in $\text{Trp53}^{\text{fl/fl}}$ $\text{Rosa26}^{\text{c-MYC/c-MYC}}$ tumours versus normal liver.

Figure 6.2: STING staining and STING target gene expression in $Cttnb1^{exon3/Wt}$ $Rosa26^{c-MYC/c-MYC}$ and $Trp53^{fl/fl}$ $Rosa26^{c-MYC/c-MYC}$ models of HCC. Panel A – STING immunohistochemistry, note heterogenous expression in $Trp53^{fl/fl}$ $Rosa26^{c-MYC/c-MYC}$. Some STING is cytosolic in top and bottom inset micrographs, whereas middle inset micrograph has weak nuclear staining for STING in the tumour epithelia. There was no epithelial expression of STING in any $Cttnb1^{exon3/Wt}$ $Rosa26^{c-MYC/c-MYC}$ tumours and very little in the tumour microenvironment. All images acquired on Leica Aperio AT-2 at 20x magnification. Representative images from $n = 6$ mice at day 160 timepoint post AAV8-TBG-Cre for $Trp53^{fl/fl}$ $Rosa26^{c-MYC/c-MYC}$, day 140 for $Cttnb1^{exon3/Wt}$ $Rosa26^{c-MYC/c-MYC}$. Panel B – Normalised gene expression counts of STING target gene expression from $Cttnb1^{exon3/Wt}$ $Rosa26^{c-MYC/c-MYC}$ and $Trp53^{fl/fl}$ $Rosa26^{c-MYC/c-MYC}$ models of HCC.



To see whether these findings were relevant to human disease before proceeding further, I then performed the same analysis on RNA-sequencing data from the Cancer Genome Atlas to see whether expression of STING1, RELA, RELB, CCL5 and CXCL10 were associated with immune infiltration. For this, I used the quantification of immune cells in human H&E tissue performed by Dr Tim Kendall. Figure 6.3 below shows the results of this and Gene Set Enrichment pathway analysis, of tumours which had no infiltrate compared with those which had high levels of immune infiltrate. Concordant with the mouse data, this analysis showed that immune infiltrated tumours had significantly higher levels of STING1, RELB, CCL5 and CXCL10 compared to those without infiltrate.

Gene set enrichment analysis of Gene Ontology (GO) terms found upregulation of leukocyte migration and activation pathways, but also significantly higher levels of innate immune response, in keeping with activity of pathways such as cGAS-STING. Interestingly, DNA repair and chromosome arrangement pathways were more highly expressed in tumours with low levels of immune infiltrate. Improved chromosome organisation and effective DNA repair may result in lower levels of dsDNA in the cytosol of these tumours and account for a lack of STING1, RELB, CCL5 and CXCL10 expression.

6.3.1 Stimulation of $Cttnb1^{\text{exon3/Wt}}$ $Rosa26^{\text{c-MYC/c-MYC}}$ and $Trp53^{\text{fl/fl}}$ $Rosa26^{\text{c-MYC/c-MYC}}$ tumour cells in-vitro with 2'3'cGAMP

To test the hypothesis that stimulation of the cGAS-STING pathway could induce pro-inflammatory cytokine signalling pathways (namely from type-I interferon responses), I performed an in-vitro experiment to ascertain the effect of exogenous 2'3'cGAMP on $Cttnb1^{\text{exon3/Wt}}$ $Rosa26^{\text{c-MYC/c-MYC}}$ cells.

An overview of this experiment can be seen in figure 6.4A. Briefly, tumour organoids were isolated from both $Cttnb1^{\text{exon3/Wt}}$ $Rosa26^{\text{c-MYC/c-MYC}}$ and $Trp53^{\text{fl/fl}}$ $Rosa26^{\text{c-MYC/c-MYC}}$ tumour bearing mice and grown in-vitro. Both organoid lines were cultured in the same media and same incubator. Experiments were performed at the same passage number. Organoids were suspended into Matrigel and plated at 5000 cells per well in 24-well plates and supplemented with organoid culture medium. Organoids were grown undisturbed for 6 days. At day 6, the media was replaced with fresh organoid media. 24 hours later, 12 wells per plate were treated with 10 ug/ml 2'3'cGAMP in fresh organoid media. This dose was selected as there are previous data in the literature on using this or higher doses. Therefore, I opted for a more conservative dose to provide more certainty in direction of any observed effect. The other 12 wells treated with fresh organoid media and the corresponding volume of sterile PBS from the same bottle used to dilute the lyophilised 2'3'cGAMP. Cells were incubated with 2'3'cGAMP or PBS for 48 hours, cells were then washed in ice-cold PBS and RNA extracted from the resulting cell pellet at 4 °C. I then enriched for mRNA and constructed sequencing libraries which were then sequenced at a minimum depth of 20M reads per sample.

Figure 6.3: Expression of cGAS-STING genes and Gene Set Enrichment of Gene Ontology (GO) terms by levels of immune infiltration from patients with HCC in the Cancer Genome Atlas. Panel A – Significantly higher levels of STING1, RELB, CCL5 and CXCL10 in patients with high immune infiltrate compared to those with no infiltration. Yellow diamonds represent mean normalised count values and error bars are \pm 95% confidence intervals. Statistical tests are Wilcoxon rank sum. Panel B – Gene Set Enrichment of Gene Ontology (GO) analysis of HCC tumours from the Cancer Genome Atlas comparing those with have no immune infiltrate versus those with high levels of infiltration scored by histopathological assessment (Dr Tim Kendall).

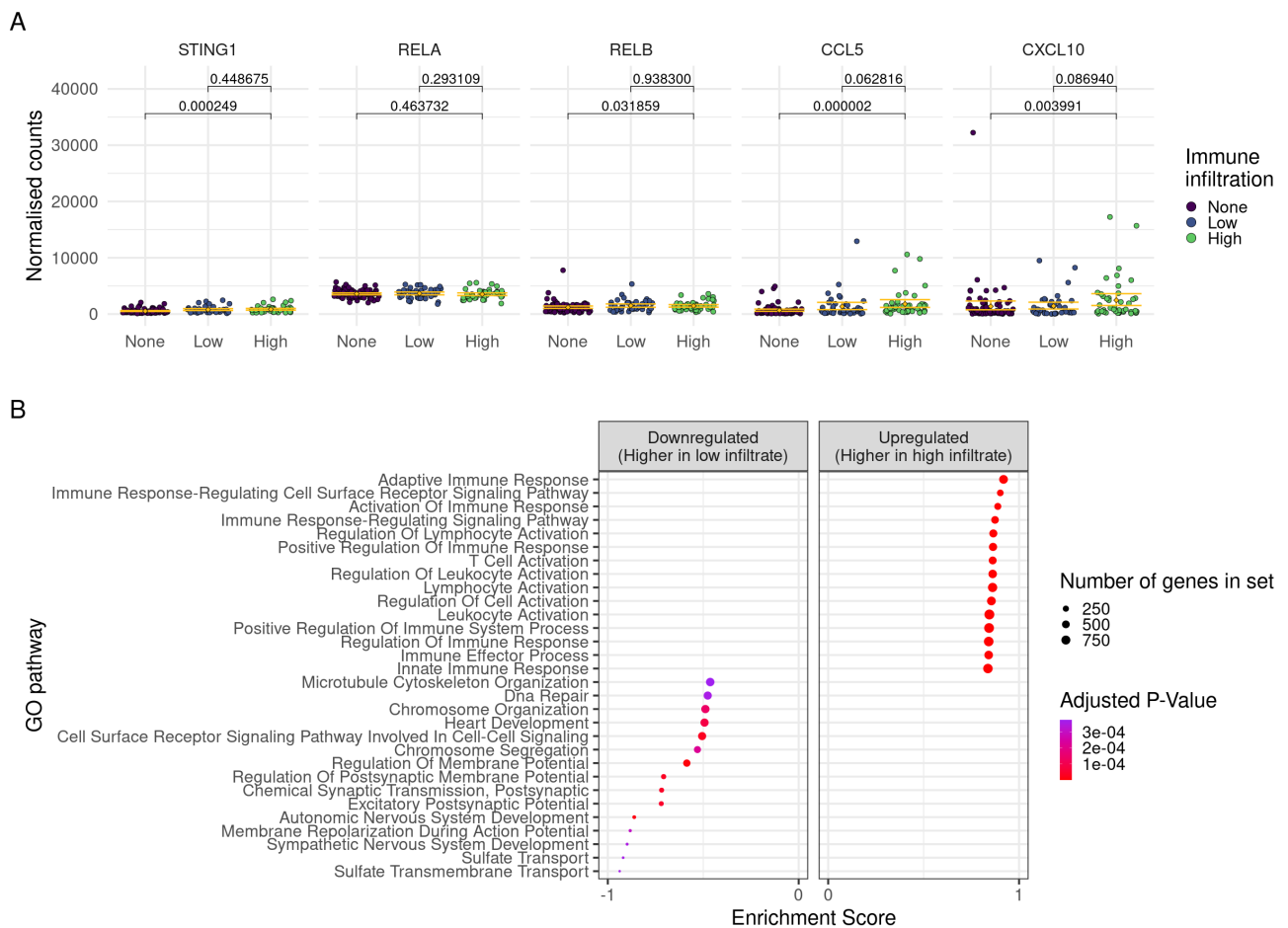
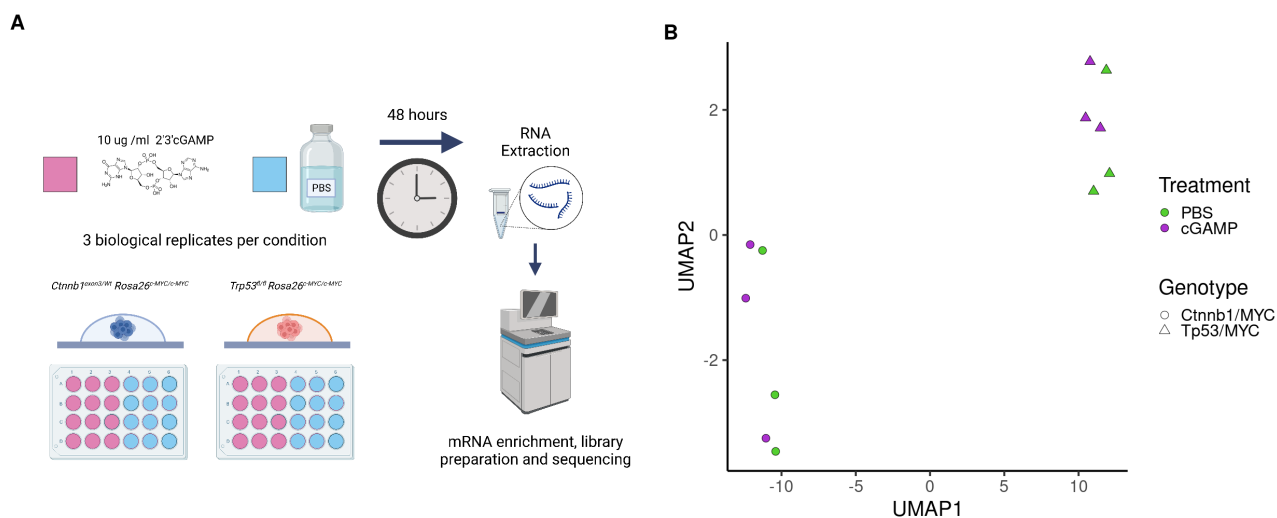


Figure 6.4: Panel A – Overview of the cGAMP stimulation experiment and clustering by genotype of organoids and treatment received. Panel B – Organoids cluster in opposite UMAP dimensions to one another by genotype.



6.3.2 Comparison of transcriptome sequencing of *Ctnnb1^{exon3/Wt} Rosa26^{c-MYC/c-MYC}* and *Trp53^{fl/fl} Rosa26^{c-MYC/c-MYC}* tumour cells following 2'3'cGAMP

Stimulation of tumour organoids with 2'3'cGAMP induced marked transcriptional changes in *Ctnnb1^{exon3/Wt} Rosa26^{c-MYC/c-MYC}* tumours, but not in and *Trp53^{fl/fl} Rosa26^{c-MYC/c-MYC}* tumours (figure 6.4, 6.5 and 6.6). Stimulation of *Ctnnb1^{exon3/Wt} Rosa26^{c-MYC/c-MYC}* tumours enhanced expression of multiple type I interferon response genes, including *Ifit1*, *Isg15*, *Ccl5* and *Cxcl10* (figure 6.6A) with over 100-fold increase in expression in some cases. Conversely, treatment of *Trp53^{fl/fl} Rosa26^{c-MYC/c-MYC}* with the same dose of 2'3'cGAMP resulted in moderately increased expression of a single gene, *Ccl5* (figure 6.6B). Comparing both 2'3'cGAMP and PBS treated *Ctnnb1^{exon3/Wt} Rosa26^{c-MYC/c-MYC}* tumours with *Trp53^{fl/fl} Rosa26^{c-MYC/c-MYC}* tumours (figure 6.6C and figure 6.6D), there were no significant differences in these type I interferon genes across genotypes in either treatment group. Taken together, this suggests that stimulation of *Trp53^{fl/fl} Rosa26^{c-MYC/c-MYC}* tumours has minimal effect, due to an already active cGAS-STING pathway.

Stimulation of this pathway in $Cttnb1^{\text{exon3/Wt}} \text{ Rosa26}^{\text{c-MYC/c-MYC}}$ tumours led to a large effect, recapitulating *Ccl5* and *Cxcl10* expression to that of $\text{Trp53}^{\text{fl/fl}} \text{ Rosa26}^{\text{c-MYC/c-MYC}}$. This can also be seen in the heatmap of cytokine related genes (figure 6.7) where 2'3'cGAMP stimulation increases expression of *Ccl5* and *Cxcl10* in $Cttnb1^{\text{exon3/Wt}} \text{ Rosa26}^{\text{c-MYC/c-MYC}}$ tumour organoids. Interestingly, stimulation with 2'3'cGAMP was also associated with increased expression of the inhibitory immune checkpoints *Cd274* (PD-L1) and *Lag3* (figure 6.8). This may suggest that activation of these checkpoint pathways is occurring in response to the damage signalling induced by 2'3'cGAMP stimulation and may suggest anti-PD1 therapy and STING pathway agonism as a rational therapeutic combination.

Figure 6.5: Overview heatmap of $Ctnnb1^{exon3/Wt}$ $Rosa26^{c-MYC/c-MYC}$ and $Trp53^{fl/fl}$ $Rosa26^{c-MYC/c-MYC}$ tumour transcriptomes following treatment with 2'3'cGAMP or PBS. Hierarchical clustering clearly segregates both genotype and treatment. There are clear differences in genes expressed following treatment with 2'3'cGAMP in $Ctnnb1^{exon3/Wt}$ $Rosa26^{c-MYC/c-MYC}$ tumour organoids, but very little difference in $Trp53^{fl/fl}$ $Rosa26^{c-MYC/c-MYC}$ tumour organoids.

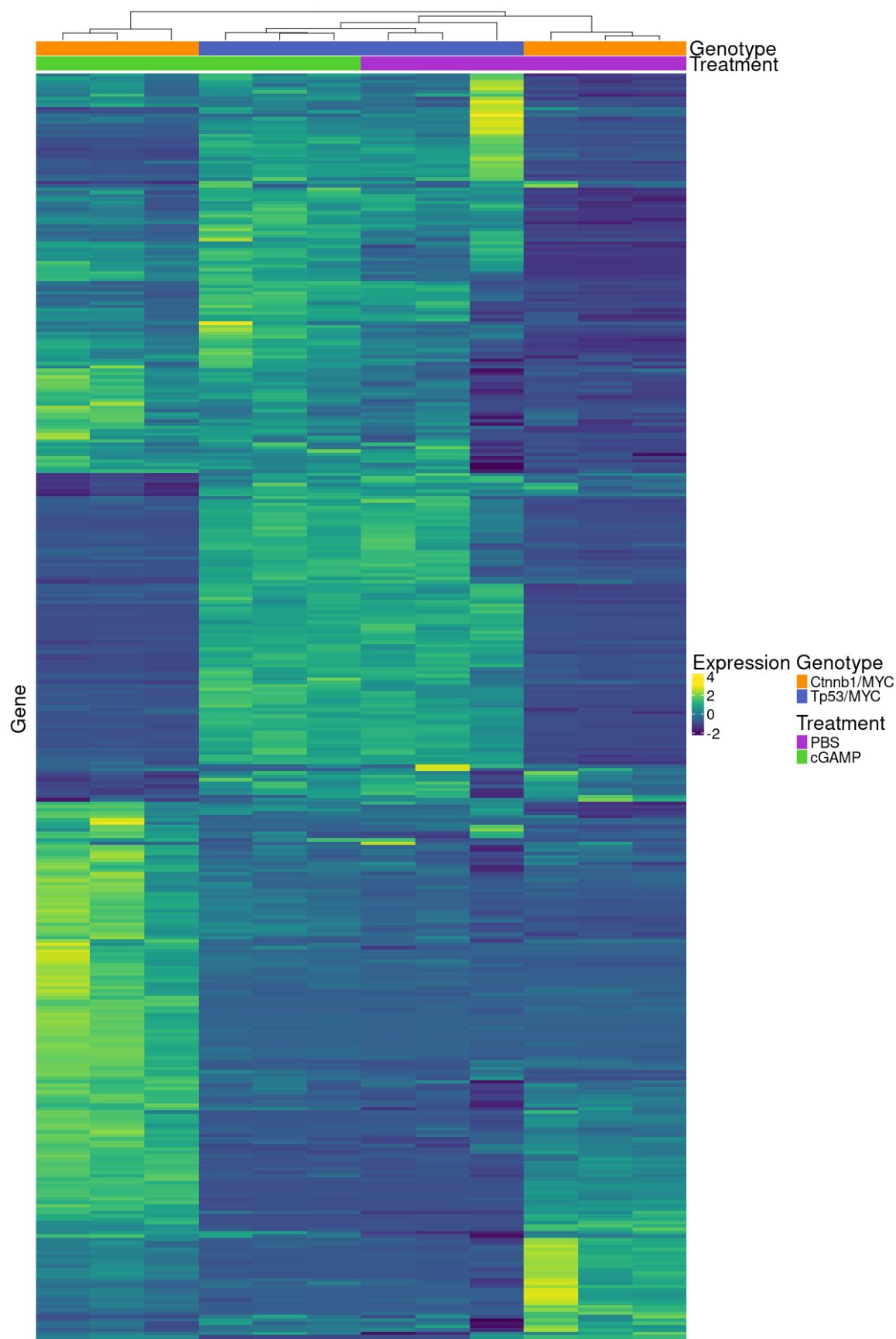
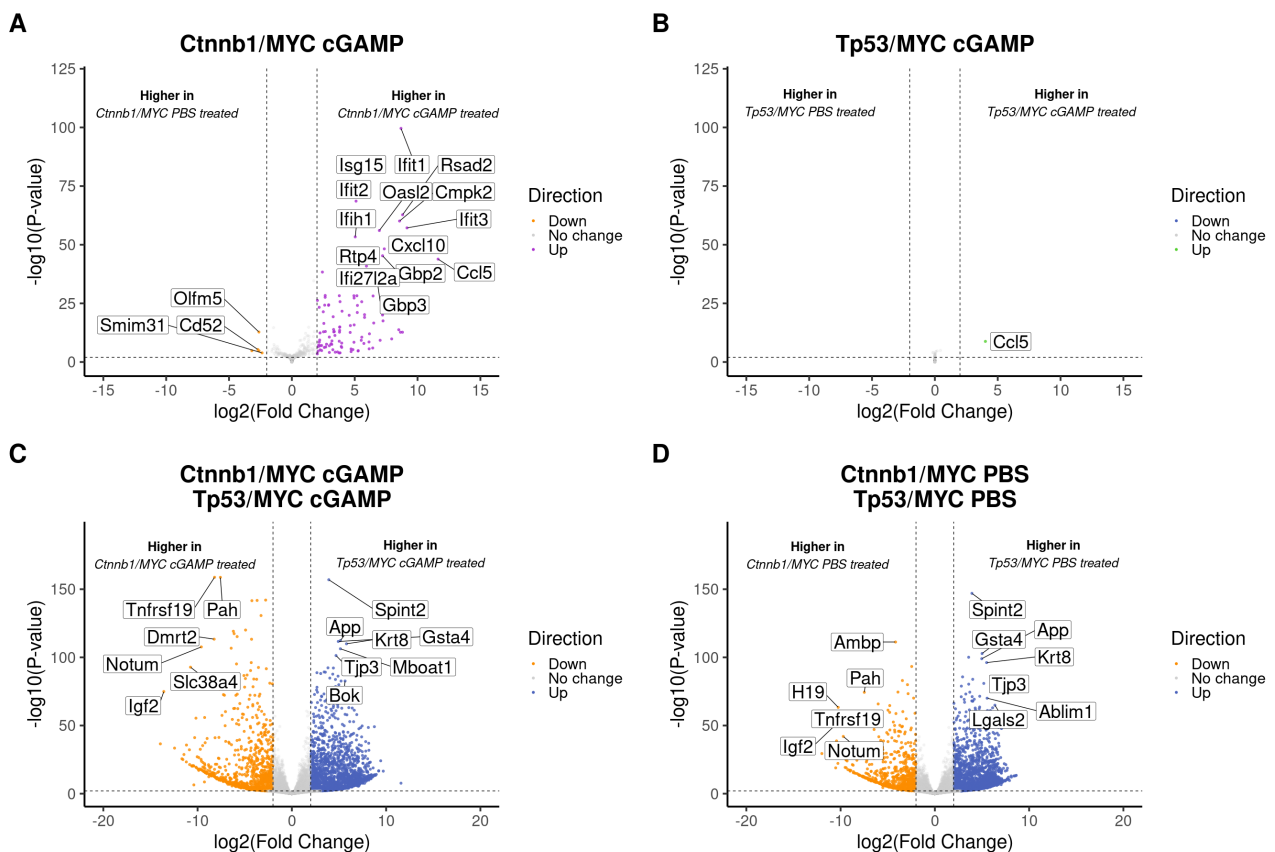


Figure 6.6: Volcano plots of most highly differentially expressed genes in the different 2'3'cGAMP treatment and genotype groups. Panel A – Effect of 2'3'cGAMP on *Ctnnb1*^{exon3/Wt} *Rosa26*^{c-MYC/c-MYC} tumour organoids. There is significantly increased expression of major type I interferon response genes which are downstream of STING, including *Ccl5* and *Cxcl10*. Panel B – Effect of 2'3'cGAMP on *Trp53*^{fl/fl} *Rosa26*^{c-MYC/c-MYC} tumour organoids. Only *Ccl5* expression was significantly increased. Panel C – Comparison of differentially expressed genes in *Ctnnb1*^{exon3/Wt} *Rosa26*^{c-MYC/c-MYC} and *Trp53*^{fl/fl} *Rosa26*^{c-MYC/c-MYC} cGAMP treated tumour organoids. Panel D – Comparison of differentially expressed genes in *Ctnnb1*^{exon3/Wt} *Rosa26*^{c-MYC/c-MYC} and *Trp53*^{fl/fl} *Rosa26*^{c-MYC/c-MYC} PBS treated tumour organoids. As can be seen in panel C and panel D, there are no differentially expressed type I interferon response genes. This suggests that 2'3'cGAMP increases type I interferon response genes downstream of STING, but to a threshold which *Trp53*^{fl/fl} *Rosa26*^{c-MYC/c-MYC} has likely already achieved.



To understand which signalling pathways were affected by 2'3'cGAMP stimulation in $Ctnnb1^{\text{exon3/Wt}} \text{ Rosa26}^{\text{c-MYC/c-MYC}}$ tumour cells I performed a Gene Set Enrichment Analysis using Gene Ontology terms (figure 6.9). Stimulation of $Ctnnb1^{\text{exon3/Wt}} \text{ Rosa26}^{\text{c-MYC/c-MYC}}$ tumour organoids led to significant upregulation of pathogen defence and cytokine response pathways, some of which were identified as being upregulated in the immune infiltrated $\text{Trp53}^{\text{fl/fl}} \text{ Rosa26}^{\text{c-MYC/c-MYC}}$ tumour model in the previous chapter (i.e. positive regulation of immune responses, inflammatory response signalling). Pattern recognition receptor signalling was also enriched in tumour organoids which were stimulated with 2'3'cGAMP. This would support activation of the STING pathway as a driver for proinflammatory programmes of gene expression, which could provide a druggable route to establishing immune infiltration in $Ctnnb1^{\text{exon3/Wt}} \text{ Rosa26}^{\text{c-MYC/c-MYC}}$ tumours.

Next, I compared PBS treated $Ctnnb1^{\text{exon3/Wt}} \text{ Rosa26}^{\text{c-MYC/c-MYC}}$ and $\text{Trp53}^{\text{fl/fl}} \text{ Rosa26}^{\text{c-MYC/c-MYC}}$ tumour organoids to determine whether in the unstimulated state there were major differences in signalling that could explain why cGAS-STING signalling was absent in $Ctnnb1^{\text{exon3/Wt}} \text{ Rosa26}^{\text{c-MYC/c-MYC}}$ tumour cells. As these tumour organoids are populations of purely tumour epithelial cells, albeit subject to selection pressure in-vitro, it provides one means of a direct epithelial comparison than bulk sequencing of whole tissue where other cell populations are present. As expected, in unstimulated $Ctnnb1^{\text{exon3/Wt}} \text{ Rosa26}^{\text{c-MYC/c-MYC}}$ tumour organoids, canonical WNT/ β -Catenin pathways were significantly upregulated compared with $\text{Trp53}^{\text{fl/fl}} \text{ Rosa26}^{\text{c-MYC/c-MYC}}$ tumour organoids. However, the most significantly upregulated pathways in $Ctnnb1^{\text{exon3/Wt}} \text{ Rosa26}^{\text{c-MYC/c-MYC}}$ cells were DNA damage response, including double-strand break (DSB) responses, and chromosome organisation pathways (figure 6.9B). This was also observed in human tumours with low levels of immune infiltrate in the Cancer Genome Atlas[20].

This finding is interesting given emerging evidence that activation of cGAS-STING can be mediated through increased chromosomal tension and formation of exposed chromosomal bridges, rather than the classically described presence of micronuclei[185]. If $\text{Trp53}^{\text{fl/fl}} \text{ Rosa26}^{\text{c-MYC/c-MYC}}$ tumours were driving cGAS-STING activation through large amounts of

Figure 6.7: Normalised cytokine counts by 2'3'cGAMP treatment and tumour organoid genotype. There is higher expression of key cytokines with 2'3'cGAMP treatment in $Cttnb1^{exon3/Wt}$ $Rosa26^{c-MYC/c-MYC}$ tumour organoids, including in $Ccl5$ and $Cxcl10$.

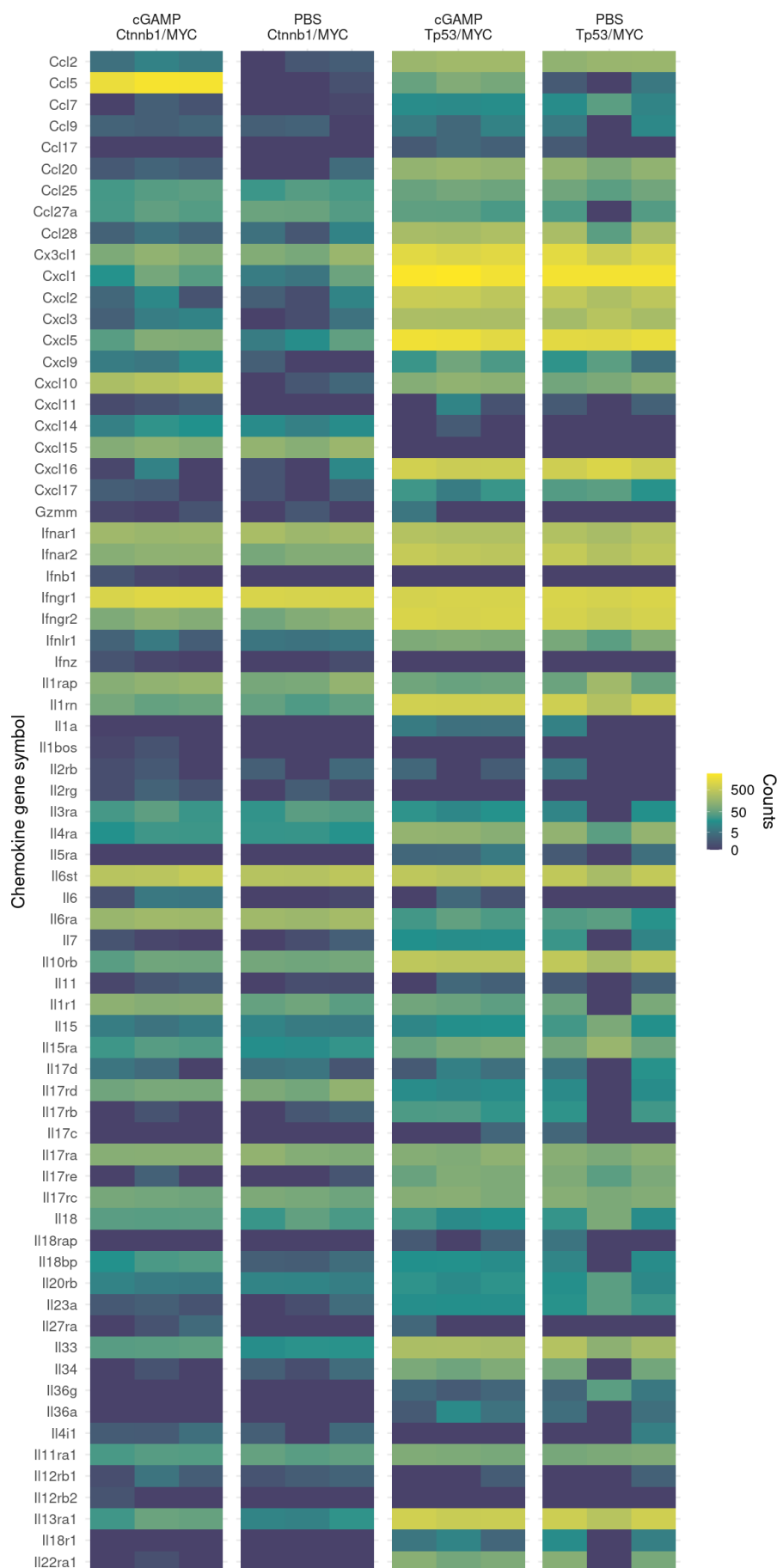
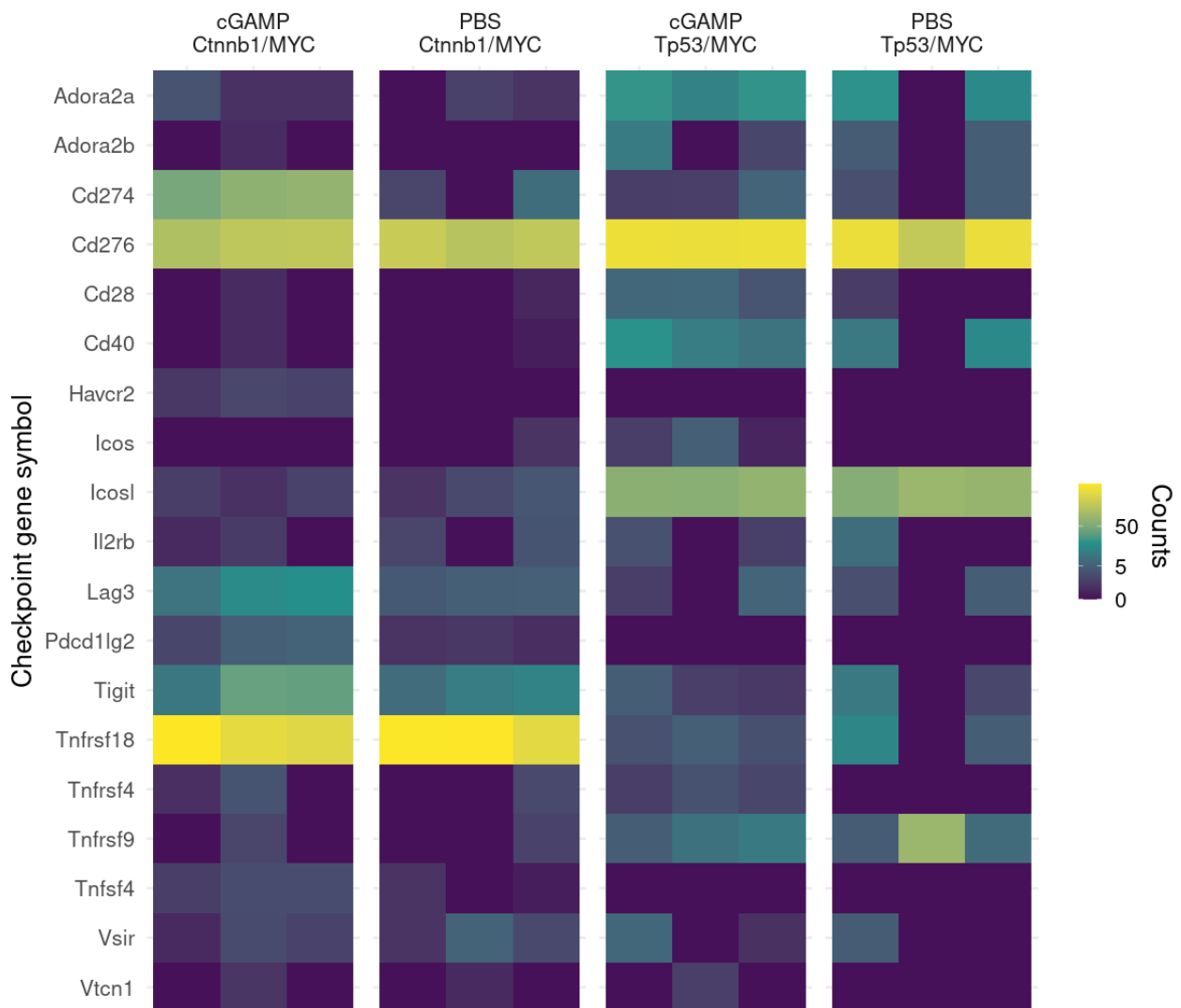


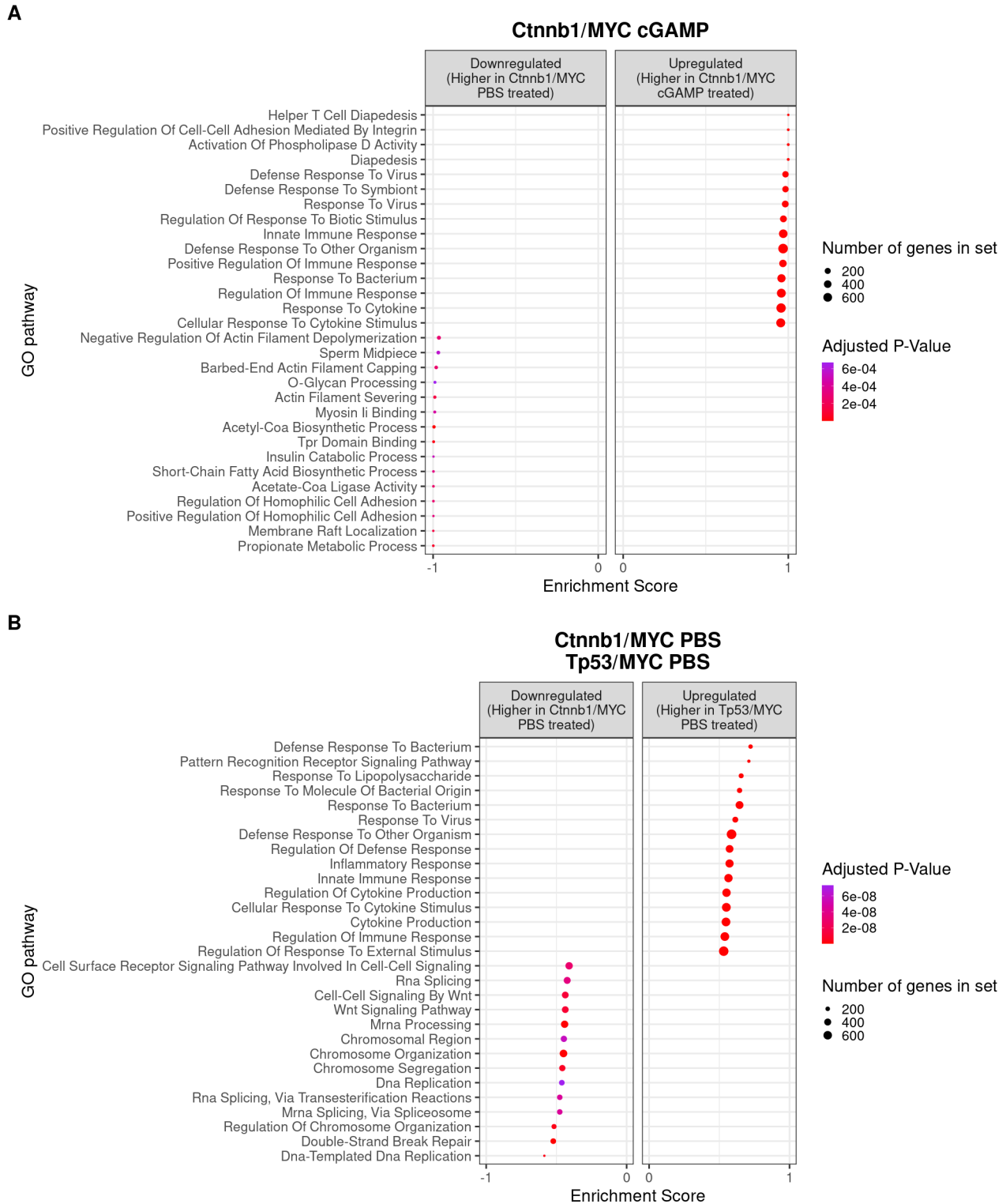
Figure 6.8: Normalised counts of immune checkpoints expressed in response to 2'3'cGAMP by treatment and genotype. In $Cttnb1^{exon3/Wt}$ $Rosa26^{c-MYC/c-MYC}$ tumour organoids treatment with 2'3'cGAMP resulted in the upregulation of inhibitory checkpoints Lag3 and Cd274 (PD-L1). This suggests anti-PD1/PD-L1 therapy may be a rational combination therapy for tumours where Cd274 expression can be induced with 2'3'cGAMP stimulation or STING agonism.



DNA damage and subsequent shedding of dsDNA into the cytosol, it might be expected that the mutational burden in this model would be significantly higher than $Ctnnb1^{\text{exon3/Wt}} \text{ Rosa26}^{\text{c-MYC/c-MYC}}$. Indeed, it could be hypothesised that with the absence of functional TP53, detecting and responding to DNA damage events would be impaired and large amounts of chromosomal instability would be present. However, given my findings that mutational burden and lack of copy number variation across $Ctnnb1^{\text{exon3/Wt}} \text{ Rosa26}^{\text{c-MYC/c-MYC}}$ and $\text{Trp53}^{\text{fl/fl}} \text{ Rosa26}^{\text{c-MYC/c-MYC}}$ tumours, this cannot fully account for the large differences in cGAS-STING activity.

Increases in DNA damage response and chromosome organisation pathways in $Ctnnb1^{\text{exon3/Wt}} \text{ Rosa26}^{\text{c-MYC/c-MYC}}$ were largely driven by spindle checkpoint assembly genes, notably Aurora Kinases, Dual specificity protein kinase TTK (Mps1), centromere arrangement and a range of double strand and nucleotide excision repair genes. Although it could be that $Ctnnb1^{\text{exon3/Wt}} \text{ Rosa26}^{\text{c-MYC/c-MYC}}$ tumour organoids were simply more proliferative, both β -Catenin and c-MYC are known to have major roles in cell-cycle progression and directing organisation of the spindle checkpoint assembly. Indeed, there is evidence that small molecule inhibition of both Aurora Kinases and Mps1 leads to mitotic catastrophe in canonical WNT and c-MYC driven tumours[186, 187]. Based on my results, and literature surrounding chromosomal and checkpoint assembly, a hypothesis arises that $Ctnnb1^{\text{exon3/Wt}} \text{ Rosa26}^{\text{c-MYC/c-MYC}}$ tumours may suppress cGAS-STING through increased spindle checkpoint fidelity, preventing exposure of long sections of exposed chromatin and minimising fibre tension, subsequently preventing cGAS coating and generation of 2'3'cGAMP. This hypothesis is supported further by the key role canonical WNT/ β -Catenin signalling plays in development and organ regeneration. It would be undesirable for cells involved in these roles to trigger innate immune responses leading to their elimination and potentially induce a autoimmunity which could lead to perpetual organ damage, particularly to the stem cell compartment (for example in liver injury or in intestine which is exposed to multiple damage-associated molecular patterns through food).

Figure 6.9: Panel A – Gene Set Enrichment Analysis of Gene Ontology (GO) terms for *Ctnnb1*^{exon3/Wt} *Rosa26*^{c-MYC/c-MYC} tumour organoids treated with 2'3'cGAMP. Panel B – Gene Set Enrichment Analysis of Gene Ontology (GO) terms for *Ctnnb1*^{exon3/Wt} *Rosa26*^{c-MYC/c-MYC} versus *Trp53*^{fl/fl} *Rosa26*^{c-MYC/c-MYC} tumour organoids.



6.4 Summary

I have shown cGAS-STING activity is associated with increased immune infiltration found in $\text{Trp53}^{\text{fl/fl}}$ $\text{Rosa26}^{\text{c-MYC/c-MYC}}$ tumours compared with immune excluded $\text{Ctnnb1}^{\text{exon3/Wt}}$ $\text{Rosa26}^{\text{c-MYC/c-MYC}}$ tumours. Expression of STING and its effector cytokines were significantly raised in $\text{Trp53}^{\text{fl/fl}}$ $\text{Rosa26}^{\text{c-MYC/c-MYC}}$ tumours, both at the transcriptional and protein level.

Stimulation of tumour organoids from $\text{Ctnnb1}^{\text{exon3/Wt}}$ $\text{Rosa26}^{\text{c-MYC/c-MYC}}$ mice with 2'3'cGAMP in-vitro lead to significant upregulation of type I interferon responses consistent with activation of the cGAS-STING pathway (Cxcl10 and Ccl5). Interestingly, stimulation of $\text{Trp53}^{\text{fl/fl}}$ $\text{Rosa26}^{\text{c-MYC/c-MYC}}$ tumours did not profoundly induce these responses, suggesting a saturation of cGAS-STING activation had been achieved in these cells or they had mechanisms of suppressing the pathway. Taken together, this suggests that triggering type I interferon responses through cGAS-STING could be a therapeutic strategy to selectively activate proinflammatory cytokine signalling in immune evasive canonical WNT/ β -Catenin driven HCC.

These features of type I IFN suppression in immune evasive tumours would fit with the current literature. There have been several reports that immune evasive tumour microenvironments are found to have low levels of type I IFN signalling[188]. Furthermore, in mouse models of HCC, systemic administration of interferon has also been demonstrated to enhance the effectiveness of anti-PD1 therapy. Interestingly this was shown by *Hu et al.* to be mediated through inhibition of FosB, a key component of AP-1 driven transcription and which I found to be present in promoter regions of the STING pathway in $\text{Ctnnb1}^{\text{exon3/Wt}}$ $\text{Rosa26}^{\text{c-MYC/c-MYC}}$ tumours [189].

A further notable finding, which should be investigated further, is the significant upregulation of DNA damage and chromosomal organisation pathways in $\text{Ctnnb1}^{\text{exon3/Wt}}$ $\text{Rosa26}^{\text{c-MYC/c-MYC}}$ tumours. This could indicate $\text{Ctnnb1}^{\text{exon3/Wt}}$ $\text{Rosa26}^{\text{c-MYC/c-MYC}}$ cells rely on increased spindle checkpoint assembly fidelity to prevent cGAS-STING activation and

thereby avoid triggering innate immune responses. As tumour cells rely on the spindle assembly checkpoint for continued proliferation, this may provide a selective means to target cancer cells and generate cytokine gradients which could promote the infiltration of anti-tumour immune cells.

Up to this point, the development of STING agonists has been hampered by major difficulties. One of the key challenges posed is selectively targeting STING agonists to tumour cells, rather than immune cells where they can be toxic and thereby impair immune response. Various strategies have been suggested, including the delivery of STING agonists through direct injection into tumours[180, 190]. One way to improve this and allow the systemic delivery of STING agonists would be to increase the baseline level of cGAS-STING activation in a tumour-specific manner prior to administration of STING agonist. This may allow lower doses of STING agonist to be given to increase cGAS-STING in cells with already active signalling, rather than leading to systemic activation of cGAS-STING in all cells. Alternatively, this could be achieved by delivering 2'3'cGAMP directly to tumour cells using tumour-targeted viral vectors, but this would be some time off, requiring extensive development and regulatory approvals. Small molecules aimed at cGAS-STING pathway agonism, and disruption of the spindle assembly checkpoint already have clinical approval or are in early phase human trials. The latter combination approach would potentially represent a faster route to clinic, should further experiments provide evidence this is a viable strategy.

6.5 Future directions

- Given the expression of inflammatory chemokines in $Ctnnb1^{\text{exon3/Wt}} \text{ Rosa26}^{\text{c-MYC/c-MYC}}$ tumours response to treatment with 2'3'cGAMP, further work should be undertaken to test if recapitulating this would be possible in-vivo. This could be done using one or a combination of the following: small molecule inhibition leading to cGAS activation (DNA damage, ENPP1 inhibition), STING agonism, or by developing a viral vector with tumour-tropism for delivering 2'3'cGAMP or biologically active analogues. It would also be useful to accurately determine levels of intracellular 2'3'cGAMP to add to these comparisons

and work to establish this assay is currently ongoing.

- Disrupting the spindle assembly checkpoint in-vivo using small molecule approaches such as inhibition of MPS1 or AURKB should be tested to test whether this directly leads to cGAS-STING activation in $Cttnb1^{\text{exon3/Wt}}$ $Rosa26^{\text{c-MYC/c-MYC}}$ tumours. If so, this could then be tested in combination with STING agonism and anti-PD1 therapy.
- Stimulation of human canonical WNT/ β -Catenin driven tumour cell lines with 2'3'cGAMP should also be performed to verify the same effect occurs in human HCC cells. The same should be performed for any small molecule agonists or inhibitors that are shown to promote cGAS-STING in mice.
- High throughput screens using cGAS-STING pathway activity as a read-out could be performed to identify novel targets which could be used for tumour selective cGAS-STING activation.
- Should these strategies of targeting cGAS-STING be shown to work, the same experiments could then be performed in $Sting1^{-/-}$ mice and in immunodeficient mice. This would test whether these effects are mediated by cGAS-STING dependent immunity.

Chapter 7

New genetically engineered mouse models to study epithelial-immune interactions in the tumour microenvironment

7.1 Introduction

Conditional genetically engineered mouse models have allowed me to study associations between different genetic drivers of cancer, the immune phenotype of the tumour microenvironment and subsequent response to immune checkpoint inhibition. Despite these findings, there are important biological questions which could be answered in a far more causal manner by using improved transgenic technology.

I decided to develop novel, conditional and temporally controllable GEMMs to answer these questions:

- Mutant β -Catenin and c-MYC are both required for tumourigenesis in the $Ctnnb1^{\text{exon3/Wt}} \text{ Rosa26}^{\text{c-MYC/c-MYC}}$ model. Does immune evasion depend on sustained mutant β -Catenin signalling? Then in turn, what happens to the immune microenvironment if mutant β -Catenin is withdrawn?
- Is lack of response to immune checkpoint therapy due to immune evasion or a lack of antigen-specific signals (lack of neoantigens)?

At present, there are no conditional mouse models of mutant β -Catenin driven HCC which allow mutant β -Catenin to be added or withdrawn. Nor are there any specific chemical probes, *in-vivo* degron tagged mutant β -Catenin, or proteolysis targeting chimeras (PROTACs), although they are under active development[191–193]. A model where mutant β -Catenin could be withdrawn would allow me to test if this results in infiltration of the tumour microenvironment by immune cells.

Adaptive immune responses require two signals, an antigen-specific signal, and a co-stimulatory signal. Antigen specific signals are provided through T-cell-receptors (TCRs) which recognise specific antigens presented by MHC molecules on cell-surfaces. Lack of response to immune checkpoint therapy in $Ctnnb1^{\text{exon3/Wt}} \text{ Rosa26}^{\text{c-MYC/c-MYC}}$ models could be due to a lack of antigens rather than immune exclusion of effector immune cells, or a

combination of the two. A model where an immunogenic neoantigen could be conditionally expressed and withdrawn would help to attribute how much each mechanism contributes toward immunotherapeutic resistance.

7.2 Development of a temporally controlled model of β -Catenin driven HCC

To establish a model system where mutant β -catenin could be turned on or off in established tumours, mice with a doxycycline controlled truncated form of oncogenic β -catenin (TetO- Δ N89 β -catenin) were gifted by Professor Trevor Dale from Cardiff University[113]. The TetO- Δ N89 β -catenin is a truncated version of human β -catenin with the first (N-terminus) 89 amino acids (including those encoded by the third exon) deleted. This TetO- Δ N89 β -catenin is expressed from the *Colla1* gene trap, thus this model also retains expression of endogenous mouse β -catenin. These amino acids encode serine-threonine residues which when phosphorylated, mediate the degradation of β -Catenin through E3 Ubiquitin Ligase (β -TrCP), thus resulting in the production of an ‘un-degradable’, constitutively active form of human β -Catenin. Another advantage over *Ctnnb1*^{exon3/Wt} is that Δ N89 β -catenin uses the human CTNNB1 sequence. This may allow better study of human β -catenin and its interactions with human c-MYC, thus giving increased relevance to human disease.

Both drivers in this model (Δ N89 β -catenin and c-MYC) are from human sequences, producing a humanised system. This has several benefits, including being able to test whether small molecule inhibitors shown to work in the murine *Ctnnb1*^{exon3/Wt} models are relevant to human β -catenin and any interactions it has with c-MYC. However, there are potential drawbacks of using human alleles. First, being ‘foreign’ proteins, which are expressed only after recombination, they may trigger an immune response. When immune responses are the focus of this work, this may lead to experimental confounding. Second, human proteins may lack the relevant domains required to interact with mouse proteins. Therefore, using humanised alleles is likely to be most useful where the protein of interest and its potential

binding partners share significant homology with their murine counterparts. Both the canonical Wnt/ β -catenin and MYC signalling pathways are highly conserved between mouse and humans, which would make these suitable for study in a humanised mouse system[194, 195].

Use of Δ N89 β -catenin was first described in breast cancer models. In mammary epithelium, Δ N89 β -catenin expression driven by the Mouse mammary tumour virus (MMTV) resulted in the development of precocious lobuloalveolar branching and hyperlobular phenotype, followed by the development of aggressive adenocarcinoma at full penetrance in both breeding and virgin females[196, 197]. Subsequent work by the Dale lab combined Δ N89 β -catenin with a tetracycline response element and generated a mouse model with this allele[113]. They demonstrated that expression of Δ N89 β -catenin by administering doxycycline promotes intestinal crypt hyperplasia and leads to upregulation of canonical Wnt/ β -catenin target genes. Subsequent withdrawal of doxycycline led to reversion of both intestinal hyperplasia and canonical Wnt/ β -catenin target gene expression.

As the Rosa26 locus is frequently used as a gene trap, I sought to find an alternative region to locate a conditional tetracycline transactivator element (tTA or rtTA), which would leave the Rosa26 locus free permitting TetO- Δ N89 β -catenin to be combined with Rosa26^{c-MYC/c-MYC}. I selected a strain available from the Jackson Laboratory which conditionally expressed the ‘tet-off’ tTA2 element at the Igs2 locus (Igs2^{CAG-lsl-tTA2-T2A-H2B-TagBFP}). An overview of the alleles used in this chapter can be seen in figure 7.1. I then hypothesised that by expressing TetO- Δ N89 β -catenin in hepatocytes at the correct level in combination with Rosa26^{c-MYC/c-MYC}, it would be possible to generate a mouse model of HCC. This would enable the addition or withdrawal respectively of oncogenic β -catenin signalling by administering doxycycline.

7.2.1 Results from whole-body and conditional expression of TetO- Δ N89 β -catenin

As *Jardé et al.* did not find or report any significant toxicity with the $\text{Colla1}^{\text{TetO-}\Delta\text{N89 } \beta\text{-catenin/Wt}}$ $\text{Rosa26}^{\text{M2-rtTA}}$ ‘tet-on’ mouse in their initial report, I sought to establish whether there were signs of β -Catenin activation in the liver of the same model[113], prior to crossing on the $\text{Igs2}^{\text{CAG-lsl-tTA2-T2A-H2B-TagBFP}}$ conditional allele. I also wanted to establish the dynamics of β -Catenin activation in response to doxycycline administration. To do this, I performed a time-course experiment where mice were given either 12 mg or 24 mg of doxycycline by oral gavage and sampled tissue at 2, 4, 6 or 8 hours after administration. The experimental read-out was accumulation of nuclear β -Catenin measured by immunohistochemistry. Tissue from $\text{Ctnnb1}^{\text{exon3/Wt}}$ mice was used as a positive control. Figure 7.2 demonstrates doxycycline led to an accumulation of nuclear β -Catenin, which peaked at 4 to 6 hours after administration and had gone by 8 hours. In addition to a very short half-life which would necessitate at least twice daily dosing, within 24 hours of the first dose, all mice appeared clinically unwell, could not be gavaged and had to be killed. Although the cause of this was not established, canonical Wnt/ β -Catenin activation in other tissues, it was hypothesised this was causing obstruction of either the small intestine or oesophagus in these mice. These features of using a ‘tet-on’ whole body $\text{Rosa26}^{\text{M2-rtTA}}$ model made it unsuitable for long-term cancer studies.

Figure 7.1: Panel A – Alleles crossed onto $Col1a1^{TetO-\Delta N89\beta\text{-catenin}/Wt}$ mice. This included crossing on constitutive $Rosa26^{M2-rtTA}$ tetracycline ‘on’ and conditional $Igs2^{CAG-lsl-tTA2-T2A-H2B-TagBFP}$ tetracycline ‘off’ alleles. Panel B – In the absence of doxycycline, tetracycline ‘on’ systems with the reverse tetracycline-controlled transactivator (rtTA) cannot bind to the tetracycline response element (TRE/TetO) which promotes transgene transcription. When doxycycline is administered, in this case in the drinking water or by oral gavage, the presence of doxycycline allows rtTA to bind the promoter and activate gene transcription. In the tetracycline ‘off’ system, the tetracycline-controlled transactivator (tTA) will bind to the TRE/TetO and promote transgene transcription in the absence of doxycycline. When doxycycline is administered, tTA is bound by doxycycline preventing it binding to the TRE/TetO, preventing downstream expression of the $\Delta N89\beta\text{-catenin}$ transgene. For the conditional systems, exposure to Cre-recombinase prior to doxycycline administration.

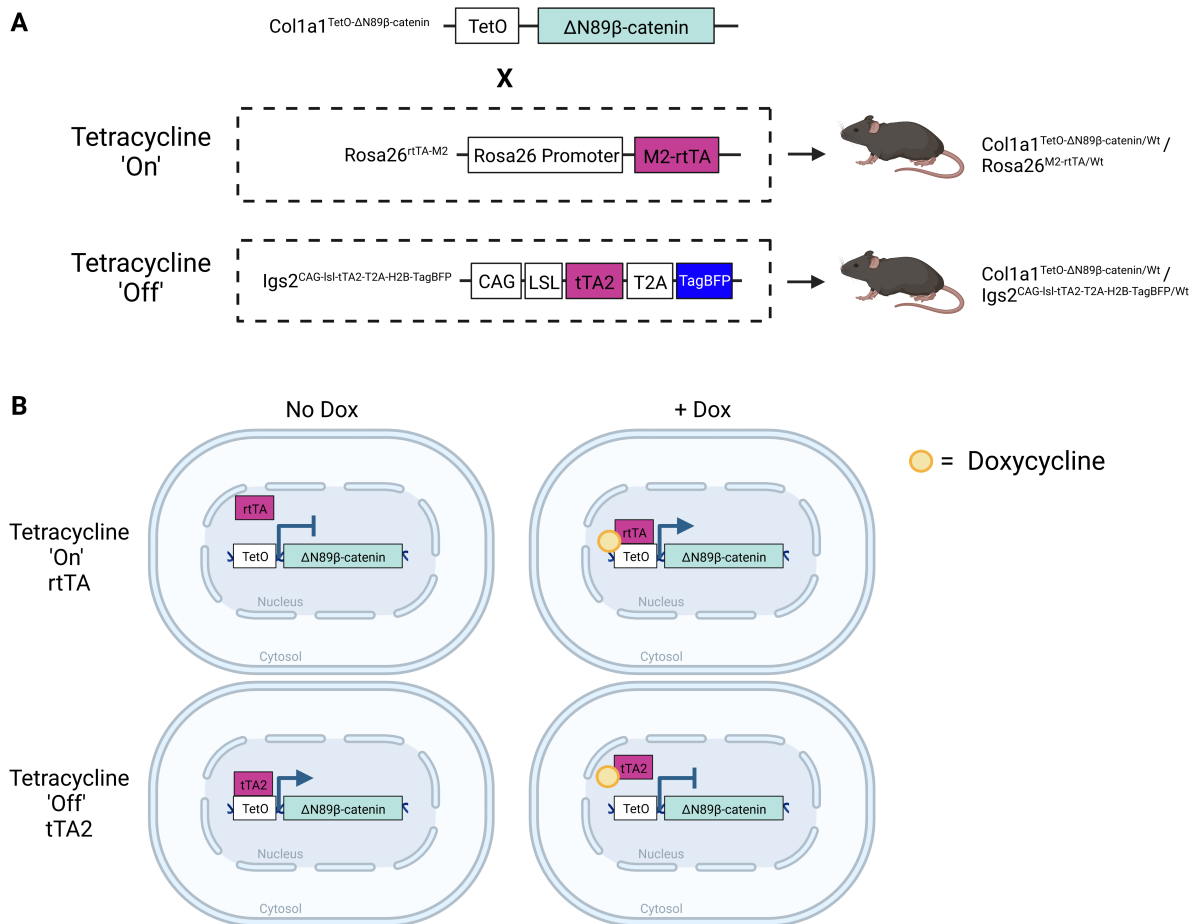
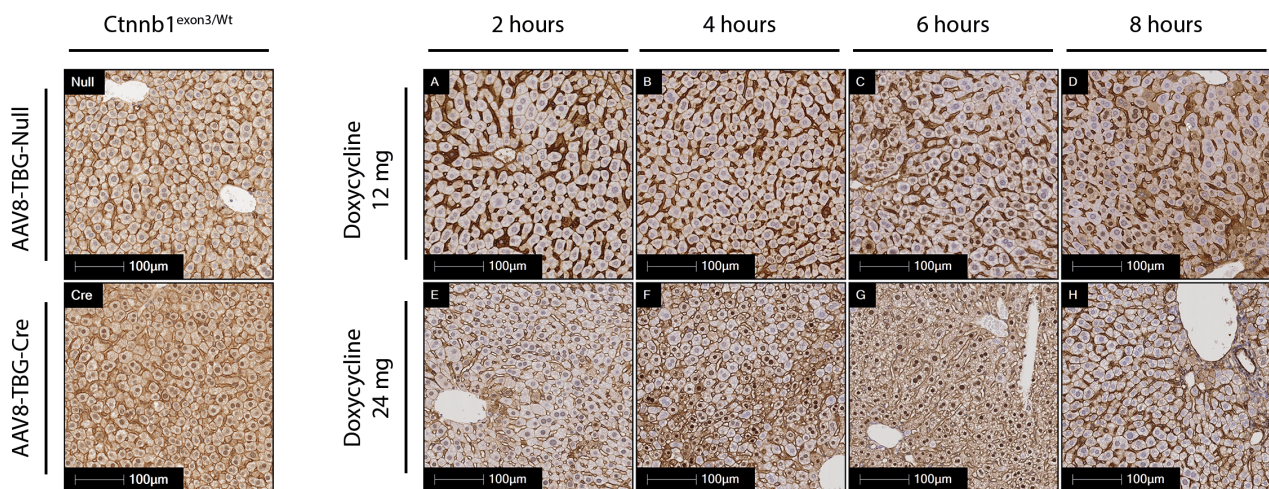


Figure 7.2: Immunohistochemical stain of β -Catenin in an experiment to identify optimal timing and dose of doxycycline administration in $Coll1a1^{TetO-\Delta N89 \beta\text{-catenin}} Rosa26^{M2\text{-rtTA}}$ ‘tet-on’ mice. All images acquired on Leica Aperio AT-2 at 20x magnification. Left panel shows $Ctnnb1^{\text{exon3}/Wt}$ mice who have received 2×10^{11} GC AAV8-TBG-Cre as a positive and negative control. Mice were administered a single dose of 12mg or 24mg of doxycycline in sterile water at hour 0 by oral gavage, tissue was sampled at 2, 4, 6 or 8 hours after administration. As can be seen in the control staining panel, activated, exon 3 deleted β -Catenin is present within the nucleus in $Ctnnb1^{\text{exon3}/Wt}$ mice who received 2×10^{11} GC AAV8-TBG-Cre. In the $Coll1a1^{TetO-\Delta N89 \beta\text{-catenin}/Wt} Rosa26^{M2\text{-rtTA}/Wt}$ mice, peak onset of nuclear β -Catenin staining was observed at 4 to 6 hours following oral gavage, with more intense induction in the 24mg group. By 8 hours, there was very little nuclear β -Catenin staining remaining. Representative micrographs from minimum $n = 2$ mice per group.



Having established the $Coll1a1^{TetO-\Delta N89 \beta\text{-catenin}/Wt}$ allele resulted in β -Catenin activation in the liver, I crossed this strain to a conditional $Igs2^{CAG\text{-lsl-tTA2-T2A-H2B-TagBFP}}$ ‘tet-off’ mouse strain. As expression of this allele relied on Cre-lox recombination, β -Catenin activation could be restricted to the liver using AAV8-TBG-Cre, addressing the toxicity caused by the whole-body $Rosa26^{M2\text{-rtTA}}$ allele. Using a ‘tet-off’ system would also allow β -Catenin activation to be continuous in the absence of doxycycline, avoiding the leaky expression of ‘tet-on’ systems and permitting continuous β -Catenin activation. I opted to provide doxycycline continuously by adding it to normal drinking water in an effort improve the kinetics of β -Catenin deactivation. $Coll1a1^{TetO-\Delta N89 \beta\text{-catenin}/Wt} Igs2^{CAG\text{-lsl-tTA2-T2A-H2B-TagBFP}/Wt}$ mice did not display any clinical signs following AAV8-TBG-Cre. Activation of β -Catenin was also present (figure 7.3) and was ablated by supplementing drinking water with 1 mg/ml doxycycline. Other canonical WNT/ β -

Figure 7.3: Immunohistochemical stain of β -Catenin to demonstrate efficacy of doxycycline in $Col1a1^{TetO-\Delta N89} \beta\text{-catenin}/Wt$ $Igs2^{CAG-lsl-tTA2-T2A-H2B-TagBFP}/Wt$ ‘tet-off’ mice. All images acquired on Leica Aperio AT-2 at 20x magnification. Mice received 2×10^{11} GC AAV8-TBG-Cre at day 0, then received either doxycycline 1 mg/ml or normal drinking water from day 4. Samples for tissue analysis were taken at day 10 following AAV8-TBG-Cre induction. Doxycycline 1 mg/ml treatment resulted in lack of nuclear β -Catenin accumulation. Expression of nuclear β -Catenin was specific to liver epithelium and other WNT-dependent tissues including the small intestine appeared morphologically normal. Representative micrographs from minimum $n = 2$ mice per group.

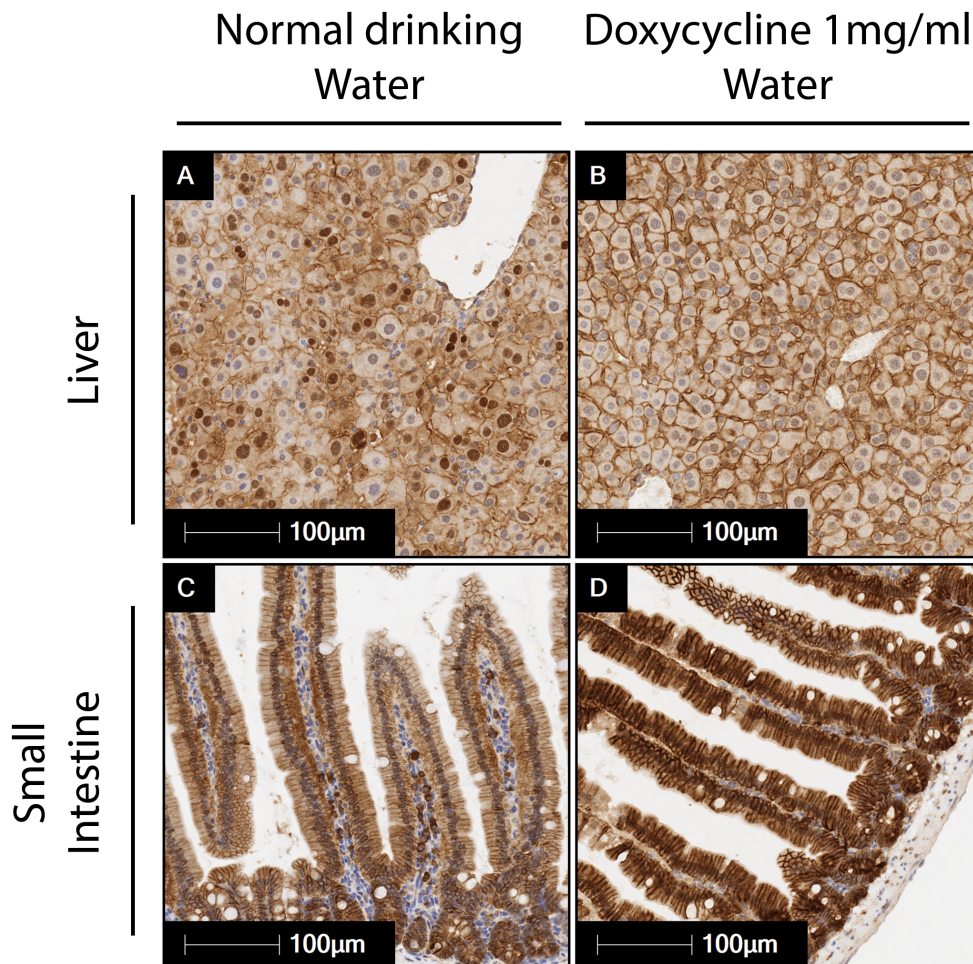
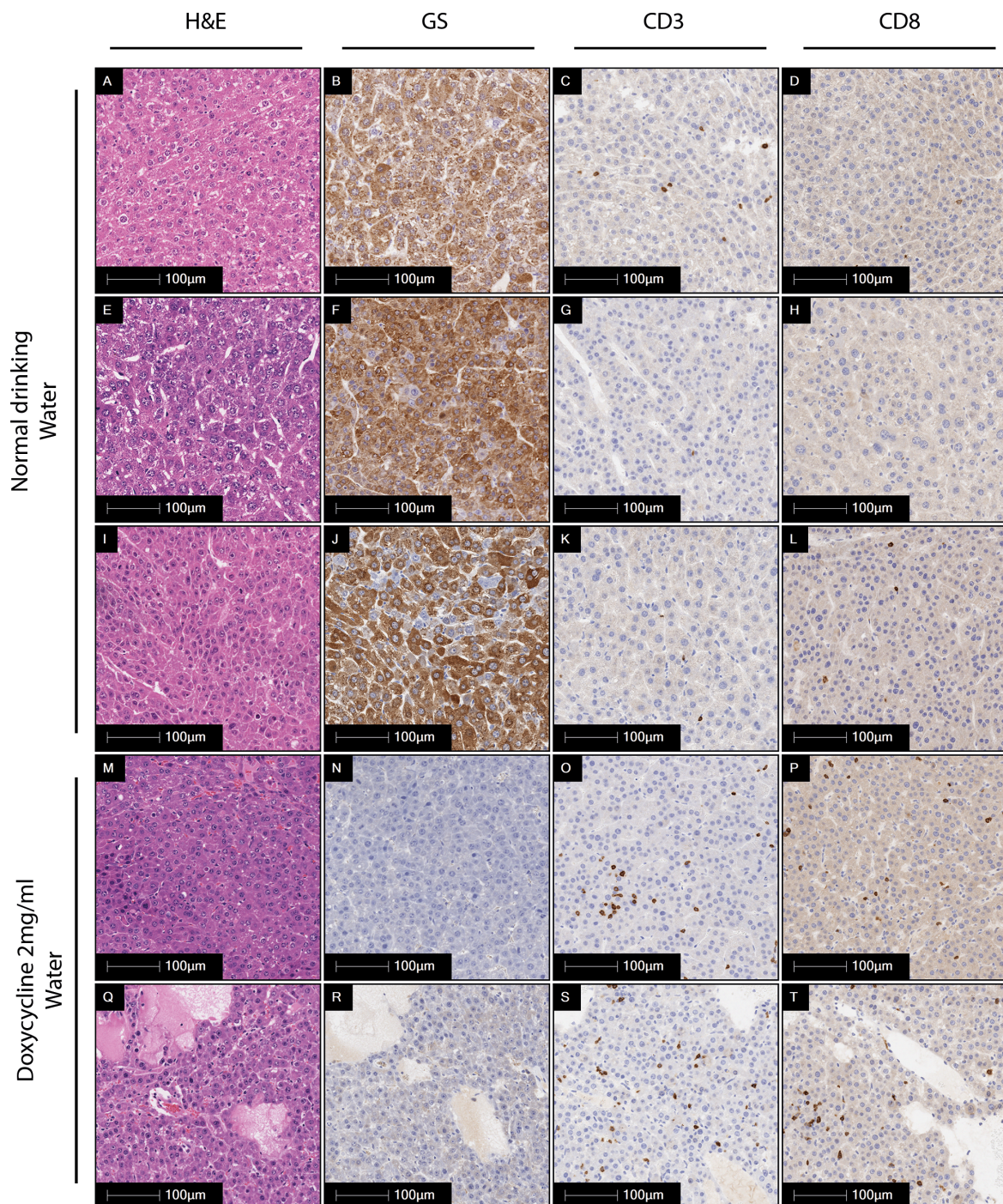


Figure 7.4: $Col1a1^{TetO-\Delta N89 \beta\text{-catenin/Wt}}$ $Rosa26^{c\text{-MYC}/c\text{-MYC}}$ $Igs2^{CAG\text{-Isl-tTA2-T2A-H2B-TagBFP/Wt}}$ mouse model of HCC with doxycycline control of β -Catenin. Haematoxylin and Eosin staining shows subtly different morphology of tumours. All images acquired on Leica Aperio AT-2 at 20x magnification. Glutamine synthetase, a canonical target of the WNT/ β -Catenin pathway is found to be expressed in $Col1a1^{TetO-\Delta N89 \beta\text{-catenin/Wt}}$ $Rosa26^{c\text{-MYC}/c\text{-MYC}}$ $Igs2^{CAG\text{-Isl-tTA2-T2A-H2B-TagBFP/Wt}}$ mice who received normal drinking water and therefore have expression of mutant Δ N89 β -Catenin. Doxycycline 2 mg/ml in drinking water resulted in formation of tumours which lacked Glutamine synthetase expression. Staining for the pan-T-cell marker CD3 suggested increased infiltration in mice who received Doxycycline 2 mg/ml ('tet-off'). Similarly, there were greater numbers of CD8 cells in mice who received Doxycycline 2 mg/ml. Representative micrographs from minimum $n = 3$ mice per group (one mouse in the doxycycline 2 mg/ml group did not have tumours).



Catenin dependent tissues appeared normal. Therefore, this system was taken forward for developing a longer-term cancer model.

To develop a doxycycline controlled model of β -Catenin driven HCC, $\text{Coll1a1}^{\text{TetO-}\Delta\text{N89 } \beta\text{-catenin/Wt}}$ $\text{Igs2}^{\text{CAG-lsl-tTA2-T2A-H2B-TagBFP/Wt}}$ ‘tet-off’ 6 mice were given 5×10^9 GC AAV8-TBG-Cre and received either sterile water ($n = 3$) or doxycycline 2 mg/ml ($n = 3$) in sterile water until day 160. Doxycycline 2 mg/ml water in light-proof bottles was replaced every 5 days to ensure activity was maintained[198]. In the sterile water group, all mice developed multifocal liver tumours, which were positive for the canonical WNT/ β -Catenin marker glutamine synthetase (figure 7.4). Two out of three mice in the doxycycline 2 mg/ml group developed singular liver tumours, which did not stain for the canonical WNT/ β -Catenin marker glutamine synthetase. Tumours from mice in the sterile water, activated β -Catenin group also had features of immune exclusion, with few CD3+ and CD8 cells present (figure 7.4).

7.2.2 Summary

I have developed a model of mutant β -Catenin driven HCC where it is possible to control expression of TetO- Δ N89 β -catenin through administration of doxycycline. I have shown as a proof-of concept that administration of doxycycline in a ‘tet-off’ model results in the formation of tumours which do not express canonical WNT/ β -catenin markers (GS). This system will not only be useful to understand the role of mutant β -Catenin plays in cancer, but also provides a humanised system test therapeutics *in-vivo* using human β -Catenin.

7.2.3 Future directions

- The next step is to use this model to demonstrate the effects of withdrawing oncogenic β -catenin signalling from cancer epithelial cells. There are multiple questions that could be explored using this system, including whether in established tumours withdrawing oncogenic β -catenin results in tumour involution, or whether c-MYC or other acquired drivers in these tumours can drive continued growth and sustain immune escape. Similarly, if oncogenic β -catenin is withdrawn, does the immune microenvironment change and can

immune cells infiltrate this? An interesting experiment would be to see the effect of withdrawing β -catenin for a short length of time (5 to 10 days) and comparing this to longer withdrawal (30+ days). As discussed in previous chapters, downregulating the DNA repair and chromosomal organisation pathways found in β -catenin driven tumours may provide an opportunity for damage to accumulate and subsequently trigger pro-inflammatory signalling. Understanding these dynamics would be useful to help inform future canonical Wnt/ β -catenin targeting strategies.

- As endogenous mouse β -catenin expression is retained in this model, it would be useful to cross $\text{Coll1a1}^{\text{TetO-}\Delta\text{N89 } \beta\text{-catenin/Wt}}$ $\text{Rosa26}^{\text{c-MYC/c-MYC}}$ $\text{Igs2}^{\text{CAG-lsl-tTA2-T2A-H2B-TagBFP}}$ mice to $\text{Ctnnb1}^{\text{fl/fl}}$ mice. This would allow the conditional deletion of mouse β -catenin and ensure that $\text{Coll1a1}^{\text{TetO-}\Delta\text{N89 } \beta\text{-catenin/Wt}}$ is driving tumorigenesis.
- One of the interesting findings of this work, particularly in the tet ‘off’ model, was the diverse phenotypes displayed across different genetic dosages of $\text{Coll1a1}^{\text{TetO-}\Delta\text{N89 } \beta\text{-catenin/Wt}}$ and $\text{Igs2}^{\text{CAG-lsl-tTA2-T2A-H2B-TagBFP}}$. At low dosages no tumours were found, whereas at high doses the entire liver was comprised of fibroblast-type cells. This suggests that there may be a dose of mutant β -catenin which is oncogenic, but at higher and lower doses it may be inadequate to drive tumours. Understanding how mutant β -catenin dosage affects oncogenic signalling and how it interacts with other pathways to initiate cancer may be useful in understanding cancer initiation processes.
- Crossing the $\text{Coll1a1}^{\text{TetO-}\Delta\text{N89 } \beta\text{-catenin/Wt}}$ $\text{Igs2}^{\text{CAG-lsl-tTA2-T2A-H2B-TagBFP}}$ onto mice with a tamoxifen controlled $\text{Rosa26}^{\text{c-MycER-T2}}$ allele would allow simultaneous and temporal control over both β -catenin and c-MYC[112]. Experiments could be conducted using both these alleles to establish how the two interact with one another. It would also be useful to study whether simultaneous or sequential activation impacts tumorigenesis and how this alters the tumour microenvironment.

7.3 Development of a conditional, tissue specific and temporally controllable model of neoantigen presentation

It is important to delineate whether anti-tumour responses in tumours are absent due to a lack of stimulatory molecules (lack of antigens or co-stimulatory molecules), exclusion of effector cells themselves (immune exclusion by epithelial cells) or a combination of both. One way to model this would be to express a model antigen in tumour epithelium in an immune excluded tumour microenvironment. If when the model antigen was expressed, infiltrating CD8 T-cells are observed and tumours regressed completely, then it could be argued that lack of expressed tumour model antigen was the cause. However, if tumours are still present without infiltration in the presence of model antigen, it is likely that immune exclusion is a more multifactorial problem. Use of a defined neoantigen would also allow the fate of antigen restricted T-cells to be traced, thus furthering our understanding of T-cell interactions in HCC.

To study this *in-vivo* a GEMM with the ability to express a model neoantigen in cancer epithelial cells is required. There are a range of existing models which do this in a constitutive or tissue specific manner, however, these systems are found to be susceptible to developing tolerance due to expression of model antigens throughout development[199, 200]. If such a model existed where a model antigen could be expressed in a tissue specific and temporally controllable manner (time and space), it would be useful to the scientific community to study antigen mediated responses in a range of diseases, including cancer.

As there are no current model systems that can currently do this, I set about developing my own GEMM to address this shortcoming.

7.3.1 Requirements for the ideal mouse model of neoantigen expression

To study neoantigen presentation in this manner, the ideal system should:

- Encode a neoantigen that is known to stimulate adaptive immune responses
- The neoantigen should have a range of existing tools available to permit study (i.e. antibodies, transgenic T cell receptors, restricted antigen specific T cells [both CD4 and CD8])
- Show an absence or very low level of ectopic expression when not ‘activated’, to prevent tolerance
- Be expressed in a conditional specific manner, so neoantigens within the tumour microenvironment can be studied in specific cell types
- Be expressed in a temporally controllable manner, so neoantigens can be studied in early tumour development or in late-stage disease
- Temporal expression must be controlled using a system with minimal leakiness or background expression
- The agent controlling temporal expression should be safe, cheap, readily available and be at low risk of confounding immune responses
- Be linked to a reporter, either by using a bicistronic construct or fusion protein so cells expressing the neoantigen can be readily identified
- Be produced on a fully inbred strain background to prevent requirement to backcross mice for many generations to obtain experimental mice

7.3.2 Design of a mouse model for study of neoantigen expression

Based on these criteria, I opted to use chicken ovalbumin as the model antigen. Ovalbumin is found in chicken egg white and therefore is readily available in large quantities. Ovalbumin has no confirmed function other than as a food source and is non-toxic[201, 202]. There are two epitopes in the full-length ovalbumin protein. The first is SIINFEKL (OVA 257-264, OVA I), an MHC class I H-2Kb restricted epitope which induces robust CD8 T-Cell responses[201]. The

second ISQAVHAAHAEINEAGR, (OVA 323-339, OVA II), binds to I-A(d) MHC class II[203]. There are a wide range of established tools available to study ovalbumin and its specific epitopes. Transgenic mice and readily available cell lines that contain specific TCRs to both OVA-I and OVA-II[204, 205].

Ovalbumin containing transgenes have been typically used in 3 forms; the full-length secreted protein, a membrane-bound transferrin receptor fusion protein and a truncated cytosol restricted protein. As secreted ovalbumin could have systemic effects, this would not be suitable. Cytosolic OVA is restricted to the cytosolic compartment and is not secreted, therefore limiting any systemic effects and allowing the study of TCR engagement of T-cells with cancer epithelial cells expressing this epitope on the cell surface[201]. The membrane-bound transferrin receptor fusion protein may also be used, but in terms of studying the specific mechanisms where neoantigen in the cytosol is presented to the cell surface, the cytosolic epitope was felt to be the most optimal choice.

To identify which cells are expressing the construct, cOVA is followed by a porcine teschovirus 2A self-cleaving linker peptide and the mCherry fluorescent protein. I selected mCherry as this is a rapidly maturing, and is red-shifted, therefore more suited to deep tissue imaging than other fluorescent proteins with shorter emission lengths. The immunogenicity of mCherry is uncertain.

To allow tissue specific, conditional expression of the cOVA-P2A-mCherry cassette, there are two sets of lox sites within the construct. The first set flank the neo-lox-stop-lox cassette and in the presence of Cre recombinase, lead to the excision of the cassette and allow pCAG driven gene expression. The cOVA-P2A-mCherry expression cassette is flanked by lox66 and lox71 and undergoes Cre mediated inversion at the same time as the neo lox-stop-lox cassette is excised. The loxP sites in each region are incompatible, therefore ensuring the construct is recombined in the desired orientation. The TetO-3G promoter then drives cOVA-P2A-mCherry expression in the presence of doxycycline, with rtTA expression driven by the strong pCAG promoter.

I opted to use a third-generation tetracycline ‘on’ (TetO-3G) system to control the temporal expression of cOVA and mCherry. The TetO-3G system has several advantages over other controlled systems, namely Tamoxifen controlled Estrogen Receptor fusion systems and to a lesser extent the later Cumate-controlled system[206–208]. First, the TetO-3G system is well established and has been shown to work reliably *in-vivo* with a low level of leakiness compared to Estrogen Receptor fusion systems. Second, tetracycline antibiotics are readily available from a wide range of suppliers unlike cumate systems and are less hazardous to handle than tamoxifen. Third, tetracycline antibiotics have more limited effects on mammalian cells than tamoxifen and given there is a clear role for sex-divergent immune responses in mammals, using tamoxifen may plausibly confound the study of immune response and neoantigen presentation, making experiments more complex to design and adequately power. Finally, using doxycycline over tamoxifen also allows this allele to be used in breast cancer research, including in Estrogen Receptor positive models, which is not possible in Estrogen Receptor fusion systems.

These elements were subsequently combined into the final vector layout in collaboration with Dr Arielle Byran, design specialist at Ingenious targeting laboratories (Ronkonkoma, New York, USA). The model was named the ‘NeoTAP’, an abbreviation for NEOantigen expression in Time And sPace.

7.3.2.1 Production of the NeoTAP model

The NeoTAP mouse was produced using C57BL/6 embryonic stem cells by Ingenious targeting laboratories (Ronkonkoma, New York) as described in the methods section. A colony was established at the Cancer Research UK Beatson Institute by rederivation into C57BL/6J mice.

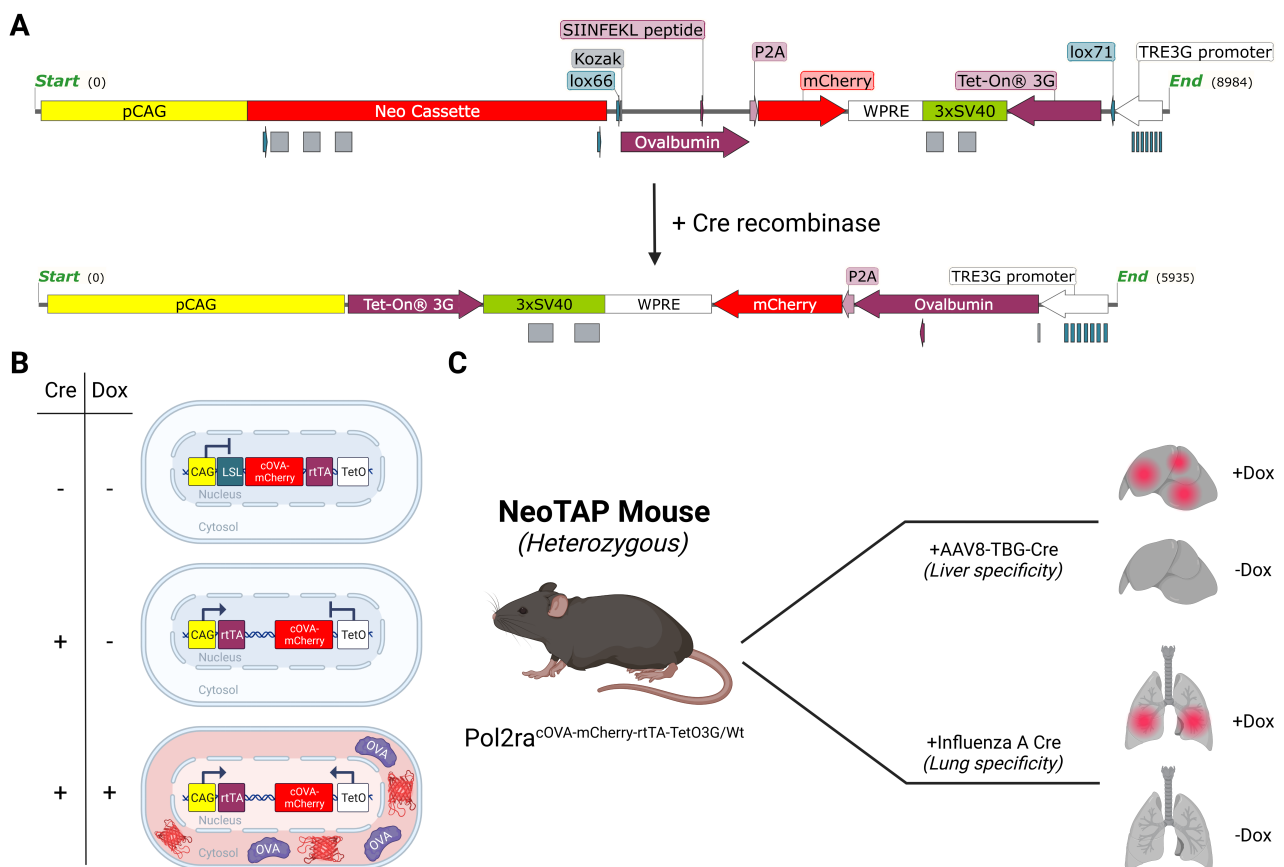
7.3.3 Comparison with the inversion controlled joined neoantigen mouse model

During the development of this model, the iNversion controlled Joined neoantigen (NINJA) mouse model was published and made available to the scientific community through the Jackson laboratory repository[200, 209]. To enable expression of the lymphocytic choriomeningitis virus GP33-43 and GP66-77 epitopes, the NINJA system requires crossing onto a mouse with a tetracycline transactivator allele, followed by Cre-recombination and administration of both tetracycline and tamoxifen. These multiple layers of regulation are aimed to prevent ectopic expression of GP33-43 and GP66-77 in the thymus and hence avoid non-response caused by central tolerance.

In addition to the issues posed by tamoxifen as discussed above, there are several limitations of the NINJA system, which limits its practicality for the study of neoantigen presentation in cancer models. First, the NINJA model uses antigens derived from the rodent-borne lymphocytic choriomeningitis virus (LCMV). This is commonly found in rodents and has a high incidence in animal handling facilities[210] of up to 21%. Therefore, it is important that facilities using this model routinely test NINJA colonies for LCMV to ensure results are not confounded by prior exposure and ensure appropriate controls are used in experiments.

Second, the NINJA allele is found at the Rosa26 locus, which is frequently required for the expression of other alleles (e.g. Rosa26^{c-MYC/c-MYC}). Instead, I opted to insert the allele at the Pol2ra locus, thereby avoiding conflict with other alleles at Rosa26. Third, the NINJA allele requires mice to be crossed with tetracycline transactivator strains, which leads to complex breeding requirements should other alleles (such as oncogenic drivers) be added on. By using an ‘all-in-one’ design, my model dispenses with the need for tetracycline transactivator strains. However, by opting for this, my model cannot be used with a tetracycline ‘off’ approach, but should constitutive expression be required, the model could simply be crossed with a tTA tetracycline ‘off’ strain.

Figure 7.5: Overview of the NeoTAP model. Panel A – Genetic construct layout prior to Cre-mediated excision-inversion and after Cre-recombination. Two elements feature in this design, expression of pCAG driven rtTA in the 5' to 3' direction and TetO controlled expression of Ovalbumin-P2A-mCherry in the 3' to 5' direction. Panel B – In the absence of Cre-recombinase gene expression is stopped by the neo-lox-stop-lox cassette. On Cre-mediated excision and inversion, the transgene becomes correctly orientated, but in the absence of doxycycline rtTA cannot bind the TetO response element. In the presence of both Cre-recombinase and doxycycline, rtTA can bind the TetO response element preceding cOVA-P2A-mCherry and activate transgene expression. On translation, the P2A linker is cleaved, resulting in the expression of cytosolic ovalbumin with OVA I + OVA II epitopes and mCherry fluorescent protein. Panel C – Examples of tissue specificity which could be used to validate the NeoTAP model and demonstrate its utility.



A limitation of both my system and the NINJA system is they employ fluorescent proteins (mCherry for my system, GFP in case of ninja) fused to the neoantigen. Use of a longer wavelength red fluorescent protein may improve performance in deep tissue imaging applications, however, as it does not emit in the near-infrared spectrum it is not as optimal as a near-infrared fluorescent protein such as iRFP713. Both GFP and mCherry, like any fluorescent proteins, both are antigenic, so experiments should be controlled using GFP/mCherry expressing mice.

The OT-I and OT-II transgenic TCR mice have inserts in Tcr α and Tcr β genes which allow them to produce SIINFEKL CD8 (OT I) and ISQAVHAAHAEINEAGR CD4 (OT II) restricted T-cells[204, 205]. They are extremely well characterised and are widely used in immunology research. Cells from these OT-I or OT-II mice can be expanded and modified *in-vitro*, then used as models of adoptive cell therapy and used to study mechanisms of resistance to future cell-based therapies.

7.3.4 Validation of tissue-specific expression

To validate the expression of cOVA-mCherry, I designed an experiment to test the leakiness of cOVA-mCherry in the recombined (with and without doxycycline) and non-recombined states. These experiments were kindly led and performed by Dr. Toshiyasu Suzuki. Mice were assigned to receive either doxycycline 2 mg/ml in drinking water followed by 2×10^{11} GC AAV8-TBG-Cre, normal drinking water followed by 2×10^{11} GC AAV8-TBG-Cre or doxycycline 2 mg/ml in drinking water followed by 2×10^{11} GC AAV8-TBG-Null (empty vector). Mice were sampled 5 days following AAV8 administration.

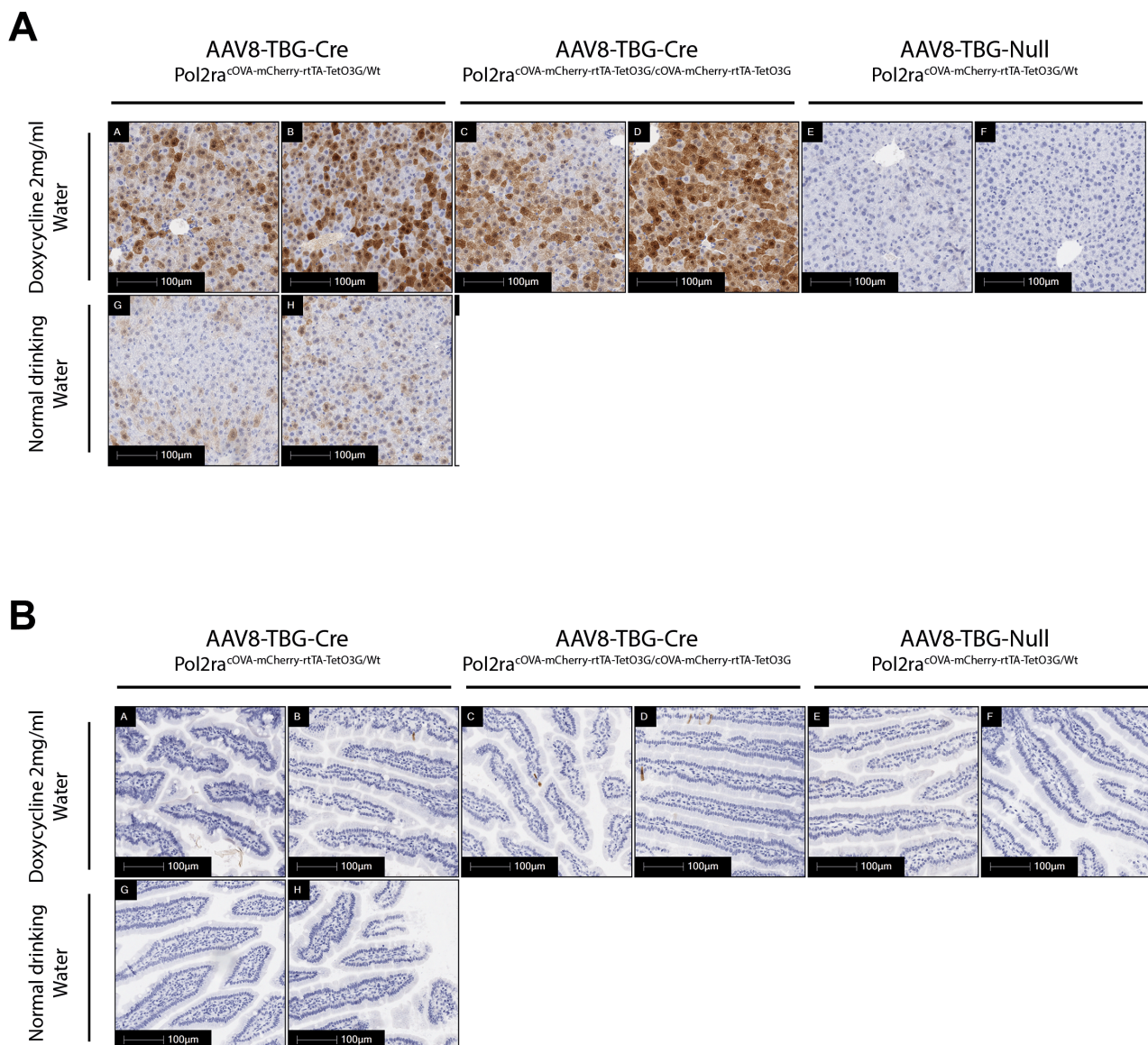
Expression of mCherry was clearly present in the target organ (liver) of $\text{Pol2ra}^{\text{cOVA-mCherry-rtTA-TetO3G/Wt}}$ mice who received high-dose AAV8-TBG-Cre together with doxycycline drinking water (figure 7.6A). Whereas in $\text{Pol2ra}^{\text{cOVA-mCherry-rtTA-TetO3G/Wt}}$ mice who received high-dose AAV8-TBG-Null with doxycycline in drinking water, expression of mCherry in the liver was absent.

$\text{Pol2ra}^{\text{cOVA-mCherry-rtTA-TetO3G/Wt}}$ mice who received high-dose AAV8-TBG-Cre but only had normal drinking water had some, very low expression of mCherry, suggesting leakiness with Cre-recombinase alone. In homozygous $\text{Pol2ra}^{\text{cOVA-mCherry-rtTA-TetO3G/cOVA-mCherry-rtTA-TetO3G}}$ mice, expression of mCherry was stronger, suggesting a genetic dose response. To examine whether there was any off-target expression in other tissues, I also assessed expression of mCherry in the small intestine (figure 7.6B). In mice who received AAV8-TBG-Cre and doxycycline, extremely small numbers of intestinal cells positively stained for mCherry. In mice which didn't receive AAV8-TBG-Cre, there were no traces of mCherry in the intestine. These findings suggest $\text{Pol2ra}^{\text{cOVA-mCherry-rtTA-TetO3G}}$ is expressed in a tissue specific and reasonably non-leaky manner. However, further characterisation of off-target expression should be performed, including in tissues where AAV8 has specific tropism (heart, skeletal muscle, and pancreas).

7.3.5 Summary

The NeoTAP mouse allows highly controlled expression of the model chicken ovalbumin antigen. Minimal expression was observed in non-target tissues. This suggests there is unlikely

Figure 7.6: Immunohistochemical staining for mCherry protein (using anti-Red Fluorescent Protein antibody) expression in liver and small intestine following AAV8-TBG-Cre or AAV8-TBG-Null, with or without 2 mg/ml Doxycycline Hydrochloride in drinking water. All images acquired on Leica Aperio AT-2 at 20x magnification. Panel A – shows hepatocyte specific expression following recombination with AAV8-TBG-Cre, with no expression of mCherry in the absence of Cre-recombinase. Expression was stronger in Pol2racOVA-mCherry-rtTA-TetO3G/cOVA-mCherry-rtTA-TetO3G mice compared with Pol2racOVA-mCherry-rtTA-TetO3G/Wt mice. Panel B – shows small intestine from the same mice assessing for tissue specificity. This shows that at least in small intestine, there is very low off-target expression of Pol2racOVA-mCherry-rtTA-TetO3G. Representative micrographs from minimum n=2 mice per group.



to be central tolerance, a key issue with current ovalbumin expressing models. There was some expression of mCherry in liver tissue of mice which received AAV8-TBG-Cre but did not receive Doxycycline in drinking water, suggesting a mild degree of leakiness. This was observed at high AAV8-TBG-Cre doses and should be further validated with lower dose AAV8-TBG-Cre doses.

Further validation is required to determine whether the cytosolic ovalbumin expressed in this system can induce adaptive immune responses and these experiments are underway. Nevertheless, this new model allows study of neoantigens in a tissue specific and temporally controlled manner, with significant advantages over currently available models.

7.3.6 Future directions

- Further validation is required to show Pol2ra^{cOVA-mCherry-rtTA-TetO3G} is not centrally expressed in the thymus and that it can induce adaptive immune responses. This could be done by staining T-cells from these mice with OVA I + II fluorescent tetramers, or quantifying cytokine release using Elispot assays following *in-vitro* co-culture of Pol2ra^{cOVA-mCherry-rtTA-TetO3G} expressing cells and OT-I T-cells in the presence or absence of doxycycline.
- Tumour cells in solid cancers are known to downregulate antigen presentation machinery, to prevent detection and subsequent destruction by the immune system. This allele should be bred on to different GEMMs of cancer in a range of tissues, to understand the different mechanisms cancer cells engage to prevent antigen presentation or promote tolerogenic responses. It would be interesting to compare both early and late stages to understand how early-stage cancer cells evade immunosurveillance to become established in their relevant tissue niche.
- Tumour organoids or cell lines could be subsequently derived from GEMM tumours from different genotypes and used for genetic or small molecule sScreens to identify compounds which promote neoantigen presentation. This could be done by fluorescent staining of nuclei, cell membranes and ovalbumin (with staining of H2-Kb bound SIINFEKL), followed by high content imaging to count the number of ovalbumin

molecules on the cell surface versus found in the cytosol. An alternative method could be through co-culture with labelled OT-I cells and using high-throughput flow cytometry assays to count dying epithelial cells and OT-I cell activation. Labelling OT-I cells with a fluorescent protein or dye allow these to be easily distinguished from epithelial cells. Live cells can then be CRISPR-Cas9 edited to knock-out genes in a genome wide fashion, co-cultured with labelled OT-I cells, then stained with a vital stain such as DAPI to quantify viability at the end of the co-culture experiment. Identified targets could then be rationally combined with immune checkpoint therapies or cell-based (i.e. CAR-T) therapies and tested *in-vivo*.

- The NeoTAP model also opens the door to addressing therapeutic resistance to adoptive cell therapies. Immune cold tumours exclude infiltrating immune cells, which could plausibly extend to adoptive cell therapies as well. By using the NeoTAP model using a standardised antigen and TCR, genome wide genetic screens can be set-up *in-vivo*, to identify genetic alterations that could be engineered into future adoptive cell-based therapies. An example could be transduction and selection of OT-I cells with a genome wide CRISPR library or overexpression library, followed by injection into mice with ova expressing tumours. After a short period of time, tumours could be sampled and the infiltrating engineered OT-I cells isolated using fluorescence activated cell sorting (FACS). The guide RNA sequences found in the OT-I cells could then be captured and sequenced to identify the most overrepresented guides. These overrepresented guides would correspond to pathways which could be manipulated in subsequent validation experiments to engineer adoptive cell therapies which could overcome an immune excluded microenvironment.
- This system is also likely to be useful for the study of other diseases, namely autoimmune conditions. Within the liver and biliary tree, conditions such as autoimmune hepatitis and primary biliary cirrhosis are thought to occur due to response to self-antigens. One theory is that the failure to develop tolerance to these antibodies, or when a critical mass of antigen is reached, autoimmune responses and autoantibodies are raised against self-

antigens. Using the NeoTAP model, mechanisms of these diseases could be studied and new therapies to promote tolerance developed, providing a more specific treatment than current systemic immunosuppressive therapies.

Chapter 8

Conclusions

8.1 Key findings

Using clinically relevant *in-vivo* models of HCC, I have shown significant differences in signalling across canonical WNT/ β -Catenin immune excluded and immune infiltrated Trp53^{fl/fl} Rosa26^{c-MYC/c-MYC} models. A key, and exciting finding is type I IFN responses in both mouse and human disease were lower in canonical WNT/ β -Catenin driven tumours. In turn, I showed type I IFN responses in canonical WNT/ β -Catenin driven disease can be restored through agonism of the cGAS-STING pathway. This could provide a therapeutic means of promoting immune infiltration and subsequent sensitisation to immune checkpoint blockade through exploiting key vulnerabilities in canonical WNT/ β -Catenin driven tumours. Further work is required to identify drugs that can trigger cGAS-STING activation in these tumours, but my work demonstrates this is indeed plausible.

Resistance to immune checkpoint blockade is likely to be multifactorial and mediated in a context-dependent manner. Specifically, I have shown by using genetically engineered, immunocompetent models, that different underlying genetic drivers of HCC have a major role in governing sensitivity to immune checkpoint inhibition. Figure 8.1 shows a summary of my findings and the mechanisms which may be underpinning these observations.

This body of work has generated novel *in-vivo* models and strategies for investigating therapy resistance in HCC which will be a resource for the scientific community. Notably, I have developed conditional, temporally controlled mouse models of mutant TetO- Δ 89 β -Catenin expression and a model of antigen expression using cytosolic ovalbumin as a model antigen. In addition to these models, I have developed a genetically defined cell line from the Trp53^{fl/fl} Rosa26^{c-MYC/c-MYC} GEMM and developed techniques which allow 2D cell-lines to be generated from tumour organoids for orthotopic transplantation with a high engraftment rate.

Although there are numerous directions future work could take, expanding the range of orthotopic transplant lines and further validation of the TetO- Δ 89 β -Catenin and NeoTAP ovalbumin mouse models should be a priority. For the orthotopic model, a line which

produces immune excluded tumours would be incredibly useful. This would allow immune infiltrated and immune excluded tumour producing cells to be manipulated *in-vitro* using overexpression vectors or CRISPR-Cas9, then subsequently transplanted, to rapidly test which genes are involved in producing an immune excluded microenvironment. This could then be further validated using the more heterogeneous GEMMs.

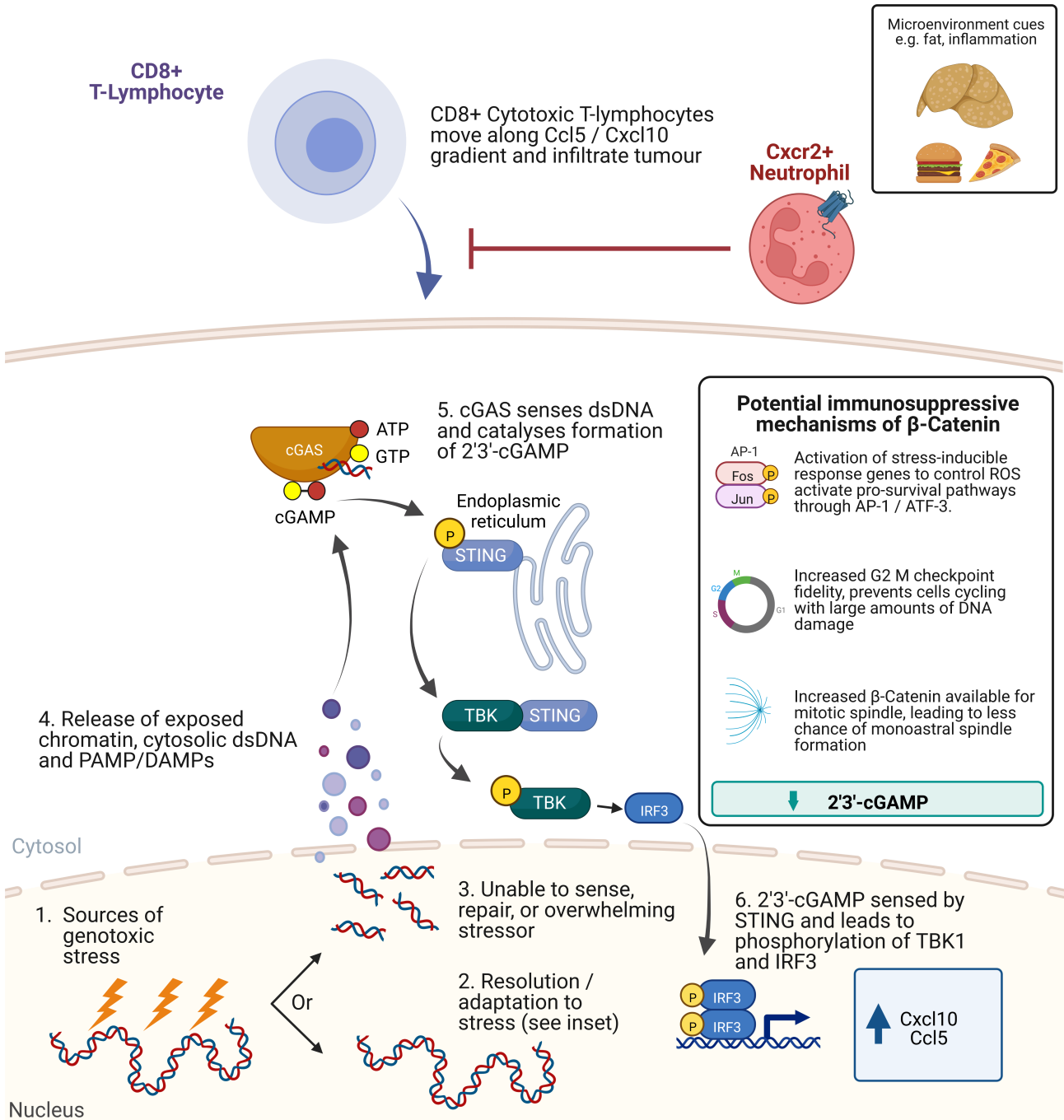
For the TetO- $\Delta 89$ β -Catenin system, I have shown that administering doxycycline suppresses the development of ‘classical’ glutamine-synthetase expressing canonical WNT/ β -Catenin driven tumours. The next step would be to establish whether administration of doxycycline could ‘turn-off’ canonical WNT/ β -Catenin in established tumours. If switching ‘off’ β -Catenin by administering doxycycline led to an increase in immune cell infiltrate over time, this would demonstrate a causal role for β -Catenin and provide extensive opportunities to investigate how it exerted its effects. Tumours from these mice could be sampled at timepoints following administration of doxycycline and analysed with methods I’ve used elsewhere in my thesis, such as pseudotime trajectory modelling and single-cell RNA sequencing. This would show which genes in different cell populations change in response to switching β -Catenin ‘off’. Thus, giving critical insights into which components of the canonical WNT/ β -Catenin are implicated promoting immune evasion.

Finally, although I have demonstrated the NeoTAP ovalbumin model expresses the mCherry reporter in response to Cre and doxycycline, the construct I bicistronic and expression of cytosolic ovalbumin should also be confirmed. Cytosolic ovalbumin has a very short half-life before it is degraded and requires presentation via MHC Class I to trigger an immune response. Therefore, showing expression could be achieved through fluorescent tetramer staining of T-cells in this model or by using co-culture experiments *in-vitro*. Plating cells from NeoTAP mice who have received Cre recombinase vector and co-culturing with OT-I cells in the presence of doxycycline should show increased cell killing or Elispot responses against cells expressing ovalbumin derived epitopes.

8.1.1 Cancer cell intrinsic mechanisms underpinning immune exclusion

To identify possible mechanisms that promote anti-tumour immune response, I developed and characterised an immunotherapy-responsive $\text{Trp53}^{\text{fl/fl}}$ $\text{Rosa26}^{\text{c-MYC/c-MYC}}$ murine model of HCC. Generating this allowed me to compare the molecular characteristics of this model to the immunotherapy resistant $\text{Ctnnb1}^{\text{exon3/Wt}}$ $\text{Rosa26}^{\text{c-MYC/c-MYC}}$ model using an integrative, multiomic approach to identify potential mechanisms of therapy resistance.

Figure 8.1: Potential mechanisms underpinning immunotherapeutic resistance in β -Catenin mutant HCC arising from this thesis.



With the demonstration of repressive transcription factor binding and upregulation of DNA repair and chromosome organisation pathways in $Cttnb1^{\text{exon3/Wt}} \text{ Rosa26}^{\text{c-MYC/c-MYC}}$ tumours, it appears there are two central mechanisms which may lead to the suppression of CCL5 and CXCL10.

First, β -Catenin driven tumours suppress the production of 2'3'cGAMP and other cell intrinsic PAMP/DAMP signalling molecules, namely through high levels of DNA repair and increased spindle assembly checkpoint fidelity. These pathways were found to be significantly upregulated in β -Catenin driven tumours, both in the Cancer Genome Atlas, in mice and in organoids derived from these mice. As STING activation requires a threshold of 2'3'cGAMP to be reached[179], it's plausible that by enhancing DNA repair and spindle assembly checkpoint fidelity, β -Catenin tumours reduce the amount of broken DNA or the physical stress in DNA fibres, thus preventing 2'3'cGAMP accumulation[185].

Second, suppression of CCL5 or CXCL10 could be due to β -Catenin mediated transcription. This effect may be direct (β -Catenin directly binding regulatory elements) or indirect, with β -Catenin target genes promoting gene transcription programmes which then suppress CCL5 or CXCL10. My findings of AP-1 transcription factor footprints in promoter regions of cGAS-STING pathway genes suggests the indirect model is more likely. There is considerable literature describing the cooperation between β -Catenin and AP-1, including β -Catenin being found in complex with c-JUN and c-FOS[175, 176, 211]. Interestingly, *Spranger et al.* found β -Catenin mediated immune exclusion in melanoma depended on ATF3, which has been found to be both a target of β -Catenin and to form complexes with AP-1[88, 176, 212–214].

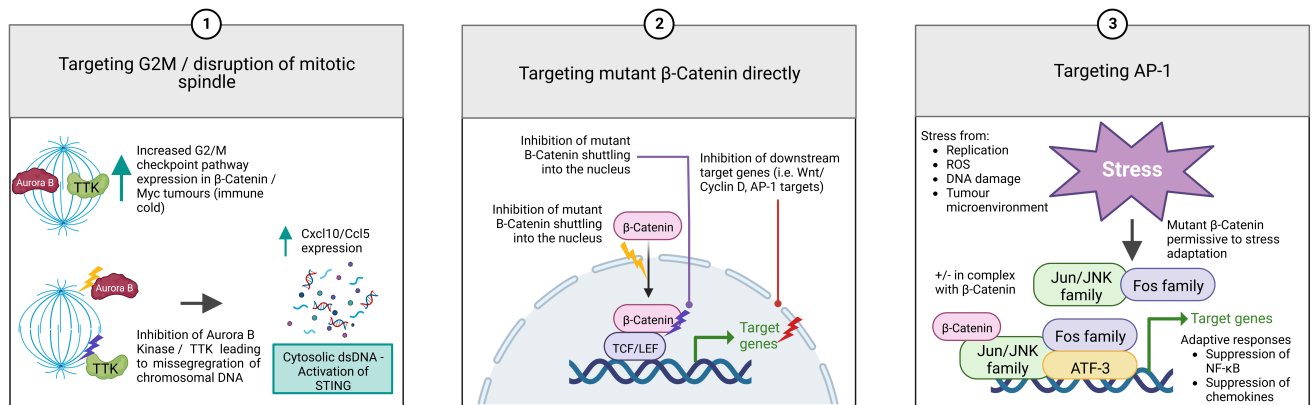
Both components of this hypothetical model may act separately or in combination, and further work should be undertaken to establish whether this provides β -Catenin driven cancers with multiple layers of defence against immunotherapies.

The observation that immune infiltration appears to be dependent on epithelial CCL5 and CXCL10 expression is provocative, given that these have been identified as predictors of response in human disease in samples from patients with HCC who have received anti-PD1

therapy[188]. It would therefore be useful to show causally in the GEMMs I have used, that CCL5 and CXCL10 are critical cytokines required to promote immune-cell infiltration into liver tumours would help greatly. This could be achieved either through conditional or CRISPR-Cas9 knock-out *in-vivo* and would provide reassuring data to support further research investigating how expression of CCL5 and CXCL10 can be restored in immunotherapy-resistant tumours. Other researchers in the field have done this and shown CCL5 over expression restored anti-tumour immunity in immune excluded tumours driven by β -Catenin[101]. My work not only supports the current literature but takes it one step further by suggesting CCL5 expression could be induced using 2'3'cGAMP. This opens the door to using the upstream cGAS-STING signalling pathway to provide an avenue for clinical translation.

An overview of the mechanisms in mutant β -Catenin HCC and how they can be targeted are outlined in figure 8.1 and figure 8.1.1.

Figure 8.2: Potential therapeutic targets for reversing immunotherapeutic resistance in β -Catenin mutant HCC.



8.1.2 Epithelial cytokine expression can be induced by targeting the cGAS-STING pathway

Immunotherapy-resistant tumours were found to have very low levels of STING expression, whereas immunotherapy sensitive tumours contained had strong expression of STING which coincided closely with the spatial distribution of infiltrating lymphocytes. As CCL5 and CXCL10 are the downstream effectors of canonical STING signalling, taken together, this association suggests $Ctnnb1^{\text{exon3}/\text{Wt}}$ driven tumours may regulate pro-inflammatory STING expression to limit lymphocyte infiltration and hence evade anti-tumour immune responses through this pathway. Treatment of $Ctnnb1^{\text{exon3}/\text{Wt}}$ $Rosa26^{\text{c-MYC}/\text{c-MYC}}$ tumour organoids with 2'3'cGAMP restored expression of CCL5 and CXCL10, suggesting that $Ctnnb1^{\text{exon3}/\text{Wt}}$ does not suppress STING expression directly, but is more likely to play a role in regulating upstream pathways to limit production of intracellular 2'3'cGAMP.

Given that 2'3' cGAMP is largely produced by the presence of cytosolic DNA, this finding gives rise to an intriguing question, what is the role of canonical Wnt signalling in maintaining genome or mitochondrial DNA stability and DNA repair? Understanding these functions may allow vulnerabilities in canonical WNT/ β -Catenin driven tumours to be targeted and drive production of pro-inflammatory messenger molecules in tumour cells that

are otherwise ‘immune-cold’. Indeed, work published in GEMMs in the last few years would suggest that CCL5 overexpression can extend survival in immunotherapy resistant excluded canonical WNT/ β -Catenin driven HCC[101]. Using the cGAS-STING to target this may then make this a druggable target.

The study by *de Galeretta et al.* [101] used transcriptional comparison of $\Delta 90$ β -Catenin MYC and Trp53^{-/-} MYC tumours to identify CCL5 as a differentially expressed cytokines. I have gone further in my analysis using multiomic comparison in two autochthonous models. The autochthonous models may be superior in several ways. 1) Tumourigenesis is slower, 2) Tumourigenesis is not dependent upon hydrodynamic tail vein injection, which causes liver damage, 3) c-MYC is expressed at a more physiological level by using the native Rosa26 promoter, 4) Genetic drivers of HCC are found in defined genomic locations, as opposed to sleeping beauty transposons, which may be inserted across the whole genome and disrupt the function of other genes.

Previous work has shown that cGAS localises to the presence of exposed dsDNA which may include micronuclei or chromatin bridges[185]. The presence of cGAS-coated chromatin bridges under mechanical load are potent inducers of the cGAS/STING pathway and can be generated by inhibition of MPS1[179, 185]. This has been shown to prime immunogenicity in an immune excluded model of lung cancer and MPS1 inhibition has been shown to be effective in HCC cell lines and in a Trp53^{-/-} c-MYC hydrodynamic mouse model[148, 187]. As MPS1 is upregulated compared to normal liver in models of Ctnnb1^{exon3/Wt} Rosa26^{c-MYC/c-MYC} HCC, this may be a useful strategy to prime to generate epithelial cGAS/STING activation, prior to treatment with immune checkpoint blockade. A rational next step would be to examine whether inhibition of MPS1 using orally bioavailable small molecules such as BAY1161909 or BAY1217389 induces STING and downstream CCL5 and CXCL10 expression in Ctnnb1^{exon3/Wt} Rosa26^{c-MYC/c-MYC} HCC tumour models as a timepoint study. Inhibition of MPS1 as a monotherapy or in combination with taxanes are currently under evaluation in phase 1 and 2 clinical trials[215, 216]. Of the trials that have reported studying the current compounds which have been studied in humans (S81694, CFI-402257,

BAY1161909 (Empesertib) and BAY1217389), toxicities occurred in half or more of patients, suggesting long-term tolerability of these agents is likely to be limited[217]. However, as has been shown in preclinical models of lung cancer, a short course of therapy may be better tolerated and could allow the priming of an immune-cold microenvironment through accumulation of micronuclei or chromatin bridges which subsequently sensitise ‘immune-cold’ tumours to immune checkpoint blockade[148, 185]. It must also be considered that this may not be a ‘one-size-fits-all’ therapy, as many HCC arise because of inflammation and exacerbating this by triggering CXCL10 and CCL5 expression may have a deleterious effect.

To robustly demonstrate the dependence on STING for promoting lymphocyte infiltration into tumours it would be useful to compare $Cttnb1^{exon3/Wt}$ $Rosa26^{c-MYC/c-MYC}$ mice with $Trp53^{fl/fl}$ $Rosa26^{c-MYC/c-MYC}$ and $Trp53^{fl/fl}$ $Rosa26^{c-MYC/c-MYC}$ $Sting1^{-/-}$ mice, to identify whether loss of STING leads to an immune-cold microenvironment or affects sensitivity to immune checkpoint blockade. If MPS1 inhibition is shown to be effective in sensitising $Cttnb1^{exon3/Wt}$ $Rosa26^{c-MYC/c-MYC}$ tumours to immune checkpoint blockade, the requirement for STING could be demonstrated by comparing with MPS1 inhibitor treated $Cttnb1^{exon3/Wt}$ $Rosa26^{c-MYC/c-MYC}$ $Sting1^{-/-}$ mice and examining whether loss of STING restores resistance to immune checkpoint blockade.

8.2 Further research questions and limitations

8.2.1 Do other cell types contribute to immunotherapy resistance in HCC?

A key finding of my work is how the genetic and liver microenvironment context both have profound effects on immunotherapy resistance in models of HCC. The presence of NASH/NAFLD (Appendix A) prevented anti-PD1 therapy working in models of HCC that were previously sensitive to therapy. As part of a collaboration, I helped to show this was dependent on CXCR2 signalling in myeloid populations, which when targeted with CXCR2 small molecule inhibitors, led to reversal of the immunotherapy resistant phenotype. These

findings raise an additional question around the precise role of CXCR2+ cells and whether CXCR2i acts directly upon myeloid cells in the tumour microenvironment or indirectly by targeting NASH associated inflammation. It would therefore be interesting to establish whether longer-term treatment of mice on a high-fat diet leads to different NASH phenotypes and patterns of fat deposition in hepatocytes. If CXCR2 inhibition could reverse established NASH/NAFLD, this would have important and more wide-ranging clinical applications than just in patients with NASH/NAFLD HCC. If CXCR2i exerts its effect by reversing fatty infiltrates and associated inflammation, this in turn leads to an even more interesting question. Could diet or exercise therefore improve immunotherapy responses in certain types of cancer or affect the chances of tumourigenesis in premalignant states?

In GEMMs of HCC, there were generally far fewer myeloid infiltrates than in the DEN-ALIOS tumour models. Trp53^{fl/fl} Rosa26^{c-MYC/c-MYC} models typically had high levels of F4/80 macrophages and Kupffer cells, whereas Ctnnb1^{exon3/Wt} Rosa26^{c-MYC/c-MYC} was largely devoid of any leukocytes besides Kupffer cells. In the GEMMs there were very few if any neutrophils present, suggesting CXCR2i is unlikely to have a major impact in at least some of these models. Now more relevant GEMMs have been developed, these can be combined with dietary or environmental exposures to model the effects of different liver disease aetiologies. Given very few patients develop HCC without liver disease, it is essential to model this aspect in conjunction with the GEMM approach. This could be using high-fat diets such as ALIOS, supplementing diets with ethanol to model alcoholic liver disease, or by giving agents such as carbon tetrachloride to model liver fibrosis. The natural next step to combine the NASH/NAFLD-HCC and GEMM streams of work would be to test whether combining a high-fat diet with the Trp53^{fl/fl} Rosa26^{c-MYC/c-MYC} model, led to the infiltration of neutrophils and subsequent CXCR2-dependent resistance to anti-PD1 therapy.

In this thesis I have focussed predominantly on the role of cancer epithelial cells and how these may coordinate the tumour microenvironment. Although epithelial cells arguably orchestrate a tumour microenvironment to support their growth (otherwise tumours could exist without epithelial cells), the microenvironment milieu is an often-complex mixture of

immune (macrophages, Kupffer cells, T-cells, B-cells etc.) and mesenchymal cells (endothelial cells, sinusoidal cells, hepatic stellate cells, fibroblasts etc.). Response to PAMP/DAMP molecules is mediated by a wide range of different cells, including Kupffer cells and recruited monocyte/macrophages. These cells, depending on their phenotype (pro-inflammatory or pro-repair) may then orchestrate different immune responses[64, 82].

Furthermore, simplifying what is a complex process of lymphocyte recruitment into a diseased environment and explaining this solely by cytokine expression and chemotaxis is likely to be rather too simplistic. One of the main cell-types involved in lymphocyte recruitment are endothelial cells, which express receptors and adhesion molecules. Expression of these molecules may be in response to crosstalk between different cells within the tumour microenvironment and it is well known that tumour endothelium express different molecules compared to normal healthy liver. Finally, the unique cell types found in the liver are likely to mean findings applicable to other cancers may not translate across. For example, liver sinusoidal endothelial cells (LSECs) are unique to the liver and express different sets of receptors and adhesion molecules. Intriguingly, it has been shown that compared with normal endothelium, lymphocytes take different transmigration routes across LSECs. Failure to consider these factors may have consequences for the recruitment of lymphocytes into otherwise immune excluded tumours, even if cytokine signalling can be successfully induced[2, 8].

To address these limitations of my work, high-throughput technologies such as single-cell RNA sequencing or high-resolution spatial transcriptomics would allow unbiased phenotyping and localisation of genes which mediate immunotherapy resistance in these models. With adequate resources, this would represent an important investment in understanding these models in a far greater depth, explain the contributions made by different cell types, and be used to prioritise new therapeutic targets.

8.2.2 How does c-MYC cooperate with different drivers to limit or promote anti-tumour immunity?

In this thesis I comprehensively characterised the differences between $Ctnnb1^{\text{exon3/Wt}}$ $Rosa26^{\text{c-MYC/c-MYC}}$ and $Trp53^{\text{fl/fl}}$ $Rosa26^{\text{c-MYC/c-MYC}}$ HCC GEMMs. One of the reasons I decided to undertake this comparison was due to the comparability between the genotypes - the only difference being $Ctnnb1^{\text{exon3/Wt}}$ or $Trp53^{\text{fl/fl}}$ in combination with $Rosa26^{\text{c-MYC/c-MYC}}$. Although the presence of $Rosa26^{\text{c-MYC/c-MYC}}$ did not change across these comparisons, it is widely known that c-MYC can play a major role in evading anti-tumour immunity[131].

Although c-MYC overexpression was present in both GEMMs, if c-MYC has different effects in combination with $Ctnnb1^{\text{exon3/Wt}}$ compared to $Trp53^{\text{fl/fl}}$, the analyses presented here may not be able to account fully for any cooperation. Without c-MYC, $Ctnnb1^{\text{exon3/Wt}}$ and $Trp53^{\text{fl/fl}}$ alone do not form tumours, making it difficult to study these in isolation. To address this, an inducible c-MYC-ER model could be used to elucidate the specific effects of c-MYC and identify how it cooperates with $Ctnnb1^{\text{exon3/Wt}}$ and $Trp53^{\text{fl/fl}}$ to drive immune evasion[112]. Recombination would be performed using AAV8-TBG-Cre as I have done here, but mice would be given tamoxifen in their chow to turn on c-MYC. Tamoxifen could then be withdrawn to see how c-MYC affects the immune microenvironment and responses to immunotherapy.

8.2.3 Can β -Catenin be targeted as an adjuvant to immunotherapy?

Targeting β -Catenin has traditionally been a difficult member of the canonical Wnt signalling pathway to target pharmacologically. Multiple inhibitors of the canonical Wnt signalling pathway have been developed, however, many are targeted at upstream components of the pathway or elements involved in paracrine Wnt signalling such as Dvl, Dkk or porcupine and are of limited use in the context of constitutively active mutant β -Catenin. Therefore, disrupting binding of β -Catenin to its nuclear cofactors, inhibiting its shuttling into the nucleus, or repressing β -Catenin target gene transcription are likely to be more suitable approaches. Although not specifically examined in this thesis, there are examples where targeting upstream elements of the canonical Wnt/ β -Catenin signalling pathway using

approaches such as DKK or Tankyrase inhibition enhances immunotherapy responses in other cancer types[218].

Key questions going forward will be which patients to include in these studies and how the trials of these agents will be designed. A range of compounds targeting β -Catenin are in preclinical and early-phase clinical development, however, there is not yet a suitable compound that has demonstrated efficacy or gained approval for routine clinical use. Once an effective compound is identified it will need to be determined whether this is especially in β -Catenin mutant disease. However challenging, this is an exciting area, as should a compound be shown to be effective in a particular molecular subtype this could introduce routine molecular testing into clinical practice and further widen the opportunities for stratified trials in other disease subtypes.

As β -Catenin plays a key physiological role in the maintenance of different tissues, it is important to establish whether direct or indirect targeting of β -Catenin will lead to off-target effects, or whether β -Catenin inhibition may affect the proliferation of both normal hepatocytes and immune cells that mount anti-tumour responses. Understanding potential side-effects will help to inform clinical trials and design dosing regimens that are better tolerated, thus increasing the likelihood of patient benefit. It remains unclear in the preclinical setting whether combination therapies are required continuously alongside immune checkpoint therapies, or whether a ‘short-course’ regimen of an immunosensitising β -Catenin targeted agent, followed by immune checkpoint blockade is a better strategy. In addition to identifying the optimal sequence for targeted anti- β -Catenin therapies, future studies should systematically investigate the role of different β -Catenin nuclear co-factors, to identify which co-factors promote tumorigenesis and immunosuppression.

It is plausible that β -Catenin has different nuclear co-factors in homeostasis and in tumorigenesis. These could play divergent roles and as such, understanding whether β -Catenin has different co-factors could help to identify better drug targets which are more selective for HCC, rather than other tissues where β -Catenin is physiologically required. One way to investigate this, which would also help to answer whether β -Catenin is found in

complex with AP-1, would be to perform an immunoprecipitation experiment to pull-down nuclear β -Catenin. The resulting immunoprecipitated β -Catenin can then be run through liquid chromatography and into a mass spectrometer to identify which proteins it is found in complex with. This could be further enhanced by treating with endonucleases such as Benzonase to release complexes bound to DNA, allowing DNA bound fractions to be examined.

8.3 Immunotherapy for HCC in context

Central to any future work must be a focus on translating findings into clinical practice, in a meaningful and patient-centred way. To effectively translate my findings, there are several experiments that need to be performed to establish the best translation strategy. Unlike mice, patients with HCC are likely to have a wide range of comorbidities and degrees of frailty, which can contribute to significant complications arising from anti-cancer therapy. Most notably the presence of background liver disease and associated liver dysfunction is the most common reason for ineligibility for systemic therapy currently.

However, a broader question remains. How can outcomes for patients with HCC be drastically improved? Treatments for patients with advanced, inoperable cancer are likely to only provide modest survival benefit and are associated with very high costs. Detecting greater numbers of people who have HCC at a stage where curative surgery is feasible would result in far greater impact than marginal improvements in efficacy of systemic therapy given with palliative intent. Finding where in the patient pathway immunotherapies have the most impact should be prioritised. One example of where immunotherapy could be useful is the neoadjuvant setting prior to surgery or ablation. Neoadjuvant therapy prior to surgery is commonly used in other cancer types and reduces the risk of local recurrence[219, 220]. Neoadjuvant immune checkpoint blockade in HCC is under investigation in at least 30 clinical trials for HCC which at the time of writing are still ongoing, but may be promising[72]. Data from these trials, including response biomarkers and molecular profiling would be very useful to establish whether addition of therapies such as cGAS-STING agonism would be useful in

combination with immune checkpoint blockade in the neoadjuvant setting and in which patients. In other words – the ‘right therapy’ for the ‘right patient’ at the ‘right time’.

Given most cases of HCC and HCC-related deaths occur in low-middle income settings, how expensive immunotherapies and novel targeted agents may impact patients and their families in these settings must be considered. Access to immunotherapies in these settings is a major challenge[30]. Immunotherapies often come in the form of monoclonal antibodies which require temperature-controlled logistics and are administered in specialist healthcare facilities. Following administration, side effects of anti-cancer therapy are common and requires specialist care to ensure complications are safely managed. The comprehensive nature of the multidisciplinary team required to support multimodal cancer services for HCC patients (radiology, gastroenterology and hepatology, oncology, surgery, pathology, allied health professionals) makes this a particularly complex undertaking. In many low-middle income countries, the number of specialist oncologists in the national cancer workforce is in the single digits and many countries do not have any oncologists. In the event care is accessible, the prohibitively expensive costs of therapy in ‘patient-pays’ systems poses an insurmountable barrier to therapy, or results in catastrophic healthcare expenditure for the patient and their family.

The current development of targeted anti-cancer therapies is primarily based upon molecular data collected in high-income countries, which includes agents that are intended for the treatment of HCC. Similarly, clinical trials of therapies for advanced HCC which are the current standard-of-care have not been performed in low-middle income settings. Therefore, there is a risk that novel HCC therapies may not only be too expensive in these settings, but may not even be effective. It is imperative that therapies for HCC are developed and tested in equitable partnership with communities who are most affected by incurable disease to avoid further exacerbating disparities in global cancer outcomes.

Collectively, the data presented in this thesis show the development of new models which will be useful to help understand how HCC develops and responds to therapy. By using enhanced models which can more accurately recapitulate complex aspects of the tumour

microenvironment, it is more likely that preclinical therapies can be successfully translated into benefit for patients. However, it is important to acknowledge that although these immunocompetent models are more complex than many existing models, these are still only models of disease – and mice are not humans. These models should not be used in isolation, but in combination with other model systems, including human xenografts or human co-culture experiments. By triangulating results from multiple model systems, this will provide information on whether targets are valid and could highlight challenges or further opportunities for clinical translation.

Significant progress in the field is urgently needed, both in terms of new treatment strategies and enabling more people to receive curative therapy. These models will help catalyse new immunotherapeutic discoveries and help to meet this urgent need. With innovation and better means of early detection, will come improved access to treatment. Together, this will allow better outcomes for people with HCC worldwide.

Bibliography

1. Abdel-Misih, S. R. Z. & Bloomston, M. Liver Anatomy. *Surgical Clinics of North America* **90**, 643–653. ISSN: 0039-6109. <https://www.sciencedirect.com/science/article/pii/S0039610910000526> (2010).
2. Shetty, S., Lalor, P. F. & Adams, D. H. Liver sinusoidal endothelial cells — gatekeepers of hepatic immunity. *Nature Reviews Gastroenterology and Hepatology* **15**, 555–567. ISSN: 17595053. <http://dx.doi.org/10.1038/s41575-018-0020-y> (2018).
3. Horst, A. K., Neumann, K., Diehl, L. & Tiegs, G. Modulation of liver tolerance by conventional and nonconventional antigen-presenting cells and regulatory immune cells. *Cellular & Molecular Immunology* **13**, 277–292. ISSN: 1672-7681 (2016).
4. Robinson, M. W., Harmon, C. & Farrelly, C. O. Liver immunology and its role in inflammation and homeostasis. *Cellular & Molecular Immunology* **13**, 267–276 (2016).
5. Heymann, F. & Tacke, F. Immunology in the liver — from homeostasis to disease. *Nature Reviews Gastroenterology and Hepatology* **4**, 1–23 (2016).
6. Drake, T. M. & Harrison, E. M. Malignant liver tumours. *Surgery* **35**, 707–714. ISSN: 0263-9319. <https://doi.org/10.1016/j.mpsur.2017.09.008> (2017).
7. Rungay, H. *et al.* Global burden of primary liver cancer in 2020 and predictions to 2040. *Journal of Hepatology* **77**, 1598–1606. ISSN: 16000641. <https://doi.org/10.1016/j.jhep.2022.08.021> (2022).
8. Llovet, J. M. *et al.* Hepatocellular carcinoma. *Nature Reviews Disease Primers* **7**. ISSN: 2056676X. <http://dx.doi.org/10.1038/s41572-020-00240-3> (2021).
9. Global Burden of Disease 2019 Cancer Collaboration. Cancer Incidence, Mortality, Years of Life Lost, Years Lived With Disability, and Disability-Adjusted Life Years for 29 Cancer Groups From 2010 to 2019 A Systematic Analysis for the Global Burden of Disease Study 2019. *JAMA Oncology* **8**, 420–444 (2022).
10. Yuen, M.-f. *et al.* Hepatitis B virus infection. *Nature Reviews Disease Primers* **4**, 1–21. <http://dx.doi.org/10.1038/nrdp.2018.35> (2018).
11. Mak, L.-y. *et al.* Global Epidemiology, Prevention, and Management of Global Epidemiology of HBV. *American Society of Clinical Oncology*, 262–279. http://ascopubs.org/doi/pdfdirect/10.1200/EDBK%7B%5C_%7D200939 (2019).

12. Serag, H. B. E. Epidemiology of Viral Hepatitis and Hepatocellular Carcinoma. *Gastroenterology* **142**, 1264–1273.e1. ISSN: 0016-5085. <http://dx.doi.org/10.1053/j.gastro.2011.12.061> (2012).
13. Chiaramonte, M. *et al.* Rate of incidence of hepatocellular carcinoma in patients with compensated viral cirrhosis. *Cancer* **85**, 2132–2137. ISSN: 0008-543X (Print) (May 1999).
14. Bengtsson, B. *et al.* The risk of hepatocellular carcinoma in cirrhosis differs by etiology, age and sex: A Swedish nationwide population- based cohort study. *United European Gastroenterology Journal* **10**, 465–476 (2022).
15. GBD 2017 Cirrhosis Collaborators. The global, regional, and national burden of cirrhosis by cause in 195 countries and territories, 1990–2017: a systematic analysis for the Global Burden of Disease Study 2017. *The Lancet Gastroenterology & Hepatology* **5**, 245–266 (2020).
16. Torrens, L. *et al.* Hepatocellular Carcinoma in Mongolia Delineates Unique Molecular Traits and a Mutational Signature Associated with Environmental Agents. *Clinical Cancer Research* **28**, 4509–4520. ISSN: 15573265 (2022).
17. Álvarez, E. G. *et al.* Aberrant integration of Hepatitis B virus DNA promotes major restructuring of human hepatocellular carcinoma genome architecture. *Nature Communications* **12**, 1–12 (2021).
18. Matthews, P. C., Brown, R. & Goulder, P. Sexual Dimorphism in Chronic Hepatitis B Virus (HBV) Infection: Evidence to Inform Elimination Efforts. *Wellcome Open Research* **7**, 1–22. ISSN: 2398502X (2022).
19. Manns, M. P. *et al.* Hepatitis C virus infection. *Nature Reviews Disease Primers* **3**, 1–19 (2017).
20. Ally, A. *et al.* Comprehensive and Integrative Genomic Characterization of Hepatocellular Carcinoma. *Cell* **169**, 1327–1341.e23. ISSN: 10974172 (2017).
21. Schulze, K. *et al.* Exome sequencing of hepatocellular carcinomas identifies new mutational signatures and potential therapeutic targets. *Nature Genetics* **47**, 505–511. ISSN: 15461718 (2015).

22. Alexandrov, L. B. *et al.* The repertoire of mutational signatures in human cancer. *Nature* **578**, 94–101. ISSN: 14764687 (2020).
23. Seitz, H. K. *et al.* Alcoholic liver disease. *Nature Reviews Disease Primers*. ISSN: 2056-676X. <http://dx.doi.org/10.1038/s41572-018-0014-7> (2018).
24. Petrick, J. L. *et al.* Tobacco, alcohol use and risk of hepatocellular carcinoma and intrahepatic cholangiocarcinoma: The Liver Cancer Pooling Project. *British Journal of Cancer* **118**, 1005–1012. ISSN: 15321827. <http://dx.doi.org/10.1038/s41416-018-0007-z> (2018).
25. Lieber, C. S. The Discovery of the Microsomal Ethanol Oxidizing System and Its Physiologic and Pathologic Role. *Drug Metabolism Reviews* **36**, 511–529. ISSN: 0360-2532. <https://doi.org/10.1081/DMR-200033441> (Jan. 2004).
26. Wei, R. *et al.* Comprehensive analysis reveals distinct mutational signature and its mechanistic insights of alcohol consumption in human cancers. *Briefings in Bioinformatics* **22**, 1–14. ISSN: 14774054 (2021).
27. Fairfield, C. J. *et al.* Genome-Wide Association Study of NAFLD Using Electronic Health Records. *Hepatology Communications* **6**, 297–308. ISSN: 2471254X (2022).
28. Abdel-Rahman, O. *et al.* Cigarette smoking as a risk factor for the development of and mortality from hepatocellular carcinoma: An updated systematic review of 81 epidemiological studies. *Journal of Evidence-Based Medicine* **10**, 245–254. ISSN: 17565391 (2017).
29. Kumar, P., Mahato, D. K., Kamle, M. & Mohanta, T. K. Aflatoxins : A Global Concern for Food Safety , Human Health and Their Management. *Frontiers in Microbiology* **7**, 1–10 (2017).
30. Drake, T. M., Knight, S. R., Harrison, E. M. & Søreide, K. Global inequities in precision medicine and molecular cancer research. *Frontiers in Oncology* **8**. ISSN: 2234943X (2018).
31. Aguilar, F., Hussain, S. P. & Cerutti, P. Aflatoxin B1 induces the transversion of G – T in codon 249 of the p53 tumor suppressor gene in human hepatocytes. *Proceedings of the National Academy of Sciences of the United States of America* **90**, 8586–8590 (1993).

32. Pfister, N. T. & Prives, C. Transcriptional regulation by wild-type and cancer-related mutant forms of p53. *Cold Spring Harbor Perspectives in Medicine* **7**, 1–26. ISSN: 21571422 (2017).
33. Brunt, E. M. *et al.* Nonalcoholic fatty liver disease. *Nature Reviews Disease Primers* **1**, 15080. ISSN: 2056-676X. <https://doi.org/10.1038/nrdp.2015.80> (2015).
34. Wong, V. W.-s., Ekstedt, M., Wong, G. L.-h. & Hagström, H. Changing epidemiology, global trends and implications for outcomes of NAFLD. *Journal of Hepatology* **In-press**. ISSN: 0168-8278. <https://doi.org/10.1016/j.jhep.2023.04.036> (2023).
35. Liu, Y.-L. *et al.* Carriage of the PNPLA3 rs738409 C >G polymorphism confers an increased risk of non-alcoholic fatty liver disease associated hepatocellular carcinoma. *Journal of Hepatology* **61**, 75–81. ISSN: 0168-8278. <https://doi.org/10.1016/j.jhep.2014.02.030> (July 2014).
36. Rada, P. Understanding lipotoxicity in NAFLD pathogenesis : is CD36 a key driver ? *Cell Death and Disease*. ISSN: 2041-4889. <http://dx.doi.org/10.1038/s41419-020-03003-w> (2020).
37. Masarone, M. *et al.* Review Article Role of Oxidative Stress in Pathophysiology of Nonalcoholic Fatty Liver Disease. *Oxidative Medicine and Cellular Longevity*, 1–14 (2018).
38. Pfister, D. *et al.* NASH limits anti-tumour surveillance in immunotherapy-treated HCC. *Nature* **592**, 450–456. ISSN: 14764687 (2021).
39. Brissot, P. *et al.* Haemochromatosis. *Nature Reviews Disease Primers* **4**. ISSN: 2056676X (2018).
40. Czlonkowska, A. *et al.* Wilson disease. *Nature Reviews Disease Primers*, 1–20 (2018).
41. Llovet, J. M. *et al.* Sorafenib in Advanced Hepatocellular Carcinoma. *New England Journal of Medicine* **359**, 378–390. ISSN: 0028-4793 (2008).
42. Pfeiffenberger, J. *et al.* Hepatobiliary malignancies in Wilson disease. *Liver international*, 1615–1622 (2015).
43. National Institute on Drug Abuse. Substance Use in Women Research Report Substance Use in Women Research Report. *National Institute on Drug Abuse* (2020).

44. Naugler, W. E. *et al.* Gender Disparity in Liver Cancer Due to Sex Differences in MyD88-Dependent IL-6 Production. *Science* **317**, 121–124. <https://doi.org/10.1126/science.1140485> (July 2007).
45. Wang, S. H. *et al.* Estrogen Receptor α Represses Transcription of HBV Genes via Interaction With Hepatocyte Nuclear Factor 4a. *Gastroenterology* **142**, 989–998.e4. ISSN: 0016-5085. <http://dx.doi.org/10.1053/j.gastro.2011.12.045> (2012).
46. Simon, F. R. *et al.* Multihormonal regulation of hepatic sinusoidal Ntcp gene expression. *American Journal of Physiology - Gastrointestinal and Liver Physiology* **287**, 782–794 (2004).
47. Klein, S. L. & Flanagan, K. L. Sex differences in immune responses. *Nature Reviews Immunology* **16**, 626–638. ISSN: 14741741 (2016).
48. Pellicoro, A., Ramachandran, P., Iredale, J. P. & Fallowfield, J. A. Liver fibrosis and repair: Immune regulation of wound healing in a solid organ. *Nature Reviews Immunology* **14**, 181–194. ISSN: 14741733 (2014).
49. Albillos, A., Lario, M. & Álvarez-Mon, M. Cirrhosis-associated immune dysfunction: Distinctive features and clinical relevance. *Journal of Hepatology* **61**, 1385–1396. ISSN: 16000641 (2014).
50. Zhu, M. *et al.* Somatic Mutations Increase Hepatic Clonal Fitness and Regeneration in Chronic Liver Disease. *Cell* **177**, 608–621.e12. ISSN: 10974172. <https://doi.org/10.1016/j.cell.2019.03.026> (2019).
51. Arroyo, V. *et al.* Acute-on-chronic liver failure in cirrhosis. *Nature Reviews Disease Primers*, 3–7 (2016).
52. Simon, T. G. *et al.* Association of Aspirin with Hepatocellular Carcinoma and Liver-Related Mortality. *New England Journal of Medicine* **382**, 1018–1028. ISSN: 0028-4793 (2020).
53. Bravi, F., Bosetti, C., Tavani, A., Gallus, S. & La Vecchia, C. Coffee reduces risk for hepatocellular carcinoma: An updated meta-analysis. *Clinical Gastroenterology and Hepatology* **11**, 1413–1421.e1. ISSN: 15423565 (2013).

54. Cainzos-achirica, M. *et al.* Methodological Issues in Nutritional Epidemiology Research — Sorting Through the Confusion. *Current Cardiovascular Risk Reports* **12**, 1–9 (2018).
55. Adeniji, N. Current and Emerging Tools for Hepatocellular Carcinoma Surveillance. *Hepatology Communications* **5**, 1972–1986 (2021).
56. Singal, A. G. *et al.* Utilization of hepatocellular carcinoma surveillance among American patients: A systematic review. *Journal of General Internal Medicine* **27**, 861–867. ISSN: 08848734 (2012).
57. Haq, M. I. *et al.* Effect of hepatocellular carcinoma surveillance programmes on overall survival in a mixed cirrhotic uk population: A prospective, longitudinal cohort study. *Journal of Clinical Medicine* **10**, 1–13. ISSN: 20770383 (2021).
58. Chernyak, V., Fowler, M. S. K. J., Kamaya, A. & Kielar, A. Z. Liver Imaging Reporting and Data System (LI-RADS) Version 2018: Imaging of Hepatocellular Carcinoma in At-Risk Patients. *Radiology* **289**, 816–830 (2018).
59. Brierley, J. D. *TNM Classification of Malignant Tumours, 8th edition* ISBN: 978-1-119-26356-2 (Wiley-Blackwell, 2016).
60. Reig, M. *et al.* Review BCLC strategy for prognosis prediction and treatment recommendation : The 2022 update q. *Journal of Hepatology* **76**, 681–693. ISSN: 0168-8278. <https://doi.org/10.1016/j.jhep.2021.11.018> (2022).
61. Bruix, J. *et al.* Regorafenib for patients with hepatocellular carcinoma who progressed on sorafenib treatment (RESORCE): a randomised, double-blind, placebo-controlled, phase 3 trial. *The Lancet* **389**, 56–66. ISSN: 0140-6736. [https://doi.org/10.1016/S0140-6736\(16\)32453-9](https://doi.org/10.1016/S0140-6736(16)32453-9) (Jan. 2017).
62. Kudo, M. *et al.* Lenvatinib versus sorafenib in first-line treatment of patients with unresectable hepatocellular carcinoma: a randomised phase 3 non-inferiority trial. *The Lancet* **391**, 1163–1173. ISSN: 1474547X. [http://dx.doi.org/10.1016/S0140-6736\(18\)30207-1](http://dx.doi.org/10.1016/S0140-6736(18)30207-1) (2018).
63. Abou-Alfa, G. K. *et al.* Cabozantinib in Patients with Advanced and Progressing Hepatocellular Carcinoma. *New England Journal of Medicine* **379**, 54–63. ISSN: 0028-4793 (2018).

64. Keenan, B. P., Fong, L. & Kelley, R. K. Immunotherapy in hepatocellular carcinoma: The complex interface between inflammation, fibrosis, and the immune response. *Journal for ImmunoTherapy of Cancer* **7**, 1–13. ISSN: 20511426 (2019).
65. El-Khoueiry, A. B. *et al.* Nivolumab in patients with advanced hepatocellular carcinoma (CheckMate 040): an open-label, non-comparative, phase 1/2 dose escalation and expansion trial. *The Lancet* **389**, 2492–2502. ISSN: 1474547X. [http://dx.doi.org/10.1016/S0140-6736\(17\)31046-2](http://dx.doi.org/10.1016/S0140-6736(17)31046-2) (2017).
66. Zhu, A. X. *et al.* Pembrolizumab in patients with advanced hepatocellular carcinoma previously treated with sorafenib (KEYNOTE-224): a non-randomised, open-label phase 2 trial. *The Lancet Oncology* **19**, 940–952. ISSN: 14745488 (2018).
67. Finn, R. S. *et al.* Pembrolizumab As Second-Line Therapy in Patients With Advanced Hepatocellular Carcinoma in KEYNOTE-240: A Randomized, Double-Blind, Phase III Trial. *Journal of clinical oncology* **38**, 193–202. ISSN: 15277755 (2020).
68. Yau, T. *et al.* Nivolumab versus sorafenib in advanced hepatocellular carcinoma (CheckMate 459): a randomised, multicentre, open-label, phase 3 trial. *The Lancet Oncology* **23**, 77–90. ISSN: 14745488. [http://dx.doi.org/10.1016/S1470-2045\(21\)00604-5](http://dx.doi.org/10.1016/S1470-2045(21)00604-5) (2022).
69. Finn, R. S. *et al.* Atezolizumab plus Bevacizumab in Unresectable Hepatocellular Carcinoma. *New England Journal of Medicine* **382**, 1894–1905. ISSN: 0028-4793 (2020).
70. Abou-Alfa, G. K. *et al.* Tremelimumab plus Durvalumab in Unresectable Hepatocellular Carcinoma. *New England Journal of Medicine* **1**, 1–12. ISSN: 2766-5526 (2022).
71. Brahmer, J. R. *et al.* Management of Immune-Related Adverse Events in Patients Treated With Immune Checkpoint Inhibitor Therapy: American Society of Clinical Oncology Clinical Practice Guideline. *Journal of Clinical Oncology* **36**, 1714–1768. ISSN: 0732-183X. <https://doi.org/10.1200/JCO.2017.77.6385> (Feb. 2018).
72. Marron, T. U. *et al.* Neoadjuvant cemiplimab for resectable hepatocellular carcinoma: a single-arm, open-label, phase 2 trial. *The Lancet Gastroenterology & Hepatology* **7**, 219–229. ISSN: 24681253. [https://doi.org/10.1016/S2468-1253\(21\)00385-X](https://doi.org/10.1016/S2468-1253(21)00385-X) (Mar. 2022).

73. Cercek, A. *et al.* PD-1 Blockade in Mismatch Repair–Deficient, Locally Advanced Rectal Cancer. *New England Journal of Medicine* **386**, 2363–2376. ISSN: 0028-4793 (2022).
74. Zhu, A. X. *et al.* Molecular correlates of clinical response and resistance to atezolizumab in combination with bevacizumab in advanced hepatocellular carcinoma. *Nature Medicine* **28**, 1599–1611. ISSN: 1546170X (2022).
75. Müller, M. *et al.* Human-correlated genetic HCC models identify combination therapy for precision medicine. *Research Square*. <https://www.researchsquare.com/article/rs-1638504/v1> (2022).
76. Nault, J. C. *et al.* High frequency of telomerase reverse-transcriptase promoter somatic mutations in hepatocellular carcinoma and preneoplastic lesions. *Nature Communications* **4**, 1–7. ISSN: 20411723 (2013).
77. Nault, J. C. *et al.* Telomerase reverse transcriptase promoter mutation is an early somatic genetic alteration in the transformation of premalignant nodules in hepatocellular carcinoma on cirrhosis. *Hepatology* **60**, 1983–1992. ISSN: 15273350 (2014).
78. Hoshida, Y. *et al.* Integrative transcriptome analysis reveals common molecular subclasses of human hepatocellular carcinoma. *Cancer Research* **69**, 7385–7392. ISSN: 00085472 (2009).
79. Hanahan, D. & Weinberg, R. A. Review Hallmarks of Cancer : The Next Generation. *Cell* **144**, 646–674. ISSN: 0092-8674. <http://dx.doi.org/10.1016/j.cell.2011.02.013> (2011).
80. Elia, I. & Haigis, M. C. Metabolites and the tumour microenvironment: from cellular mechanisms to systemic metabolism. *Nature Metabolism* **3**, 21–32. ISSN: 25225812. <http://dx.doi.org/10.1038/s42255-020-00317-z> (2021).
81. Hanahan, D. Hallmarks of Cancer: New Dimensions. *Cancer Discovery* **12**, 31–46. ISSN: 21598290 (2022).
82. Patten, D. A., Wilkinson, A. L., O’Keeffe, A. & Shetty, S. Scavenger Receptors: Novel Roles in the Pathogenesis of Liver Inflammation and Cancer. *Seminars in Liver Disease* **42**, 61–76. ISSN: 10988971 (2022).

83. Donnell, J. S. O., Teng, M. W. L. & Smyth, M. J. Cancer immunoediting and resistance to T cell-based immunotherapy. *Nature Reviews Clinical Oncology*. ISSN: 1759-4782. <http://dx.doi.org/10.1038/s41571-018-0142-8>.
84. Cruz-Muñoz, M. E., Valenzuela-Vázquez, L., Sánchez-Herrera, J. & Santa-Olalla Tapia, J. From the “missing self” hypothesis to adaptive NK cells: Insights of NK cell-mediated effector functions in immune surveillance. *Journal of Leukocyte Biology* **105**, 955–971. ISSN: 19383673 (2019).
85. Friman, T. K. *et al.* Cancer risk and mortality after solid organ transplantation: A population-based 30-year cohort study in Finland. *International Journal of Cancer* **150**, 1779–1791. ISSN: 10970215 (2022).
86. Chen, D. S. & Mellman, I. Oncology meets immunology: The cancer-immunity cycle. *Immunity* **39**, 1–10. ISSN: 10747613 (2013).
87. Sia, D. *et al.* Identification of an Immune-specific Class of Hepatocellular Carcinoma, Based on Molecular Features. *Gastroenterology* **153**, 812–826. ISSN: 15280012 (2017).
88. Spranger, S., Bao, R. & Gajewski, T. F. Melanoma-intrinsic β -catenin signalling prevents anti-tumour immunity. *Nature* **523**, 231–235. ISSN: 14764687 (2015).
89. Pardoll, D. M. The blockade of immune checkpoints in cancer immunotherapy. *Nature Reviews Cancer* **12**, 252–264. ISSN: 1474175X. arXiv: NIHMS150003. <http://dx.doi.org/10.1038/nrc3239> (2012).
90. Suntharalingham, G. *et al.* Cytokine Storm in a Phase 1 Trial of the Anti-CD28 Monoclonal Antibody TGN1412. *New England Journal of Medicine* **355**, 1018–1028 (2006).
91. Brown, Z. J., Heinrich, B. & Greten, T. F. Mouse models of hepatocellular carcinoma: an overview and highlights for immunotherapy research. *Nature Reviews Gastroenterology and Hepatology* **15**, 536–554. ISSN: 17595053. <http://dx.doi.org/10.1038/s41575-018-0033-6> (2018).
92. Kress, S. *et al.* p53 mutations are absent from carcinogen-induced mouse liver tumors but occur in cell lines established from these tumors. *Molecular Carcinogenesis* **6**, 148–158. ISSN: 0899-1987. <https://doi.org/10.1002/mc.2940060210> (Jan. 1992).

93. Darlington, G. J., Bernhard, H. P., Miller, R. A. & Ruddle, F. H. Expression of Liver Phenotypes in Cultured Mouse Hepatoma Cells. *JNCI : Journal of the National Cancer Institute* **64**, 809–819. ISSN: 0027-8874 (1980).
94. Yuen, V. W. H. *et al.* Using mouse liver cancer models based on somatic genome editing to predict immune checkpoint inhibitor responses. *Journal of Hepatology* **78**, 376–389. ISSN: 16000641. <https://doi.org/10.1016/j.jhep.2022.10.037> (2023).
95. Coral, H. *et al.* AKT and N-Ras co-activation in the mouse liver promotes rapid carcinogenesis via mTORC1, FOXM1/SKP2, and c-Myc pathways. *Hepatology* **55**, 833–45. ISSN: 1946-6242. arXiv: NIHMS150003 (2012).
96. Zhan, N. *et al.* The effect of selective c-MET inhibitor on hepatocellular carcinoma in the MET-Active, β -Catenin-Mutated mouse model. *Gene Expression* **18**, 135–147. ISSN: 10522166 (2018).
97. Jonkers, J. & Berns, A. Conditional mouse models of sporadic cancer. *Nature Reviews Cancer* **2**, 251–265. ISSN: 1474175X (2002).
98. Orban, P. C., Chui, D. & Marth, J. D. Tissue- and site-specific DNA recombination in transgenic mice. *Proceedings of the National Academy of Sciences of the United States of America* **89**, 6861–6865. ISSN: 00278424 (1992).
99. Morton, J. P. *et al.* Mutant p53 drives metastasis and overcomes growth arrest/senescence in pancreatic cancer. *Proceedings of the National Academy of Sciences of the United States of America* **107**, 246–251. ISSN: 10916490 (2010).
100. Sekiya, S. & Suzuki, A. Intrahepatic cholangiocarcinoma can arise from Notch-mediated conversion of hepatocytes. *The Journal of Clinical Investigation* **122**, 3914–3918 (2012).
101. De Galarreta, M. R. *et al.* β -catenin activation promotes immune escape and resistance to anti-PD-1 therapy in hepatocellular carcinoma. *Cancer Discovery* **9**, 1124–1141. ISSN: 21598290 (2019).
102. Deane, N. G. *et al.* Hepatocellular carcinoma results from chronic cyclin D1 overexpression in transgenic mice. *Cancer Research* **61**, 5389–5395. ISSN: 00085472 (2001).

103. Connor, F. *et al.* Mutational landscape of a chemically-induced mouse model of liver cancer. *Journal of Hepatology* **69**, 840–850. ISSN: 16000641. <https://doi.org/10.1016/j.jhep.2018.06.009> (2018).
104. Harvey, M. *et al.* Spontaneous and carcinogen- induced tumorigenesis in p53-deficient mice. *Nature Genetics* **5**, 225–229 (1993).
105. Tsuchida, T. *et al.* A simple diet- and chemical-induced murine NASH model with rapid progression of steatohepatitis, fibrosis and liver cancer. *Journal of Hepatology* **69**, 385–395. ISSN: 16000641. <https://doi.org/10.1016/j.jhep.2018.03.011> (2018).
106. Tetri, L. H., Basaranoglu, M., Brunt, E. M., Yerian, L. M. & Neuschwander-Tetri, B. A. Severe NAFLD with hepatic necroinflammatory changes in mice fed trans fats and a high-fructose corn syrup equivalent. *American Journal of Physiology - Gastrointestinal and Liver Physiology* **295**. ISSN: 01931857 (2008).
107. Esteban-Fabró, R. *et al.* Cabozantinib Enhances Anti-PD1 Activity and Elicits a Neutrophil-Based Immune Response in Hepatocellular Carcinoma. *Clinical Cancer Research* **28**, 2449–2460. ISSN: 1078-0432. <https://doi.org/10.1158/1078-0432.CCR-21-2517> (June 2022).
108. Muto, S. *et al.* Tumor β -catenin expression is associated with immune evasion in non-small cell lung cancer with high tumor mutation burden. *Oncology Letters* **21**, 1–9. ISSN: 17921082 (2021).
109. Du Sert, N. P. *et al.* Reporting animal research: Explanation and elaboration for the arrive guidelines 2.0. *PLoS Biology* **18**, 1–65. ISSN: 15457885 (2020).
110. Harada, N. *et al.* Intestinal polyposis in mice with a dominant stable mutation of the β -catenin gene. *EMBO Journal* **18**, 5931–5942. ISSN: 02614189 (1999).
111. Marino, S., Vooijs, M., Van Der Gulden, H., Jonkers, J. & Berns, A. Induction of medulloblastomas in p53-null mutant mice by somatic inactivation of Rb in the external granular layer cells of the cerebellum. *Genes and Development* **14**, 994–1004. ISSN: 08909369 (2000).

112. Murphy, D. J. *et al.* Distinct Thresholds Govern Myc's Biological Output In Vivo. *Cancer Cell* **14**, 447–457. ISSN: 15356108. <http://dx.doi.org/10.1016/j.ccr.2008.10.018> (2008).
113. Jardé, T. *et al.* In vivo and in vitro models for the therapeutic targeting of Wnt signaling using a Tet-O Δ N89 β -catenin system. *Oncogene* **32**, 883–893. ISSN: 09509232 (2013).
114. Tasaka, G.-i. *et al.* Article The Temporal Association Cortex Plays a Key Role in Auditory-Driven Maternal Plasticity The Temporal Association Cortex Plays a Key Role in Auditory-Driven Maternal Plasticity. *Neuron* **107**, 566–579.e7. ISSN: 0896-6273. <https://doi.org/10.1016/j.neuron.2020.05.004> (2020).
115. Hochedlinger, K., Yamada, Y., Beard, C. & Jaenisch, R. Ectopic expression of Oct-4 blocks progenitor-cell differentiation and causes dysplasia in epithelial tissues. *Cell* **121**, 465–477. ISSN: 00928674 (2005).
116. Ewels, P. A. & Peltzer, A. The nf-core framework for community-curated bioinformatics pipelines. *Nature Biotechnology* **38**, 271. ISSN: 15461696 (2020).
117. Benjamin, D. *et al.* Calling Somatic SNVs and Indels with Mutect2. *bioRxiv*, 861054. <https://www.biorxiv.org/content/10.1101/861054v1.abstract> (2019).
118. McLaren, W. *et al.* The Ensembl Variant Effect Predictor. *Genome Biology* **17**, 1–14. ISSN: 1474760X. <http://dx.doi.org/10.1186/s13059-016-0974-4> (2016).
119. Plagnol, V. *et al.* A robust model for read count data in exome sequencing experiments and implications for copy number variant calling. *Bioinformatics* **28**, 2747–2754. ISSN: 13674803 (2012).
120. Li, H. & Durbin, R. Fast and accurate short read alignment with Burrows-Wheeler transform. *Bioinformatics* **25**, 1754–1760. ISSN: 13674803 (2009).
121. Zhang, Y. *et al.* Model-based analysis of ChIP-Seq (MACS). *Genome Biology* **9**. ISSN: 14747596 (2008).
122. Li, Z. *et al.* RGT: a toolbox for the integrative analysis of high throughput regulatory genomics data. *BMC Bioinformatics* **24**, 1–12. ISSN: 14712105. <https://doi.org/10.1186/s12859-023-05184-5> (2023).

123. La Manno, G. *et al.* RNA velocity of single cells. *Nature* **560**, 494–498. ISSN: 14764687. <http://dx.doi.org/10.1038/s41586-018-0414-6> (2018).
124. Qiu, X. *et al.* Reversed graph embedding resolves complex single-cell trajectories. *Nature Methods* **14**, 979–982. ISSN: 15487105 (2017).
125. Broutier, L. *et al.* Human primary liver cancer-derived organoid cultures for disease modeling and drug screening. *Nature Medicine* **23**, 1424–1435. ISSN: 1546170X (2017).
126. Zincarelli, C., Soltys, S., Rengo, G. & Rabinowitz, J. E. Analysis of AAV serotypes 1-9 mediated gene expression and tropism in mice after systemic injection. *Molecular Therapy* **16**, 1073–1080. ISSN: 15250024. <http://dx.doi.org/10.1038/mt.2008.76> (2008).
127. Kiourtis, C. *et al.* Specificity and off-target effects of AAV8-TBG viral vectors for the manipulation of hepatocellular gene expression in mice. *Biology Open* **10**, 1–11. ISSN: 20466390 (2021).
128. Jackstadt, R., Hodder, M. C. & Sansom, O. J. WNT and β -Catenin in Cancer: Genes and Therapy. *Annual Review of Cancer Biology* **4**, 177–196. ISSN: 24723428 (2020).
129. Mosimann, C., Hausmann, G. & Basler, K. β -Catenin hits chromatin: Regulation of Wnt target gene activation. *Nature Reviews Molecular Cell Biology* **10**, 276–286. ISSN: 14710072 (2009).
130. Lourenco, C. *et al.* MYC protein interactors in gene transcription and cancer. *Nature Reviews Cancer* **21**, 579–591. ISSN: 14741768. <http://dx.doi.org/10.1038/s41568-021-00367-9> (2021).
131. Muthalagu, N. *et al.* Repression of the type I interferon pathway underlies MYC- and KRAS-dependent evasion of NK and B cells in pancreatic ductal adenocarcinoma. *Cancer Discovery* **10**, 872–887. ISSN: 21598290 (2020).
132. Campbell, P. J. *et al.* Pan-cancer analysis of whole genomes. *Nature* **578**, 82–93. ISSN: 14764687 (2020).
133. Vousden, K. H. & Lu, X. Live or let die: The cell's response to p53. *Nature Reviews Cancer* **2**, 594–604. ISSN: 1474175X (2002).
134. Horikawa, I. *et al.* Differential cis-regulation of human versus mouse TERT gene expression in vivo: Identification of a human-specific repressive element. *Proceedings of*

- the National Academy of Sciences of the United States of America* **102**, 18437–18442. ISSN: 00278424 (2005).
135. Olive, K. P. *et al.* Mutant p53 gain of function in two mouse models of Li-Fraumeni syndrome. *Cell* **119**, 847–860. ISSN: 00928674 (2004).
136. Du, Y. *et al.* In Vivo Mouse Models for Hepatitis B Virus Infection and Their Application. *Frontiers in Immunology* **12**, 1–12. ISSN: 16643224 (2021).
137. Peng, W. *et al.* Loss of PTEN promotes resistance to T cell-mediated immunotherapy. *Cancer Discovery* **6**, 202–216. ISSN: 21598290 (2016).
138. Cretella, D., Digiacomio, G., Giovannetti, E. & Cavazzoni, A. PTEN Alterations as a Potential Mechanism for Tumor Cell Escape from PD-1/PD-L1 Inhibition. *Cancers* **11**, 1–17 (2019).
139. Zhou, Y. *et al.* CDKN2A promoter methylation and hepatocellular carcinoma risk: A meta-analysis. *Clinics and Research in Hepatology and Gastroenterology* **42**, 529–541. ISSN: 2210741X. <http://dx.doi.org/10.1016/j.clinre.2017.07.003> (2018).
140. Adib, E. *et al.* CDKN2A alterations and response to immunotherapy in solid tumors. *Clinical Cancer Research* **27**, 4025–4035. ISSN: 15573265 (2021).
141. Serrano, M. *et al.* Role of the INK4a locus in tumor suppression and cell mortality. *Cell* **85**, 27–37. ISSN: 00928674 (1996).
142. The Jackson Laboratory. *Physiological Data Summary – Aged C57BL/6J (000664)* tech. rep. (The Jackson Laboratory, 2023). <https://www.jax.org/-/media/jaxweb/files/jax-mice-and-services/phenotypic-data/aged-b6-physiological-data-summary.pdf>.
143. Jost-Brinkmann, F. *et al.* Atezolizumab plus bevacizumab in unresectable hepatocellular carcinoma: Results from a German real-world cohort. *Alimentary Pharmacology & Therapeutics*, 1313–1325. ISSN: 0269-2813 (2023).
144. Lacoste, B., Raymond, V. A., Cassim, S., Lapierre, P. & Bilodeau, M. Highly tumorigenic hepatocellular carcinoma cell line with cancer stem cell-like properties. *PLoS ONE* **12**, 1–19. ISSN: 19326203 (2017).

145. Baklaushev, V. P. *et al.* Luciferase expression allows bioluminescence imaging but imposes limitations on the orthotopic mouse (4T1) model of breast cancer. *Scientific Reports* **7**, 1–17. ISSN: 20452322 (2017).
146. Capone, I., Marchetti, P., Ascierto, P. A., Malorni, W. & Gabriele, L. Sexual Dimorphism Of Immune Responses: A new perspective in cancer immunotherapy. *Frontiers in Immunology* **9**, 1–8. ISSN: 16643224 (2018).
147. Gal-Oz, S. T. *et al.* ImmGen report: sexual dimorphism in the immune system transcriptome. *Nature Communications* **10**. ISSN: 20411723. <http://dx.doi.org/10.1038/s41467-019-12348-6> (2019).
148. Kitajima, S. *et al.* MPS1 inhibition primes immunogenicity of KRAS-LKB1 mutant lung cancer. *Cancer Cell* **40**, 1128–1144.e8. ISSN: 1535-6108. <https://doi.org/10.1016/j.ccell.2022.08.015> (Oct. 2022).
149. Wang, Y. *et al.* Anti-PD-1/L1 lead-in before MAPK inhibitor combination maximizes antitumor immunity and efficacy. *Cancer Cell* **39**, 1375–1387.e6. ISSN: 18783686. <https://doi.org/10.1016/j.ccell.2021.07.023> (2021).
150. Park, B. V. *et al.* TGF β 1-mediated SMAD3 enhances PD-1 expression on antigen-specific T cells in cancer. *Cancer Discovery* **6**, 1366–1381. ISSN: 21598290 (2016).
151. Isoyama, S. *et al.* Cancer immunotherapy with PI3K and PD-1 dual-blockade via optimal modulation of T cell activation signal. *Journal for ImmunoTherapy of Cancer* **9**, 1–15. ISSN: 20511426 (2021).
152. Gurjao, C., Tsukrov, D., Imakaev, M., Luquette, L. J. & Mirny, L. A. Is tumor mutational burden predictive of response to immunotherapy? *eLife* **12**. ISSN: 2050084X (June 2023).
153. Tate, J. G. *et al.* COSMIC: The Catalogue Of Somatic Mutations In Cancer. *Nucleic Acids Research* **47**, D941–D947. ISSN: 13624962 (2019).
154. Zehir, A. *et al.* Mutational landscape of metastatic cancer revealed from prospective clinical sequencing of 10,000 patients. *Nature Medicine* **23**, 703–713. ISSN: 1546170X (2017).
155. Wu, L. *et al.* Landscape of somatic alterations in large-scale solid tumors from an Asian population. *Nature Communications* **13**, 1–11. ISSN: 20411723 (2022).

156. Yoshida, R. *et al.* Molecular cloning of a novel human CC chemokine EBI1-ligand chemokine that is a specific functional ligand for EBI1, CCR7. *Journal of Biological Chemistry* **272**, 13803–13809. ISSN: 00219258. <http://dx.doi.org/10.1074/jbc.272.21.13803> (1997).
157. Yoshida, R. *et al.* Secondary lymphoid-tissue chemokine is a functional ligand for the CC chemokine receptor CCR7. *Journal of Biological Chemistry* **273**, 7118–7122. ISSN: 00219258. <http://dx.doi.org/10.1074/jbc.273.12.7118> (1998).
158. Shields, J. D., Kourtis, I. C., Tomei, A. A., Roberts, J. M. & Swartz, M. A. Induction of Lymphoidlike Stroma and Immune Escape by Tumors That Express the Chemokine CCL21. *Science* **328**, 749–752. <https://www.science.org> (2010).
159. Marchi, S., Guilbaud, E., Tait, S. W., Yamazaki, T. & Galluzzi, L. Mitochondrial control of inflammation. *Nature Reviews Immunology* **23**, 159–173. ISSN: 14741741 (2023).
160. Kim, J., Kim, H. S. & Chung, J. H. Molecular mechanisms of mitochondrial DNA release and activation of the cGAS-STING pathway. *Experimental and Molecular Medicine*. ISSN: 20926413 (2023).
161. Seth, R. B., Sun, L., Ea, C. K. & Chen, Z. J. Identification and characterization of MAVS, a mitochondrial antiviral signaling protein that activates NF- κ B and IRF3. *Cell* **122**, 669–682. ISSN: 00928674 (2005).
162. Simpson, E., Scott, D. & Chandler, P. THE MALE-SPECIFIC HISTOCOMPATIBILITY ANTIGEN, H-Y:A History of Transplantation, Immune Response Genes, Sex Determination and Expression Cloning. *Annual Review of Immunology* **15**, 39–61. ISSN: 0732-0582. <https://doi.org/10.1146/annurev.immunol.15.1.39> (Apr. 1997).
163. Collison, A. M. *et al.* TRAIL signals through the ubiquitin ligase MID1 to promote pulmonary fibrosis. *BMC Pulmonary Medicine* **19**, 1–11. ISSN: 14712466 (2019).
164. Gu, L., Fullam, A., McCormack, N., Höhn, Y. & Schröder, M. DDX3 directly regulates TRAF3 ubiquitination and acts as a scaffold to co-ordinate assembly of signalling complexes downstream from MAVS. *Biochemical Journal* **474**, 571–587. ISSN: 0264-6021. <https://doi.org/10.1042/BCJ20160956> (Feb. 2017).

165. Oshiumi, H., Sakai, K., Matsumoto, M. & Seya, T. DEAD/H BOX 3 (DDX3) helicase binds the RIG-I adaptor IPS-1 to up-regulate IFN- β -inducing potential. *European Journal of Immunology* **40**, 940–948. ISSN: 00142980 (2010).
166. Mermel, C. H. *et al.* GISTIC2.0 facilitates sensitive and confident localization of the targets of focal somatic copy-number alteration in human cancers. *Genome Biology* **12**, 1–14. ISSN: 14747596 (2011).
167. Agostino, M., Pohl, S. Ö. G. & Dharmarajan, A. Structure-based prediction of Wnt binding affinities for frizzled-type cysteine-rich domains. *Journal of Biological Chemistry* **292**, 11218–11229. ISSN: 1083351X (2017).
168. Fan, T. W. *et al.* De novo synthesis of serine and glycine fuels purine nucleotide biosynthesis in human lung cancer tissues. *Journal of Biological Chemistry* **294**, 13464–13477. ISSN: 1083351X. <http://dx.doi.org/10.1074/jbc.RA119.008743> (2019).
169. Yin, K. *et al.* Senescence-induced endothelial phenotypes underpin immune-mediated senescence surveillance. *Genes and Development* **36**, 533–549. ISSN: 15495477 (2022).
170. Kukurba, K. R. & Montgomery, S. B. RNA sequencing and analysis. *Cold Spring Harbor Protocols* **2015**, 951–969. ISSN: 15596095 (2015).
171. Crawford, A., Angelosanto, J. M., Nadwodny, K. L., Blackburn, S. D. & Wherry, E. J. A role for the chemokine RANTES in regulating CD8 T cell responses during chronic viral infection. *PLoS Pathogens* **7**. ISSN: 15537366 (2011).
172. Ku, H. C. & Cheng, C. F. Master Regulator Activating Transcription Factor 3 (ATF3) in Metabolic Homeostasis and Cancer. *Frontiers in Endocrinology* **11**, 1–16. ISSN: 16642392 (2020).
173. Ortabozkoyun, H. *et al.* CRISPR and biochemical screens identify MAZ as a cofactor in CTCF-mediated insulation at Hox clusters. **54**, 202–212. ISSN: 15461718 (2022).
174. Trimarchi, J. M., Fairchild, B., Wen, J. & Lees, J. A. The E2F6 transcription factor is a component of the mammalian Bmi1-containing polycomb complex. *Proceedings of the National Academy of Sciences of the United States of America* **98**, 1519–1524. ISSN: 00278424 (2001).

175. Cao, L. *et al.* Genotoxic stress-triggered β -catenin/JDP2/PRMT5 complex facilitates reestablishing glutathione homeostasis. *Nature Communications* **10**, 1–17. ISSN: 20411723. <http://dx.doi.org/10.1038/s41467-019-11696-7> (2019).
176. Toualbi, K. *et al.* Physical and functional cooperation between AP-1 and β -catenin for the regulation of TCF-dependent genes. *Oncogene* **26**, 3492–3502. ISSN: 09509232 (2007).
177. Stevenson, N. J. *et al.* CCL11 blocks IL-4 and GM-CSF signaling in hematopoietic cells and hinders dendritic cell differentiation via suppressor of cytokine signaling expression. *Journal of Leukocyte Biology* **85**, 289–297. ISSN: 0741-5400. <https://doi.org/10.1189/jlb.0708394> (Feb. 2009).
178. Sadik, C. D., Kim, N. D. & Luster, A. D. Neutrophils cascading their way to inflammation. *Trends in Immunology* **32**, 452–460. ISSN: 1471-4906. <https://doi.org/10.1016/j.it.2011.06.008> (Oct. 2011).
179. Decout, A., Katz, J. D., Venkatraman, S. & Ablasser, A. The cGAS–STING pathway as a therapeutic target in inflammatory diseases. *Nature Reviews Immunology* **21**, 548–569. ISSN: 14741741. <http://dx.doi.org/10.1038/s41577-021-00524-z> (2021).
180. Samson, N. & Ablasser, A. The cGAS–STING pathway and cancer. *Nature Cancer* **3**, 1452–1463. ISSN: 26621347 (2022).
181. Dufour, J. H. *et al.* IFN- γ -Inducible Protein 10 (IP-10; CXCL10)-Deficient Mice Reveal a Role for IP-10 in Effector T Cell Generation and Trafficking. *The Journal of Immunology* **168**, 3195–3204. ISSN: 0022-1767 (2002).
182. Burke, S. J. *et al.* Synergistic Expression of the CXCL10 Gene in Response to IL-1 β and IFN- γ Involves NF- κ B, Phosphorylation of STAT1 at Tyr701, and Acetylation of Histones H3 and H4. *The Journal of Immunology* **191**, 323–336. ISSN: 0022-1767 (2013).
183. Dou, Z. *et al.* Cytoplasmic chromatin triggers inflammation in senescence and cancer. *Nature* **550**, 402–406. ISSN: 14764687. <http://dx.doi.org/10.1038/nature24050> (2017).
184. Dixon, C. R. *et al.* STING nuclear partners contribute to innate immune signaling responses. *iScience* **24**, 103055. ISSN: 25890042. <https://doi.org/10.1016/j.isci.2021.103055> (2021).

185. Flynn, P. J., Koch, P. D. & Mitchison, T. J. Chromatin bridges, not micronuclei, activate cGAS after drug-induced mitotic errors in human cells. *Proceedings of the National Academy of Sciences of the United States of America* **118**, 1–8 (2021).
186. Dauch, D. *et al.* A MYC-aurora kinase A protein complex represents an actionable drug target in p53-altered liver cancer. *Nature Medicine* **22**, 744–753. ISSN: 1546170X (2016).
187. Chan, C. Y.-K. *et al.* CFI-402257, a TTK inhibitor, effectively suppresses hepatocellular carcinoma. *Proceedings of the National Academy of Sciences of the United States of America* **119**, e2119514119. ISSN: 1091-6490 (Electronic) (Aug. 2022).
188. Haber, P. K. *et al.* Molecular Markers of Response to Anti-PD1 Therapy in Advanced Hepatocellular Carcinoma. *Gastroenterology* **164**, 72–88.e18. ISSN: 15280012. <http://dx.doi.org/10.1053/j.gastro.2022.09.005> (2023).
189. Hu, B. *et al.* IFN α Potentiates Anti-PD-1 Efficacy by Remodeling Glucose Metabolism in the Hepatocellular Carcinoma Microenvironment. *Cancer Discovery* **12**, 1718–1741. ISSN: 21598290 (2022).
190. Le Naour, J., Zitvogel, L., Galluzzi, L., Vacchelli, E. & Kroemer, G. Trial watch: STING agonists in cancer therapy. *OncoImmunology* **9**. ISSN: 2162402X. <https://doi.org/10.1080/2162402X.2020.1777624> (2020).
191. Yesbolatova, A. *et al.* The auxin-inducible degron 2 technology provides sharp degradation control in yeast, mammalian cells, and mice. *Nature Communications* **11**. ISSN: 20411723. <http://dx.doi.org/10.1038/s41467-020-19532-z> (2020).
192. Sun, X. *et al.* A chemical approach for global protein knockdown from mice to non-human primates. *Cell Discovery* **5**, 1–13. ISSN: 20565968. <http://dx.doi.org/10.1038/s41421-018-0079-1> (2019).
193. Macdonald, L. *et al.* Rapid and specific degradation of endogenous proteins in mouse models using auxin-inducible degrons. *eLife* **11**, 1–25. ISSN: 2050084X (2022).
194. Clevers, H. Wnt/ β -Catenin Signaling in Development and Disease. *Cell* **127**, 469–480. ISSN: 00928674 (2006).
195. Bernard, O., Cory, S., Gerondakis, S., Webb, E. & Adams, J. M. Sequence of the murine and human cellular myc oncogenes and two modes of myc transcription resulting from

- chromosome translocation in B lymphoid tumours. *The EMBO journal* **2**, 2375–2383. ISSN: 02614189 (1983).
196. Imbert, A., Eelkema, R., Jordan, S., Feiner, H. & Cowin, P. N89 B-Catenin Induces Precocious Development, Differentiation, and Neoplasia in Mammary Gland. *The Journal of Cell Biology* **153**, 555–568 (2001).
197. Teissedre, B. *et al.* MMTV-Wnt1 and Δ N89 β -catenin induce canonical signaling in distinct progenitors and differentially activate hedgehog signaling within mammary tumors. *PLoS ONE* **4**. ISSN: 19326203 (2009).
198. Redelsperger, I. M. *et al.* Stability of doxycycline in feed and water and minimal effective doses in tetracycline-inducible systems. *Journal of the American Association for Laboratory Animal Science* **55**, 467–474. ISSN: 15596109 (2016).
199. Xing, Y. & Hogquist, K. A. T-Cell Tolerance : Central and Peripheral. *Cold Spring Harbor perspectives in biology* **4**, 1–16 (2012).
200. Damo, M. *et al.* Inducible de novo expression of neoantigens in tumor cells and mice. *Nature Biotechnology* **39**, 64–73. ISSN: 15461696. <http://dx.doi.org/10.1038/s41587-020-0613-1> (2021).
201. Shen, L. & Rock, K. L. Cellular protein is the source of cross-priming antigen in vivo. *Proceedings of the National Academy of Sciences of the United States of America* **101**, 3035–3040. ISSN: 00278424 (2004).
202. Rostamabadi, H. *et al.* Ovalbumin, an outstanding food hydrocolloid: Applications, technofunctional attributes, and nutritional facts, A systematic review. *Food Hydrocolloids* **139**, 108514. ISSN: 0268005X (2023).
203. Rasmussen, I. B., Lunde, E., Michaelsen, T. E., Bogen, B. & Sandlie, I. The principle of delivery of T cell epitopes to antigen-presenting cells applied to peptides from influenza virus, ovalbumin, and hen egg lysozyme: Implications for peptide vaccination. *Proceedings of the National Academy of Sciences of the United States of America* **98**, 10296–10301. ISSN: 00278424 (2001).
204. Hogquist, K. A. *et al.* T cell receptor antagonist peptides induce positive selection. *Cell* **76**, 17–27. ISSN: 00928674 (1994).

205. Barnden, M. J., Allison, J., Heath, W. R. & Carbone, F. R. Defective TCR expression in transgenic mice constructed using cDNA- based α - and β -chain genes under the control of heterologous regulatory elements. *Immunology and Cell Biology* **76**, 34–40. ISSN: 08189641 (1998).
206. Wüst, R. C., Houtkooper, R. H. & Auwerx, J. Confounding factors from inducible systems for spatiotemporal gene expression regulation. *Journal of Cell Biology* **219**, 2–5. ISSN: 15408140 (2020).
207. Mullick, A. *et al.* The cumate gene-switch: A system for regulated expression in mammalian cells. *BMC Biotechnology* **6**, 1–18. ISSN: 14726750 (2006).
208. Sato, S. *et al.* Generation of mouse iPS cells using an inducible expression of transgenes via the cumate gene-switch. *Analytical Biochemistry* **599**, 113748. ISSN: 10960309. <https://doi.org/10.1016/j.ab.2020.113748> (2020).
209. Fitzgerald, B. *et al.* A mouse model for the study of anti-tumor T cell responses in Kras-driven lung adenocarcinoma. *Cell Reports Methods* **1**, 100080. ISSN: 26672375. <https://doi.org/10.1016/j.crmeth.2021.100080> (2021).
210. Knust, B. *et al.* Lymphocytic choriomeningitis virus in employees and mice at multipremises feeder-rodent operation, United States, 2012. *Emerging Infectious Diseases* **20**, 240–247. ISSN: 10806040 (2014).
211. Gan, X. Q. *et al.* Nuclear Dvl, c-Jun, β -catenin, and TCF form a complex leading to stabilization of β -catenin-TCF interaction. *Journal of Cell Biology* **180**, 1087–1100. ISSN: 00219525 (2008).
212. Mittelstadt, M. L. & Patel, R. C. AP-1 mediated transcriptional repression of matrix metalloproteinase-9 by recruitment of histone deacetylase 1 in response to interferon β . *PLoS ONE* **7**, 1–11. ISSN: 19326203 (2012).
213. Zhao, J., Li, X., Guo, M., Yu, J. & Yan, C. The common stress responsive transcription factor ATF3 binds genomic sites enriched with p300 and H3K27ac for transcriptional regulation. *BMC Genomics* **17**, 1–14. ISSN: 14712164. <http://dx.doi.org/10.1186/s12864-016-2664-8> (2016).

214. Kwon, J. W. *et al.* Activating transcription factor 3 represses inflammatory responses by binding to the p65 subunit of NF- κ B. *Scientific Reports* **5**, 1–9. ISSN: 20452322 (2015).
215. Wesolowski, R. *et al.* TWT-203: Phase 1b/2 dose-confirming study of CFI-402257 as a single agent in advanced solid tumors and in combination with fulvestrant in patients with ER+/HER2- advanced breast cancer after disease progression on prior CDK4/6 and endocrine therapy. *Journal of Clinical Oncology* **40**, TPS1123–TPS1123. ISSN: 0732-183X. https://doi.org/10.1200/JCO.2022.40.16%7B%5C_%7Dsuppl.TPS1123 (June 2022).
216. Reig, M. *et al.* NMS-01940153E, an MPS1 inhibitor with anti-tumor activity in relapsed or refractory unresectable Hepatocellular carcinoma. *European Journal of Cancer* **174**, S2. ISSN: 18790852. [https://doi.org/10.1016/S0959-8049\(22\)00813-9](https://doi.org/10.1016/S0959-8049(22)00813-9) (2022).
217. Atrafi, F. *et al.* A Phase i Study of an MPS1 Inhibitor (BAY 1217389) in Combination with Paclitaxel Using a Novel Randomized Continual Reassessment Method for Dose Escalation. *Clinical Cancer Research* **27**, 6366–6375. ISSN: 15573265 (2021).
218. Waaler, J. *et al.* Tankyrase inhibition sensitizes melanoma to PD-1 immune checkpoint blockade in syngeneic mouse models. *Communications Biology* **3**, 1–13. ISSN: 23993642. <http://dx.doi.org/10.1038/s42003-020-0916-2> (2020).
219. Swedish Rectal Cancer Trial. Improved Survival With Preoperative Radiotherapy in Resectable Rectal Cancer. *New England Journal of Medicine* **336**, 980–987. ISSN: 00973521 (1997).
220. Morton, D. *et al.* Preoperative Chemotherapy for Operable Colon Cancer: Mature Results of an International Randomized Controlled Trial. *Journal of clinical oncology* **41**, 1541–1552. ISSN: 15277755 (2023).
221. Margetts, J. *et al.* Neutrophils: Driving progression and poor prognosis in hepatocellular carcinoma? *British Journal of Cancer* **118**, 248–257. ISSN: 15321827. <http://dx.doi.org/10.1038/bjc.2017.386> (2018).
222. Thomas, C. E. *et al.* Neutrophil-lymphocyte ratio in relation to risk of hepatocellular carcinoma in patients with non-alcoholic fatty liver disease. *Cancer Medicine* **12**, 3589–3600. ISSN: 20457634 (2023).

223. H., Y. *et al.* Neutrophil-lymphocyte ratio (NLR) could be better predictor than C-reactive protein (CRP) for liver fibrosis in non-alcoholic steatohepatitis(NASH). *Annals of clinical and laboratory science* **45**, 278–286. ISSN: 0091-7370. <http://ovidsp.ovid.com/ovidweb.cgi?T=JS%7B%5C%7DPAGE=reference%7B%5C%7DD=med8%7B%5C%7DNEWS=N%7B%5C%7DAN=26116591%7B%5C%7D0Ahttp://www.annclinlabsci.org/content/45/3/278.full.pdf%7B%5C%7D0Ahttp://ovidsp.ovid.com/ovidweb.cgi?T=JS%7B%5C%7DPAGE=reference%7B%5C%7DD=emed17%7B%5C%7DNEWS=N%7B%5C%7DAN=605068416> (2015).
224. Hwang, S., Yun, H., Moon, S., Cho, Y. E. & Gao, B. Role of Neutrophils in the Pathogenesis of Nonalcoholic Steatohepatitis. *Frontiers in Endocrinology* **12**, 1–16. ISSN: 16642392 (2021).
225. Papayannopoulos, V. Neutrophil extracellular traps in immunity and disease. *Nature Reviews Immunology* **18**, 134–147. ISSN: 14741741 (2018).
226. Fridlender, Z. G. *et al.* Polarization of Tumor-Associated Neutrophil Phenotype by TGF- β : "N1" versus "N2" TAN. *Cancer Cell* **16**, 183–194. ISSN: 15356108. <http://dx.doi.org/10.1016/j.ccr.2009.06.017> (2009).
227. Geh, D. *et al.* Neutrophils as potential therapeutic targets in hepatocellular carcinoma. *Nature Reviews Gastroenterology and Hepatology* **19**, 257–273. ISSN: 17595053 (2022).
228. Metzemaekers, M., Gouwy, M. & Proost, P. Neutrophil chemoattractant receptors in health and disease: double-edged swords. *Cellular and Molecular Immunology* **17**, 433–450. ISSN: 20420226. <http://dx.doi.org/10.1038/s41423-020-0412-0> (2020).
229. Zhou, S. L. *et al.* CXCR2/CXCL5 axis contributes to epithelial-mesenchymal transition of HCC cells through activating PI3K/Akt/GSK-3 β /Snail signaling. *Cancer Letters* **358**, 124–135. ISSN: 18727980. <http://dx.doi.org/10.1016/j.canlet.2014.11.044> (2015).
230. Leslie, J. *et al.* CXCR2 inhibition enables NASH-HCC immunotherapy. *Gut* **71**, 2093–2106. ISSN: 14683288 (2022).
231. Aran, D. *et al.* Reference-based analysis of lung single-cell sequencing reveals a transitional profibrotic macrophage. *Nature Immunology* **20**, 163–172. ISSN: 15292916. <http://dx.doi.org/10.1038/s41590-018-0276-y> (2019).

232. Heng, T. S. P., Painter, M. W., Immunological, T. & Project, G. The Immunological Genome Project: networks of gene expression in immune cells. *Nature Immunology* **9**, 1091–1094 (2008).
233. Grieshaber-Bouyer, R. *et al.* The neutrotine transcriptional signature defines a single continuum of neutrophils across biological compartments. *Nature Communications* **12**, 1–21. ISSN: 20411723 (2021).
234. Dennis, K. L. *et al.* T-cell expression of IL10 is essential for tumor immune surveillance in the small intestine. *Cancer Immunology Research* **3**, 806–814. ISSN: 23266074 (2015).
235. Groux, H., Bigler, M., de Vries, J. E. & Roncarolo, M.-G. Inhibitory and Stimulatory Effects of IL-10 on Human CD8+ T Cells. *The Journal of Immunology* **160**, 3188–3193. ISSN: 0022-1767 (1998).
236. Zander, R. *et al.* CD4+ T Cell Help Is Required for the Formation of a Cytolytic CD8+ T Cell Subset that Protects against Chronic Infection and Cancer. *Immunity* **51**, 1028–1042.e4. ISSN: 10974180. <https://doi.org/10.1016/j.immuni.2019.10.009> (2019).
237. Evans, T. R. *Clinical trial of whether AZD5069 combined with immunotherapy (durvalumab) is effective for patients with advanced primary liver cancer* 2022. <https://www.isrctn.com/ISRCTN12669009>.
238. Koide, S. L., Inaba, K. & Steinman, R. M. INTERLEUKIN I ENHANCES T-DEPENDENT IMMUNE RESPONSES BY AMPLIFYING THE FUNCTION OF Evidence that soluble factors are important in T cell mitogenesis began with experiments in which leukocyte-conditioned media enhanced growth in the presence of lectin (1. *Journal of Experimental Medicine* **165**, 515–530 (1987).
239. Van Rooijen, N. & Sanders, A. Kupffer cell depletion by liposome-delivered drugs: comparative activity of intracellular clodronate, propamidine, and ethylenediaminetetraacetic acid. *Hepatology (Baltimore, Md.)* **23**, 1239–1243. ISSN: 0270-9139 (Print) (May 1996).
240. Huang, D. Q., El-Serag, H. B. & Loomba, R. Global epidemiology of NAFLD-related HCC: trends, predictions, risk factors and prevention. *Nature Reviews Gastroenterology*

- and Hepatology* **18**, 223–238. ISSN: 17595053. <http://dx.doi.org/10.1038/s41575-020-00381-6> (2021).
241. O’Byrne, P. M. *et al.* Efficacy and safety of a CXCR2 antagonist, AZD5069, in patients with uncontrolled persistent asthma: a randomised, double-blind, placebo-controlled trial. *The Lancet Respiratory Medicine* **4**, 797–806. ISSN: 22132619. [http://dx.doi.org/10.1016/S2213-2600\(16\)30227-2](http://dx.doi.org/10.1016/S2213-2600(16)30227-2) (2016).

Appendix A

Resistance to immune checkpoint
inhibitors in non-alcoholic
steatohepatitis induced hepatocellular
carcinoma

A.1 Introduction

Non-alcoholic steatohepatitis and non-alcoholic fatty liver disease are risk factors for the development of HCC. Inflammation and T-cell mediated cytotoxic immune responses play key roles in both the pathogenesis of HCC and in mediating anti-tumour immune responses. There is increasing evidence that the presence of NASH/NAFLD promotes the development of an exhausted T-cell phenotype, thus leading to immunotherapy resistance[38].

Persistent inflammation is a key hallmark of NASH. Neutrophils are the first cells involved in responding to tissue injury and play a dual role, either by driving further inflammation or promoting resolution[33]. In patients with NASH/NAFLD, neutrophils have been implicated in more severe hepatocyte injury, which is reflected in peripheral blood counts, with higher high neutrophil to lymphocyte ratios in those with the most severe NASH/NAFLD and in those who develop HCC[221–223]. Similarly, in animal models of NASH/NAFLD, antibody depletion of neutrophils has been shown to reduce liver injury, steatosis, fibrosis and hepatic stellate cell activation[224].

In other cancer types, tumour associated neutrophils have been shown to suppress T-cell mediated anti-tumour immune responses through a diverse range of mechanisms including through cytokine receptor signalling (IL-10, CCL17, ARG1, TGF β), neutrophil extracellular traps, and recruitment of immunosuppressive cell populations[225, 226]. Given this close association with poor clinical outcomes following immune checkpoint inhibitors and their relative abundance in NASH/NAFLD, targeting neutrophils in the NASH-HCC microenvironment may be a useful strategy to improve immunotherapy responses in this patient group[227].

One of the key regulators of neutrophil trafficking and maturation is CXC motif chemokine receptor 2 (CXCR2), a G-protein coupled receptor (GPCR)[228]. As neutrophils mature within the bone marrow, they gain expression of CXCR2, which allows maturing neutrophils to migrate out of the bone marrow and into the systemic circulation in response

to CXCL2. In addition to CXCL2, CXCR2 also can be bound by CXCL1, CXCL3, CXCL5, CXCL6, CXCL7 and CXCL8[228]. Engagement of these chemokines with CXCR2, activates several signalling pathways including PI3K/AKT and p38 MAPK, which both play major roles in neutrophil migration and survival[229]. Expression of CXCR2 has also been shown to be critical for both chemotaxis and transepithelial migration of neutrophils through tissues[227, 228]. Given the association between neutrophils and NASH/NAFLD HCC, CXCR2 may be a good therapeutic target to manipulate neutrophil infiltration and reprogramme neutrophil-associated immunosuppressive signalling within the tumour microenvironment.

The central objective of this chapter is to build upon previous work by our group in collaboration with Newcastle University investigating the role of neutrophils within NASH/NAFLD-HCC. This programme of work, which I contributed to, took place during my PhD fellowship. A key output of this programme was a paper which we published in the journal Gut. In this article, we demonstrated that CXCR2smi combination therapy sensitised models of NASH/NAFLD-HCC to anti-PD1 therapy[230]. Although we had previously shown effect of the treatment, it was unclear which transcriptional programmes were underlying this and if neutrophils were likely to be the primary explanation for this effect. Some of our data from this piece of work suggested mature neutrophils may exert an immunosuppressive effect, but how this was mediated was not clear. Therefore, using single-cell RNA sequencing, I set out to explore this question.

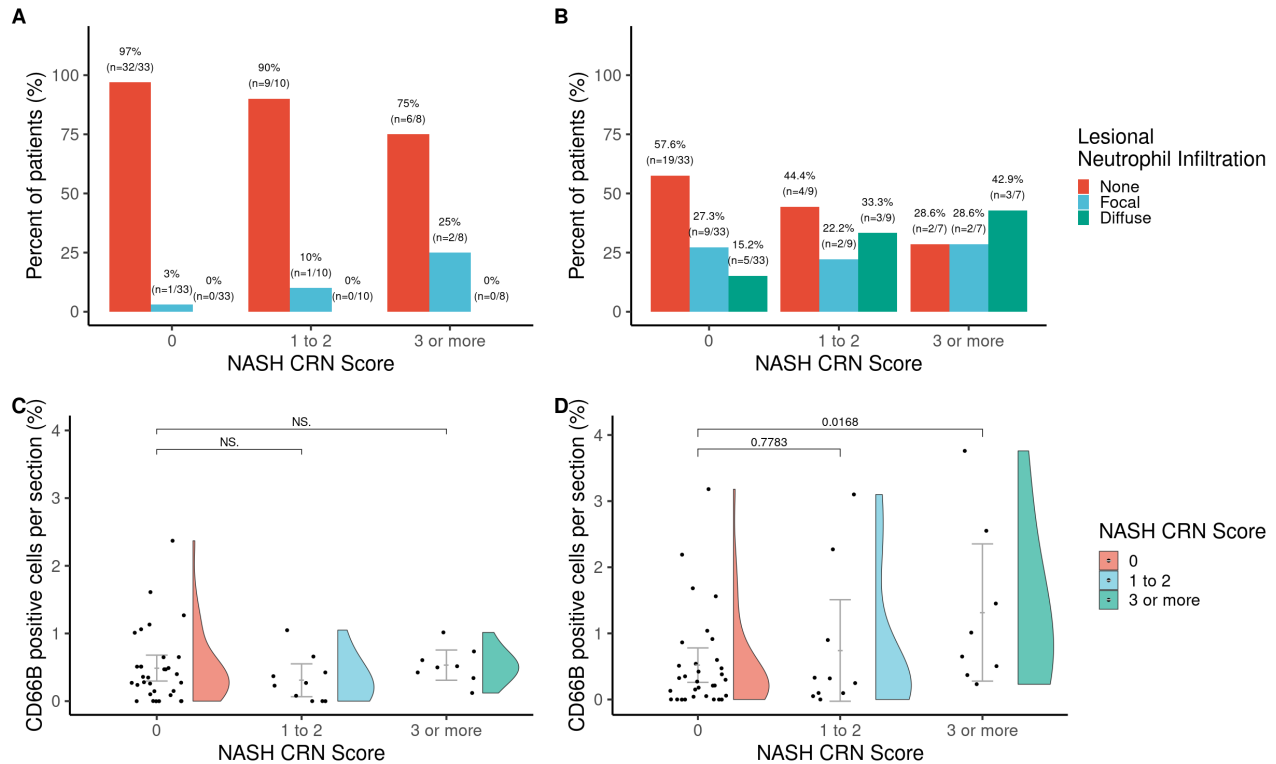
A.2 Hypothesis

- Combination CXCR2 inhibition with anti-PD1 therapy reprogrammes neutrophils in the NASH/NAFLD-HCC tumour microenvironment to an immature phenotype and restores cytotoxic anti-tumour responses.

A.3 Neutrophils in human NASH/NAFLD-HCC

Several reports suggest that myeloid populations, including neutrophils, play a key role in the development of NASH/NAFLD HCC and drive pro-tumorigenic programmes of chronic inflammation. To establish whether this is clinically relevant, I examined whether patients with NASH/NAFLD-HCC had higher levels of neutrophils in both lesional and non-lesional liver tissue. This anonymised tissue was obtained from a cohort of 49 patients who had undergone resection for HCC in NHS Lothian. The H&E sections were examined by a consultant hepatobiliary histopathologist (Dr. Tim Kendall) and scored for the presence of neutrophils and assigned a NASH Clinical Research Network (NASH CRN) score. The NASH CRN score measures the severity of NASH based on the following histopathological features; steatosis, lobular inflammation, hepatocyte ballooning and fibrosis. Sections were also immunohistochemically stained for CD66B at Newcastle University, before being scanned on an Aperio AT2 brightfield slide scanner at the CRUK Beatson Institute histology core facility. Scans were then annotated and quantified using QuPath scripting on the Cancer Research UK Beatson Institute High Performance Computing cluster.

Figure A.1: Pathological assessment and automated quantification of HCC resection patient cohort. Panel A – NASH CRN Score by neutrophil infiltration in non-lesional liver, Panel B – NASH CRN Score by neutrophil infiltration in lesional HCC tissue, XC NASH CRN Score by CD66B in non-lesional liver (each point represents percentage contained in one slide, grey bars are mean \pm 95% confidence interval), Panel C – NASH CRN Score by CD66B in non-lesional liver (each point represents percentage contained in one slide, grey bars are arithmetic mean \pm 95% confidence interval), Panel D – NASH CRN Score by CD66B in lesional HCC tissue (each point represents percentage contained in one slide, grey bars are arithmetic mean \pm 95% confidence interval). Tests are Wilcoxon signed rank.



The results of this analysis are shown in figure A.1. In non-lesional liver, focal neutrophil infiltration was higher in people with mild histopathological NASH features (NASH CRN 1 to 2) compared to those with a NASH CRN score of 0 (3% n=1/33 NASH CRN 0, 10% n=1/10 NASH CRN 1 to 2, figure A.1A). This further increased when the NASH CRN score was equal to or greater than 3 (3% n=1/33 NASH CRN 0, 25% n=2/8 NASH CRN 3 or higher, figure A.1A). Although these are small numbers, it is suggestive that in non-lesional tissue, neutrophil infiltration increases with severity of NASH. There were no patients with diffuse neutrophil infiltration in non-lesional tissue compartments.

In HCC lesions, neutrophil infiltration was more frequent (figure A.1B) in patients with

higher NASH CRN grades. Both focal and diffuse neutrophil infiltrate was least commonly found in people with NASH CRN grades of 0 (diffuse 15.2% n=5/33) and increased with NASH CRN scores (diffuse 33.3% n=3/9 in NASH CRN 1 to 2, 42.9% n=3/7 in NASH CRN 3 or higher). This suggests that in patients with NASH/NAFLD-HCC, both lesional and non-lesional neutrophil infiltration is more common compared to people without features of NASH/NAFLD. To confirm this, I quantified CD66B, a granulocyte marker, in tissue sections from the same cohort (figure A.1C). In non-lesional regions there was no increase in CD66B cell infiltration (figure A.1C), but in lesional HCC tissue there was a significantly higher proportion of CD66B positive cells in NASH CRN 3 or higher lesional HCC tissue, compared with NASH CRN 0 or NASH CRN 1 to 2 (figure A.1D). Taken together, neutrophil infiltration is associated with higher NASH pathological severity and is likely a feature of human NASH/NAFLD-HCC.

A.4 Investigating the effect of CXCR2 inhibition on the tumour microenvironment

To investigate the role of CXCR2 further, I used single-cell RNA sequencing data generated from mouse models NASH-HCC to analyse the landscape of infiltrating neutrophils following treatment with isotype/vehicle control, CXCR2 inhibitor (termed CXCR2smi), anti-PD1 immune checkpoint blockade, or CXCR2 inhibitor and anti-PD1 combined (combination CXCR2smi/anti-PD1). I chose to use single-cell RNA sequencing as it provides an unbiased overview of the transcriptional activity occurring in every cell within a given sample. This also allows heterogeneity within cell populations to be examined and the discovery of new cell subpopulations.

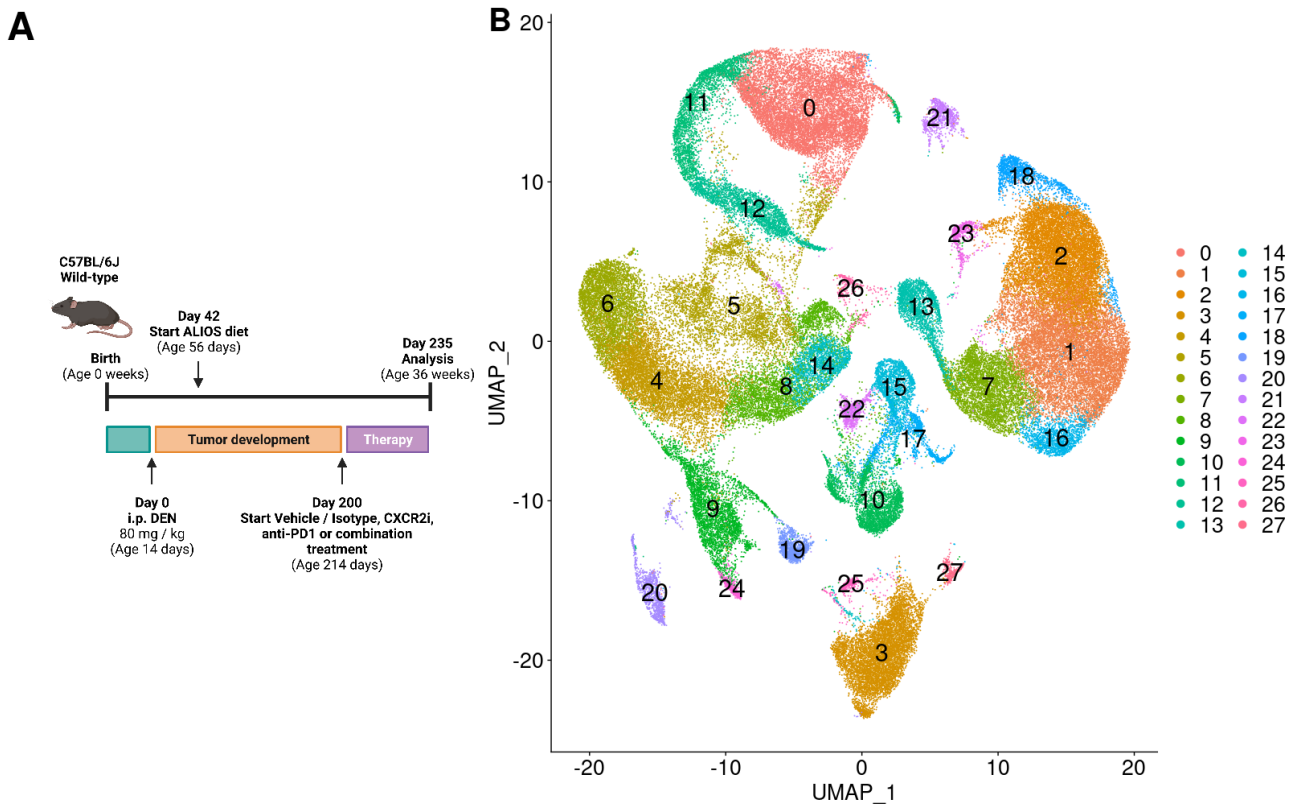
NASH-HCC mice were given a single dose of diethylnitrosamine (DEN) and then fed a high fat, high sugar ALIOS diet (DEN-ALIOS) as described in figure A.2A. Using the 10x genomics chromium platform (Thomas Jamieson, Dr. Rachel Ridgway, Dr. Amanda McFarlane, Dr. Ximena L Raffo Iraolagoitia, Dr. John Mackey and Dr. Ya-Ching Hsieh), a total of 161,620 single cell transcriptomes were obtained from 14 mice (4 vehicle/isotype treated, 3 anti-PD1, 3 CXCR2smi (AZD5069) and 4 treated with combination CXCR2smi/anti-PD1). Cells which

had less than 200 RNA features, or more than 3000 features were discarded, as were cells which had over 5% mitochondrial reads.

A.4.1 Results of single-cell RNA sequencing analysis

After filtering, a total of 90,657 cells were available for analysis (figure A.2). Next, similar cell-types were identified across the different treatment groups by using integration anchors across all conditions. This approach identifies very similar cell-cell pairings to allow cell subsets to be identified, even if treatment effects lead to large differences in expression of other genes. Analysis was as described in the methods, using an elbow plot to identify how variance was spread over the principle components, with the first 10 components used to find clusters with the UMAP function of Seurat (resolution 0.6, minimum number of neighbours 45, over 500 epochs). After identifying the relevant integration anchors, dimensionality reduction using PCA and initial clustering using Louvain community detection were applied to the dataset and non-linear dimensional reduction was performed with Uniform Manifold Approximation and Projection (UMAP). In the presented UMAP plot (figure A.2B), each point represents a single cell and the distances between each point represent the similarity between each single cell transcriptome. This resulted in a total of 27 cell clusters being identified across all conditions (figure A.3).

Figure A.2: Overview of single-cell RNA sequencing experiment in a DEN-ALIOS NASH-HCC model following treatment with vehicle/isotype control, CXCR2smi (AZD5069) alone, anti-PD1 alone, or CXCR2smi/anti-PD1 combination therapy. Panel A – Overview of experimental strategy. Panel B – UMAP projection following initial integration and filtering of cells.



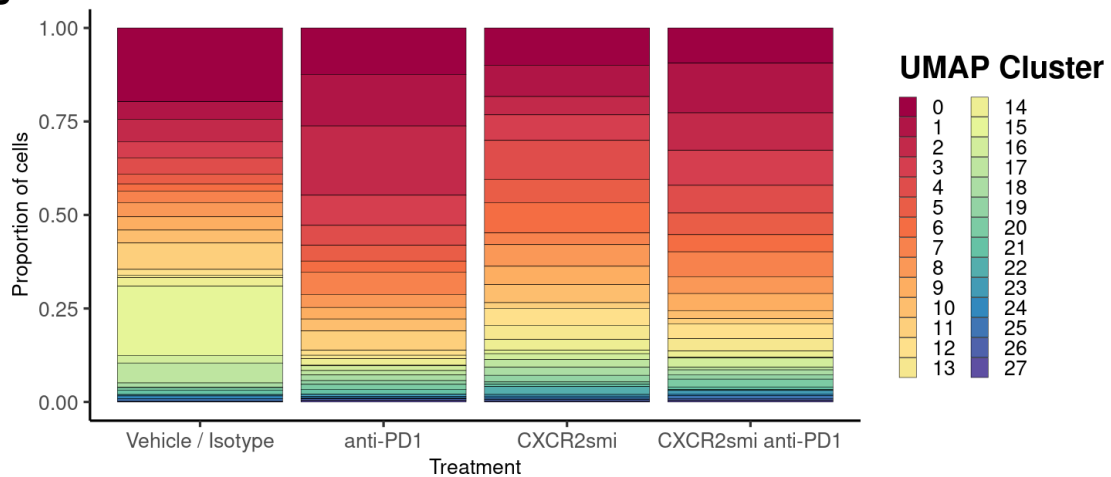
As there were small quantities of epithelial cells (3 clusters - 15, 17 and 22, figure A.2B, figure A.3 and figure A.4) within the data across different treatment conditions, these were removed from the analysis and the UMAP re-clustered to share the variance across immune and mesenchymal cell types only. Re-clustering identified a further 2 clusters and improved general cluster segregation. I next annotated by relative expression of markers to sets of well-established canonical markers. First by identifying whether the cell expressed Cd45 (Ptprc) or other major immune cell markers (figure A.4), and if so, then categorising according to major immune subsets; T-cells (Cd3d, Cd3e, Cd3g, Cd8a), myeloid derived cells including monocytes, macrophages and neutrophils (Itgam, Adgre1, Ccr2, S100a8, Cd86, Cd68), tissue resident macrophages (Clec4f), B-lymphocytes (Cd19), NK cells (Cd49b, Nkg7, Ncr1) and Dendritic cells (Cd103, Xcr1, Clec9a). Epithelial or tumour cells were identified through the expression of hepatocyte associated genes such as Alphafetoprotein (Afp), Fibrinogen (Fga or

Figure A.3: Summary of clusters by treatment group in a DEN-ALIOS NASH-HCC model following treatment with vehicle/isotype control, CXCR2smi (AZD5069) alone, anti-PD1 alone, or CXCR2smi/anti-PD1 combination therapy. Panel A – Number of cells per cluster (column percentages within in treatment group are in parentheses). Panel B – Relative proportion of cells within each UMAP cluster. Panel C – UMAP clusters split by treatment group.

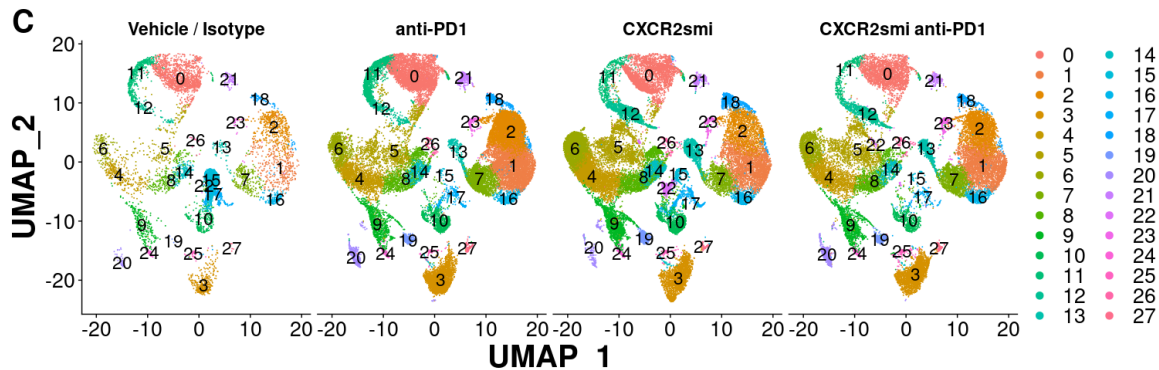
A

Cluster	Total cells	Vehicle / Isotype	anti-PD1	CXCR2smi	CXCR2smi anti-PD1
0	10384 (11.5)	1479 (19.7)	3739 (12.5)	2991 (10.0)	2175 (9.4)
1	10066 (11.1)	355 (4.7)	4126 (13.7)	2515 (8.4)	3070 (13.3)
2	9794 (10.8)	448 (6.0)	5556 (18.5)	1474 (4.9)	2316 (10.0)
3	6956 (7.7)	328 (4.4)	2418 (8.1)	2046 (6.8)	2164 (9.4)
4	6769 (7.5)	325 (4.3)	1601 (5.3)	3128 (10.4)	1715 (7.4)
5	4668 (5.1)	197 (2.6)	1268 (4.2)	1871 (6.2)	1332 (5.8)
6	4521 (5.0)	142 (1.9)	885 (2.9)	2432 (8.1)	1062 (4.6)
7	4500 (5.0)	233 (3.1)	1795 (6.0)	934 (3.1)	1538 (6.7)
8	4103 (4.5)	286 (3.8)	1038 (3.5)	1739 (5.8)	1040 (4.5)
9	3724 (4.1)	266 (3.5)	925 (3.1)	1479 (4.9)	1054 (4.6)
10	3150 (3.5)	260 (3.5)	952 (3.2)	1442 (4.8)	496 (2.1)
11	2867 (3.2)	529 (7.0)	1562 (5.2)	455 (1.5)	321 (1.4)
12	2798 (3.1)	118 (1.6)	396 (1.3)	1367 (4.6)	917 (4.0)
13	2217 (2.4)	50 (0.7)	271 (0.9)	1135 (3.8)	761 (3.3)
14	1959 (2.2)	169 (2.3)	528 (1.8)	869 (2.9)	393 (1.7)
15	1745 (1.9)	1392 (18.5)	47 (0.2)	271 (0.9)	35 (0.2)
16	1582 (1.7)	152 (2.0)	379 (1.3)	468 (1.6)	583 (2.5)
17	1527 (1.7)	400 (5.3)	353 (1.2)	616 (2.1)	158 (0.7)
18	1499 (1.7)	89 (1.2)	456 (1.5)	656 (2.2)	298 (1.3)
19	1112 (1.2)	4 (0.1)	298 (1.0)	533 (1.8)	277 (1.2)
20	1109 (1.2)	50 (0.7)	402 (1.3)	176 (0.6)	481 (2.1)
21	822 (0.9)	90 (1.2)	387 (1.3)	180 (0.6)	165 (0.7)
22	703 (0.8)	3 (0.0)	0 (0.0)	647 (2.2)	53 (0.2)
23	573 (0.6)	26 (0.3)	190 (0.6)	138 (0.5)	219 (0.9)
24	442 (0.5)	58 (0.8)	129 (0.4)	145 (0.5)	110 (0.5)
25	417 (0.5)	41 (0.5)	55 (0.2)	124 (0.4)	197 (0.9)
26	361 (0.4)	15 (0.2)	122 (0.4)	129 (0.4)	95 (0.4)
27	289 (0.3)	6 (0.1)	131 (0.4)	64 (0.2)	88 (0.4)

B



C

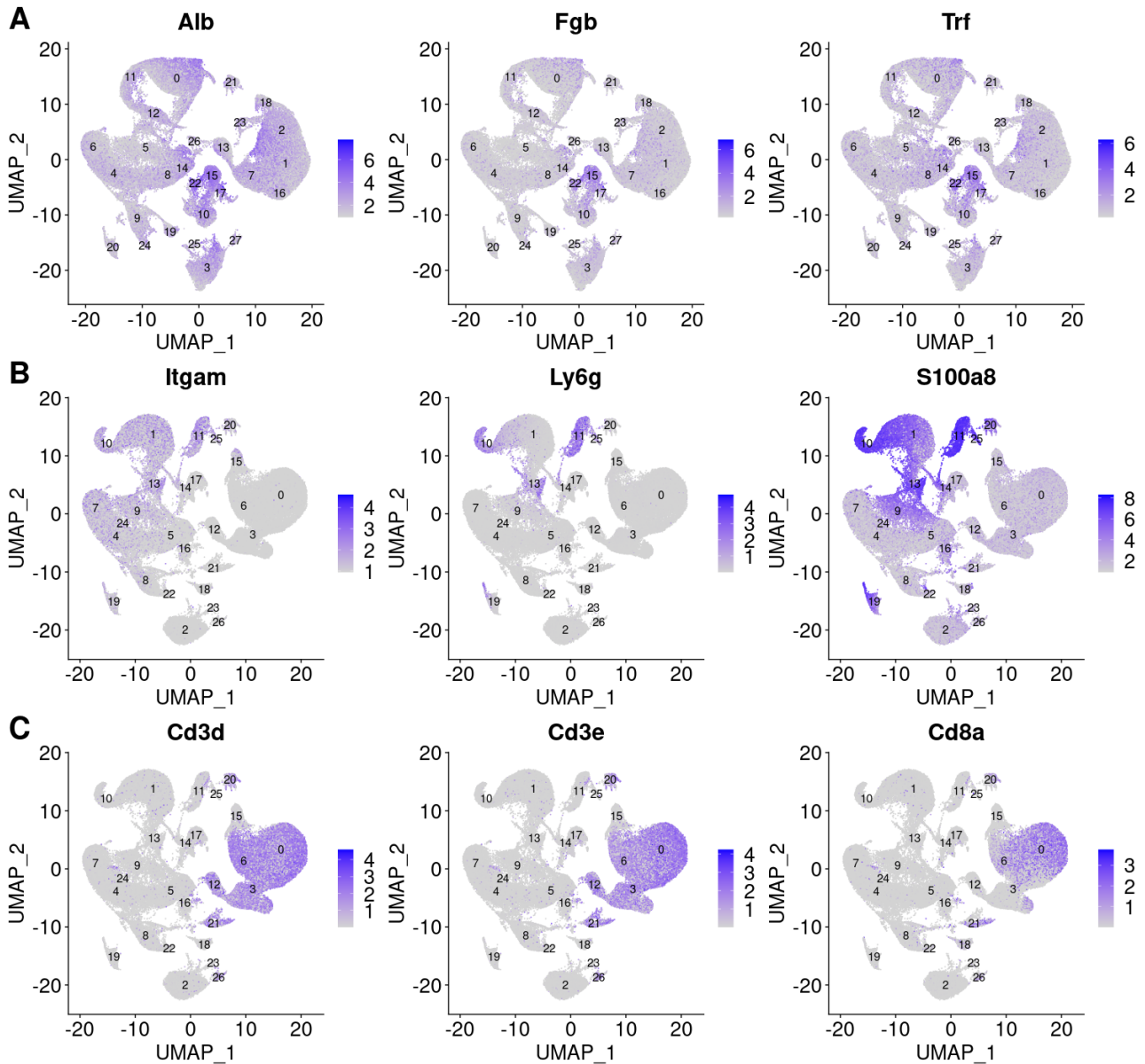


Fgb), Transferrin (Trf), albumin (Alb) and other associated secretory proteins. Endothelial and liver sinusoidal endothelial cells were identified primarily through expression of Plvap, Lyve1 and Clec4g (LSEctin). Guided annotation with the SingleR R package was then used to help annotate the remaining clusters. SingleR compares differential expression in each cluster to that of 'known' cell subtypes in the Immunological Genome project[231, 232]. For the remaining unidentified cells, the top 10 differentially expressed genes in each cluster were then studied to identify whether these genes fitted well-described canonical marker expression in the scientific literature.

A.4.2 Effect of CXCR2 inhibition in myeloid compartments of the tumour microenvironment

To further improve the resolution of the analysis in the myeloid subpopulations I repeated the clustering analysis for myeloid populations only. Re-clustering the myeloid cell population revealed 16 distinct UMAP clusters (figure A.5). Each cluster was annotated according to the canonical markers expressed by the cell groups. Stage of neutrophil development was defined according to expression of markers identified by *Grieshaber-Bouyer et al.* known as neutrotime[233]. I used neutrotime signature genes to define the stage of maturity of the 6 neutrophil clusters, with genes such as *Ltf*, *Mmp8*, *Lcn2*, *Camp*, *Lyz2* denoting early neutrotime and genes such as *Malat1*, *Il-1b*, *Ccl6*, *Csf3r* denoting late neutrotime. The UMAP projection of these cell types (figure A.5A) showed two distinct cellular partitions, the first being monocyte/macrophage and dendritic cells, with the second being neutrophils across different stages of maturity. Interestingly, the relative proportion of cells in the monocyte/macrophage and dendritic cells group did not change across the different treatment groups (figure A.5C-D). Tissue resident Kupffer cells were the most consistent, comprising between 5 and 6% of the myeloid population across every group (figure A.5D). However, in the neutrophil group, there was a 2-to-8-fold relative increase in immature neutrophils (termed ‘early’ or ‘intermediate’) in the CXCR2smi alone and combination CXCR2smi/anti-PD1 therapy groups (figure A.5D), suggesting CXCR2smi has greatest impact on the recruitment of neutrophil populations.

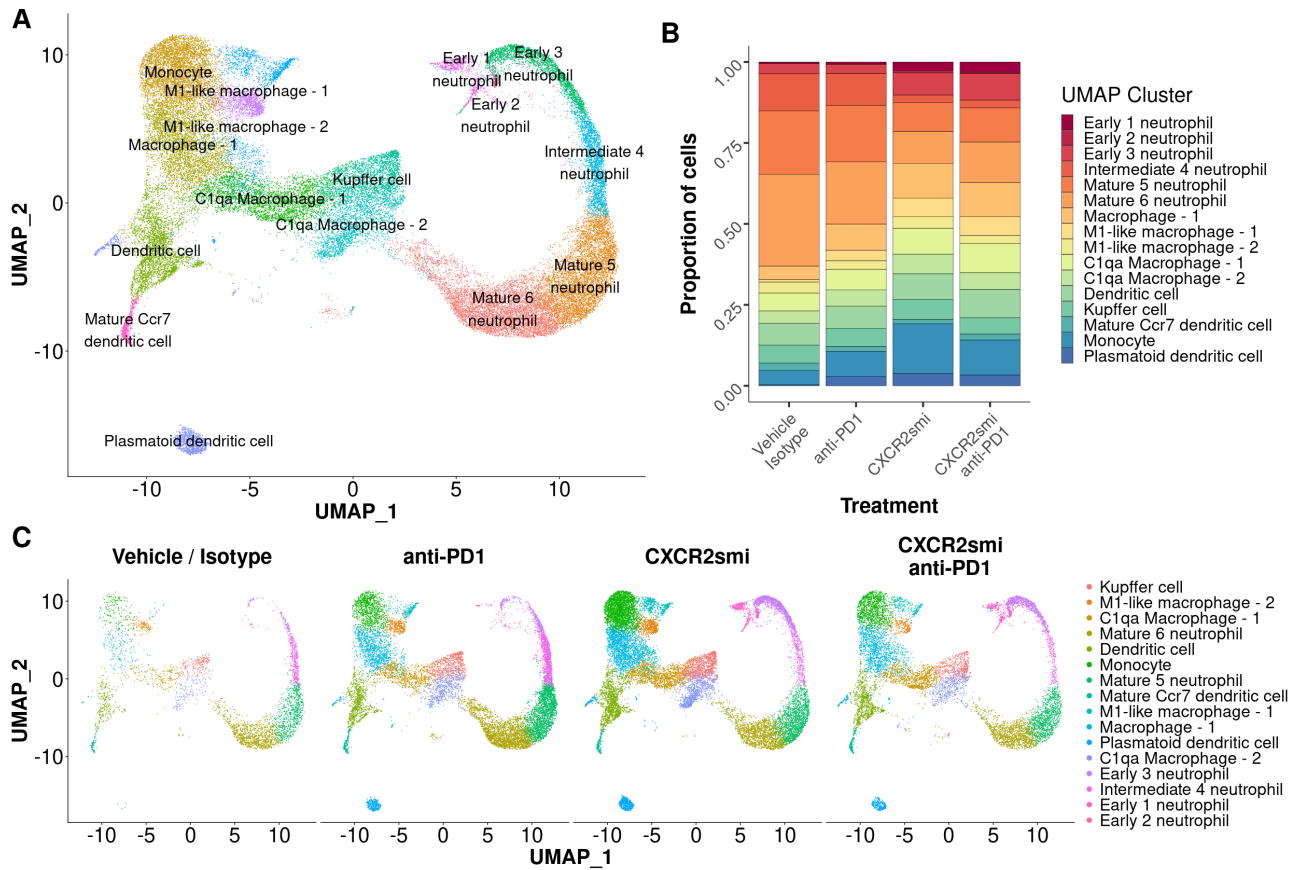
Figure A.4: Overview of a selection of cluster defining canonical epithelial and immune cell markers. Panel A – Epithelial markers albumin, fibrinogen and transferrin clearly demarcate clusters 15, 17 and 22 as epithelial cells. Due to the small numbers of these across different conditions they were later removed. Panel B – Myeloid markers Itgam (Cd11b), Ly6g and S100a8 (Mrp8). Panel C – T-cell markers Cd3d, Cd3e and Cd8a.



Although the proportion of early and intermediate class neutrophils increased in the CXCR2smi treatment groups, single cell sequencing allows the elucidation of the transcriptional programmes that underpin this and may help to suggest whether the function and phenotype of these cells is altered with CXCR2smi therapy. Therefore, I performed a gene set enrichment analysis (GSEA) on each cluster to identify which pathways were up or downregulated within each cell-type across the different CXCR2smi treatment groups. For this analysis, the reference level was taken as a composite of all treatments, to give a conservative estimate of which pathways were most strongly enriched. Figure A.6 displays the results of the GSEA analysis for selected cell types in response to combination CXCR2smi/anti-PD1 therapy.

Combination CXCR2smi/anti-PD1 therapy appears to drive upregulation of transcriptional programmes associated with leukocyte migration, chemotaxis and inflammatory response in the early-intermediate neutrophil clusters. This is accompanied by suppression of inflammatory signalling and antimicrobial responses in mature neutrophil populations. These antimicrobial response pathways are associated with the formation of neutrophil extracellular traps (NETs), which in some cancers has been previously shown to limit effective CD8+ T-cell mediated immunity[225]. It is unknown whether immature tumour associated neutrophils are more or less likely to produce NETs and if these structures differ from NETs produced by mature neutrophils. However, if immature tumour associated neutrophils are less likely to produce NETs, or if the structure of NETs is more conducive to effective antigen presentation or results in greater harm to tumour cells, this may plausibly contribute toward anti-tumour immune responses. In the monocyte cluster, there appeared to be a significant shift with combination therapy to expression of pathways promoting neutrophil chemotaxis and leukocyte migration, suggesting that monocytes may play a key role in either attracting immature neutrophils to the tumour microenvironment, or reprogramming neutrophils to maintain an ‘early’ phenotype.

Figure A.5: Re-clustering of myeloid populations identifies additional cell-types and refines cell-type classification. Panel A – Annotated UMAP projection of re-clustered myeloid subset for all treatments combined. Panel B – Proportion of different myeloid cell types by treatment group, noting an increased proportion of early/intermediate stage neutrophils. Panel C – UMAP projection by treatment group with the numerical proportions shown in table panel D.



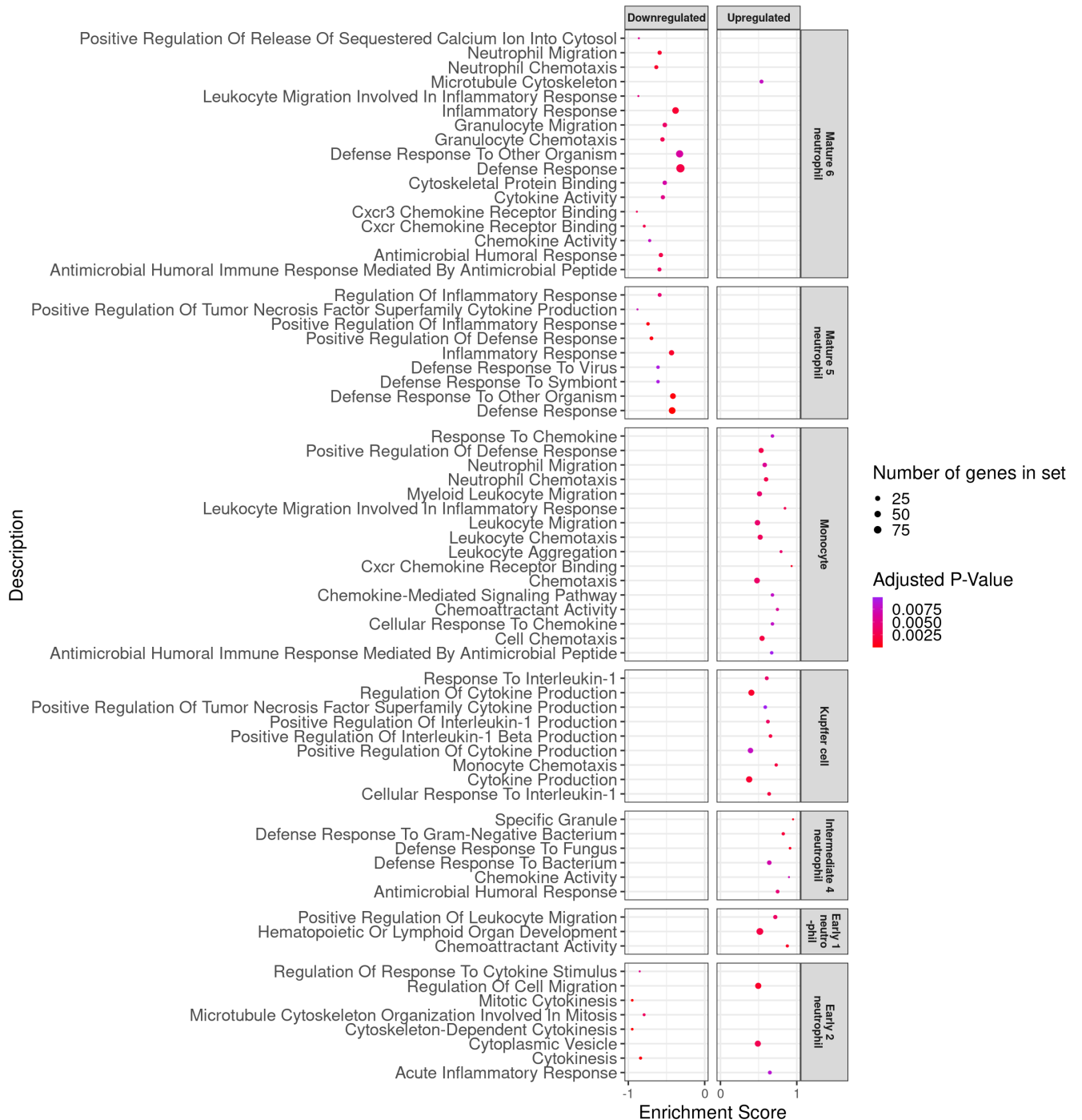
Although the proportion of Kupffer cells remained relatively constant across treatment groups, CXCR2smi combination therapy led to significant enrichment of cytokine production, most notably in the Interleukin-1 β (Il-1b) pathway. Interleukin-1 β plays a key role in stimulating cytokine production in a range of other cell-types and can work in a paracrine manner inducing the expression of molecules required for neutrophil transmigration on endothelial cells[3, 227]. This suggests that combination therapy may not just be acting on neutrophils and may also affect other cell compartments, including endothelial cells, Kupffer cells, and monocytes to promote the recruitment of immature neutrophils to the tumour microenvironment.

A.4.3 Cytokine signalling in neutrophil populations

To examine which cytokines and receptors were most likely to be responsible for the recruitment of immature neutrophils to the tumour microenvironment, I performed a pseudotime trajectory analysis using monocle3[124].

Many cellular processes occur in a dynamic fashion, responding to difference changes and cues within the microenvironment. To understand the transcriptional changes that could be underlying these changes in state, cells can be arranged along a trajectory and changes in gene expression that may be generating the trajectory. Here, I use this to draw a trajectory through stages of neutrophil maturity to identify which genes might be causing the immature neutrophil phenotype in CXCR2smi treated mice. To do this, monocle3 uses graph embedding algorithms to find key transitional hubs along given UMAP coordinates. I did this by placing a root (start) in the immature neutrophil cluster and terminated this in the mature 6 neutrophil cluster.

Figure A.6: Gene set enrichment analysis of Gene Ontology (GO) terms associated with inflammation and neutrophil migration by cell type following treatment with combination CXCR2smi/anti-PD1 therapy.



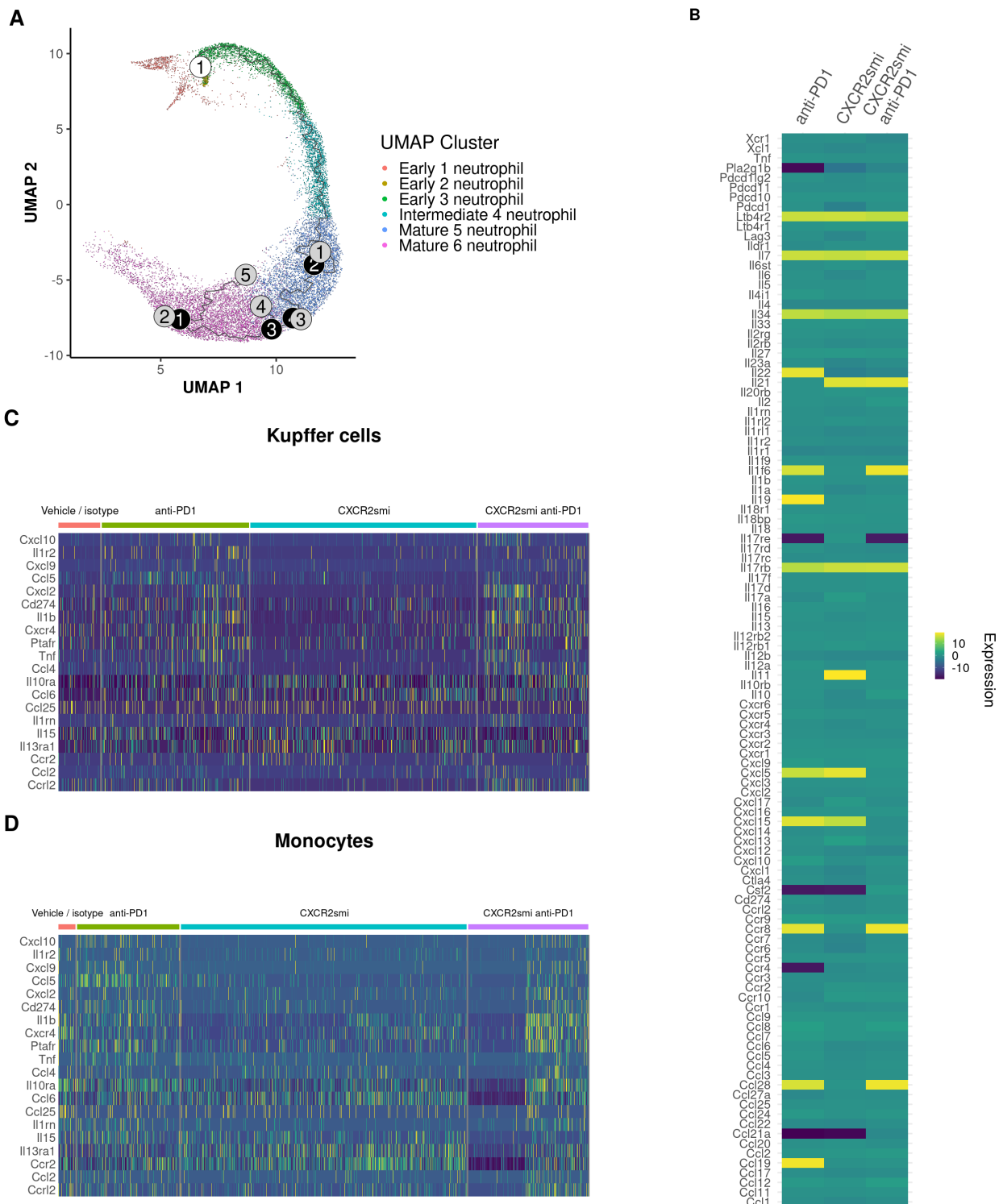
I performed a differential expression analysis along the drawn pseudo time trajectory (figure A.7A), which accounted for both cell phenotype and treatment received. This analysis allows different stages of neutrophil development to be considered to identify which changes in cytokine receptor signalling are observed.

A wide range of differentially expressed cytokines were identified (figure A.7B). Strikingly, there appeared to be differences not only between CXCR2smi treated groups and anti-PD1, but suggestion of additional differences with combination CXCR2smi/anti-PD1 therapy versus anti-PD1 or CXCR2smi alone. Several key regulators of acute inflammation and neutrophil chemotaxis were upregulated in the CXCR2smi treated groups, most notably phospholipase A2 (arachidonic acid pathway) and Ccr4 (receptor for Ccl17 and Ccl22, figure A.7B). Il-22, Il-19, Ccl19 were all down regulated after CXCR2smi treatment (either monotherapy or combination CXCR2smi/anti-PD1) and Cxcl5, Cxcl15, Il13ra2 were downregulated in the combination arm only. Csf2 was found to be significantly increased in the combination group and plays a key role in triggering the release of Interleukin-1 β from monocytes and Kupffer cells (figure A.7C and figure A.7D). Taken together, CXCR2smi and combination CXCR2smi/anti-PD1 therapy appears to downregulate key mediators of immunosuppression (Il-19) and neutrophil recruitment (Cxcl3, Cxcl5, Phospholipase A2) which may alter how other immune cells respond to inflammation in the tumour microenvironment.

A.4.4 Effect of CXCR2 inhibition in T-cell compartments of the tumour microenvironment

After re-clustering, several T-cell subsets were more clearly identified using canonical markers of T-cell subtypes (figure A.8). One cluster that could not be identified as a specific T-cell subpopulation was termed 'T-cell'. Treatment with anti-PD1 therapy drastically increased the proportion of Cd8 T-cells which also expressed cytotoxic granzyme markers (Gzma and Gzmb), but also increased the proportion of Cd8 T-cells expressing exhaustion markers including Pdcd1 (Pd1), Lag3, Havcr2 (Tim-3), Eomes, Ctla4, Tox and Cxcr6. With CXCR2smi monotherapy, the proportions of different T-cell populations were very similar to

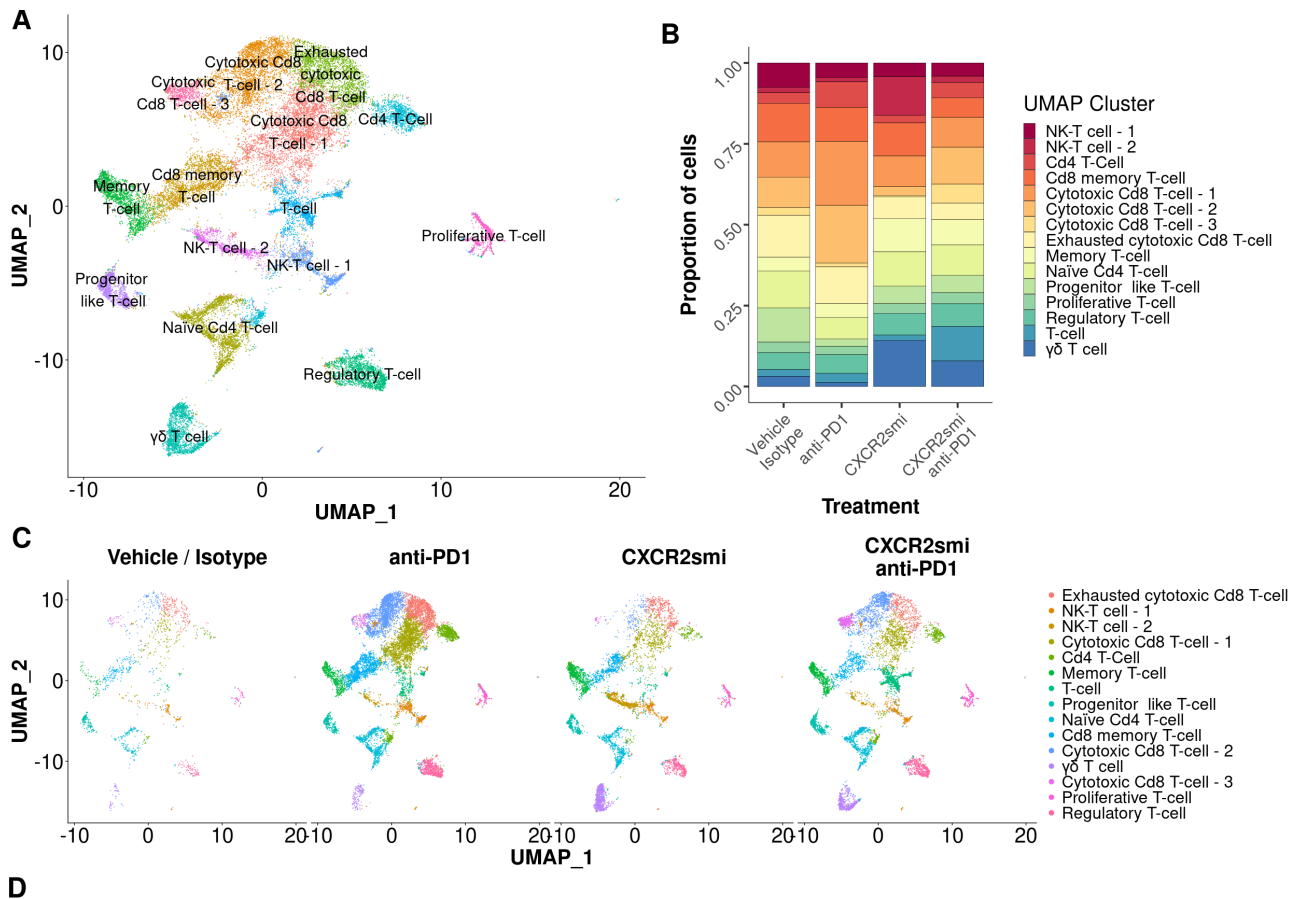
Figure A.7: Pseudotime trajectory analysis of differentially expressed genes within neutrophils and differentially expressed genes in Kupffer cells and monocytes. Panel A – Pseudotime trajectory by UMAP clusters. The white circle labelled 1 represents the start root for the trajectory, in the immature first early neutrophil cluster. The remaining circles represent hubs or ends of the trajectory. Panel B – differentially expressed cytokine genes with respect to pseudotime and treatment. Data presented as global changes in cytokine and cytokine receptors across the entire neutrophil population versus all groups together provide a proportionally unbiased view of gene expression, by controlling for differences in neutrophil maturity. Panel C – Heatmap of significantly differentially expressed cytokine genes in Kupffer cells by treatment condition, highlighting Il-1 pathways. Panel D – Heatmap of significantly differentially expressed cytokine genes in monocytes by treatment condition, again highlighting IL-1 β pathways.



the vehicle/isotype control, although there was a large increase in the proportion of $\gamma\delta$ T-cells. Combination CXCR2smi/anti-PD1 therapy led to a more diverse and even spread of T-cell types, rather than the high proportion of cytotoxic/exhausted cytotoxic Cd8 T-cells seen with anti-PD1 monotherapy (Figure A.8B, A.8C and A.8D). Crucially, a decrease in the proportion of exhausted Cd8 cytotoxic T-cells was observed, suggesting combination CXCR2smi/anti-PD1 therapy was reducing T-cell exhaustion in some way, compared with both anti-PD1 therapy and vehicle/isotype control. The unidentified T-cell population was substantially higher in the combination therapy group, suggesting this may play an important role in mediating the enhanced efficacy of combination therapy.

Although reduced Cd8 cytotoxic T-cell exhaustion and the increase in an unknown T-cell population may explain to some degree why combination therapy improved responses compared to anti-PD1 monotherapy or CXCR2smi alone, understanding the changes in the transcriptional programmes within T-cells will provide additional insight into how combination therapy is working. To do this, I performed a Gene Set Enrichment Analysis (GSEA) on each of the T-cell clusters using the global expression values, the same way I performed this previously in the myeloid clusters. Figure A.9 shows the GSEA results for statistically significant selected Gene Ontology (GO) T-cell and immunity pathways.

Figure A.8: Re-clustering of T-cell populations identifies additional cell-types and refines cell-type classification. Panel A – Annotated UMAP projection of re-clustered T-cell subset for all treatments combined. Panel B – Proportion of different T-cell cell types by treatment group, noting an increased diversity of T-cells, with a substantial reduction in the proportion of exhausted cytotoxic Cd8 T-cells, with an accompanying increase in Cd4 T-cell populations. An unidentified subset, expressing no conclusive markers, is labelled ‘T-cell’. Panel C – UMAP projection by treatment group with the numerical proportions shown in panel D.



Cluster	Total cells	Vehicle / Isotype	anti-PD1	CXCR2smi	CXCR2smi anti-PD1
Cytotoxic Cd8 T-cell - 1	4253 (13.9)	158 (11.0)	2591 (19.8)	664 (9.5)	840 (9.2)
Cytotoxic Cd8 T-cell - 2	3696 (12.1)	135 (9.4)	2334 (17.8)	188 (2.7)	1039 (11.4)
Cytotoxic Cd8 T-cell - 3	754 (2.5)	35 (2.4)	153 (1.2)	38 (0.5)	528 (5.8)
Exhausted cytotoxic Cd8 T-cell	2617 (8.5)	187 (13.0)	1492 (11.4)	466 (6.7)	472 (5.2)
NK-T cell - 1	1369 (4.5)	109 (7.6)	590 (4.5)	298 (4.3)	372 (4.1)
NK-T cell - 2	1208 (3.9)	24 (1.7)	173 (1.3)	834 (11.9)	177 (1.9)
Cd8 memory T-cell	2799 (9.1)	170 (11.8)	1368 (10.5)	710 (10.2)	551 (6.1)
Cd4 T-Cell	1679 (5.5)	48 (3.3)	1038 (7.9)	165 (2.4)	428 (4.7)
Memory T-cell	2045 (6.7)	61 (4.2)	559 (4.3)	720 (10.3)	705 (7.8)
T-cell	1492 (4.9)	31 (2.1)	372 (2.8)	119 (1.7)	970 (10.7)
Progenitor like T-cell	1322 (4.3)	152 (10.5)	297 (2.3)	381 (5.4)	492 (5.4)
Naive Cd4 T-cell	2631 (8.6)	165 (11.4)	870 (6.6)	740 (10.6)	856 (9.4)
γδ T cell	1921 (6.3)	45 (3.1)	162 (1.2)	995 (14.2)	719 (7.9)
Proliferative T-cell	894 (2.9)	47 (3.3)	328 (2.5)	209 (3.0)	310 (3.4)
Regulatory T-cell	1936 (6.3)	75 (5.2)	761 (5.8)	466 (6.7)	634 (7.0)

The GSEA analysis identified differences in pathway enrichment across most of the T-cell subtypes (figure A.9). There were several important pathways that play a key role in anti-tumour immunity and coordinating cytotoxic T-cell responses which were found to be upregulated following CXCR2smi/anti-PD1 combination therapy, along with downregulation of key immunosuppressive pathways (i.e. Il-4).

In the cytotoxic Cd8 T-cell groups, there was a significant down-regulation of immunosuppressive signalling, including Il-4, Il-17 and tumour necrosis factor pathways. Il-17 is known to play a key role in recruiting neutrophils and stimulates the production of neutrophil chemoattractants Cxcl1, Cxcl2, Cxcl5 and Cxcl8 in other cell types, which may contribute to the reduced proportions of mature neutrophils observed in the myeloid cell analysis. Differentiation pathways were also found to be downregulated in the exhausted cytotoxic T-cell subset, possibly suggesting a skew away from exhaustion. In addition to effects on cytotoxic T-cells, combination CXCR2smi/anti-PD1 therapy had profound effects on Cd4 T-cells, with significant upregulation of cytokine production pathways, in particular Il-10. Il-10 is a well-characterised cytokine, which drives Stat3 signalling through Il-10 receptors 1 and 2 and then through the Jak1 and Tyk2 signalling adapters. Although pleiotropic in its effects, Il-10 has been shown to enhance the production of cytotoxic granule formation (Granzyme B and perforin) thereby potentiating the killing effects of Cd8 T-cells in other models of cancer[234, 235].

The unidentified T-cell cluster ('T-cell') appeared to have significant activation of cytotoxic pathways, suggesting that in addition to a relative increase in this cell-type, there is an accompanying cytotoxic effect.

One of the key factors regulating cytotoxic T-cell responses and a major target for anti-cancer immunotherapy is expression of coinhibitory immune checkpoints. Although these and their ligands are typically cell-type specific, with inhibitory receptors usually expressed on T-cells and ligands on other cell types (epithelial cells, endothelial cells, macrophages), their expression on effector cells can be affected by changes within the tumour microenvironment. To understand whether combination CXCR2smi/anti-PD1 therapy affects

Figure A.9: Gene set enrichment analysis of Gene Ontology (GO) terms associated with inflammation and cytotoxic T-cell responses by cell type following treatment with combination CXCR2smi/anti-PD1 therapy.



immune checkpoint expression, I performed a differential expression analysis across the T-cell clusters. This could inform future rational combination immunotherapy or explain potential mechanisms of resistance to combination therapy. Figure A.10A shows differentially expressed immune checkpoint and cytotoxicity genes in T-cell subsets by therapy. In the anti-PD1 alone group, exhaustion markers, notably *Eomes*, *Tox*, *Cxcr6* along with a wide-range of inhibitory immune checkpoints were expressed across nearly all T-cell clusters. Combination CXCR2smi/anti-PD1 treatment, and to some extent CXCR2smi monotherapy, resulted in downregulation of these exhaustion markers but also downregulation of *Lag3* and *Havcr2* (Tim-3). Both immune checkpoints have monoclonal antibodies in active development and clinical trials. LAG3 binds MHC-II and Fibrinogen-like protein1 (FGL1), which is produced and found in abundance within the liver. When bound by its ligands, LAG3 negatively regulates activation of T-cells, including cytotoxic CD8+ subsets, thus impeding anti-tumour responses. In a similar fashion, HAVCR2 (Tim-3) is an inhibitory receptor, but also has affinity to HMGB1, Gal-9 and CD66a, which are commonly associated with PAMP/DAMP and neutrophil mediated immunity[5, 225, 233]. Therefore, downregulation of these checkpoints may have beneficial effects and plausibly enhance cytotoxic tumour responses in the combination therapy group. There was also positive regulation of some cytokine genes, but this expression amongst T-cell subsets was heterogenous and would possibly benefit from some future ligand:receptor interaction analysis to identify cross-talk between T-cell clusters (figure A.10B).

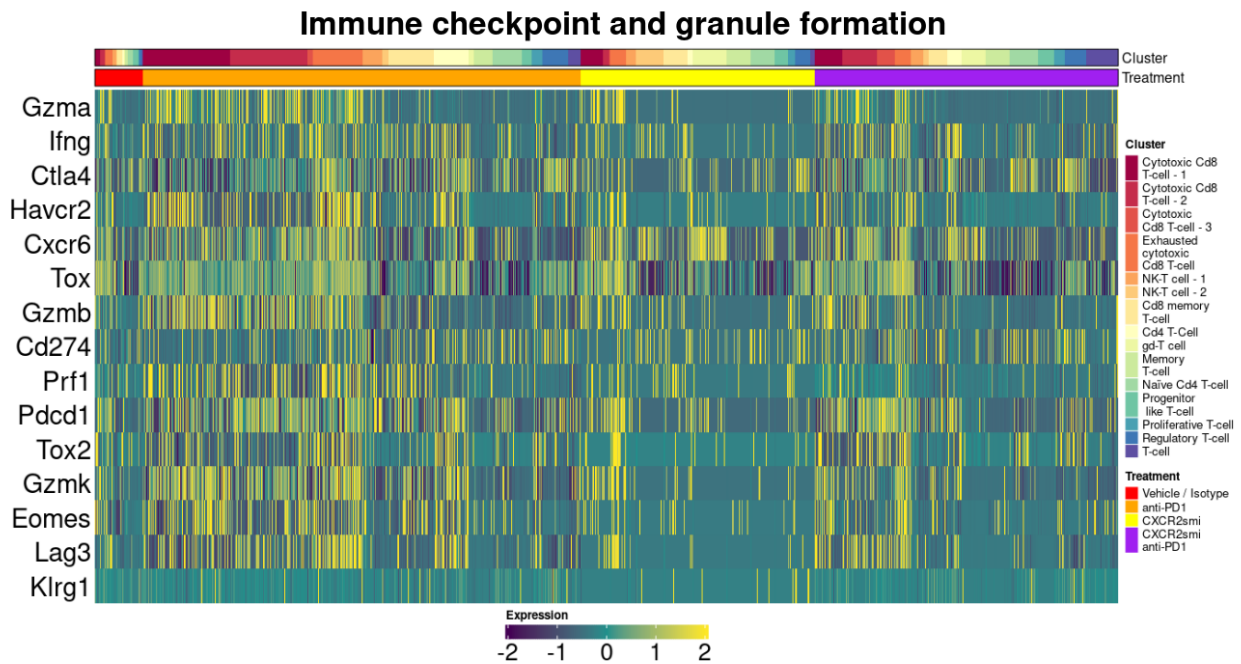
A.4.5 Effect of CXCR2 inhibition on cell state and RNA velocity in T-cell compartments

Finally, to understand which genes were driving the shift of the T-cell compartment in the combination CXCR2smi/anti-PD1 therapy group, I performed RNA velocity analysis using velocity and scVelo. RNA velocity models dynamic cellular processes using information by identifying which transcripts in single cell RNA sequencing are newly transcribed, unspliced pre-mRNAs or mature, spliced mRNAs. scVelo uses a likelihood-based dynamical model based upon this information to recover latent time and transcriptional dynamics across cells. This approach can also detect putative drivers of these transcriptional dynamics.

Figure A.11 shows the results from the dynamical models, split by treatment group with the UMAP projection. The arrows represent the direction and ‘stream’ of RNA velocity across the T-cell clusters. Stronger thicker lines mean greater RNA velocity in the indicated direction. As this is a relatively new analysis framework, the ability to quantitatively model with terms that include both treatment group and cluster is not yet established. Therefore, this is a qualitative assessment of velocity by treatment.

Figure A.10: Expression of key cytotoxicity genes, exhaustion markers and cytokines by T-cell populations by treatment condition. Panel A – Increased expression of cytotoxic granule formation genes in the anti-PD1 and CXCR2smi/anti-PD1 groups. In the anti-PD1 alone group there is substantially greater burden of T-cell exhaustion markers, namely inhibitory immune checkpoints (Lag3, Havcr2 known as Tim-3), Tox and Eomes. Panel B – Cytokines produced across different T-cell populations by treatment group. Notably reduced proportions of cells expressing Ccl3 and Ccl5, known to recruit myeloid populations including neutrophils through Ccr1, Ccr3, Ccr4 and Ccr5.

A



B

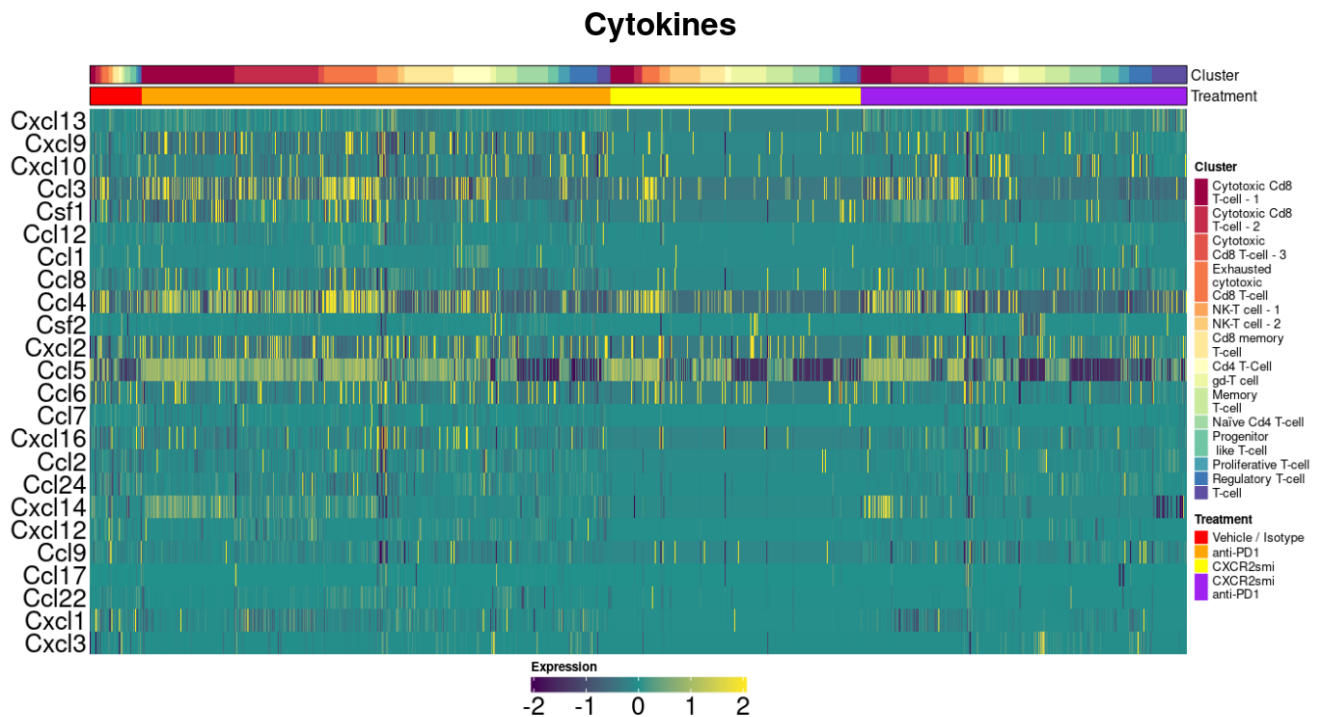
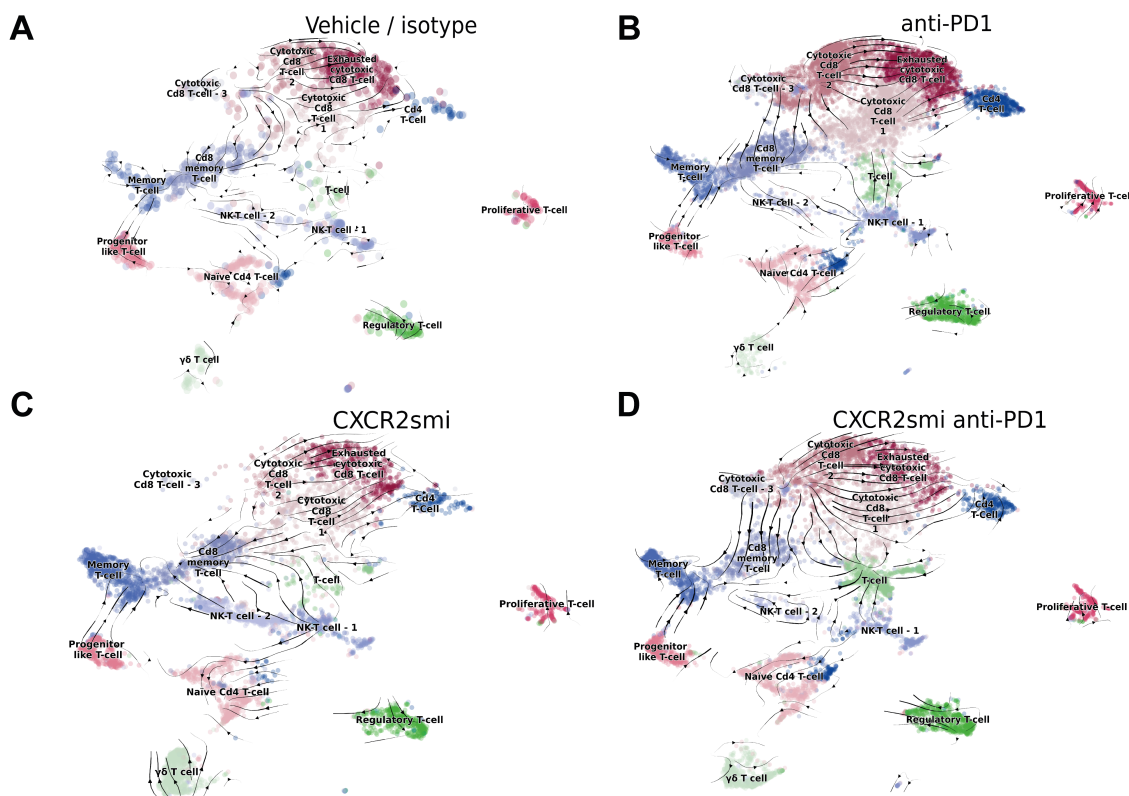


Figure A.11: RNA velocity measurements across T-cell clusters using estimates from Velocityto and processed with scVelo. Panel A – Vehicle/isotype control, note direction of low amplitude velocity toward exhausted Cd8 T-cells. Panel B – anti-PD1 alone, note direction of moderate amplitude velocity toward both exhausted Cd8 T-cells and cytotoxic Cd8 cells. Panel C – CXCR2smi monotherapy, note direction of moderate amplitude velocity toward exhausted Cd8 T-cells. Panel D – combination CXCR2smi/anti-PD1 therapy, note direction of strong amplitude velocity toward Cd4 and cytotoxic Cd8 T-cell clusters.

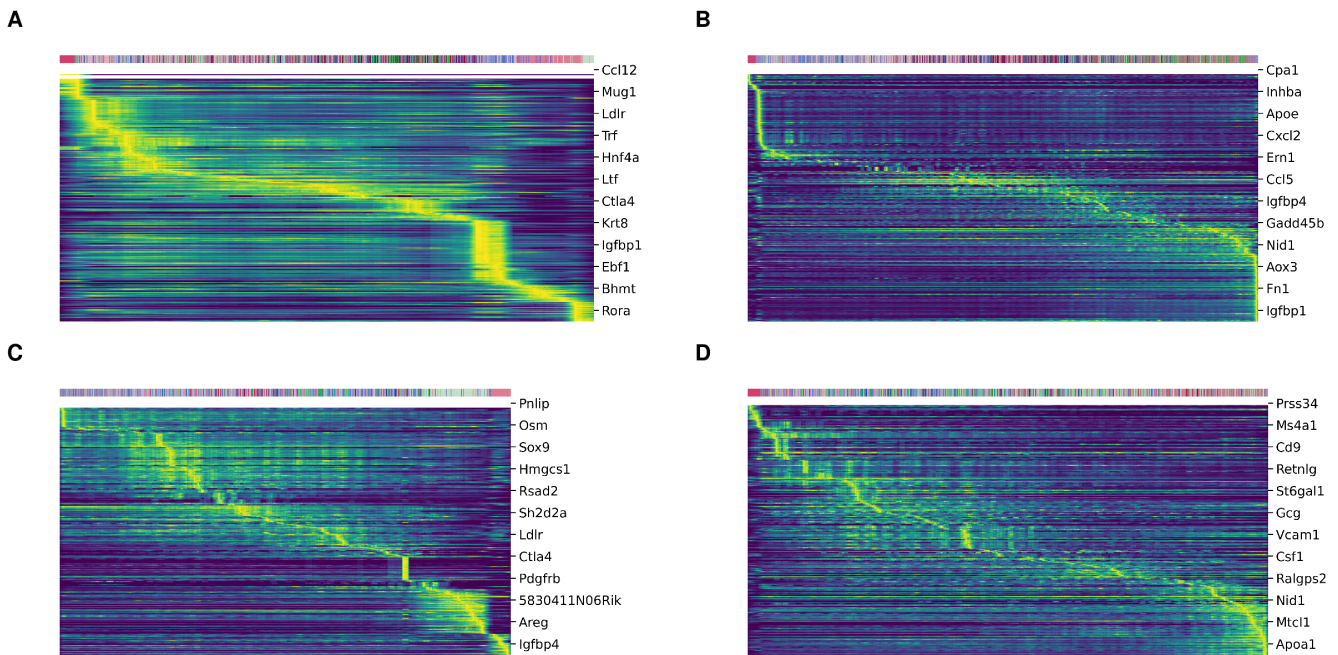


Compared with the other treatment groups, combination CXCR2smi/anti-PD1 combination treatment had greater velocity amplitude, directed toward the Cd8 cytotoxic T-cell cluster and away from the exhausted Cd8 T-cell cluster (figure A.11A to figure A.11D). This reinforces the findings of lower exhaustion markers in the combination treated group.

By analysing differentially expressed genes by the latent time contained within the different cell clusters and treatment groups, I identified several genes which may be responsible for the transition away from exhaustion and towards effective cytotoxic T-cell responses which can be seen in the heatmaps presented in figure A.12. In the vehicle/isotype

treated group, the latent time contained within the dynamical model identified the exhausted cytotoxic Cd8 T-cells as a root node, with cytotoxic Cd8 T-cells as an end node for latent time. Across latent time in the vehicle/isotype group there was expression of exhaustion associated programmes and interestingly, increased velocity of genes associated with neutrophil trafficking (*Ptgs2*) and some which are known to suppress T-cell activation (*Vegfa*). High velocity of *Vegfa* expression was also seen in the CXCR2smi monotherapy group. With anti-PD1 therapy, latent time had roots in other cytotoxic T-cell clusters, with more distributed velocity across all other groups (figure A.12B). This was accompanied with an increased velocity of neutrophil differentiation (*Ccl6*) and activation genes (*Igf1*) across latent time. Combination CXCR2smi/anti-PD1 therapy reverted the latent time root to exhausted Cd8 T-cells and toward cytotoxic Cd8 T-cells. Even in the exhausted subsets, there was an increased velocity of genes associated with T-cell activation and cytotoxic Cd8 phenotypes (*Top2a*), which gained in amplitude over latent time. This included expression of genes such as *Klra9*, which has been implicated with specific CX3CR1 positive subsets of cytotoxic anti-tumour CD8+ T-cells[236].

Figure A.12: Heatmaps of T-cell RNA velocity by latent time (left to right) and cluster (top colour map, aligns to colours of clusters in previous figure). Yellow is high expression, blue is low expression. Panel A – Vehicle/isotype control. Panel B – anti-PD1 therapy alone. Panel C – CXCR2smi monotherapy. Panel D – Combination CXCR2smi/anti-PD1 therapy.



A.4.6 Effect of combination CXCR2 inhibition on cell state and RNA velocity in tumour associated neutrophils

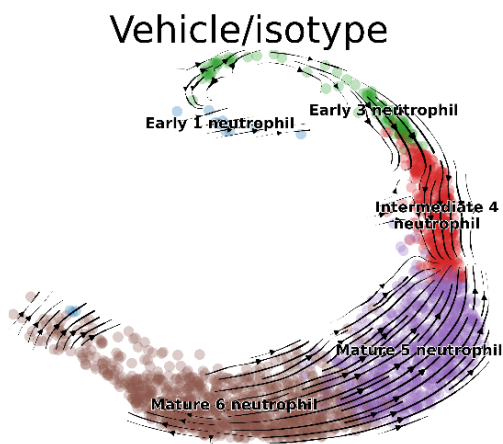
As RNA velocity helps to explain the transition between different cell states and identify genes driving these changes, I repeated the velocity analysis for the neutrophil population. Figure A.13 shows the RNA velocity across the different treatment groups. This analysis demonstrated that RNA velocity toward neutrophil maturity was relatively unimpeded by vehicle/isotype or anti-PD1 treatment. However, along with the introduction of earlier stage neutrophils, CXCR2smi appeared to markedly disrupt RNA velocity toward neutrophil maturation (figure A.13C).

When this was combined with anti-PD1 therapy, there were fewer intermediate neutrophils and the velocity stream reversed and was directed toward maintaining earlier stage neutrophil transcriptional states. Both CXCR2smi monotherapy and CXCR2smi/anti-PD1 combination therapy resulted in binodal latent time end points (one for immature and one for mature neutrophils), whereas vehicle/isotype and anti-PD1 endpoints were monocentric (mature only).

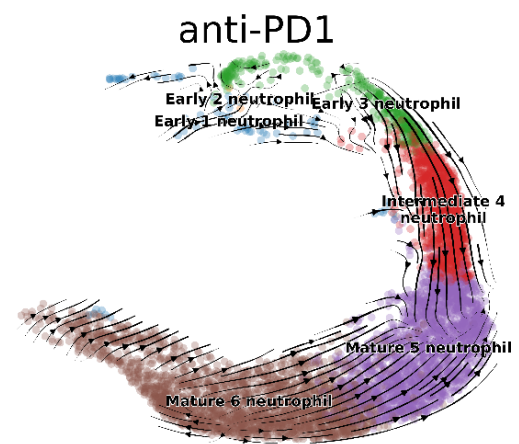
Using latent time, I next analysed the gene drivers that may be responsible for this skew toward immature neutrophil transcriptional states with CXCR2smi, shown in the heatmaps in figure A.14. This analysis identified that *Cxcl2* had an increased RNA velocity, along with key other neutrophil associated inflammatory cytokines and activity markers such as *Ptsg2* and *Furin* in mature neutrophil clusters. With CXCR2smi treatment, these genes became less prominently expressed and shifted the latent time end points toward early neutrophil transcription. Remarkably, the genes associated with early neutrophil transcriptional activity, mirrored that of those defined in neutrotime by *Grieshaber-Bouyer et al.*, with significant expression of early neutrotime genes such as *Ltf* and *Mmp8* and concurrent increases in the T-cell chemotaxis genes *Ccl4* and *Ccl5*[233]. This suggests that signalling through CXCR2 is required for mature neutrophil transcriptional programmes and CXCR2smi not only increases the relative abundance of immature neutrophils, but functionally reprogrammes them away from a mature, pro-inflammatory phenotype. The presence of these in both the neutrotime definition and in our data is strongly suggestive of this effect but should be further validated using flow cytometry or immunohistochemistry.

Figure A.13: RNA velocity measurements across neutrophil clusters using estimates from Velocityto and processed with scVelo. Panel A – Vehicle/isotype control, note direction velocity toward mature neutrophils, with clear streams through intermediate neutrophil groups. Panel B – anti-PD1 alone, note direction velocity toward mature neutrophils, with clear streams through intermediate neutrophil clusters. Panel C – CXCR2smi monotherapy, note presence of larger early neutrophil clusters, with reversal of velocity streams in the intermediate cluster, suggesting to some extent CXCR2smi prevents maturation. Panel D – Combination CXCR2smi/anti-PD1 therapy, note reversal of velocity streams now directed into early neutrophil cluster.

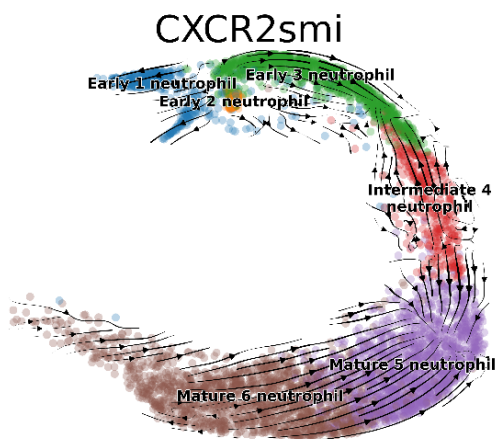
A



B



C



D

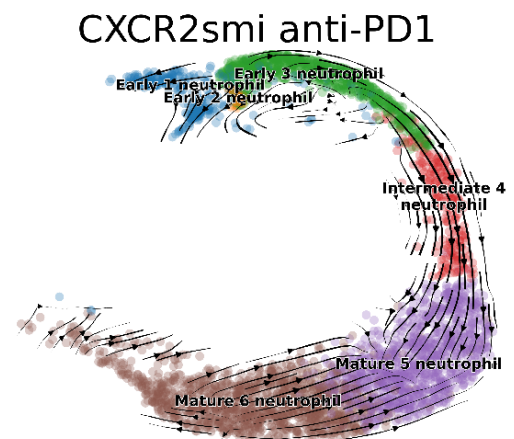
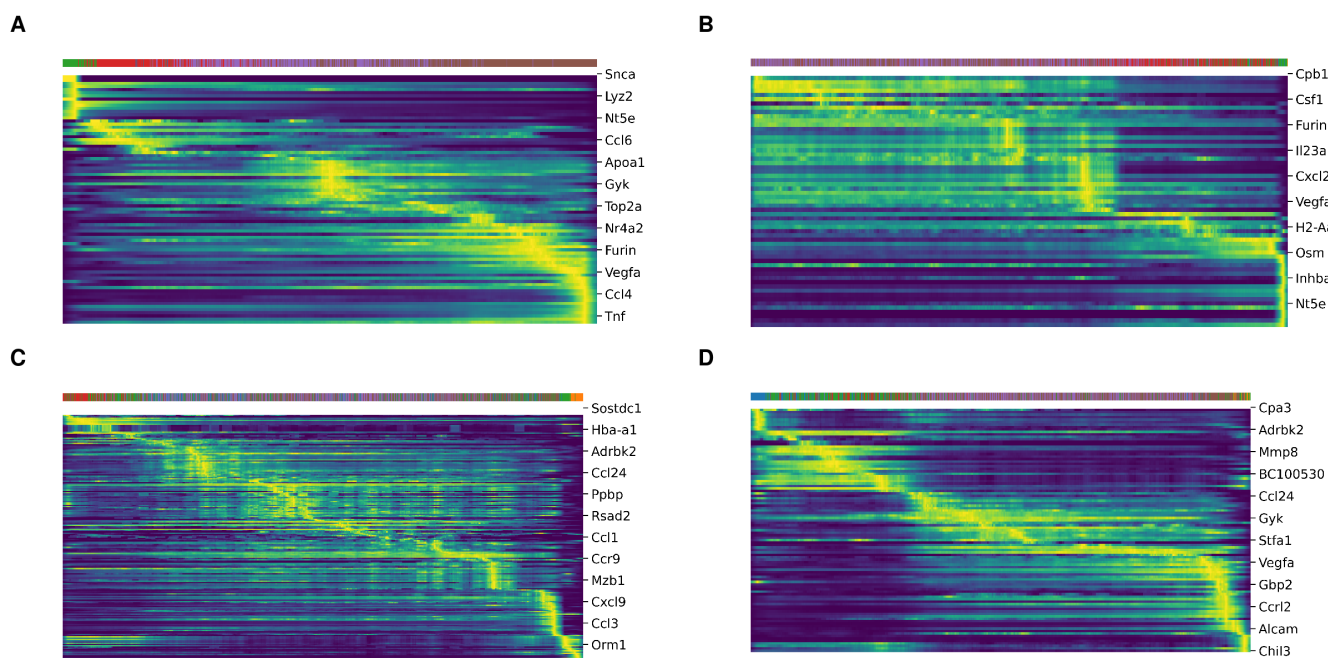


Figure A.14: Heatmaps of Neutrophil RNA velocity by latent time (left to right) and cluster (top colour map, aligns to colours of clusters in previous figure. Yellow is high expression, blue is low expression. Panel A – Vehicle/isotype control. Panel B – anti-PD1 therapy alone. Panel C – CXCR2smi monotherapy. Panel D – combination CXCR2smi/anti-PD1 therapy.



A.5 Summary

As part of a multicentre collaboration with Newcastle University and the HCC Expediter Network (HUNTER), we showed reprogramming neutrophil maturity by inhibiting CXCR2 sensitised a model of NASH/NAFLD-HCC to anti-PD1 therapy[230]. This has led to a further CRUK programme grant which aims to characterise the phenotypic and functional heterogeneity of neutrophils in HCC. Furthermore, this work has resulted in the initiation of a phase I/II clinical trial, which will assess the safety and efficacy of combining the CXCR2 small molecule inhibitor AZD5069 with Durvalumab[237].

In this chapter, I have demonstrated that in human disease NASH/NAFLD-HCC is associated with increased neutrophil infiltration. Targeting neutrophil infiltration using CXCR2smi, altered the gene expression programmes of several cell-types in a mouse model of NASH/NAFLD-HCC, resulting in an increased number of immature tumour associated

neutrophils, reprogramming transcriptional programmes toward immature neutrophil phenotypes. CXCR2 inhibition in combination with anti-PD1 therapy markedly reduced the proportion of exhausted cytotoxic Cd8 T-cells and reprogrammed T-cell transcription to favour non-exhausted cytotoxic Cd8 T-cell and Cd4 T-cell responses.

My findings support our earlier work published in the journal *Gut*, where we demonstrated shifts in neutrophil infiltration toward immature phenotypes[230]. My work not only confirms this data, but also implicates new cell types in mediating this effect and illustrates the complex effects neutrophil maturation has within the NASH/NAFLD-HCC tumour microenvironment. My findings suggest monocytes and Kupffer cells are likely to play a key role in this, through the expression of Interleukin-1 β . This may well be in response to enhanced release of PAMP/DAMPs and subsequent NLRP3 inflammasome activation arising from enhanced cell killing. In general, Interleukin-1 β is thought to oppose anti-tumour T-cell responses[227, 228] but has been shown to enhance the ability of dendritic cells to activate T-cells[238]. Further experiments such as Clec4f^{DTR} or liposomal clodronate to enable monocytic depletion or through targeting Interleukin-1 β directly using inhibitory antibodies in liver cancer models could be performed to directly test this hypothesis[239].

My findings also support previous work by *Pfister et al.*[38]. This study showed that anti-PD1 immunotherapy responses were impaired in NASH/NAFLD-HCC, primarily due to T-cell exhaustion. My analysis recapitulated the increases in exhausted Cd8 populations, which also expressed the same markers (Eomes, Tox, Cxcr6) as identified in so called ‘autoaggressive T cells’ in the study by *Pfister et al.*[38]. In addition to this, I found that expression of Tnf (TNF α), known to be toxic to T-cells and impair responses, was reduced significantly in cytotoxic T-cells using combination CXCR2smi/anti-PD1 therapy. Taken together, this suggests that CXCR2smi/anti-PD1 combination therapy may help to reverse the aberrant T-cell phenotypes seen in both *Pfister et al.* and our previous work [38, 230], thus providing a clinically relevant treatment strategy for translation into randomised clinical trials in NASH/NAFLD-HCC populations. Furthermore, in my analysis there were profound changes induced by CXCR2smi monotherapy alone. Given *Pfister et al.* showed T-cell

dysfunction was essential for promoting the development of NASH/NAFLD-HCC, given my results it would be interesting to test whether CXCR2smi monotherapy could be used as a preventative therapy for NAFLD/NASH[38].

As the number of people with NASH/NAFLD increases globally, the incidence of NASH/NAFLD-HCC is set to increase[240]. Given the challenges in access to surgery and curative interventions in this patient population, systemic therapy in either an adjuvant or neoadjuvant setting is likely to be required. I have shown that neutrophilic inflammation is a key feature of people with NASH/NAFLD-HCC and that skewing the tumour microenvironment to favour anti-tumour CD8+ T-cell responses using CXCR2 inhibition may be potentially useful. Further early phase clinical work is required, but the CXCR2 inhibitor used here, AZD5069, may be a useful candidate for translation given it has been tested already in humans with an acceptable toxicity profile[241].

A.6 Future directions

- The findings of the single cell RNA sequencing analysis should be validated through multiplex immunohistochemical staining of protein to confirm the correct cell types have been assigned and this translates to the protein-level. This would also be useful to provide a spatial context to the single cell data to identify which tumour regions this is occurring in and signs of associated steatosis normalisation or alteration in neutrophil infiltration and whether other cell populations are associated with these phenotypic changes. This should be performed both in tissue from animals included in the single-cell analysis and those which were not, to ensure these were consistent across larger experimental groups. Functional validation of the role different cell types in mediating the effect of combination CXCR2smi therapy could also be performed, for example using Il-1b knock-out to validate the role of Kupffer cell derived Interleukin-1 β .
- Understanding the functional differences between immature and mature tumour associated neutrophils would help to identify specific mechanisms underpinning the

synergistic CXCR2smi/anti-PD1 combination. For example, is this due to differences in NET formation or intra-tumoural reactive oxygen species production.

- To add further relevance to clinical disease, combination CXCR2smi/anti-PD1 therapy should be repeated in genetically engineered mouse models. Due to the large number of mutations induced across the genome with DEN carcinogen models, it is likely that a more precisely engineered model could recapitulate human disease more accurately. To do this, it would have to be established whether NASH induced immune checkpoint inhibitor resistance in a model which without fat is sensitive to immunotherapy. A good starting point would be to use either modified western or ALIOS diets with the $Tp53^{fl/fl}$ $Rosa26^{c-MYC/c-MYC}$ model, which I have shown is sensitive to immune-checkpoint inhibition in chapter 4.
- The CUBIC trial, a phase I/II clinical trial based upon this work, will assess the safety and efficacy of combining the CXCR2 small molecule inhibitor AZD5069 with Durvalumab, an anti-PD-L1 monoclonal antibody[237]. Tissue from patients in this study would be useful to assess whether treatment with CXCR2 inhibitor leads to the same effects observed in mice and whether similar transcriptomic signatures predict treatment response. Similarly, data from this trial will be useful to determine whether the combination is useful in NASH-HCC or whether benefits may extend to other classes of HCC.